

Evolution of Variscan metamorphic rocks from the Fichtelgebirge and Elstergebirge

Von der Fakultät Chemie der Universität Stuttgart
zur Erlangung der Würde eines Doktors der
Naturwissenschaften (Dr. rer. nat.) genehmigte Abhandlung

Vorgelegt von
Gelareh Rahimi
aus Teheran

Hauptberichter: Prof. Dr. Hans-Joachim Massonne
Mitberichter: Prof. Dr. Michael Hunger
Mitprüfer: Prof. Dr. Dr. Clemens Richert

Tag der mündlichen Prüfung: 05. April 2019

Institut für Mineralogie und Kristallchemie der Universität Stuttgart

2019

Inhaltsverzeichnis

Inhaltsverzeichnis.....	ii
Abkürzungsverzeichnis.....	5
Zusammenfassung.....	9
Summary.....	14
1. Introduction.....	17
1.1. Motivation and general scope of the thesis.....	17
1.2. Targets of the thesis and methodologies.....	20
2. Geological background.....	21
2.1. Variscan orogeny in Europe.....	21
2.2.1. Variscan orogeny in central Europe.....	23
2.2.2. Tectonic evolution of the Variscan orogeny in Europe.....	25
2.3. Variscan orogeny in the Bohemian Massif and Saxothuringian Zone.....	29
2.3.1. Lithostratigraphy of the Saxothuringian Zone.....	32
2.4. Variscan orogeny in the Fichtelgebirge and Elstergebirge areas.....	34
2.4.1. Geochronology and previous protolith studies of Fichtelgebirge.....	35
2.4.2. Published pressure-temperature conditions of Fichtelgebirge metamorphic rocks.....	36
3. Methods.....	37
3.1. Localities and positions of the sampled rocks.....	37
3.2. Petrography (Polarizing Microscope).....	37
3.3. Mineral chemistry.....	39
3.3.1. Sample preparation.....	39
3.3.2. An introduction to electron microprobe (EMP) analysis.....	41
3.3.3. Electron-sample interactions.....	42
3.3.4. Characteristic X-ray spectra.....	44
3.4. Bulk rock analyses.....	46
3.4.1. X-ray Fluorescence Spectrometer and Carbon Analyser.....	46
3.4.2. Verification of analytical techniques.....	48
3.5. Geothermobarometry.....	48
3.5.1. Geothermometry.....	49
3.5.1.1. Garnet-muscovite thermometry.....	49

3.6. Phase equilibria modelling (PERPLE_X).....	50
3.6.1. Introduction.....	50
3.6.2. The basic principles of PERPLE_X.....	51
3.6.2.1. Gridded minimisation.....	51
3.7. Geochronology.....	54
3.8. Geochemical characterisation for provenance and protolith.....	55
4. Pressure-temperature-time evolution of a Variscan garnet-bearing micaschist from the northeastern Fichtelgebirge, NW Bohemian Massif in central Europe.....	56
4.1. Introduction.....	57
4.2. Geological setting.....	59
4.3. Analytical techniques.....	62
4.4. Petrography and chemical compositions of the minerals.....	63
4.4.1. Modal and textural aspects.....	65
4.5. Modelling of the P-T evolution.....	72
4.5.1. Calculation method.....	72
4.5.2. P-T pseudosection.....	77
4.5.3. P-T path.....	80
4.6. Monazite dating.....	81
4.7. Discussion.....	84
4.7.1. The metamorphic P-T evolution.....	84
4.7.2. Geological interpretation of the new data.....	87
4.8. Conclusion.....	89
4.9. Acknowledgements.....	90
5. Metamorphic evolution of chloritoid-bearing micaschist from the Variscan Elstergebirge - evidence for stacking of high-pressure rocks in the Saxothuringian Zone of central Europe.....	91
5.1. Introduction.....	92
5.2. Geological background.....	94
5.3. Analytical methods.....	97
5.4. Petrography and mineral compositions.....	98
5.4.1. Micaschist samples.....	98
5.4.2. Minerals in sample 14AS6.....	100
5.5. P-T pseudosection modelling.....	105

5.5.1. Calculation method.....	105
5.5.2. Calculation results.....	110
5.5.3. P-T path reconstruction.....	112
5.6. Monazite age dating.....	115
5.7. Discussion.....	120
5.7.1. P-T evolution.....	120
5.7.2. Interpretation of monazite ages.....	122
5.7.3. Geodynamic interpretation of the P-T-t evolution.....	123
5.8. Conclusions.....	125
5.9. Acknowledgements.....	126
6. Protolith and Provenance.....	127
6.1. Protolith of metapelites.....	127
6.2. Provenance of metapelites.....	127
7. Final conclusions.....	132
8. Bibliography.....	134
Acknowledgements.....	167
Eigenständigkeitserklärung.....	169
Lebenslauf des Autor.....	170

Abkürzungsverzeichnis

Ab	Albite
ACM	Active Continental Margin
Alm	Almandine
An	Anorthite
And	Andalusite
Andr	Andradite
Apt	Apatite
BM	Bohemian Massif
BSE	Back-scatter Electron
Bt	Biotite
CB	Cheb Basin
Ch	Chlorite
CIA	Continental Island Arc
Crd	Cordierite
Crp	Carpholite
Ctd	Chloritoid
DEKORP	Deutsches Kontinentales Reflexionsseismisches Programm
dfu	double formula unit
EC	Erzgebirge crystalline complex
EMPA	Electron Microprobe Analysis
Ep	Epidote
ETSG	Elbtal Schist Gürtel
FC	Fichtelgebirge crystalline complex
Fr	Frankenberg
GC	Granulitgebirge metamorphic complex
GMC	Galicia-Massif-Central Ocean
Grs	Grossular
Gt	Garnet

HB	Hauptbohrung
Hm	Hematite
HP	High Pressure
HT	High Temperature
ICP-MS	Inductively Coupled Plasma-Mass Spectrometry
Im	Ilmenite
Kf	Potassic feldspar
KTB	Kontinentales Tiefbohrprogramm der Bundesrepublik Deutschland
Ky	Kyanite
L	Limousin
LP	Low Pressure
LT	Low Temperature
Lw	Lawsonite
M	Silicate melt
Ma	Margarite
MC	Massif Central
MGCH	Mid-German Crystalline High
MMC	Münchberg metamorphic complex
MO	Moldanubian Zone
mol%	Molar percentage
MORB	Mid Ocean Ridge Basalt
MS	Moravo-Silesian
Ms	Potassic white-mica
Mt	Magnetite
Mz	Monazite
NAM	North Armorican Massif
Nam	Na-rich amphibole
NWSG	Nossen-Wilsdruff Schist Gürtel
OIA	Oceanic Island Arc
Om	Omphacite

P	Pressure
Pa	Paragonite
pfu	per formula unit
Ph	Phengite
Pl	Plagioclase
PM	Passive Margin
Pyp	Pyrope
Qz	Quartz
RH	Renohercynian Zone
Rt	rutile
SEM	Scanning Electron Microscope
Sil	Sillimanite
Sps	Spessartine
St	Staurolite
Stl	Stilpnomelane
SZ	Saxothuringian Zone
T	Temperature
t	Time
UCC	Upper Continental Crust
V	H ₂ O vapour
vol.%	Volume percentage
W	Winklarn
Wd	Wildenfelds
Wrk	Wairakite
WS	West Sudetes
wt.%	Weight percentage
X _{Ca}	Molar fraction of the grossular + andradite component in garnet
X _{Mg}	Molar fraction of the pyrope component in garnet
X _{Mn}	Molar fraction of the spessartine component in garnet
ZEV	Zone of Erbdorf-Vohenstrauss

Zo	Zoisite
Zr	Zircon
ZTM	Zone of Tirschenreuth- Mähring
ZTT	Zone of Tepla-Taus

Zusammenfassung

Die Untersuchungsergebnisse dieser Doktorarbeit tragen entscheidend zum besseren Verständnis der Entwicklung der Variszischen Metamorphose der Glimmerschiefer im Fichtelgebirge und Elstergebirge im nordwestlichen Teil der Saxothuringischen Zone (SZ) des Bohemischen Massivs bei. Solche noch wenig untersuchten metamorphen Gesteine des Bohemischen Massivs treten auch im Fichtelgebirge (Tschechischer Name: Smrčiny Hory) und dem Elstergebirge (Tschechischer Name: Halštrovské Hory) auf. Diese befinden sich in Bayern und Sachsen an der Grenze zur Tschechischen Republik (und zu einem kleinen Teil auch in der Tschechischen Republik), im nordwestlichen Teil des Bohemischen Massivs.

Der Hauptaugenmerk der durchgeführten Untersuchungen konzentriert sich auf die Erarbeitung eines P-T (Druck-Temperatur) Pfades fuer unterschiedliche Proben metamorpher Gesteine. Diese Gesteine, die aus ehemaligen Sedimenten entstanden sind, durchliefen unterschiedliche Gleichgewichte auf ihrem P-T Pfad bis zum Zeitpunkt ihres Erscheinens auf der Erdoberflaeche.

Zur Erreichung des Untersuchungsziels wurden die nachfolgend aufgeführten Untersuchungsmethoden angewandt. Die Analysen fuer jede Probe sind in der Tabelle 1 aufgelistet:

1. Optische Mikroskopie: Duennschliffe der Gesteinsproben wurden zur Auswahl von geeigneten Proben fuer weitere detailliertere Untersuchungen untersucht.
2. Mikrosonden (EMP) Analysen: Die chemische Zusammensetzung der Mineralien wurde untersucht. Die Gefuegeverhaeltnisse wuden durch Bilder rückgestreuter Elektronen ermittelt. Elementverteilungskarten wurden zur Festlegung der chemischen Zonierung der Minerale erstellt. Zur Altersbestimmung wurden die U, Th und Pb Gehalte von Monazit gemessen und ausgewertet.
3. Röntgen-Fluoreszenz-Spektroskopie: Die chemische Zusammensetzung der Gesteinsproben wurde für die Hauptelemente durchgeführt. Dabei wurden Glasscheiben aus Gesteinsmehl und Spectro-Melt (Li-Borat: $\text{Li}_2\text{B}_4\text{O}_7$) hergestellt. Spurenelemente wurden mittels Presslingen, bei denen Gesteinsmehl mit Wachs verpresst wurde, bestimmt.

Eine wichtige Methode zur Bewertung der analytischen Ergebnisse und ihrer Verwendung zur Bestimmung des P-T Pfades war die Berechnung von P-T Pseudoschnitten (diagrammatische Druck-

Temperatur Querschnitte). Dazu wurde das Computer Programm PERPLE_X auf das chemische System $\text{Na}_2\text{O-K}_2\text{O-CaO-FeO-O}_2\text{-MnO-MgO-Al}_2\text{O}_3\text{-SiO}_2\text{-TiO}_2\text{-H}_2\text{O}$ angewandt. Diese Pseudoschnitte wurden durch Isoplethen für unterschiedliche modale und chemische Parameter wie z.B. Volumenprozent (vol.%) von Granaten und dem Siliziumgehalt in kaliumreichen Hellglimmern konturiert.

Teil 1 (Kapitel 4): Granat-reiche Glimmerschiefer (Probe 13F18) ca. 100 m südlich des Weilers Lauterbach (4 km NNE des Zentrums von Selb), im nördlichen Fichtelgebirge (FC) (Koordinaten: N: 50,20349°, E: 12,14639°).

Drei P-T-Pseudoschnitte wurden für die Massengesteinszusammensetzung dieses Gesteins berechnet und konturiert. Aus der Zusammensetzung der variablen Komponenten Granat und Phengit und deren Isoplethen wurden P-T Pfade abgeleitet. Dieser Pfad für Glimmerschiefer ist durch Spitzendrücke von ~ 10 kbar bei 505°C gekennzeichnet.

Die nachfolgende metamorphe Entwicklung, begleitet von Granatwachstum und Weiterwachstum wahrscheinlich von deformierten Hellglimmerschuppen, ist durch eine Druckentlastung auf 5 kbar und leicht ansteigende Temperaturen auf 535°C gekennzeichnet.

Die anschließende Temperaturerhöhung auf 565°C bei leicht abnehmendem Druck auf 4,5 kbar führte jedoch zum Abbau dieser Minerale, einschließlich teilweisem Ersatz des Granatrandes und des Kaliumglimmers durch Staurolith und Biotit.

Es darf angenommen werden, dass dieser Temperaturanstieg durch die Einlagerung großer post-tektonischer Granitkörper im FC verursacht wurde.

Die U-Th-Pb Altersbestimmung von Monazit mit der EMP ergab ein Alter zwischen 200 und 480 Ma. Entstehungszeiten jünger als 315 Ma sind eindeutig mit der Einlagerung der FC-Granite und den darauffolgenden hydrothermalen Prozessen verbunden, während im ehemaligen klastischen Sediment eine unterdevonische bis ordovizische Entstehungszeit dem detritischen Monazit zugeordnet wird. Der Alterscluster von $384,5 \pm 1,8$ (2σ) Ma bleibt unklar, aber wir sind der Ansicht, ihn auf den Zeitraum der HP Metamorphose zu beziehen.

Der Alterscluster bei $362,3 \pm 1,0$ Ma entspricht eher dem Ende der Heraushebung auf 15-20 km. Die Signalspitze bei $325,0 \pm 0,7$ Ma der Altersbestimmung könnte durch post-kollisionsbedingte granitische Schmelzen des älteren intrusiven Komplexes des FC verursacht worden sein. Diese Schmelzen waren in einen kristallinen Deckenstapel eingedrungen, der sich möglicherweise durch ein

zweites Kollisionsereignis von Gondwana und einem peri-gondwanischen Terrane gebildet hatte, das nach Schließung des Rheischen Ozeans bereits in spätdevonischer Zeit an Laurussia akkretioniert worden war. Nach unserer Interpretation führte dieses Ereignis dazu, dass kristalline Decken des FC, von dem die granathaltige Glimmerschiefer-Einheit unserer Probe einen unteren Teil bildete, auf die laurussische Kruste aufgeschoben wurden.

Teil 2 (Kapitel 5): Der untersuchte chloritoid-reichem Glimmerschiefer (Probe 14AS6) stammt aus einem Aufschluss, der 4,5 km nordöstlich der Stadt Asch/Aš im westlichen Teil des Elstergebirges liegt, ~ 2,5 km nordwestlich von Bad Brambach (Koordinaten: N: 50 ° 14,698', E: 12 ° 16,613').

Seine klar definierten Mineraltexturen und Strukturen wurden untersucht, um seine P-T-Evolution zu entschlüsseln.

Zwei P-T Pseudoschnitte wurden durch Isoplethen verschiedener Parameter konturiert, einschließlich molarer Anteile von Granatbestandteilen, Si in Phengit und X_{Mg} ($Mg / (Mg + Fe^{2+})$) in Chloritoid und Chlorit. Unter Verwendung solcher Isoplethen wurde die P-T Entwicklung ermittelt, wobei der untersuchte chloritoid-führende Glimmerschiefer bei 505 °C durch Bedingungen bei etwa 15.5 kbar und eine anschließende nahezu isotherme Heraushebung zu intermediären Bedingungen von 540 °C und 10-11 kbar und Endtemperaturen um 4.7 kbar und 618 °C erlebte.

Um die Altersabfolge dieser metamorphen Evolution zu verstehen, wurde die U-Th-Pb-Datierung an bis zu 100 µm großen Monazitkörnern mit der EMP durchgeführt. Die Alter von 113 Monazitanalysen liegen zwischen 315 und 480 Ma mit den prominentesten Maxima und Nebenmaxima bei $346,0 \pm 1,1$ (2σ), $357,3 \pm 2,3$ und $368,3 \pm 1,7$ Ma. Solche älter als 380 Ma wurden Detritus-Monazit und damit dem Herkunftsgebiet zugeordnet.

Folglich sollten die Protolithen der Glimmerschiefer spätdevonische Sedimente sein. Alter jünger als 335 Ma wurden späten variszischen Ereignissen wie Plutonismus in der Nähe des Studiengebiets zugewiesen. Das Alter nahe 370 Ma wurde auf das Hochdruckereignis bezogen, das Ergebnis der Kontinent-Kontinent-Kollision von Laurussia und Gondwana nach Schließung des Rheischen Ozeans ist. Diese Kollision verursachte eine signifikante Verdickung der Kruste. Die darauffolgende Heraushebung in obere Krustenniveaus geschah bereits im Visean.

Teil 3 (Kapitel 6): Die Haupt- und Spurenelementmuster der untersuchten Glimmerschieferproben (Tabelle 6.1) zeigen, dass die Protolithen der Metapelite des Fichtelgebirges und des Elstergebirges Schiefer- und Wacken-Zusammensetzungen aufweisen nach verschiedenen

Klassifikationsdiagrammen sind Proben des Fichtelgebirges - Elstergebirges PM (Passiver Rand - passive margin), CIA (Kontinentaler Inselbogen - continental island arc) und ACM (aktiver Kontinentalrand - active continental margin) zuzuordnen. Dies und die Anreicherung in LREE und die Dominanz von inkompatiblen Spurenelementen gegenüber kompatiblen Spurenelementen, sowie die hohen Th/Sc Verhältnisse, deuten auf das Vorherrschen der UCC (obere kontinentale Kruste - (upper continental crust)) als Ausgangsmaterial hin, und nicht auf die untere kontinentale Kruste oder den Erdmantel.

Die oben genannten Ergebnisse haben zu den folgenden neuen wichtigen Ergebnissen geführt: 1) Hochdruckgesteine ($P \geq 10$ kbar) aus dem Fichtelgebirge und dem Elstergebirge der SZ wurden im Oberdevon bis zu Tiefen von 15-20 km ($\sim 4,5$ kbar) exhumiert anschließende Aufheizung bis auf 565 °C - 590 °C war im Unterkarbon beendet. (2) Gesteine, die Drücken von ~ 16 kbar ausgesetzt waren, Teil eines tiefgelegenen Exhumierungskanals. (3) Granitische Schmelzen der älteren FC Intrusiva aus der Nach-Kollisions-Zeit um $325,0 \pm 0,7$ Ma. intrudierten eine Kristalldecke. Dieses Ereignis war durch die Überschiebungen des FC ueber die Laurussische Kruste ausgelöst worden. (4) Die mineralogischen und geochemischen Eigenschaften dieser Schiefer entsprechen gut einer hochgradigen, oberproterozoischen bis Ordovizischen Sedimentfolge in der Referenzregion der Fichtelgebirge-Elstergebirge Anticline.

Table 1. The studied samples and the corresponding analytical works. “Parts 1 to 3”: See text. Abbreviations: And, andalusite; Bt, biotite; Ch, chlorite, Ctd, chloritoid; Gt, garnet; Im, ilmenite; Kf, potassic-feldspar; Mz, monazite; Ms, potassic white-mica; Pl, plagioclase; Rt, rutile; and St, staurolite.

	Samples	Coordinates	Localities	XRF		EMP		
				Major element analyses	Trace element analyses	Spot analyses	X-ray maps	Monazite analyses for dating
Part 1 Chapter 4	Micaschist (13F18)	N: 50.20349° E: 12.14639°	4 km NNE of Selb town	1	1	141 Gt, 264 Ms, 159 Ch, 202 Bt, 13 Pl, 34 St, 36 And, 64 Im	2 Gt, 2 Ms 1 Mz	168 Mz
Part 2 Chapter 5	Micaschist (14AS6)	N: 50° 14.698 E: 12° 16.613	4.5 km NE of Asch/Aš town	1	1	192 Gt, 191 Ms, 56 Ch, 15 Bt, 65 Ctd, 19 Rt	2 Gt, 2 Ms 2 Ctd 3 Mz	128 Mz
Part 3 Chapter 6	Phyllite (13F7)	N: 50° 02.256 E: 12° 02.375	~ 7 km NE of Bad Alexandersbad (Dünkelhammer)	1	1	275 Ms, 34 Ch 70 Bt	1 Bt, 3 Ms	
	Phyllite (13F11)	N: 50° 05.787 E: 11° 80.812	~ 1.2 km NE of Bischofsgrün	1	1		1 Bt, 3 Ms	
	Phyllite (13F13)	N: 50° 23.705 E: 12° 06.890	2.5 km SE of Rehau to Selb at Fohrenreuth	1	1			
	Phyllite (13F15)	N: 50° 21.710 E: 12° 09.173	2.7 km NE of Schönwald	1	1			
	Micaschist (14AS4)	N: 50° 13.832/841 E: 12° 17.269/ 262	~1.5-2 Km NW of Bad Brambach	1	1	115 Gt, 116 Ms 35 Ch, 12 Kf	2 Gt, 2 Ms	
	Micaschist (14AS5)	N: 50° 14.418 E: 12° 16.731	~ 1.5 km SW of Raun	1	1	281 Gt, 190 Ms 84 Ch, 80 Rt	2 Gt, 2 Ms 2 Mz	38 Mz
	Micaschist (14AS11)	N: 50° 13.730 E: 12° 12.080	~ 1 km NE of Asch/Aš town	1	1	242 Gt, 183 Ms, 36 Ch, 38 Bt, 8 Kf	4 Gt, 4 Ms	
	Micaschist (14AS13)	N: 50° 14.390 E: 12° 12.360	~ 1.5 km SSE of Neuberg/Podhradí	1	1	123 Gt, 127 Ms 13Ch, 25 Rt	2 Gt, 2 Ms 3 Mz	130 Mz
Micaschist (14AS18)	N: 50° 14.777 E: 12° 13.543	~ 1.5 km NW Niederreuth/Dolní Paseky	1	1	232 Gt, 112 Ms 42 Bt	2 Gt, 2 Ms		

Summary

This thesis contributes to enhance the understanding of the Variscan metamorphic evolution of rocks in the NW part of the Saxothuringian Zone (SZ) in the Bohemian Massif. The so far poorly studied micaschists and gneisses of the SZ in the Bohemian Massif also occur in the Fichtelgebirge (Czech: Smrčiny Hory) and the Elstergebirge (Czech: Halštrowské Hory), which are located in Bavaria and Saxony close to the border to the Czech Republic (to some extent on the Czech side as well).

The major focus of the study was to establish P-T paths for these rocks with different bulk rock compositions. Such rocks, which formed from pre-existing sediments, suffer from steady states of equilibrium along their metamorphic P-T path evolution until they are exhumed. To reach the goal, the following analytical methods were applied. The numbers of analyses achieved on each sample studied in detail are listed in Table 1:

1. Optical microscopy: Thin sections of abundant rock samples were checked for the selection of samples to be studied in detail. Textural relations of minerals were recognized.

2. Electron microprobe (EMP) analytics: Chemical compositions of minerals were determined. Textural relations were documented by back scattered electron images. X-ray maps were produced to recognize the chemical zonation of minerals. Monazite was analysed to date this mineral based on U, Th, and Pb contents.

3. X-ray fluorescence (XRF) spectrometry: Chemical bulk rock compositions were determined for major elements using glass discs prepared from rock powder and Spectromelt (Li-borate: $\text{Li}_2\text{B}_4\text{O}_7$). Trace elements were analysed on discs obtained by pressing rock powder with wax.

A major part of the evaluation of the analytical work and its use to determine P-T paths was related to the calculation of P-T pseudosections. For this purpose, the computer program package PERPLE_X was applied to the chemical system $\text{Na}_2\text{O-K}_2\text{O-CaO-FeO-O}_2\text{-MnO-MgO-Al}_2\text{O}_3\text{-SiO}_2\text{-TiO}_2\text{-H}_2\text{O}$. These pseudosections were contoured by isopleths for diverse modal and chemical parameters such as vol.% of garnet, Si content in potassic white-mica per formula unit.

Part 1, (Chapter 4): Garnet-bearing micaschist (sample 13F18) from ~ 100 m south of the hamlet of Lauterbach (4 km NNE of the centre of Selb), in the northern Fichtelgebirge complex (FC) (coordinates: N: 50.20349°, E: 12.14639°). Three P-T pseudosections were calculated for the bulk rock compositions of these rocks and contoured. Using mainly the variable garnet and phengite

compositions and these isopleths, P-T paths were derived. This path for the micaschist is characterized by peak pressures of ~ 10 kbar at 505 °C.

The subsequent metamorphic evolution accompanied by garnet growth and re-growth probably of stressed white-mica flakes, is characterized by a pressure release down to 5 kbar and slightly rising temperatures to 535 °C. However, the subsequent temperature increase to 565 °C at slightly decreasing pressure to 4.5 kbar resulted in the partial decomposition of these minerals, including partial replacement of the garnet rim and of potassic white-mica by staurolite and biotite. We assume that this temperature increase was caused by the emplacement of large post-tectonic granite bodies in the FC. U-Th-Pb dating of monazite with the EMP resulted in ages between 200 and 480 Ma. Ages younger than 315 Ma are clearly related to the emplacement of the FC granites and subsequent hydrothermal processes, whereas Lower Devonian to Ordovician ages are assigned to detrital monazite in the former clastic sediment. The age cluster of 384.5 ± 1.8 (2σ) Ma remains unclear, but we prefer to relate it to the age of the HP metamorphic event.

The age cluster at 362.3 ± 1.0 Ma rather corresponds to the end of the exhumation to 15-20 km. The age peak at 325.0 ± 0.7 Ma might have caused by post-collisional granitic melts of the older intrusive complex of the FC. These melts had intruded a crystalline nappe pile that might have formed by a second collisional event of Gondwana and the peri-Gondwanan terrane which had been accreted to Laurussia after closure of the Rheic Ocean already in Late Devonian times. According to our interpretation, this event caused the overriding of crystalline nappes of the FC, of which the garnet-bearing micaschist unit of our sample was a lower part of, onto the Laurussian crust.

Part 2, (Chapter 5): The studied chloritoid-bearing micaschist (sample 14AS6) comes from outcrops lying 4.5 km NE of the town of Asch/Aš in west part of Elstergebirge, ~ 2.5 km NW of Bad Brambach (coordinates: N: $50^\circ 14.698'$, E: $12^\circ 16.613'$). The relatively fresh chloritoid-bearing micaschist with clearly defined mineral textures and structures was studied to decipher its P-T evolution.

Two P-T pseudosections were calculated and contoured by isopleths of various parameters, including molar fractions of garnet components, modal contents of garnet in vol.%, Si content in potassic white-mica, and X_{Mg} ($Mg/(Mg + Fe^{2+})$) in chloritoid and chlorite. Such isopleths were used to derive P-T paths. The studied chloritoid schist experienced peak P-T conditions around 16 kbar at 505 °C and a subsequent nearly isothermal exhumation with intermediate conditions of 540 °C and 10-11 kbar and exhumation to 15-20 km depths (~ 5 kbar) at slight heating to 555 °C followed. Subsequently, an isobaric heating to ~ 600 °C occurred. To understand the timing of this metamorphic

evolution, U-Th-Pb dating was performed on up to 100 μm sized monazite grains with the EMP. The ages obtained from 113 monazite analyses range between 315 and 480 Ma with the most prominent maxima and side maxima at 346.0 ± 1.1 (2σ), 357.3 ± 2.3 , and 368.3 ± 1.7 Ma. Several ages older than 380 Ma were related to detrital monazite and, thus, to the provenance area. Consequently, the protoliths of the micaschists should have been Late Devonian sediments. The isobaric heating event at 325 Ma were assigned to late Variscan events such as plutonism in the vicinity of the study area. We relate the ages close to 370 Ma to the high pressure event being the result of the continent-continent collision of Laurussia and Gondwana after closure of the Rheic Ocean in the Upper Devonian. The corresponding rocks were subsequently exhumed to 15-20 km depth in the early Carboniferous. This collision caused significant crustal thickening. The subsequent exhumation to upper crustal levels was already accomplished in the Viséan.

Part 3, (Chapter 6): Major and trace element geochemical features of the investigated metasedimentary samples (Table 6.1) demonstrate that the protoliths of these rocks from the Fichtelgebirge-Elstergebirge were shales, feldspar-rich sandstones, and wackes. According to different classifications plots, these samples from the Fichtelgebirge-Elstergebirge are PM (passive margin), CIA (continental island arc) and ACM (active continental margin) and the enrichment in LREE and other incompatible trace elements over compatible ones, as well as the high Th/Sc ratios, points to the predominance of upper continental crust (UCC) as parent material and not the lower crust or the mantle.

The aforementioned achievements have resulted in the following new major findings: 1) high pressure ($P \geq 10$ kbar) rocks from the Fichtelgebirge and Elstergebirge of the SZ in Upper Devonian and exhumation to 15-20 km depths (~ 4.5 kbar) following by heating to 565 °C - 590 °C ended in the Early Carboniferous. (2) Rocks which had experienced pressures of ~ 16 kbar, were involved in a deep portion of the exhumation channel. (3) Post-collisional granitic melts of the older FC intrusive complex, which intruded a crystalline nappe at $\sim 325.0 \pm 0.7$ Ma, were caused by the overriding of crystalline nappes of the FC onto the Laurussian crust. (4) Mineralogical and geochemical features of these schists correspond well with a high grade, Upper Proterozoic to Ordovician sedimentary succession in the reference region of the Fichtelgebirge-Elstergebirge Anticline.

1. Introduction

1.1. Motivation and general scope of the thesis

Low-medium grade Variscan metamorphic rocks of the Bohemian Massif occur in the Fichtelgebirge (Czech: Smrčiny Hory) and Elstergebirge (Czech: Halštrovské Hory), which are located in Bavaria and Saxony close to the border to the Czech Republic (to some extent on the Czech side as well). As this part in the northwestern Bohemian Massif was poorly petrologically studied so far, it motivated to undertake studies to decipher the metamorphic evolution of these rocks. The crustal structure and the geotectonic development of the Variscan Belt of Europe have been controversial for a long time. Traditionally, the Variscides of central and Western Europe have been regarded as the key areas of this orogeny (Kroner and Romer, 2013). Most structural and evolutionary models for the Variscides and the assemblage of Pangea are based on these areas. For instance, the classical zonation of the Variscides (Suess, 1888, 1926; Kossmat, 1927; Stille, 1951; Zwart, 1967) was established in and west of the Bohemian Massif. Because of obvious similarities in stratigraphy, structure, metamorphism and magmatism, this model was expanded to Iberia (Lotze, 1945). The classical zonation model for the central European Variscides (Kossmat, 1927), which is an anticipation of modern structural concepts stimulated by plate tectonics are still widely in use and has served as template for the arrangement of pre-Variscan plates and their boundaries in some plate tectonic models (e.g., Franke, 1989, 2000; Matte, 1991; Oncken et al., 1999).

However, due to significant differences with the classical areas of the Variscan orogen and the areas overprinted by the Alpine orogeny, this classical zonation does not apply to the geometry of the entire orogen (von Raumer and Neubauer, 1993; Stampfli, 1996). The discovery of high pressure metamorphic rocks, ophiolite sequences (Haydoutov, 1989; Pin et al., 2002) and important nappe thrusts has among others justified the application of plate-tectonic concepts. There is broad consensus on the large-scale plate-tectonic development of the Variscides. In the Cambrian, the pre-Variscan crust was broadly part of the Gondwana plate, i.e., the peri-Gondwanan Avalonian-Cadomian belt (Nance and Murphy, 1994).

Studies on the sedimentology (e.g., Wurm, 1925, 1961; Kukul, 1971; Sdzuy, 1971; Geyer and Wiefel, 1997), deformation, metamorphism (e.g., Reinhard and Kleemann, 1994; Fielitz and Mansy, 1999; Kalt et al., 2000; Cooke and O'Brien, 2001; Will and Schmädicke, 2001; Willner et al., 2002) and geochronology (e.g., Zeh et al., 2001; Linnemann et al., 2004, 2008, 2014; Drost et al., 2011) of the Palaeozoic rocks of NE Bavaria have been carried out. Furthermore, based on the results of the

KTB (Kontinentales Tiefbohrprogramm der Bundesrepublik Deutschland) pre-site investigations including deep seismic profiling, the deep borehole was expected to penetrate through a medium- to high pressure metamorphic nappe relic Erbendorf-Vohenstrauß Zone (ZEV) into the cryptic suture between the Moldanubian and Saxothuringian terranes and thus to confirm the nappe tectonic concept of the Variscan belt which had been revived since the late 1970s (Behr et al., 1984; Franke, 1989; Weber and Vollbrecht, 1989) (see Fig. 2.7).

The German Continental Deep Drilling (KTB) activities started in 1987. In 1989, the Vorbohrung (pilot hole; KTB-VB) was stopped at a depth of 4000 m, on October 12, 1994, the Hauptbohrung (main hole, KTB-HB) reached a final depth of 9101 m (Hirschmann, 1996). One of the basic scientific targets of the KTB was the investigation of the structure and evolution of the crust in the internal zones of the central European Variscides (Hirschmann, 1996).

The drill site is 40 km southeast of Bayreuth in the Oberpfalz at the western edge of the Bohemian Massif. This area is characterized by the juxtaposition of several tectonometamorphic units or terranes such as Moldanubian, Saxothuringian, Mariánské Lázně Complex and Münchberg-Teplá terrane (DEKORP (Deutsches Kontinentales Reflexionsseismisches Programm) research Group, 1994; Matte et al., 1990). The Fichtelgebirge and Elstergebirge areas are located in the NW part of the Bohemian Massif and at the western margin of the Saxothuringian Zone (SZ) of this massif. (see, Fig. 1.1 and 2.1). The geological record of the Saxothuringian Zone is in many respects typical for the continental crust of the European Variscides. The structure of this crust is controlled by at least two orogenies: the Cadomian and Variscan one. Sedimentary successions as well as tectonomagmatic and metamorphic events from the latest Precambrian until the Upper Palaeozoic witness this long-lasting process and led to complex relationships (Kroner et al., 2007).

Kroner et al. (2007) think that, in contrast to data from petrology, geochronology, and geochemistry, which led to a reassessment of significant lithological units during the past years, the generally accepted structural geometry has changed little since Kossmat (1927). For example, most of the metamorphic basement rocks earlier believed to be of Precambrian age because of lithostratigraphic considerations (Lorenz and Hoth, 1990) were recognized to be of Lower Carboniferous age (von Quadt, 1993; Kröner et al., 1998; Romer and Rötzler, 2001).

Ultrahigh pressure minerals in rocks of the Saxothuringian crust (Massonne, 1999) require a specific tectonic process such as continental subduction or lithospheric delamination with the involvement of continental crust, with all its tectonometamorphic consequences.

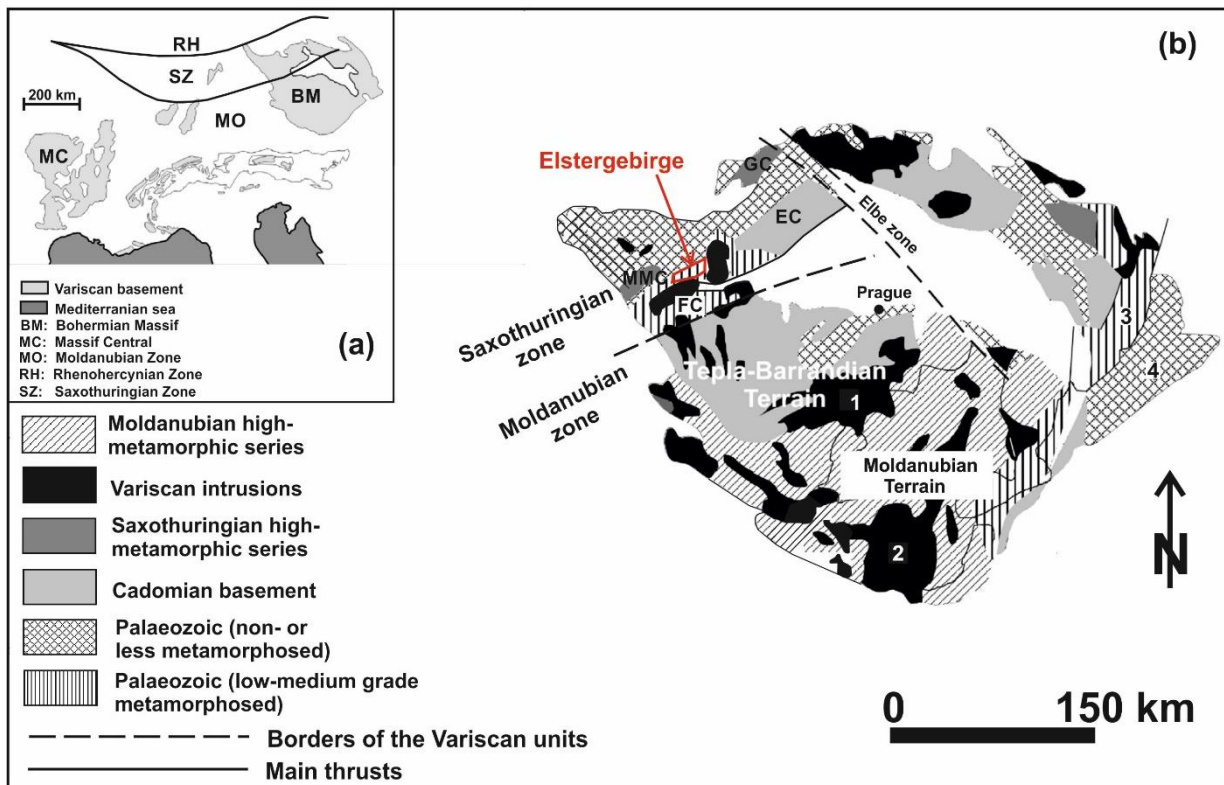


Fig. 1.1. (a) Map of the Variscan basement located in central Europe with its main geological units; and (b) Simplified geological map of the Bohemian Massif with coarse tectonometamorphic subdivision 1) central-Bohemian pluton; 2) central Moldanubian pluton; 3) and 4) Moravo-Silesian (modified after Sturm, 2017). Abbreviations: EC, Erzgebirge crystalline complex; FC, Fichtelgebirge crystalline complex; GC, Granulitgebirge metamorphic complex; and MMC, Münchberg metamorphic complex.

However, as some previous works (e.g., Mielke and Schreyer, 1969, 1972; Mielke and Abraham, 1980; Mielke et al., 1979; Schäfer et al., 1997) illustrated that the metamorphic rocks of these areas underwent a low pressure - low temperature (LP-LT) regional metamorphism, and due to the lack of well-constrained P-T data of metamorphic rocks in the SZ, it is not clear if these rocks were subject to similar P-T conditions as considered previously.

With this study, it will be demonstrated that (1) the metamorphic evolution of the Fichtelgebirge-Elstergebirge metamorphic rocks can be successfully derived and (2) important conclusions can be drawn to characterize the geodynamic processes behind the formation of these rocks.

1.2. Targets of the thesis and methodologies

The primary aim of the doctoral thesis was to derive P-T paths of metapelites combining the thermodynamic calculation of pseudosections with analysed chemical compositions of minerals, which can be chemically zoned such as garnet. In addition, the protolith character of metasedimentary rocks should be recognized. Monazite dating should be performed on metapelite. These methods provide information for a better understanding of the collisional situation of the target area in Variscan times. Detailed research objectives:

- (1) Careful study of mineral chemistry and mineral paragenesis in metasedimentary rocks from different locations. Finally, their P-T paths and tectonic evolutions should be reconstructed.
- (2) Comparison of the P-T evolutions of metapelites from different localities in the study area using the previously derived metamorphic evolution.
- (3) Defining the geotectonic settings of the protoliths of sampled metasedimentary rocks by discriminating diagram.
- (4) Geochronological achievements of U-Th-Pb electron microprobe (EMP) ages on monazite in metapelites.

In order to reach these goals, 4 phyllites and 7 metapelites from the Fichtelgebirge-Elstergebirge, in spite of the poor exposures were sampled (Fig. 1.1), based on the geological maps (scale 1:25.000, 1:200.000, 1:400.000 and 1:500.000) that exist for the entire area (Bernstein et al., 1973; Emmert et al., 1981; Stettner, 1958, 1975, 1980, 1981). Two of these metapelites studied to decipher the metamorphic evolution of the area (see chapters 4 and 5) and the other samples (phyllites and metapelites) to recognize the tectonic and protoliths of these metasediments.

2. Geological background

In fact, in the Anglo-Saxon literature the term Hercynian is frequently used as a synonym for Variscan (German word “variszisch”), which is used in preference to the term Hercynian throughout the thesis. Relics of the Variscan mountain chain are well known from many places in Europe (e.g., Iberia, Armorica, the French Massif Central, the Saxothuringian and Moldanubian domains, and Alpine pre-Mesozoic basement areas; Fig. 2.1). Modern reviews reveal their complex evolution since the Devonian (Dallmeyer and Martínez García, 1990; von Raumer and Neubauer, 1993, 1994; Keppie, 1994; Dallmeyer et al., 1995; Matte, 1998; Arenas et al., 2000; Franke et al., 2000). Pre-Variscan elements in these areas mostly appear as polymetamorphic domains, as a consequence of Variscan and/or Alpine orogenic events. Geotectonic nomenclature and zonation in these classical areas of Variscan evolution mirror the main Variscan tectonic structures (e.g., Suess, 1903; Kossmat, 1927; Stille, 1951), and evidently cannot be valid for the description of pre-Variscan elements. Relics of distinct geological periods from the Proterozoic to the Ordovician have been observed in many of the basement units. The Rheic Ocean named for the titan Rhea, sister of Iapetus in the Greek mythology—is arguably the most important ocean of the Palaeozoic in central Europe (Nance and Linnemann, 2008). Following the Silurian closure of the Iapetus Ocean, the Rheic Ocean separated the major palaeocontinents of Laurussia (Laurentia-Baltica-Avalonia) from Gondwana (Fig. 2.2). Subsequent closure of the Rheic Ocean resulted in the Ouachita-Alleghanian-Variscan orogeny and the assembly of the supercontinent of Pangea (Nance and Linnemann, 2008).

2.1. Variscan orogeny in Europe

This long-lasting orogeny (c. 120 Ma) is restricted to central, western and southeastern Europe (Fig. 2.1). Subduction processes persisted from Late Silurian to Early Carboniferous times as demonstrated by the age of high pressure metamorphism as well as the coeval existence of magmatic arcs (Kroner et al., 2008). Compressional tectonics lasted until the earliest Permian as demonstrated by the final deformation of the Cantabria-Asturias Arc in northern Spain (Weil et al., 2001), the syn- to post-kinematic intrusion of voluminous granitoids in Iberia (Fernández-Suárez et al., 2000) as well as the termination of ductile and brittle deformation along the northern external fold-and-thrust belt (Quinn et al., 2005).

2. Geological background

The remnants of the oldest subduction stage are referred to as the Early Variscan stage lasting from the Silurian to the Devonian (Matte, 2001). During the Mid-Variscan stage (c. Early Carboniferous) continental crust to the south of the Rheic suture was affected by a large-scale tectonometamorphic overprint including high pressure - high temperature (HP-HT) metamorphism, and this was followed by a large-scale low pressure - high temperature (LP-HT) event. The final geometry of the orogeny characterized by vast fold-and-thrust belts affecting voluminous foreland sediments is the result of the Late Variscan stage (Late Carboniferous-Early Permian) (Kroner et al., 2008).

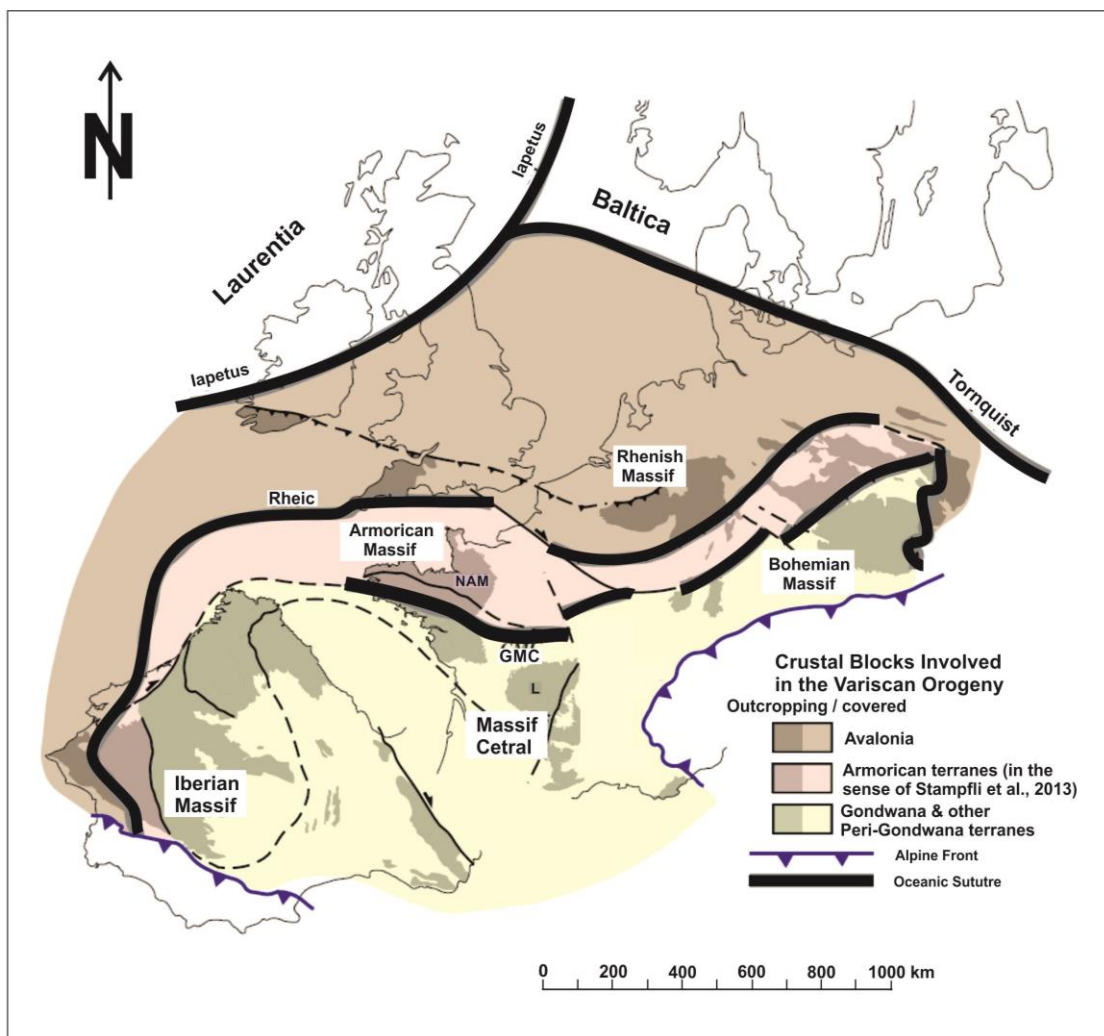


Fig. 2.1. Sketch map of the crustal blocks involved in the Variscan orogeny, adapted from Ballèvre et al. (2014). Yellow star highlights the location of the study area. Oceanic sutures: GMC, Galicia-Massif-Central Ocean. Regional subdivisions: NAM, North Armoric Massif; and L, Limousin (Western Massif Central).

2.2.1. Variscan orogeny in central Europe

The central European Variscides rank among the most intensively studied crustal sections on Earth with a plethora of publications being available and part of them now stored in various databases. These investigations started more than a century ago when the term Variscides was first coined by Suess (1888). Central and Eastern Europe have a polyorogenic history, so that the geological and structural setting especially of central Europe is attributed to the Caledonian, Variscan and Alpine orogenic events, the latter of which is still ongoing. Each stage is the consequence of a significant geodynamic setting of crustal plates.

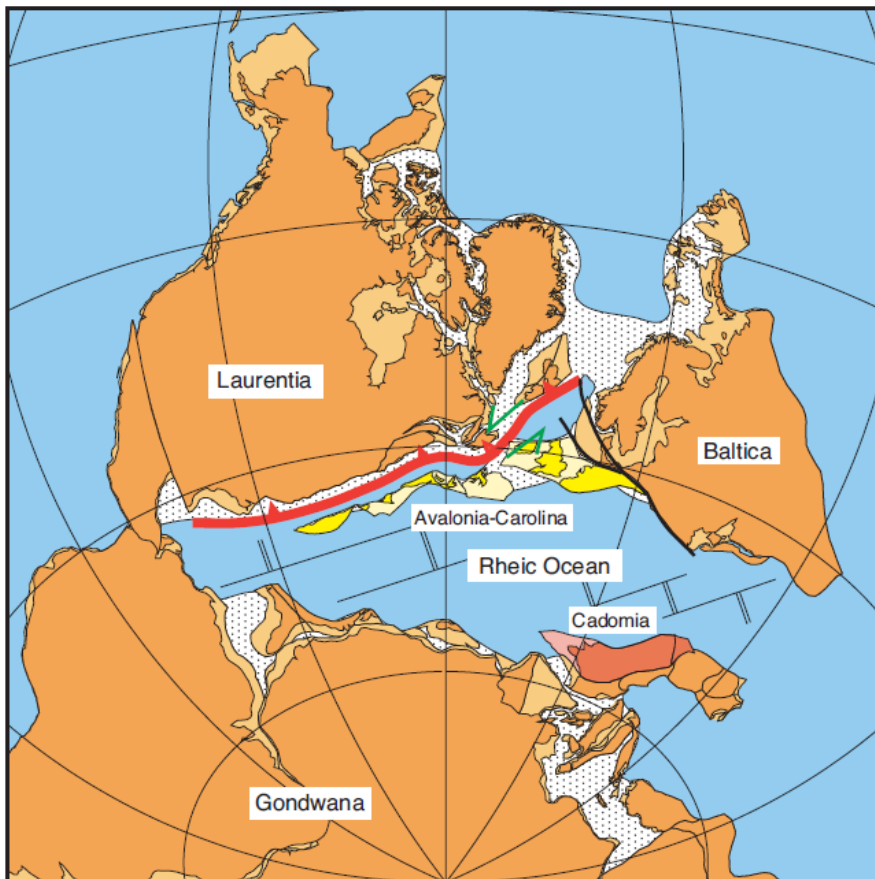


Fig. 2.2. Early Silurian reconstruction of the Rheic Ocean immediately prior to the closure of the Iapetus ocean by its subduction beneath Laurentia (toothed red line) (Nance et al., 2010). Stippled areas denote inferred regions of thinned and/or anomalous thickness of continental and arc crust. Rheic ridge-transform systems are purely schematic. Heavy black lines trace the Tornquist suture zone.

2. Geological background

Present day Europe consists of several Palaeozoic and older blocks or massifs. This configuration is the result of successive convergence and amalgamation stages of terranes and microplates since Late Precambrian or beginning of Phanerozoic times. Recently, there have been a number of volumes published summarizing the Variscan history of Europe (e.g., Dallmeyer et al., 1995; Franke et al., 2000; Neubauer and Handler, 2000; Kroner et al., 2007; Kroner and Romer, 2013; Schulmann et al., 2014). The classical subdivision of the Variscan area of central Europe into a number of distinct geotectonic zones was made by several authors (e.g., Suess, 1888, 1926; Kossmat, 1927; Stille, 1951; Zwart, 1967) (Fig. 2.3).

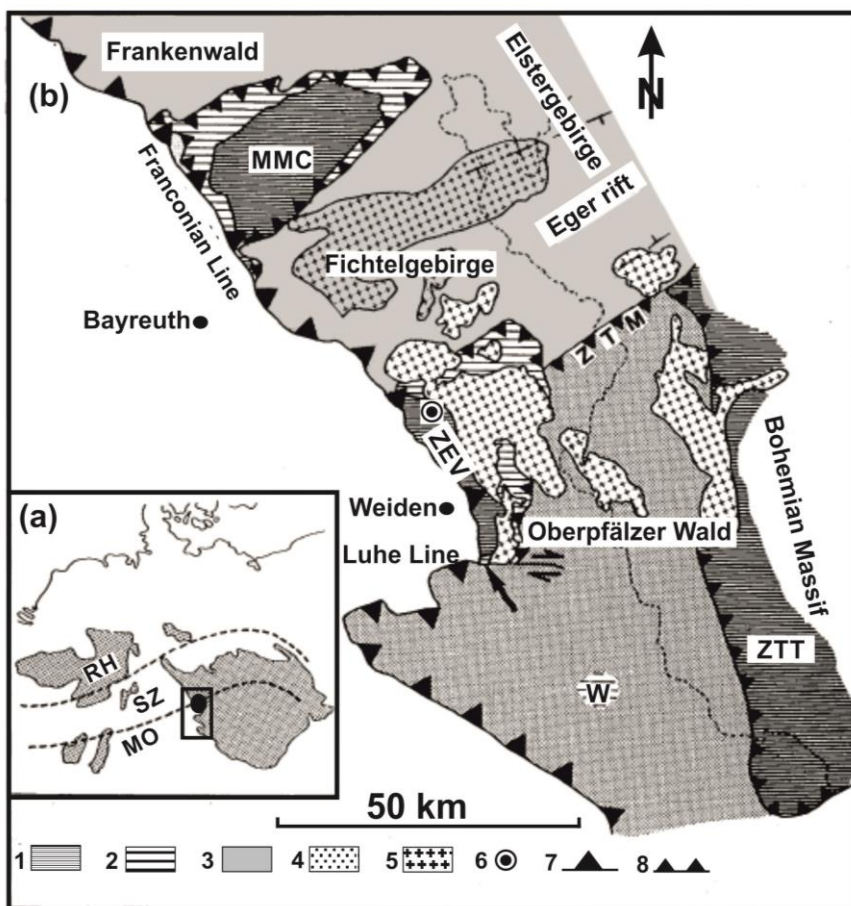


Fig. 2.3. (a) Variscan basement in mid-Europe with zones after Kossmat (1927), and sketch map of the western margin of the Bohemian Massif in NE Bavaria. RH, Rhenohercynian Zone; SZ, Saxothuringian Zone; and MO, Moldanubian Zone; and (b) Main tectonometamorphic units. 1) Medium pressure metamorphic nappes; MMC, Münchberg metamorphic complex; ZEV, Zone of Erbendorf-Vohenstrauss; ZTT, Zone of Tepla-Taus; ZTM, Zone of Tirschenreuth-Mährling; and W, Winklarn; 2) lower nappes; 3) Saxothuringian; 4) Moldanubian; 5) Late- to post-Variscan granites; 6) KTB drill site; 7) Franconian line; and 8) Overthrusts. (Modified after Vollbrecht et al., 1989)

From north to south these are the Westphalian (originally the Subvariszische Saumsenke, i.e., Variscan Foredeep), the Rhenohercynian, the Saxothuringian and Moldanubian Zones (Fig. 2.4) which together constitute the western Variscan fold belt (Kossmat 1927). Subsequent modifications of Kossmat's original scheme have included the identification of the Mid-German Crystalline High (MGCH) by Scholtz (1930) as a zone of crystalline rocks located between Kossmat's Rhenohercynian and Saxothuringian Zones. Although these books provide much-needed information concerning the nature and style of deformation during the Variscan orogeny, they are delimitedly concerned with the metamorphic evolution of the studied regions. Traditionally, the Variscides of central and Eastern Europe have been regarded as the key areas of this orogeny.

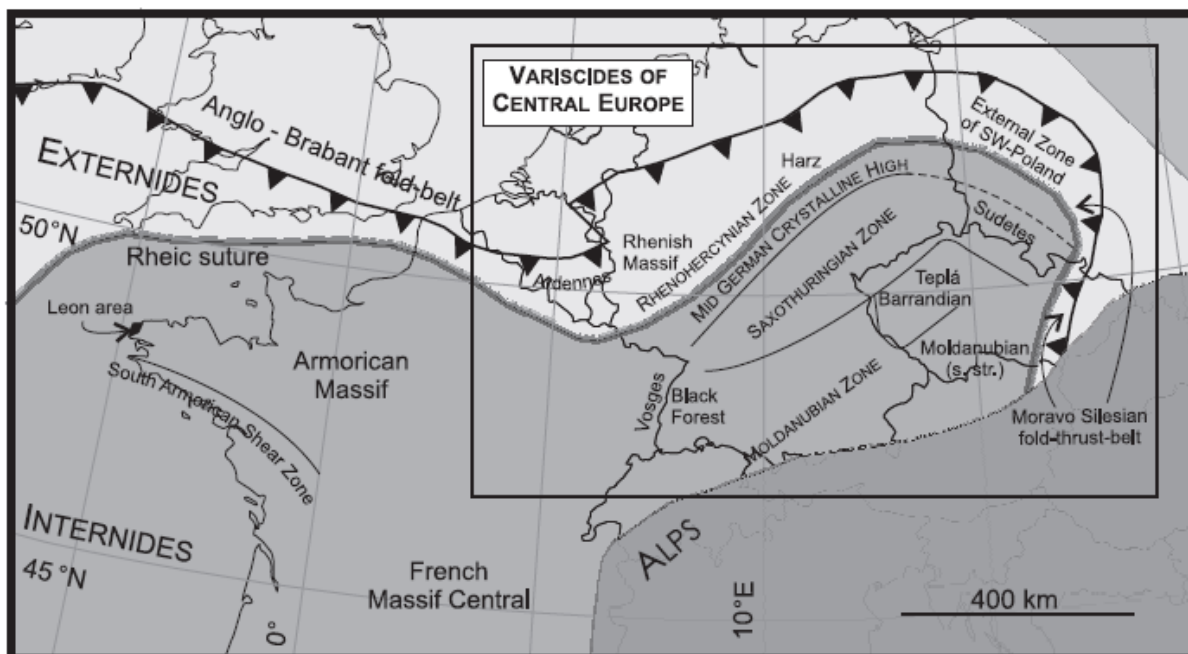


Fig. 2.4. Schematic sketch map of the central European Variscides (see, Kroner et al., 2008)

2.2.2. Tectonic evolution of the Variscan orogeny in Europe

The Variscan orogeny is related to complex tectonic scenarios. In the early and middle stages of the Variscan orogeny especially, compressional, extensional, and strike-slip tectonics occur coevally in different areas of the orogen. As with sedimentary, magmatic, and metamorphic processes, deformation within the orogen is diachronous along the orogenic belt. High pressure metamorphic belts indicate that convergent tectonics eventually leading to continental subduction

must represent the primary cause for the orogeny (e.g., Engel et al., 1983b; Echtler and Malavieille, 1990; Čizěk and Tomek, 1991; Behrmann and Tanner, 1997). During the Palaeozoic era, the interactions between the continents of Laurentia, Baltica and Gondwana were governed by two major oceans: Iapetus and Rheic (Fig. 2.5). The Iapetus Ocean, which opened in the Late Ediacaran/Early Cambrian, gave rise to the extensive Early Palaeozoic passive margin of eastern North America and was responsible for the formation of the Caledonide orogen and several accretionary orogenic episodes in the Appalachians. Iapetus was the first pre-Mesozoic ocean to be recognized with the advent of plate tectonics (Wilson, 1966) and its history is both widely known and well documented (e.g., Cocks and Fortey, 1990; Torsvik et al., 1996; Mac Niocaill et al., 1997; van Staal et al., 1998, 2009; Cocks and Torsvik, 2006, 2011).

To highlight the importance of the Rheic Ocean and clarify its role in Palaeozoic tectonics, this section provides a brief, illustrative review of the history of this ocean from its initial rifting to its final closure. An alternative tectonic setting for the inception of the Rheic Ocean is provided by a model proposed by Waldron et al. (2011) to account for the relatively rapid onset of subduction (only 20-40 Ma after initial rifting) of the Iapetus Ocean. Following the proposal of Murphy et al. (2011) for the Rheic Ocean these authors suggest that the highly depleted mantle source, indicated isotopically for many Iapetan ophiolitic complexes, points to a history of magmatism that predates the opening of Iapetus, suggesting that the complexes preserve oceanic lithosphere that was captured from the adjacent palaeo-Pacific in a manner analogous to the capture of the Caribbean plate by the Atlantic realm in the Mesozoic-Cenozoic. If this was the case and capture occurred between Baltica and Gondwana (Fig. 2.5), the Avalonian Cadomian margin of Gondwana would have occupied a tectonic position similar to those along the northern and southern sides of the present-day Caribbean plate and, hence, could have witnessed a diachronous transition from arc to transform as the captured lithosphere moved westward into Iapetus (Nance et al., 2012).

An option for the tectonic evolution of the Variscan orogeny in Europe, which is distinguished by the fate of Gondwanan island arcs (upper allochthonous unit) formed during the Late Cambrian-middle Ordovician (500-460 Ma). In this model (Fig. 2.6) (Abati, 2010; Martínez Catalán et al., 2009; Díez Fernández et al., 2012b; Gómez Barreiro et al., 2007) suggests that an island arc (upper allochthonous unit) was caused by calc-alkaline and alkaline plutons during 470-495 Ma (Abati et al., 2010), and then drifted away to open the Rheic Ocean during the middle Ordovician at c. 465-440 Ma (Martínez Catalán et al., 2009) (Fig. 2.6b, c). At c. 425-390 Ma, the arc accreted to Laurussia while the Rheic Ocean was still open (Fig. 2.6c).

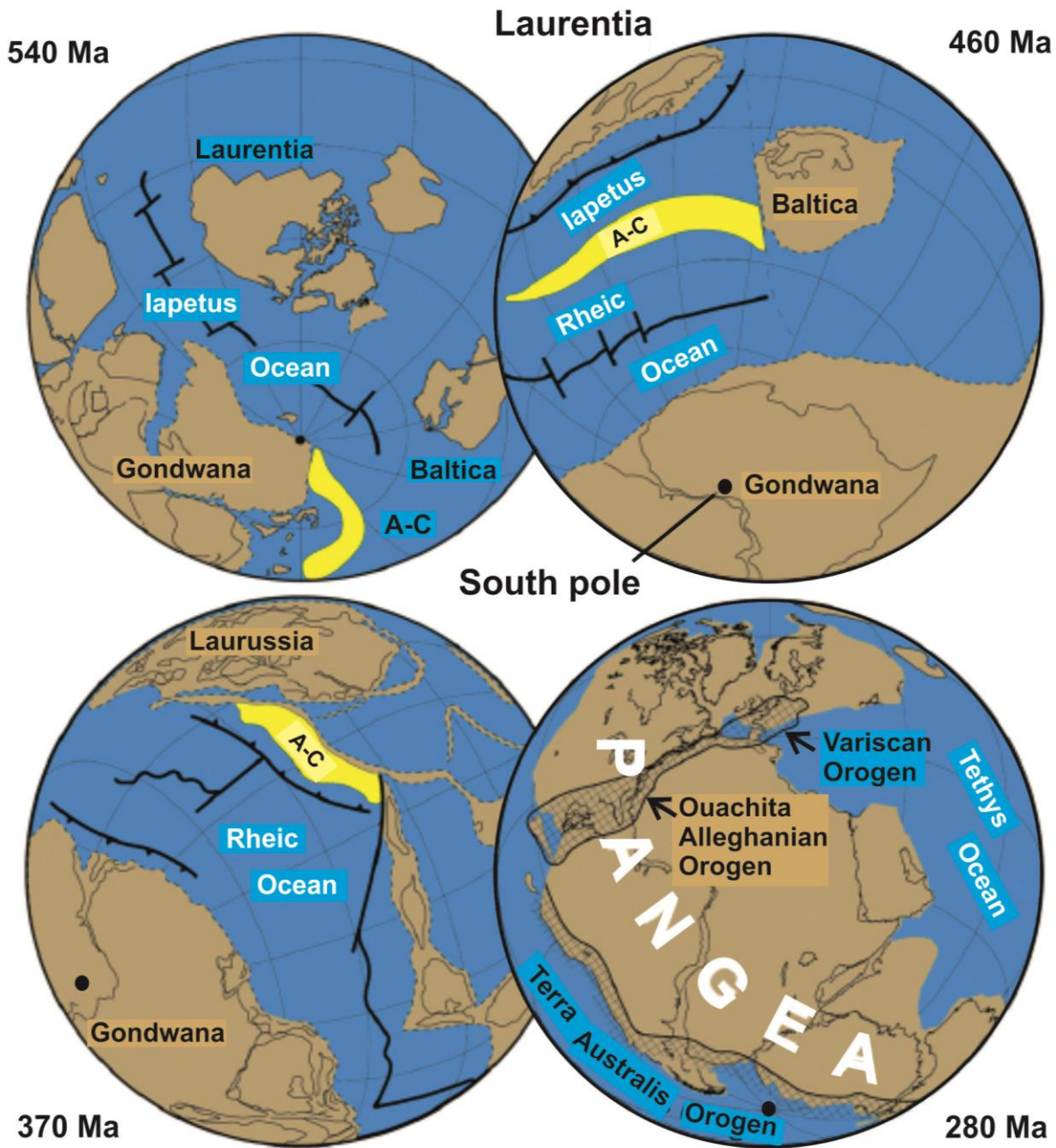


Fig. 2.5. Palaeozoic reconstructions (modified from Scotese, 1997; Cocks and Torsvik, 2002; Stampfli and Borel, 2002) at 540 Ma, 460 Ma, 370 Ma and 280 Ma showing the evolution of the Iapetus and Rheic Oceans between Gondwana and Laurentia-Baltica. A-C, Avalonia Carolina (from Murphy and Nance, 2008).

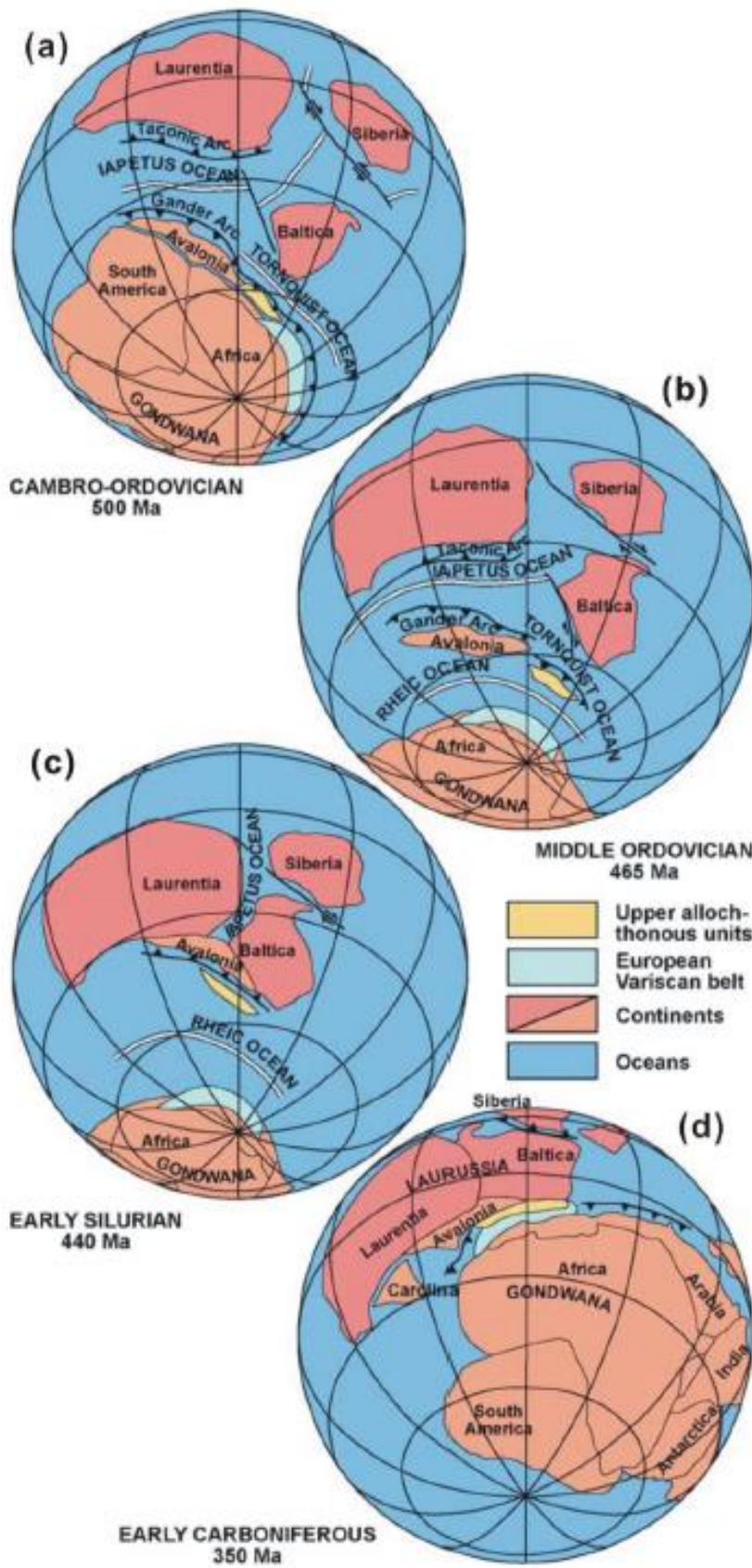


Fig. 2.6. Distribution of continental masses during the Palaeozoic, showing the suggested palaeopositions of the European Variscides and the ensialic arc preserved in the upper allochthonous units (Gómez Barreiro et al., 2007; Winchester et al., 2002; Martínez Catalán et al., 2009).

Subduction of a part of the arc involved tectonometamorphic events in the high-P and high-T units. The last stage of subduction related to Early Variscan convergence happened between 375 and 365 Ma (Rodríguez et al., 2003; Santos Zalduegui et al., 1995). The Rheic Ocean closed and Gondwana and Laurussia collided. At c. 350 Ma, the Laurussia-Gondwana convergence continued, the Variscan orogen formed finally (Fig. 2.6d) (Martínez Catalán et al., 2009).

2.3. Variscan orogeny in the Bohemian Massif and Saxothuringian Zone

The Bohemian Massif represents a relic of the Variscan orogenic belt in central Europe (Fig. 1.1). The present day structure of the Bohemian Massif shows that its tectonic evolution was controlled by the Devonian-Carboniferous subduction of an oceanic crust (so called Saxothuringian Ocean, situated at the southeastern side of the present day Saxothuringian Domain; Fig. 1.1) underneath the continental domains representing various tectonic units in the central and eastern Czech Republic, southern Poland and northern Austria (Konopásek, 2011) (Fig. 1.1). The subduction lasted at least from c. 400 Ma, which is the oldest record of high pressure metamorphism at the western margin of the Bohemian Massif, and culminated in the Early Carboniferous at c. 340 Ma by a continental collision responsible for the development of a deep orogenic root in the back-arc region of the orogen (Schulmann et al., 2005; 2009). Episodic exhumation of deeply buried rocks and/or middle crustal segments occurred in various parts of this subduction/collisional system, as documented in particular units of the Bohemian Massif (Konopásek, 2011). The Bohemian Massif is bounded to the north and the NE by the Mid-German Crystalline Zone (Fig. 2.7), which most likely represents the suture formed during the closure of the Rheic Ocean in the Late Devonian to Early Carboniferous period. To the south and southeast the Bohemian Massif is covered by the Meso-Cenozoic of the Alps and the Carpathians orogenies.

Steeply dipping faults in the southwest, such as the Franconian Line and the Danube Fault, divide the basement rocks from Mesozoic platform sediments and the Alpine molasses (Linneman, 2007). The easternmost segment of the European Variscides, is formed by four major zones: (i) the Moravo-Silesian (Brunovistulian Block); (ii) the Teplá-Barrandian Block; (iii) the Moldanubian; and (iv) the Saxothuringian Zones (Fig. 1.1).

The peri-Gondwana-derived terranes (Linnemann et al., 2004) rifted from the Gondwanan margin during the Early Ordovician. This basic division reflects the existence of four independent crustal fragments separated originally by oceanic domains, the traces of which are indicated today by the occurrences of ophiolite complexes and/or belts with high pressure and mantle rocks (Mariánské Lázně complex, Letovice ophiolite complex, blueschists of Železný Brod crystalline complex and Rýchory ridge, high temperature and high pressure rocks of the Gföhl Unit) (Grygar, 2016).

The Saxothuringian Zone (SZ) of Bohemian Massif of the Variscan belt in central Europe is a northeast trending basin, bounded to the northwest by the Mid-German Crystalline High (MGCH), and to the southeast by the northwestern margin of the Barrandian (Fig. 2.7) (Schätz et al., 2002), which mainly consists of Palaeozoic volcano-sedimentary successions, formed after the Cadomian orogeny in the course of northward drift of the Avalonian microterrane after it had split off the northern Gondwana margin at 500-480 Ma (e.g., Linnemann et al., 2007; Nance et al., 2012). These successions resulted from the deposition in the Rheic Ocean (Linnemann et al., 2007) as part of a more complex system of Palaeozoic basins between Avalonia, the “Armorican Terrane Assemblage” and Gondwana (Franke et al., 1995; Crowley et al., 2000). Some of these successions exhibit a huge variety of volcanic rocks of different ages, e.g., exposed in the Frankenwald area of northeast Bavaria. They can provide useful information on the geotectonic settings of formation and thus on the likely tectonic evolution of the area between the Cadomian and Variscan orogenies (Höhn et al., 2018). The pre- to Early Variscan evolution of the SZ is mostly constrained by studies on (meta) sedimentary rocks, comprising palaeontological, sedimentological and geochemical methods, as well as U-Pb ages derived from detrital zircon grains (e.g., Linnemann et al., 2004; Gerdes and Zeh 2006; Bahlburg et al., 2010; Geyer et al., 2014). This zone includes a complex association of different autochthonous and allochthonous units recording very low grade to granulite facies metamorphic conditions (Linnemann et al., 2010a). In the autochthonous domain of the SZ, most of the pre-Variscan geological record is preserved. Similarly, the metamorphic pile of the Erzgebirge contains the characteristic features of the autochthonous domain (Kroner et al., 2007). Geochemical signatures reported from the high pressure (HP) metamorphic rocks of the western Erzgebirge, compared to those from the autochthonous domain, reveal that the protoliths principally belong to the same crustal type (Mingram, 1998). Thus, the precursors of the entire SZ seem to belong to the same crust, although there are quantitative differences.

For instance, most of the subducted and exhumed HP- ultra HP orthogneisses in the western Erzgebirge have Ordovician protoliths (Mingram et. al., 2004). Such large volumes of Ordovician magmatic rocks, however, are not observed in the autochthonous domain of the SZ.

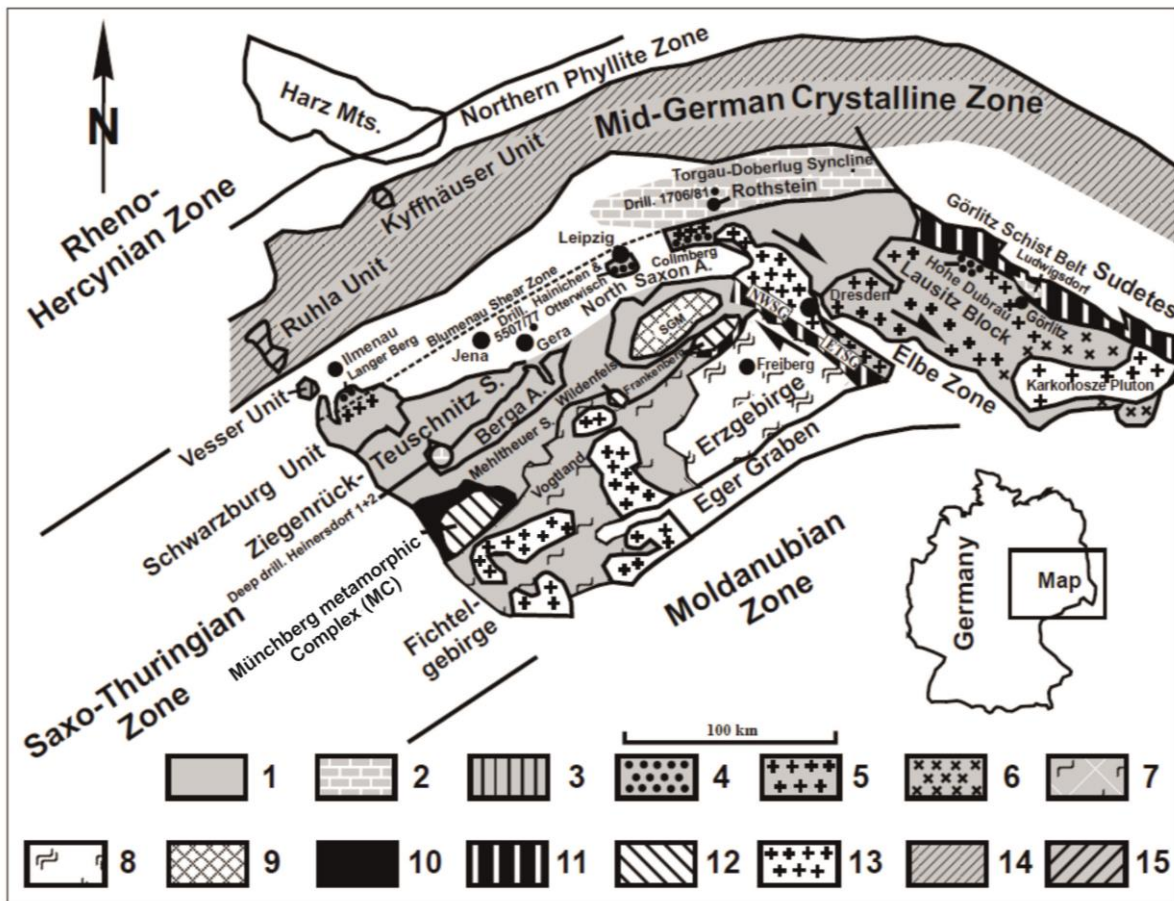


Fig. 2.7. Simplified geological map of the Saxothuringian Zone showing the distribution of Palaeozoic sedimentary rocks of the Thuringian and the Bavarian facies (modified after Linnemann et al., 2000, 2010a). NWSG, Nossen-Wilsdruff Schist Belt; ETSG, Elbtal Schist Belt (both are parts of the schist belt of the Elbe Zone). 1) general distribution of Cadomian basement and overlying Palaeozoic sedimentary rocks of the Thuringian facies; 2) lower to Middle Cambrian of the Thuringian facies; 3) middle to Upper Cambrian rocks of the Vesser Unit; 4) external segment of the Saxothuringian Zone where Ordovician rocks are present only as very thick, bedded, and highly mature Tremadocian quartzites; 5) cadomian plutons (~ 540 Ma); 6) lower Ordovician plutons (~ 490 Ma); 7) metamorphosed Palaeozoic rocks of the Thuringian facies (phyllites and garnet phyllites of the mid pressure - low temperature and the low pressure - low temperature units of the nappe pile of the Erzgebirge and adjoining areas); 8) mid pressure - mid temperature metamorphosed Cadomian basement rocks of the Freiberg and Reizenhain gneiss domes and Palaeozoic rocks of the and the high pressure - high temperature nappes of the Erzgebirge; 9) high grade metamorphosed rocks of the Saxonian Granulite Massif; 10) Palaeozoic sedimentary rocks of the Bavarian facies; 11) Palaeozoic sedimentary rocks with mixed distribution of Thuringian and Bavarian facies; 12) high grade metamorphic rocks of the nappes of the Münchberg

metamorphic complex (MMC) and the Zwischengebirge of Wildenfels and Frankenberg; 13) Variscan granites (~ 335-325 Ma); 14) metamorphic rocks of the Mid-German Crystalline Zone (covered by post-Variscan strata); and 15) metamorphic rocks of the Mid-German Crystalline Zone (outcrop).

2.3.1. Lithostratigraphy of the Saxothuringian Zone

The Saxothuringian Zone (SZ) consists of very low to high grade sedimentary and volcanic rocks with ages spanning from the Cambrian to the Early Carboniferous, deposited on Neoproterozoic crust in a rift basin (Engel et al., 1983a; Franke et al., 2017). The onset of extension is seen in Cambrian plutonic rocks and bimodal volcanic rocks dated at around 500 Ma, possibly relating to back-arc spreading in the west African crust (Linnemann et al., 2010a). Most authors have adopted the classical concept of Gümbel (1879), who distinguished a “Thuringian” facies (Cambro-Ordovician shelf and Silurian-Devonian hemipelagic deposits) from a deeper water “Bavarian” facies in the Palaeozoic (Fig. 2.8; latest review in Heuse et al., 2010).

The Thuringian rocks represent the less deformed externalides of the Variscan orogen, with very low metamorphic grade to the northwest and higher grades in the Fichtelgebirge-Erzgebirge to the southeast: see Fig. 2.7). Early Ordovician meta-granitoids represent the rift stage of the basin. Glacial marine debris-flow deposits (“Lederschiefer”) relating to the Saharan glaciation (Steiner and Falk, 1981) reveal proximity to the main Gondwanan Craton and relatively high latitudes up to the latest Ordovician. The ubiquitous Silurian black shales are overlain by Devonian shales with lenses of hemipelagic limestones. Some Early Devonian sandstones contain Neoproterozoic detrital micas derived from a northerly source (Huckriede et al., 2002).

The Bavarian facies only occurs in tectonic nappe aligned in a north-east-trending synform within the Thuringian facies (nappe of Münchberg, Wildenfels and Frankenberg, Fig. 2.8), where the allochthonous, low grade Bavarian facies rocks are overlain by metamorphic nappes which display inversion of metamorphic grade with eclogites near the top (Behr et al., 1982; Klemd, 2010). Ordovician metabasalts of very low metamorphic grade are present in the lower part of the allochthon, but metagabbros of Ordovician protolith ages transformed into eclogite also occur at the top of the Münchberg pile and, locally, in the Mariánske Lázně complex at the north-western margin of the Teplá-Barrandian block adjacent to the southeast (Timmermann et al., 2004). Metagabbros from the Münchberg greenschist nappe and the overlying “Randamphibolit” have La-ICP-MS magmatic crystallization ages of around 400 Ma (= Emsian) and MORB to Island Arc geochemical fingerprints (Franz et al., 2014; Koglin et al., 2015), which are within the age range of

the bathymetrically deepest deposits in the Bavarian facies (graptolite shales and radiolarian cherts of Silurian to Late Devonian ages, Falk et al., 1995).

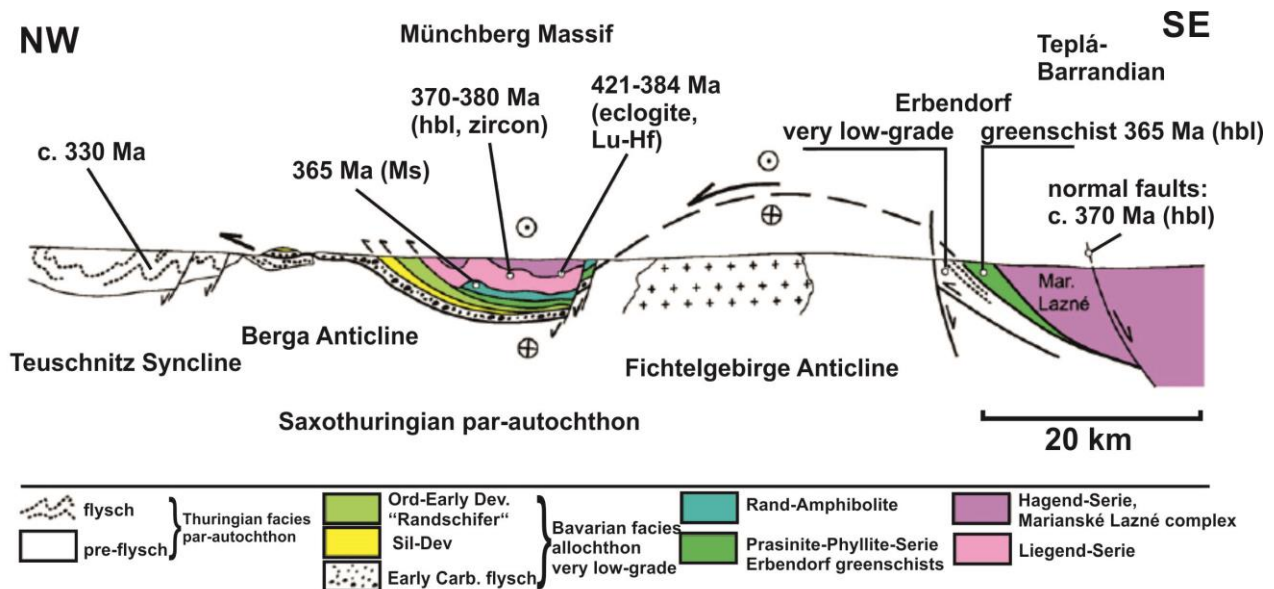


Fig. 2.8. Cross section through the Saxothuringian Zone and adjacent units, with vertical exaggeration, modified from Franke (2000). For ages of deformation, metamorphism and cooling see reviews by Franke (2000) and Klemd (2010). Felsic magmatic rocks, dated at c. 500 Ma, occur both in the Thuringian facies par-autochthon (Fichtelgebirge, north-western Frankenwald) and in the Liegend-Serie. Both island arc-type metabasalts in the Phyllite-Prasinite Unit and MORB-type metagabbro in Randamphibolite Unit gave U-Pb Laser ICP-MS zircon ages of 400 Ma (Franz et al., 2014, Koglin et al., 2015). hbl, hornblende.

The Early Devonian mafic rocks and the Bavarian-type deep-water sediments are interpreted to represent the Saxothuringian Ocean. The onset of convergence is indicated by first southerly-derived greywacke turbidites in Late Frasnian radiolarian cherts of the Bavarian facies (Zitzmann, 1968). Closure of the basin by collision with the Teplá-Barrandian block is documented by the first greywacke turbidites deposited in the Early Famennian on the parautochthonous Thuringian facies foreland in northwestern Bavaria (Adam and Reuter, 1981; Franke et al., 1992; Schäfer et al., 1997). That age of collision is corroborated by c. 380 Ma medium pressure metamorphism in the crystalline allochthonous (Klemd, 2010) and by Famennian and Early Carboniferous hemipelagic limestones, which unconformably overlie deformed Neoproterozoic and Early Palaeozoic rocks in the eastern Teplá-Barrandian.

2.4. Variscan orogeny in the Fichtelgebirge and Elstergebirge areas

The so-called Saxothuringian region comprises Palaeozoic units in the Frankenwald area, the Fichtelgebirge (Smrčiny Hory), the Elstergebirge (Halštrowské Hory) in western part of Erzgebirge (Krušné Hory), and the northernmost part of the Oberpfälzer Wald (Upper Palatinate Forest) (see Figs. 2.3 and 2.7). These units are formed by several northeast-southwest-trending anticlinal and synclinal structures offset by prominent northeast-southwest-trending fault zones, which experienced polyphase post-Variscan tectonics (e.g., the Franconian Lineament = Fränkische Linie in German, and the Mariánské Lázně Fault) (Holzförster et al., 2011).

Whereas the units of the Frankenwald are non-metamorphosed or only weakly metamorphosed, the rocks in the other areas underwent polyphase metamorphism. Late Variscan metamorphism reached low to medium pressure conditions and temperatures of up to 650 °C (Holzförster et al., 2011). In the Saxothuringian region two lithological sequences are distinguished: (i) the Thuringian facies, consisting of Cambrian to Early Carboniferous marine sediments with intercalated intra-plate volcanics, and of an Upper Devonian sequence with intercalated, widespread submarine basaltic volcanics; and (ii) the central Fichtelgebirge sequence, which comprises gneisses, micaschists, phyllites, quartzites, marbles, and calcsilicates. Their protoliths were deposited during Cambrian and Ordovician times. Furthermore, there are metamagmatites such as leucocratic, feldspar-rich orthogneisses. Protoliths for these orthogneisses might be Ordovician acid volcanics and/or intrusives (e.g., granites). Late Variscan granites intruded into the central Fichtelgebirge sequence (Holzförster et al., 2011) (Fig. 2.3). On the northwestern border of the Bohemian Massif (northeastern Bavaria) the Saxothuringian comprises the rocks of the Frankenwald, the Fichtelgebirge, the Elstergebirge and the Erzgebirge (see Figs. 2.3 and 2.7).

Together with the Erzgebirge, the Fichtelgebirge forms an anticlinal zone situated in the northwestern part of the Bohemian Massif, strikes ENE-WSW and is characterized in the geophysical maps by a significant gravity minimum of less than 100 mgal that may be traced southward into the Moldanubian Zone, discussed in the following section (Behr et al., 1989). This anticline structures originated in the Late Palaeozoic during a Late Variscan deformation phase (Stein, 1988). Two main intrusive complexes have been distinguished in the eastern part of this Variscan anticline, in the Erzgebirge (Tischendorf and Förster 1994; Sebastian, 2013).

The entire intrusive suite began with an older series, aged 330 through 310 Ma, that is of monzogranitic composition and of a mixed I/S type affiliation. Separated by a period of igneous quiescence, a younger series followed with ages of intrusion in the range 305-290 Ma. It is mostly of I-type with some A-type affinities. In the western part of the anticline, geomorphologically termed Fichtelgebirge, the felsic intrusive rocks have some basic to intermediate predecessors, ranging in their chemical composition from gabbroic, through dioritic into granodioritic which were given the collective term “redwitzite” after the town of Marktrechwitz located in the region (Richter and Stettner, 1979). The core of the Fichtelgebirge anticline consists of a metamorphosed sequence of variable lithological character: the “Bunte Gruppe” (the “variegated group” in the sense of the diverse lithology; Stettner, 1980) is composed of metapelites and metagraywackes with intercalations of marbles (Wunsiedler Marmor), calc-silicate rocks, and minor metabasites of alkaline basaltic affinity (Kreuzer et al., 1989). In the lower part of the Fichtelgebirge anticline there are transitions to the “Monotone Gruppe” (“monotonous group”) with a predominance of pelitic to psammitic metasediments. Stettner (1980) regarded the core sequence as Late Proterozoic on the basis of a comparison of the “Bunte Gruppe” with the Spilite Group of Inner Bohemia (Vejnar, 1965). The marginal areas of the Fichtelgebirge anticline are made up of pelitic and psammitic metasediments with intercalated acidic metavolcanics (“epigneisses”), resembling the Cambro-Ordovician rocks of the Thuringian lithofacies (Stettner, 1975, 1980; Emmert et al., 1981).

Immediately to the west of the northeast-southwest oriented Erzgebirge, the Elstergebirge forms a geomorphological contrast (Grünthal et al., 1990), lies at the southernmost tip of Saxony in the German-Czech border region between Fichtelgebirge and Erzgebirge (Fig. 2.3). According to the geological maps (e.g., Bernstein et al., 1973, 1:400.000), schists and phyllites, assigned to the Cambrian and Ordovician, and micaschists are the dominant rocks of the Elstergebirge (Stumm, 2002). These rocks show similarities to those of the Micaschist-Eclogite and (Garnet)-Phyllite Units of the Erzgebirge crystalline complex, being adjacent to the northeast, although eclogite was never reported from the Elstergebirge.

2.4.1. Geochronology and previous protolith studies of Fichtelgebirge

Rb-Sr age dating on orthogneiss of the town of Wunsiedel in the Fichtelgebirge, yielded an age of 480 ± 4 Ma. Sm-Nd isotope data from three orthogneiss units (Wunsiedel, Selb,

Waldershof) revealed an age of 560 ± 45 Ma which is consistent with an Early Ordovician intrusion age (Siebel et al., 1997).

According to U-Pb data of Teufel (1988) and Wiegand (1996), extrusion of metavolcanic rocks occurred at ~ 450 Ma. K-Ar age dating of Fichtelgebirge orthogneiss on muscovite and biotite range from 316-298 Ma, and from 306-280 Ma respectively, demonstrating thermal influences from Late Visean to Late Stephanian (325-290 Ma) granite intrusions (Siebel et al., 1997). Three phyllites from the Steinach Valley (part of the western Fichtelgebirge) yielded the oldest muscovite dates 330-325 Ma. The chloritoid schist from the western Fichtelgebirge (Mausbach Valley), and the two phyllites from the northeastern Fichtelgebirge (Perlenhaus) gave muscovite dates between 320 and 316 Ma (Kreuzer et al., 1989).

2.4.2. Published pressure-temperature conditions of Fichtelgebirge metamorphic rocks

The Fichtelgebirge metamorphic complex (FC) sequences underwent a low pressure metamorphism ranging from greenschist to amphibolite facies (Kreuzer et al., 1989). At the highest metamorphic grade reached, the following assemblages were stable (Mielke and Schreyer, 1969; Mielke et al., 1979): staurolite + andalusite, and almandine + biotite + muscovite + quartz. Relict minerals from an older medium pressure event were recently recognized by Lenz (1986) in the northern Fichtelgebirge, northwest of Selb. Mielke and Schreyer (1972) concluded that the paragenesis magnetite-rutile found in metapelitic rocks of the FC indicates relatively low temperatures between 450 and 500 °C. The occurrence of andalusite in FC metapelites was regarded as an indication of relatively low metamorphic pressures which were estimated to 3.5-5.5 kbar (Mielke et al., 1979).

3. Methods

Field sampling (Fig. 3.1a-b) in the northwestern Fichtelgebirge and western Elstergebirge (Fig. 1.1) was undertaken in September 2013 and October 2014. Approximately 50 samples (Fig. 3.1c) were collected, including micaschist, gneiss, granite, phyllite and quartzite. These samples represent almost all types of rocks occurring in different tectonic settings in the study area. From the collected samples, eleven were chosen for further studies.

3.1. Localities and positions of the sampled rocks

Sample 13F18 (see chapter 4) was hit from a larger block in the northern Fichtelgebirge area (Figs. 3.2 and 4.1) at latitude $50^{\circ} 20.349'$ N and longitude $12^{\circ} 14.639'$ E. Sample 14AS6 (see chapter 5) was taken from an outcrop in the western part of the Elstergebirge, ~ 4.5 km NE Asch/Aš town (see Fig. 5.1c) (coordinates: N: $50^{\circ} 14.698'$, E: $12^{\circ} 16.613'$) (Table 1). Some more samples were also studied in more detail, in order to investigate the protolith and tectonic setting of the rocks. Their descriptions are summarized in Table 1.

3.2. Petrography (Polarizing Microscope)

Polished thin sections (Fig. 3.1d) with an average thickness of 30 μm were prepared from all samples for mineral identification and microtextural observations using polarizing optical microscopy (Fig. 3.3). In Fig. 3.3, the transmitted light path is indicated. The thin sections were placed on the rotatable stage. Then, they were studied both in plane polarized light and under crossed nicols. With the digital camera, which is connected to a computer, images could be taken. More details concerning the microscope are provided in Murphy (2001), Klein and Philpotts (2013) as well as Nesse (2013).

This study allow the selection of fresh and representative samples for further detailed studies. In addition, the study also enables the selection of samples containing fresh white-mica and eventually garnet, the most important minerals for deciphering P-T conditions of metamorphism. Altogether 41 samples from micaschist, phyllite, quartzite outcrops or blocks were collected in both areas of the Fichtelgebirge and Elstergebirge, but 2 suitable rock samples for our study (parts 1 and

2) and 9 more samples for protolith and provenance investigation were used (see Table 6.1 and chapter 6).

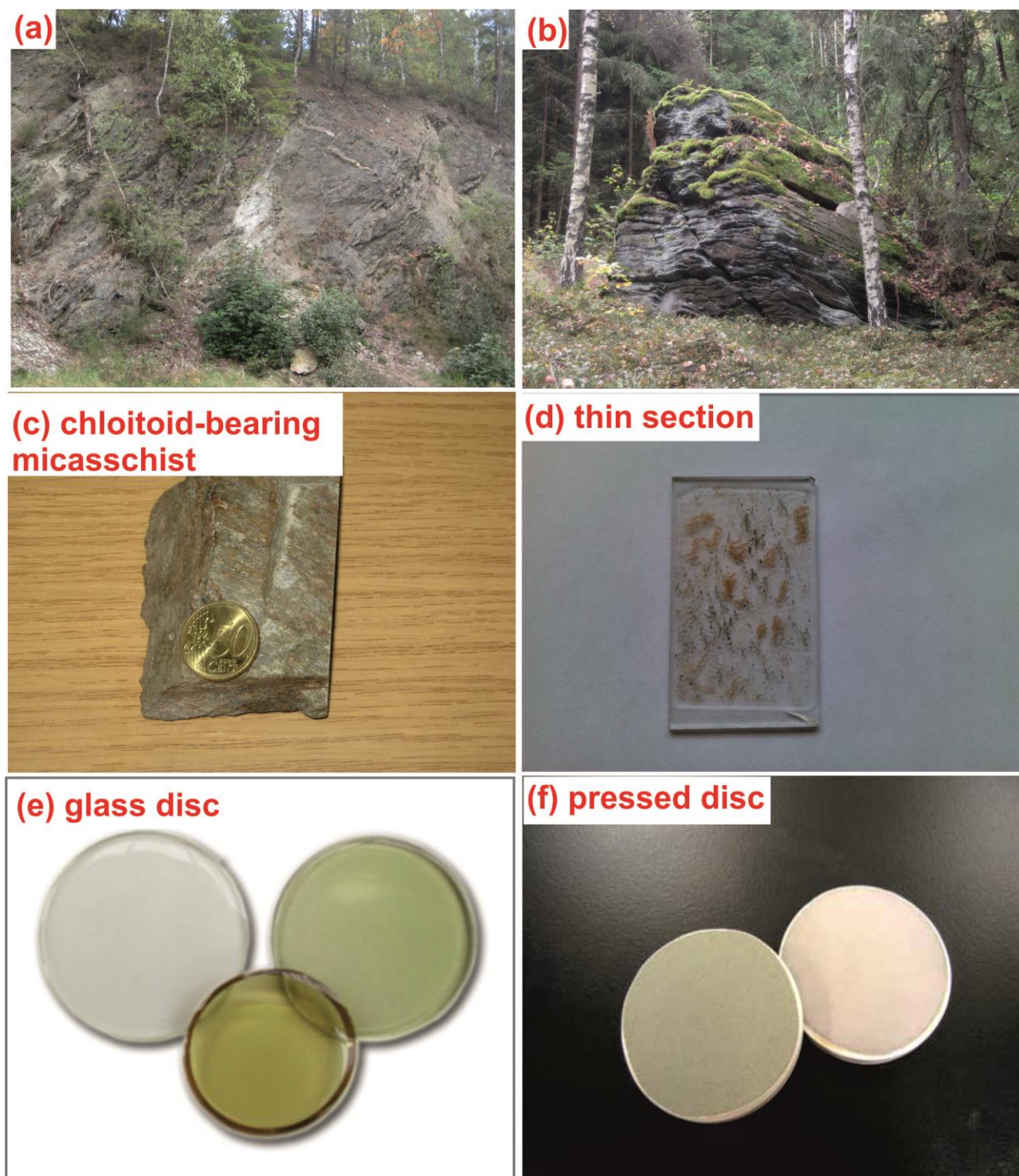


Fig. 3.1. Sample collection and preparation process. (a) field overview between Rehau and Selb; (b) orthogneiss in an outcrop near the road from Asch/Aš to Niederreuth/Dolní Paseky; (c) collected

chloritoid-bearing micaschist (sample 14AS6); (d) thin-section of garnet-bearing micaschist (sample 13F18); (e) and (f) glass disc and pressed disc prepared for major element and trace element analyses respectively, using XRF.

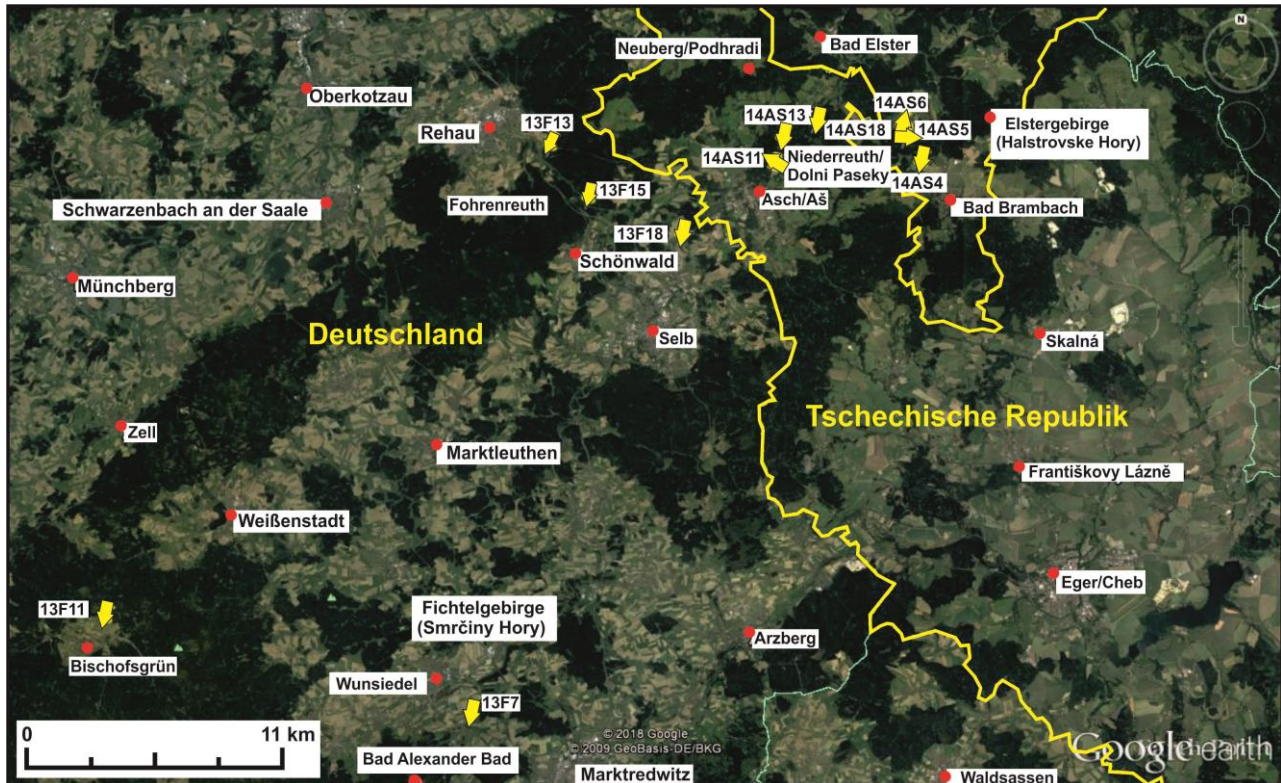


Fig. 3.2. Satellite map of the localities and geographical positions of the studied samples (the yellow arrows), according to the Google earth version 2018.

3.3. Mineral chemistry

The chemical compositions of minerals were obtained with a CAMECA SX100 electron microprobe (EMP). This instrument was used for silicate analysis, monazite dating, and as an aid to identify unknown mineral phases.

3.3.1. Sample preparation

As the polished thin sections used for ordinary microscopy were prepared using lead disks with embedded microdiamonds, hand-polished thin sections were also produced for metapelites and

lead-free thin sections for Th-U-Pb monazite dating. Conventional lead disks are not suitable for the production of thin sections for Th-U-Pb dating with the EMP, because they deposit lead at grain boundaries and fill surface irregularities, thus contaminating the sample (Scherrer et al., 2000). The analytical parameters and procedures are reported in chapters 4 and 5.

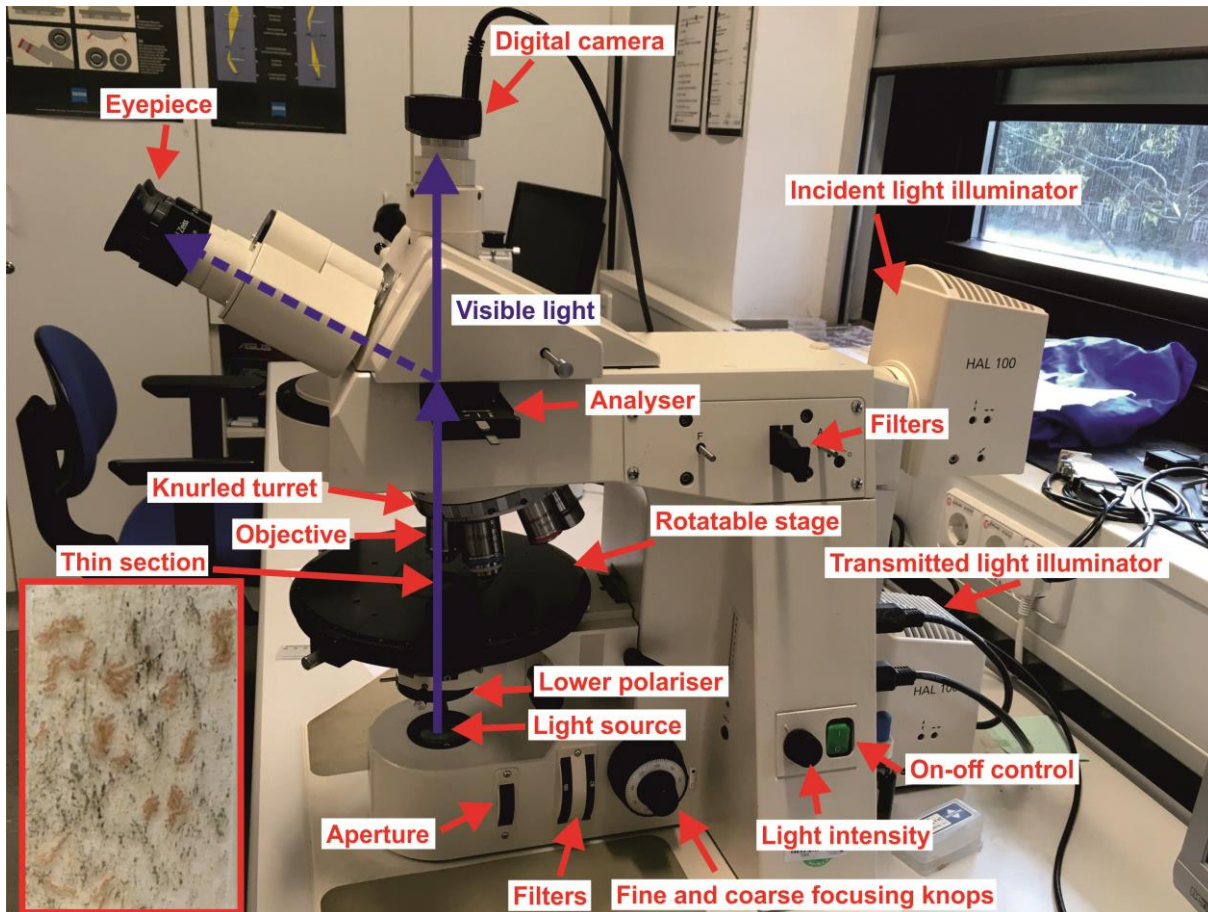


Fig. 3.3. Image of a polarizing optical microscopy (ZEISS Axioplan) with a digital camera in the Institut für Mineralogie und Kristallchemie (IMK) at Universität Stuttgart used for analysing thin sections.

Before EMP analysis, the conventional and lead-free thin sections were coated with a c. 20-30 nm carbon film to make the surface conductive. This is to prevent the sample from charging during electron bombardment. The carbon coating was achieved in a vacuum chamber where a carbon yarn was burned by an electric impulse. The thickness of the coating was controlled by the interference colour produced on a polished brass plate in the chamber (Ogenhall, 2010).

3.3.2. An introduction to electron microprobe (EMP) analysis

A typical arrangement of an EMP is a vertical electron-beam column, an array of detectors placed around the sample chamber block, a sample entry vacuum lock, a console to control operating conditions, screens to view control interfaces and sample output, and a computer for control of data acquisition (Fig. 3.4). The used EMP was a Cameca SX100 equipped with (Figs. 3.4, 3.5):

1. five wavelength dispersive spectrometers (WDSs) around the sample chamber for quantitative mineral chemical analysis,
2. an energy dispersive spectrometer (EDS) used for (semi-)quantitative mineral chemical analysis,
3. a tungsten filament as electron source,
4. a series of alignment coils, two condenser lenses, and objective lens located in the column of the instrument adjusted to condense and focus the electron beam,
5. a sample chamber that houses a brass stage to move specimens in X, Y, and Z direction, and
6. an optical microscope used to focus and view the area to be analysed.

The EMP was operated under constant vacuum to reduce the influence of molecules from the atmosphere from interfering with the electron beam.

Mineral analyses and elemental X-ray maps were performed with a Cameca SX 100 EMP around the sample chamber for full analyses (beam spot diameter of 1-5 μm) to determine the concentrations of F, Na, Mg, Al, Si, K, Ca, Ti, Cr, Mn, Fe, and Ba at the Institut für Mineralogie und Kristallchemie. Conditions for obtaining high-quality data can be set according to the specific minerals to be analysed. The operating parameters for punctual analyses were: 15 kV acceleration voltage, 30 nA beam current for analysing garnet and 10 nA for the other minerals, between 1 and 5 μm beam diameter (1 μm for the micro inclusions) and 20 s counting time on peak for each element and on the background except for F (30 s). Synthetic and natural minerals, glasses (e.g., Ba glass for the $\text{BaL}\alpha_1$ -peak), and pure oxides were used as standards. Errors of the applied method were reported by Massonne (2012). Element concentration maps for major elements were prepared by step-wise movement of the thin section under the electron beam of the EMP and subsequent computer aided evaluation. The EMP was operated at 20 kV. Counting times per step were 80 ms. An electric current of 40 nA and 20 nA was applied for scanning areas with garnet and potassic white-mica, respectively. EMP Th-U-Pb analyses of monazite crystals are carried out with beam spots of about 10 μm , an acceleration voltage of 20 kV and a beam current of 150 nA. Age data

were obtained after data processing with the Isoplot/Ex program by Ludwig (1999). Structural formulae were calculated with the CalcMin and MINCALC programs (Brandelik, 2009) as follows: garnet = 24 oxygens and 10 six and eight-fold coordinated cations, potassic white-mica (11 oxygen, per formulae unit = pfu) = 11 O, 21 - (Ca + Ba) valencies, chlorite (pfu) = 14 oxygen and the negligence of large cations (Na, Ca), chloritoid = 12 O, Ti + Al + Fe + Mn + Mg = 6, $\text{Fe}^{3+} = 4 - (\text{Al} + 2 \cdot \text{Ti})$, aluminosilicate (Al_2SiO_5) = three cations, feldspar (plagioclase) = 8 oxygen, biotite = 11 oxygen (pfu), rutile = 2 oxygen and ilmenite = 3 oxygen. Analysed minerals in the rock samples are given in Table 1.

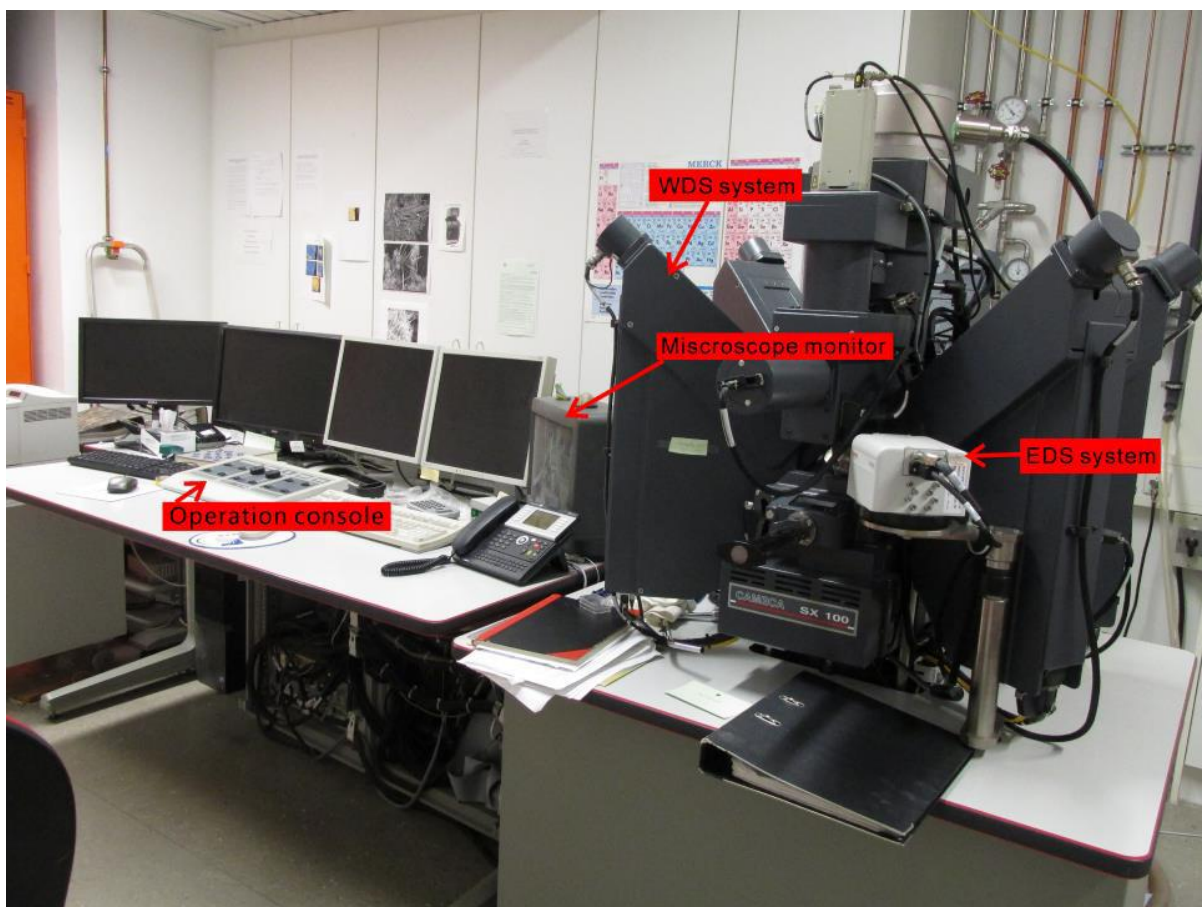


Fig. 3.4. Electron microprobe (Cameca SX100) at IMK in the Universität Stuttgart.

3.3.3. Electron-sample interactions

Electrons are produced by heating a tungsten filament to high temperatures (in the gun). These electrons are accelerated from the filament towards the sample surface. The electrons as

charged particles can be directed and focused on this surface by using electron static lenses (gun alignment, condensers) (Fig. 3.5).

The electron beam colliding with the sample surface excites mainly back-scattered electrons (elastic scattering at the nucleus partially with low energy loss = Bremsstrahlung) and characteristic X-rays (at the electron shell: high energy loss). The intensity of back-scattered electrons contains information on the mean atomic number. The characteristic X-rays, having a specific wavelength, are used to analyse the concentration of elements in the specimen.

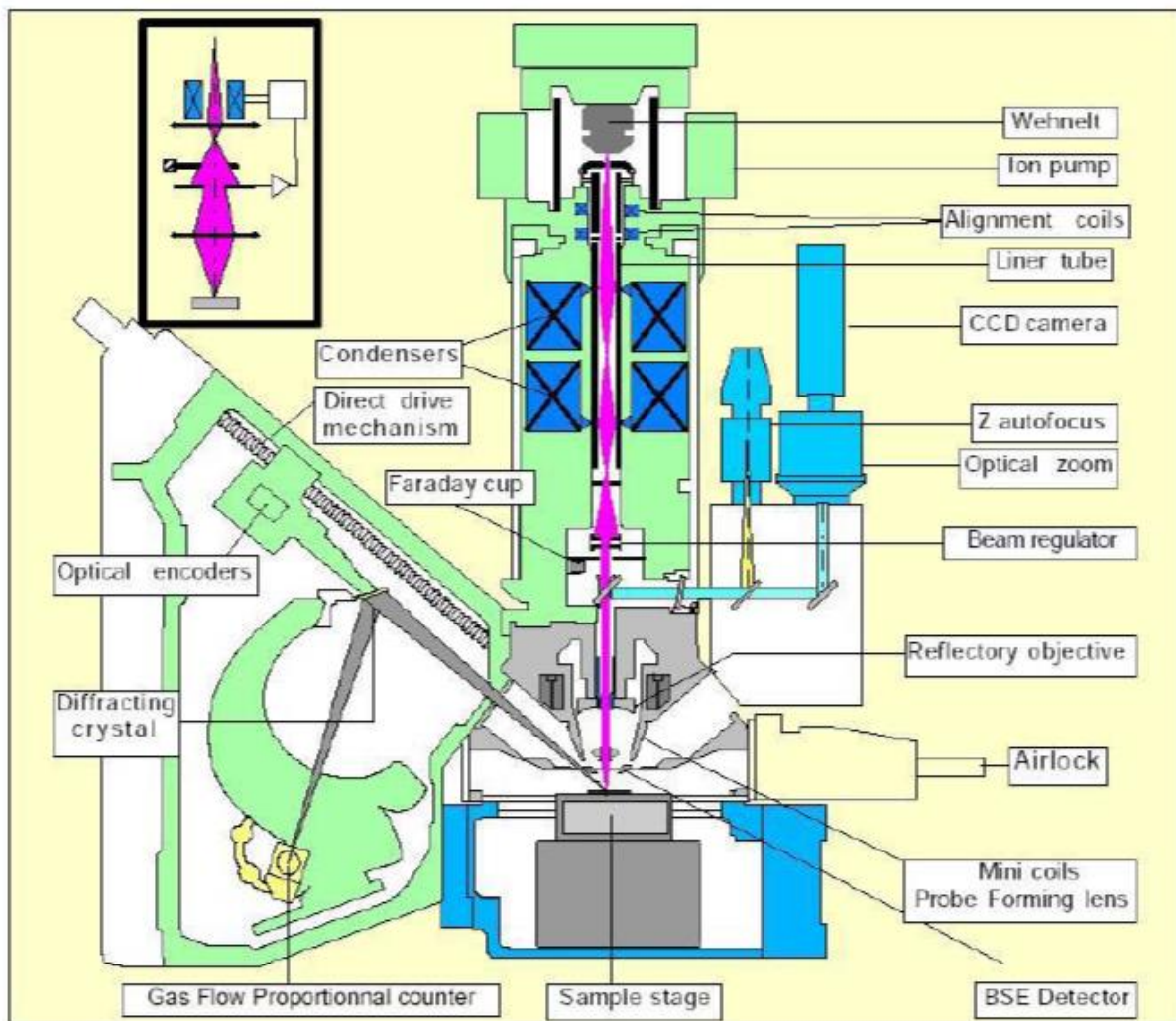


Fig. 3.5. Cross section of an electron microprobe (Cameca SX100), modified from a Cameca leaflet printed in 1999.

The intensity of X-rays with a specific wavelength is statistically counted using either an EDS or the system with WDSs. The EDS accumulates all wavelengths produced by interaction of a

volume of the specimen with the electron beam, whereas the WDS system uses X-ray diffraction at an analysing crystal to select and count a specific X-ray wavelength of interest. At the IMK, TAP, PET, and LIF (Table 3.1) were used as analysing crystal. In fact, multi-elemental analyses can be much faster obtained with an EDS but the WDS system is significantly better for obtaining high-quality analyses.

Table 3.1. The applied analysing crystals and elements commonly analysed with them (from: <http://web.mit.edu/e-probe/www/courses.shtml>).

	Atomic Number										
	6	14	22	30	38	46	54	62	70	78	86
TAP	8O	15P	24Cr	41Nb	46Pd	79Au					
PET	13Al	25Mn	36Kr	65Tb	70Yb						
LIF		13K	37Rb	48Cd							

K α, β	L α, β	M α, β, γ
-------------------	-------------------	---------------------------

3.3.4. Characteristic X-ray spectra

Characteristic X-rays are emitted as a result of the transition of an electron from an outer to an inner electron shell of an atom (Fig. 3.6 left) (Reed, 2005). The corresponding energy difference depends on the shells and the element. When irradiating an atom with an electron beam, an electron from this atom can be expelled. Thus, a ‘hole’ in a shell, for instance, the K-shell is generated. The atom wants to restore the original configuration, which is achieved by transferring an electron from an outer shell such as the L-shell to the hole in the K-shell. An L-shell electron has a higher energy than a K-shell electron. Consequently, when an L-shell electron is transferred to the K-shell, the energy surplus can be emitted as an X-ray photon (Brouwer, 2006). The X-ray photon energy is equal to the difference between the energies of the initial and final levels for the relevant transition of electrons (Reed, 2005) (Fig. 3.6). In a spectrum, this is seen as a specific line (Fig. 3.7).

In EMP analytics, one is mainly concerned with X-ray energies up to about 10 keV, and the K α_1 -line is used for the analysis of elements of atomic number up to about 30. For atoms with

higher atomic number, the $L\alpha_1$ line is usually used (or the $M\alpha_1$ line for the heaviest elements) (Reed, 2005).

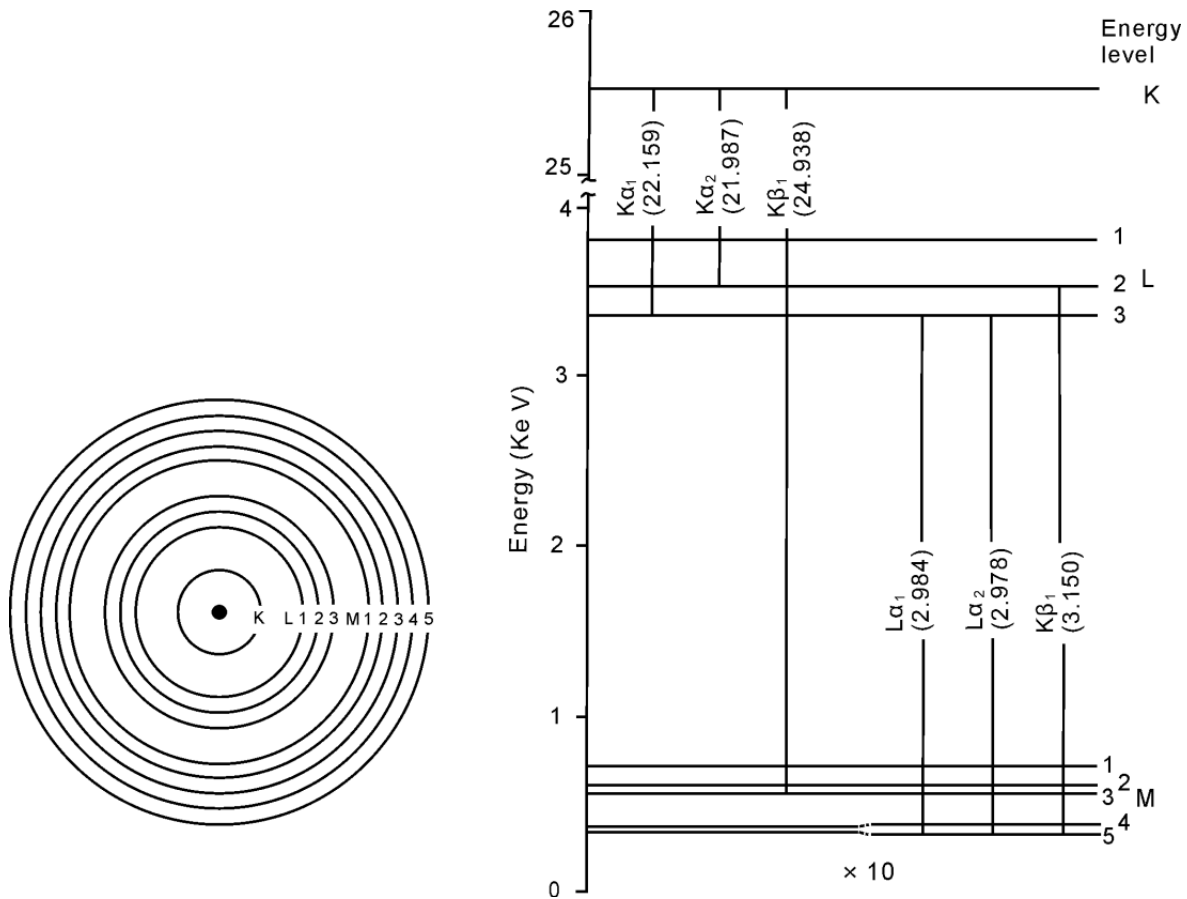


Fig. 3.6. Left: Schematic diagram of inner atomic electron shells. Right: Energy level diagram for silver (the number of electrons: $Z = 47$); characteristic X-ray energy (given in kiloelectronvolts) is equal to the difference in energy between the levels involved in the transition (Reed, 2005).

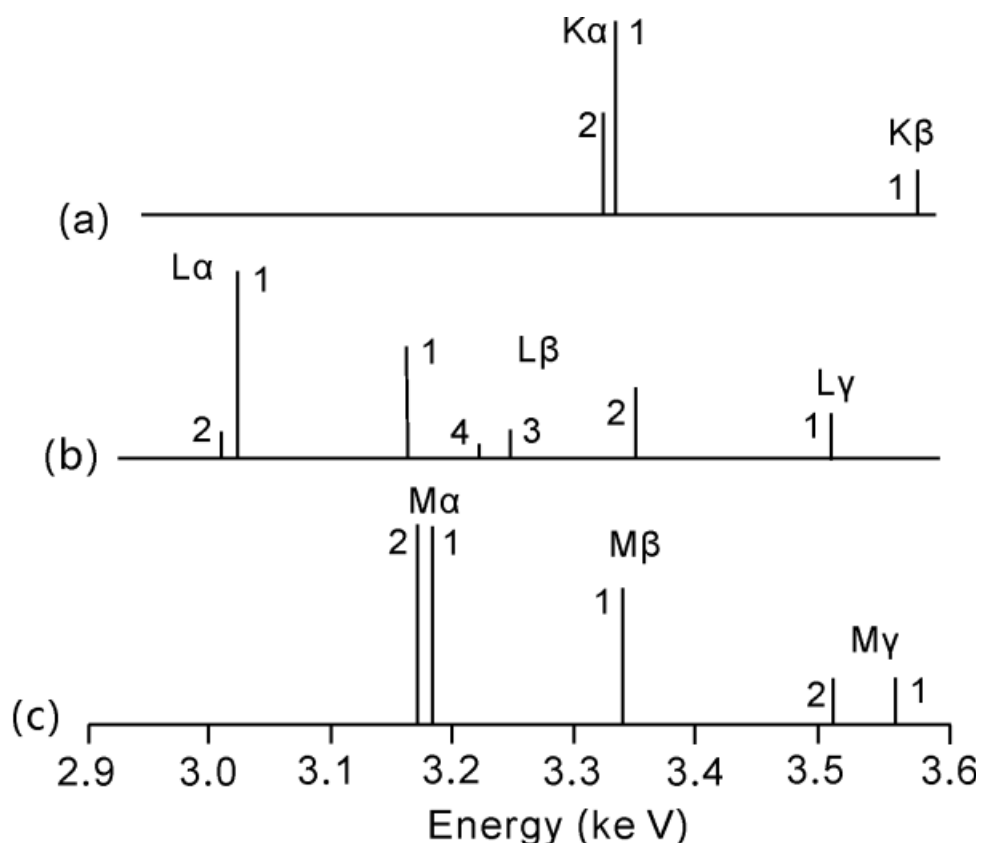


Fig. 3.7. Typical examples of characteristic X-ray spectra (principal lines only shown) (Reed, 1996): (a) K spectrum of potassium ($Z = 19$); (b) L spectrum of silver ($Z = 47$); and (c) M spectrum of uranium ($Z = 92$).

3.4. Bulk rock analyses

The concentrations of major and trace elements were determined for all selected samples. X-ray fluorescence (XRF) spectrometry was used for bulk rock analyses.

3.4.1. X-ray Fluorescence Spectrometer and Carbon Analyser

Major and trace elements of a bulk rock (Tables. 4.1, 5.1 and 6.1) were analysed on an powdered rock slab of the representative sample by X-ray fluorescence spectroscopy (XRF) FeO considering certified geostandards. XRF spectrometry is a widely-used technique for the routine determination of major elements as well as a large number of geochemically important trace elements in geological samples. Here, a PHILIPS PW2400 XRF spectrometer was used with a

WDS system. The WDS system physically separates the X-rays according to their wavelengths as in the EMP (Fig. 3.8). However, the detector is placed at a fixed position, but the analysing crystal is rotated so that different wavelengths are diffracted into the detector. Rocks were crushed and milled to obtain homogeneous powders for whole-rock analyses. A glass disc was prepared by melting 0.6 g sample powder + 3.6 g Li-borate = Spectromelt® or 0.5 g sample powder and 5 g Spectromelt®). Other discs were produced by pressing 12 g sample powder and 3 g wax-C. Before analyses, the calibration of the XRF spectrometer was checked using geostandards. Bulk rock major elements were analysed on glass discs (Fig. 3.1e). Trace elements were determined on pressed discs (Fig. 3.1f).

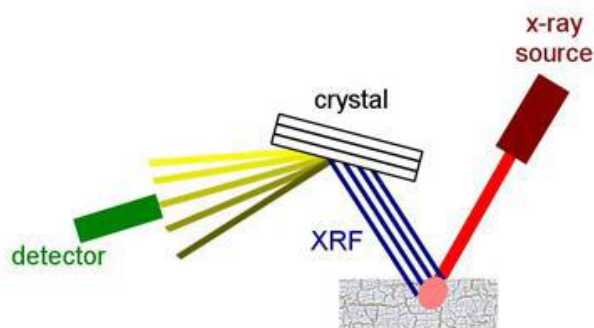


Fig. 3.8. The key components of a typical WD-XRF spectrometer (<http://www.horiba.com/scientific/products/x-ray-fluorescence-analysis/tutorial/>).

For the determination of trace element contents powdered samples were mixed with wax and pressed for producing pellets. The contents of H_2O (+) and organic C (after CO_2) in the rock powder were determined with a LECO RC-412 C-O-H multiphase determinator after drying at 110°C for several hours. A P-T pseudosection for fixed bulk composition was calculated in the Na_2O - K_2O - CaO - FeO - O_2 - MnO - MgO - Al_2O_3 - SiO_2 - TiO_2 - H_2O system with the software package PERPLE_X (see Connolly, 2005), version from August 2011 downloaded from the internet site <http://www.perplex.ethz.ch/>), using the internally consistent thermodynamic dataset and equation of state for H_2O of Holland and Powell (1998, updated 2002) and contoured it by isopleths of various parameters such as the molar fractions of garnet components.

3.4.2. Verification of analytical techniques

Knowledge on thermodynamics is a key to understand physicochemical changes occurring in the Earth's crust, producing metamorphic rocks. All systems naturally tend to the minimum energetic configuration, i.e., equilibrium.

Chemical equilibrium implies no change over time. Thus, equilibration conditions attained by a mineral assemblage would preserve the characteristics of the phases involved in the system at a certain moment, e.g., the P-T formation conditions of a metamorphic rock. As soon as the conditions (e.g., P or T) change, the system will immediately tend to a new equilibrium state. But since diffusion is involved, the scale at which the equilibrium will be achieved depends on the particular conditions (especially the temperature), on the character of the phases involved (e.g., diffusion in fluids is much faster than in solids), and on the available time.

If the conditions change rapidly, the scale of equilibration will be small. However, it can be argued that even in this case the system will develop local equilibria - small domains where equilibrium is achieved or approached (e.g., Korzhinskii, 1959; Thompson, 1959).

3.5. Geothermobarometry

As part of determining the evolution of rocks and regions, geologists have for a long time attempted to estimate the temperature and/or pressure of formation of igneous and metamorphic rocks. Early approaches were mostly qualitative. The classic pelitic index minerals, for example, were qualitative indicators of metamorphic grade (mostly temperature) and were used to estimate the relative conditions of metamorphism across a terrane or to compare one terrane to another. Certain minerals, such as andalusite and cordierite, also indicate low pressures, whereas other minerals, such as jadeite and glaucophane, indicate high pressures. Estimation of the stratigraphic overburden above shallow plutons at the time of emplacement was also used to approximate the pressure of igneous crystallization and contact metamorphism (Winter, 2010).

During the past 30 years the range of numerical tools and instrumentation available to the metamorphic petrologist has expanded beyond imagination. Examples include thermodynamic modelling and in situ analytical methods for U-Th-Pb isotope and trace element chemistry of minerals, and for mineral characterization. One approach to estimate the temperature and/or pressure of a rock is to select an appropriate geothermometer or geobarometer from those available

on the basis of the mineral assemblages available in the field. Although the use of in situ U-Th-Pb geochronology (e.g., the SHRIMP) on accessory minerals was developed during the 1980s and became accepted during the 1990s (Williams, 2013), it was only with the advent of routine in situ trace element analysis of minerals, particularly zircon, monazite and garnet (Harley and Kelly, 2007; Harley et al., 2007; Rubatto and Hermann, 2007), that it has become possible to link ages reliably to calculated P-T conditions.

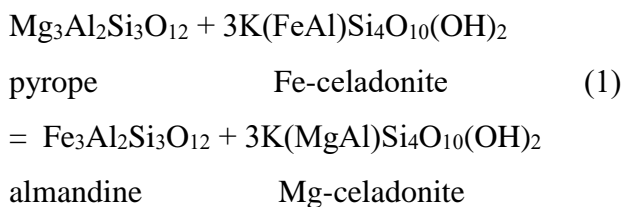
3.5.1. Geothermometry

In the chapters 4 and 5, Garnet-muscovite thermometry was used for calculating metamorphic temperature at peak pressure of metapelites.

3.5.1.1. Garnet-muscovite thermometry

Muscovite is ubiquitous in greenschist- to amphibolite facies metapelites, thus making the garnet-muscovite (GM) geothermometer very important in determining the metamorphic T conditions of metapelitic rocks (Wu and Cheng, 2006).

The Fe and Mg exchange between coexisting garnet and muscovite can be described as (Krogh and Råheim, 1978; Green and Hellman, 1982; Hynes and Forest, 1988; Wu et al., 2002)



which constitutes the basis of the GM thermometer.

At equilibrium, when ignoring heat capacity, thermal expansion and compressibility of the phases involved, and assuming quartz to be a pure phase, the above three model reactions may be described respectively by the following three thermodynamic equations (Wu et al., 2002):

$$\begin{aligned} T(\text{K}) = & (\Delta_1 H^0 / \Delta_1 S^0) + [P(\text{bars}) - 1] * (\Delta_1 V^0 / \Delta_1 S^0) \\ & + (W_{\text{FeMg}}^{\text{mus}} / \Delta_1 S^0) * 3(W_{\text{Fe}}^{\text{mus}} - W_{\text{Mg}}^{\text{mus}}) \end{aligned}$$

$$+ ([W_{Mg}^{mus} Al - W_{FeAl}^{mus}] / \Delta_1 S^0] * 3 W_{Al}^{mus} \\ + (1 / \Delta_1 S^0) * [RT \ln K^{ideal}_{(1)} + (Fea - Mga) * T + (Feb - Mgb) * P + Fec - Mgc]$$

To maintain thermodynamic consistency, we used the garnet activity model of Holdaway (2000, 2001). The activity coefficients of the grossular, pyrope and almandine phases in garnet, after rearrangement, may be written respectively as

$$RT \ln \gamma_{grs}^{gt} = 3RT \ln (\gamma_{Ca}^{gt})$$

$$= Caa * T(K) + Cab * P(\text{bars}) + Cac$$

$$RT \ln \gamma_{pyp}^{gt} = 3RT \ln (\gamma_{Mg}^{gt})$$

$$= Mga * T(K) + Mgb * P(\text{bars}) + Mgc$$

$$RT \ln \gamma_{alm}^{gt} = 3RT \ln (\gamma_{Fe}^{gt}) = Fea * T(K) + Feb * P(\text{bars}) + Fec$$

3.6. Phase equilibria modelling (PERPLE_X)

3.6.1. Introduction

The present level of sophistication in thermodynamic modelling of phase equilibria has its foundation in the 1980s with the introduction of appropriate internally-consistent thermodynamic datasets (Holland and Powell, 1998, 2011; Berman, 1988) and the development and expansion of suitable activity-composition models for phases of interest in parallel with the evolution of software for quantitative phase equilibria modelling (Berman, 1988, 1991; Brown et al., 1988; Connolly, 1990, 2005, 2009; Connolly and Petrini, 2002; Connolly and Kerrick, 1987, see also the PERPLE_X website <http://www.perplex.ethz.ch/>).

PERPLE_X is James Connolly's (1990, 2005) set of programs that can calculate phase diagrams based on reactions and an internally consistent database. There are also modules for creating pseudosections for specified bulk compositions (Connolly and Petrini, 2002). The algorithm for calculating pseudosections uses a free-energy minimization approach, but the output needs some "cleaning up" in a drawing program in order to look good. P-T pseudosections for my rock samples were calculated for a few very well petrologically studied rocks with the computer program package PERPLE_X (Connolly, 2005). In the thesis, PERPLE_X was used for calculation of pseudosections and mineral properties. These pseudosections were contoured by isopleths for

various chemical and modal parameters such as the molar fractions of phengite components (Mg-Al-celadonite, Fe-Al celadonite). By combining the compositional trends of minerals such as phengite and chlorite obtained with the EMP and these contour lines, a P-T path was derived as demonstrated by Massonne and Calderon (2008) for a HP metamorphic rock with psammopelitic protolith and by Massonne and Toulkeridis (2012) also for HP rocks of other lithologies (mafic and felsic). Also, comprehensive databases on the tectonic and P-T deformation histories of metamorphic complexes within the Bohemian Massif are available (e.g., O'Brien and Carswell, 1993; Krohe, 1998; Willner et al., 2000).

Comparison with numerical modelling should lead to a better understanding of the details of the delamination process. Another important problem that should also be addressed using the numerical modelling approach is related to the recent discovery of diamond bearing quartzofeldspathic rocks (Massonne, 1999; Stöckhert et al., 2001) exposed in the Erzgebirge of the northern Bohemian Massif. The formation and exhumation of these rocks from ~ 160 km depth requires an adequate tectonic explanation and a link to the major geodynamic processes operating during delamination of the lithospheric root.

3.6.2. The basic principles of PERPLE_X

PERPLE_X is written and maintained by James Connolly (Zürich) (Connolly and Kerrick, 1987; Connolly, 1990; 2005; Connolly and Petrini, 2002), and is written in FORTRAN with the source code available. In order to produce a phase diagram, a gridded minimisation is used.

3.6.2.1. Gridded minimisation

Isochemical phase diagrams (so-called pseudosections) usually comprise several phase fields characterised by a particular phase assemblage. Within these fields the chemical composition and physical properties of the stable phases may vary continuously, but are uniquely determined at any point. A consequence of the pseudocompound approximation is that the continuous compositional variation of the individual phases becomes discrete, so that the phase fields of a true section decompose into a continuous polygonal mesh of smaller pseudodivariant fields each of which is defined by a unique pseudocompound assemblage (Fig. 3.9a).

At the lowest level of resolution the grid has n_x and n_y data sampling points on the horizontal and vertical axes. Grids of successively higher levels of resolution are generated by halving the nodal spacing (Fig. 3.9b). Partially and entirely heterogeneous cells are marked for investigation in the next step, in which each of these marked cells is split into four cells at the next higher level. The stable assemblages at any of these nodes that are not known from the previous step are determined by free energy minimisation, and heterogeneous cells are again marked for investigation. This process is repeated until the highest level is reached (Fig. 3.9c). A continuous map of the phase relations can then be constructed by associating a representative area with each point of the $N_x \times N_y$ grid (Fig. 3.9d) (Connolly, 2005). Finally, this map (pseudosection) (Fig. 3.8d) should be redrawn using, for instance, the computer software Coreldraw. All phase boundaries are smoothed to straight or simply curved lines. Individual P-T field should be filled by a designated background, marking the variance of the assemblage, and labelled.

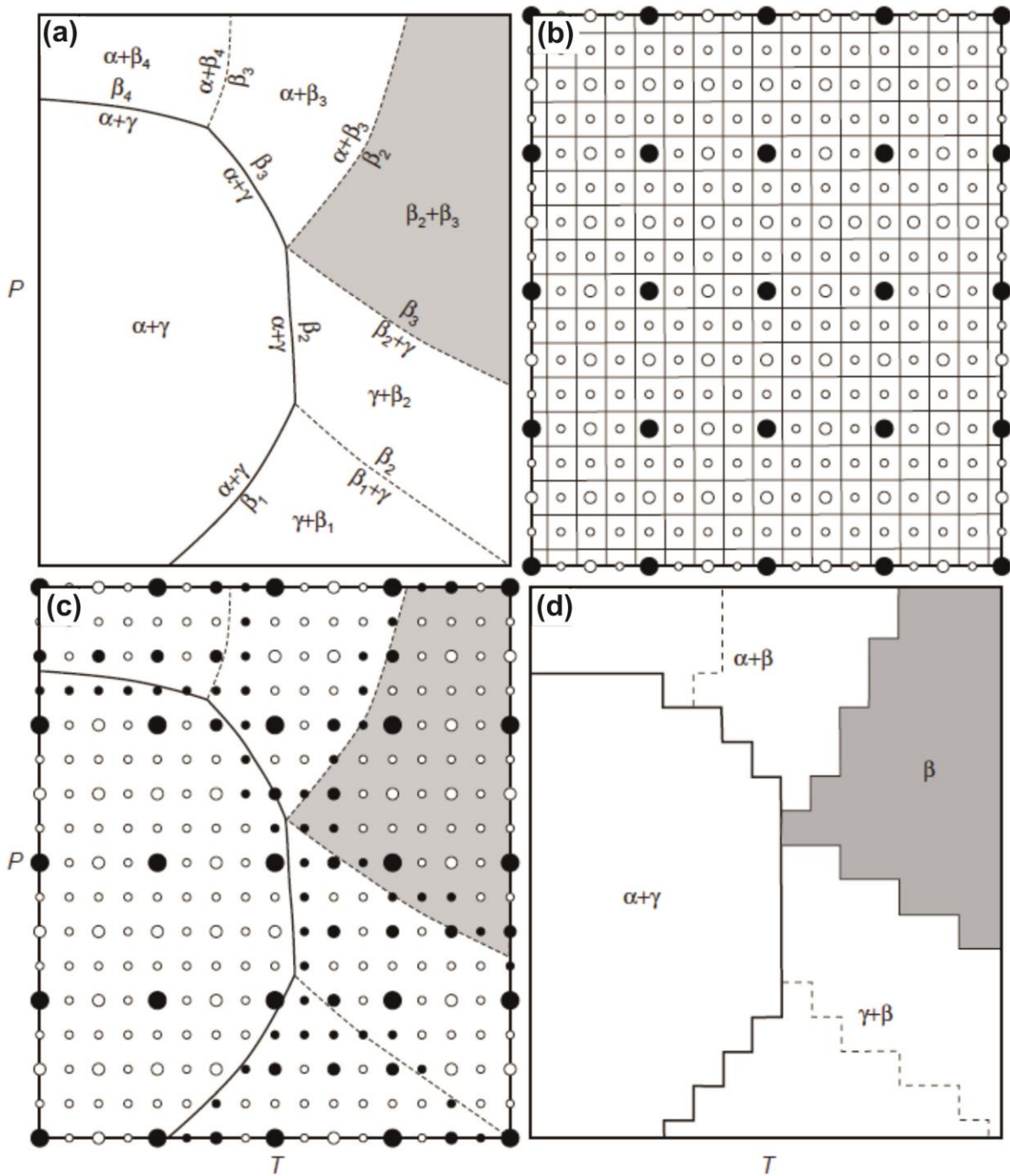


Fig. 3.9. Schematic phase pressure-temperature diagram section for a binary system with phases α , γ and β (Connolly, 2005). Only β is a solid-solution phase subdivided in a number of so-called pseudocompounds β_1 , β_2 etc; (a) Small fields are defined by unique pseudocompound assemblages; (b) A four level grid. Higher levels are indicated by circles of decreasing size; (c) Phases computed by the mapping strategy are indicated by filled circles; and (d) The final map is constructed by assuming that each node of the grid represents a finite area of the diagram.

3.7. Geochronology

Monazite is an ideal candidate for mineral dating; in addition to excluding common lead, it can incorporate significant amounts of Th and U (Spear and Pyle, 2002, and references therein), leading to accumulation of measurable amounts of radiogenic Pb in as little as 50-150 Ma.

Diffusion of Pb in monazite is negligible (Cherniak et al., 2004); for a cooling rate of 10°C/m.y., the lead closure temperature for a 10 µm grain is approximately 900°C. Monazite is also highly resistant to metamictization (Karioris et al., 1991; Meldrum et al., 1997), so the probability of lead loss due to accumulated lattice damage is low.

Suzuki and Adachi (1991) and Suzuki et al. (1994) pioneered EMP chemical dating of monazite with the CHEMical Isochron METHod (CHIME). Single-point monazite ages and statistical treatment of these ages was addressed by Montel et al. (1996), using the methods of Wendt and Carl (1991), and Williams et al. (1999) produced the first monazite age maps by running background-subtracted U, Th, and Pb pixel values through the chemical age equation for monazite (e.g., Montel et al., 1996):

$$Pb = Th / 232 [e^{\lambda^{232r}} - 1] 208 + (U / 238.04) 0.9928 \times [e^{\lambda^{238r}} - 1] 206 + (U / 238.04) 0.0072 \times [e^{\lambda^{235r}} - 1] 207 \quad (1)$$

The abundance of EMP relative to *in-situ* isotopic analysers has led to a proliferation of chemical monazite ages for both ancient and recent plutonism, sedimentation, deformational episodes, and metamorphic reactions (Kim et al., 1997; Pan and Stauffer, 2000; Cho et al., 1999; Grew et al., 2001; Asami et al., 2002; Krohe and Wawrzenitz, 2000; Williams and Jercinovic, 2002; Pyle and Spear, 2003).

Despite the apparent simplicity of the method, chemical dating of monazite is beset by a number of uncertainties and difficulties, making a rigorous assessment of the accuracy and precision associated with each chemical age a non-trivial task. Sources of error are introduced at several stages of the analytical process, including sample preparation, calibration, analysis, and post-analysis data reduction (e.g., Scherrer et al., 2000).

3.8. Geochemical characterisation for provenance and protolith

In chapter 6, the bulk rock analyses of the metamorphic rocks were used for determining possible protoliths (see Table 6.1). For this purpose classification diagrams such as $\text{Al}_2\text{O}_3 + \text{Fe}_2\text{O}_3 - \text{SiO}_2 - \text{MgO} + \text{CaO}$ (Pettijohn et al., 1987); $\log \text{SiO}_2/\text{Al}_2\text{O}_3 - \log \text{Fe}_2\text{O}_3/\text{K}_2\text{O}$ (Herron, 1988) and $\text{Zr} - 15 * \text{Al}_2\text{O}_3 - 300 * \text{TiO}_2$ (Garcia et al., 1994) were applied. The provenance of metasediments through their geochemistry have been assessed considering the relative proportion of K and Rb (Taylor and McLennan, 1985), the Th/Sc vs. Cr/Th diagram by Totten et al. (2000) or the classical discrimination diagram, based on the chemistry of major elements, by Bhatia (1983). The latter diagram allows the discrimination of four different tectonic settings (passive margin, active continental margin, continental island arc and oceanic island-arc). Besides all these discriminating diagrams, samples were characterized according to their normalized multielement patterns (Taylor and McLennan, 1985).

4. Pressure-temperature-time evolution of a Variscan garnet-bearing micaschist from the northeastern Fichtelgebirge, NW Bohemian Massif in central Europe

Abstract

The studied micaschist from the northeastern Fichtelgebirge crystalline complex (FC) contains mm-sized garnet with a foam structure. Staurolite formed at the margin of garnet. Relics of staurolite are enclosed in mm-sized andalusite porphyroblasts. Garnet exhibits prograde concentric zonation with the pyrope component increasing from 1 to 6 mol%. Cores of potassic white-mica grains locally contain Si contents up to 3.15 per formula unit (pfu). The majority of this mica is characterized by Si contents close to 3.00 pfu. Pressure-temperature (P-T) pseudosections, calculated for the micaschist, indicate conditions of 10 kbar and 505 °C for an early metamorphic stage which was followed by a pressure decrease to 5 kbar and 535 °C. Late metamorphic P-T conditions recorded by garnet are around 4.5 kbar and 565 °C, compatible with the presence of staurolite. Andalusite might have metastably formed at this stage or somewhat lower pressures. The U-Th-Pb dating of monazite with the electron microprobe yielded subordinate ages younger than 315 Ma which were assigned to the nearby emplacement of granites in the FC. Some ages older than 395 Ma were related to detrital monazite in the sedimentary protolith of the micaschist. An age cluster at 384.5 ± 1.8 (2σ) Ma is preferentially assigned to the early high pressure (HP) metamorphism resulting from the collision of Laurussia with a Peri-Gondwanan terrane. Exhumation to 15-20 km depths might have ended at 362.3 ± 1.0 Ma, but possibly the HP metamorphism occurred at this age and the 384.5 Ma age must be then referred to the provenance area of detrital monazite. The age cluster at 325.0 ± 0.7 Ma is related to a second collisional event that caused the overriding of the crystalline nappes of the FC onto the Laurussian crust.

Keywords: Fichtelgebirge crystalline complex, Garnet, Monazite dating, Variscan orogeny, P-T path

4.1. Introduction

The Variscan belt of southwestern and central Europe (Fig. 4.1a) extends from the Iberian peninsula to the Bohemian Massif and is a collage of anchimetamorphic to high grade metamorphic terranes resulting from the collision of (fragments of) the Gondwana and Laurussia plates in Devonian to Carboniferous times (e.g., Dallmeyer et al., 1995; Massonne, 2005; McCann et al., 2008; Schulmann et al., 2014).

The Bohemian Massif in Central Europe represents a large segment in the east of this belt. This massif and additional, westerly-situated crystalline complexes of the Variscan belt were traditionally subdivided into two tectonostratigraphic domains (Kossmat, 1927), the Saxothuringian Zone (SZ) and the Moldanubian Zone (Fig. 4.1a). These zones could represent Gondwana-derived terranes that were separated from this continent during the Late Cambrian and later and subsequently amalgamated to Laurussia by the closure of oceans (Rheic, Rhenohercynian, Saxothuringian - see, Franke et al., 2017 and references therein). However, numerous geodynamic views, differing by the number of oceans, subduction direction, etc., exist in the literature concerning the Variscan collision of plates (e.g., Franke, 2000; Holder and Levrige, 1986; Kroner and Romer, 2013; Massonne, 2003a; Matte, 1986; O'Brien, 2000; Zeh and Gerdes, 2010). In order to discriminate between diverse interpretations on the progress of the Variscan kinematics, various constraints from the involved rocks such as the pressure (P) - temperature (T) - time (t) evolution of metamorphic rocks are required. We have focused on an area between the dominantly medium grade metamorphic rocks of the Münchberg metamorphic complex (MMC) and the Erzgebirge crystalline complex (EC) of the SZ. For this area, the northern portion of the Fichtelgebirge crystalline complex (FC, Kreuzer et al., 1989), P-T-t paths were not reconstructed so far probably because the dominant rocks are of low metamorphic grade. These low grade rocks are pelitic and psammitic rift-related metasediments with intercalated acidic metavolcanics (called “epigneisses”) resembling nearby Cambro-Ordovician rocks of the Thuringian lithofacies (Emmert et al., 1981; Mingram and Rötzler, 1999; Stettner, 1975, 1980).

However, geological mapping campaigns have also revealed a km-wide strip of garnet-bearing medium grade metamorphic rocks (Stettner, 1958) between the low grade metasediments and the main bodies of late Variscan granites in the FC.

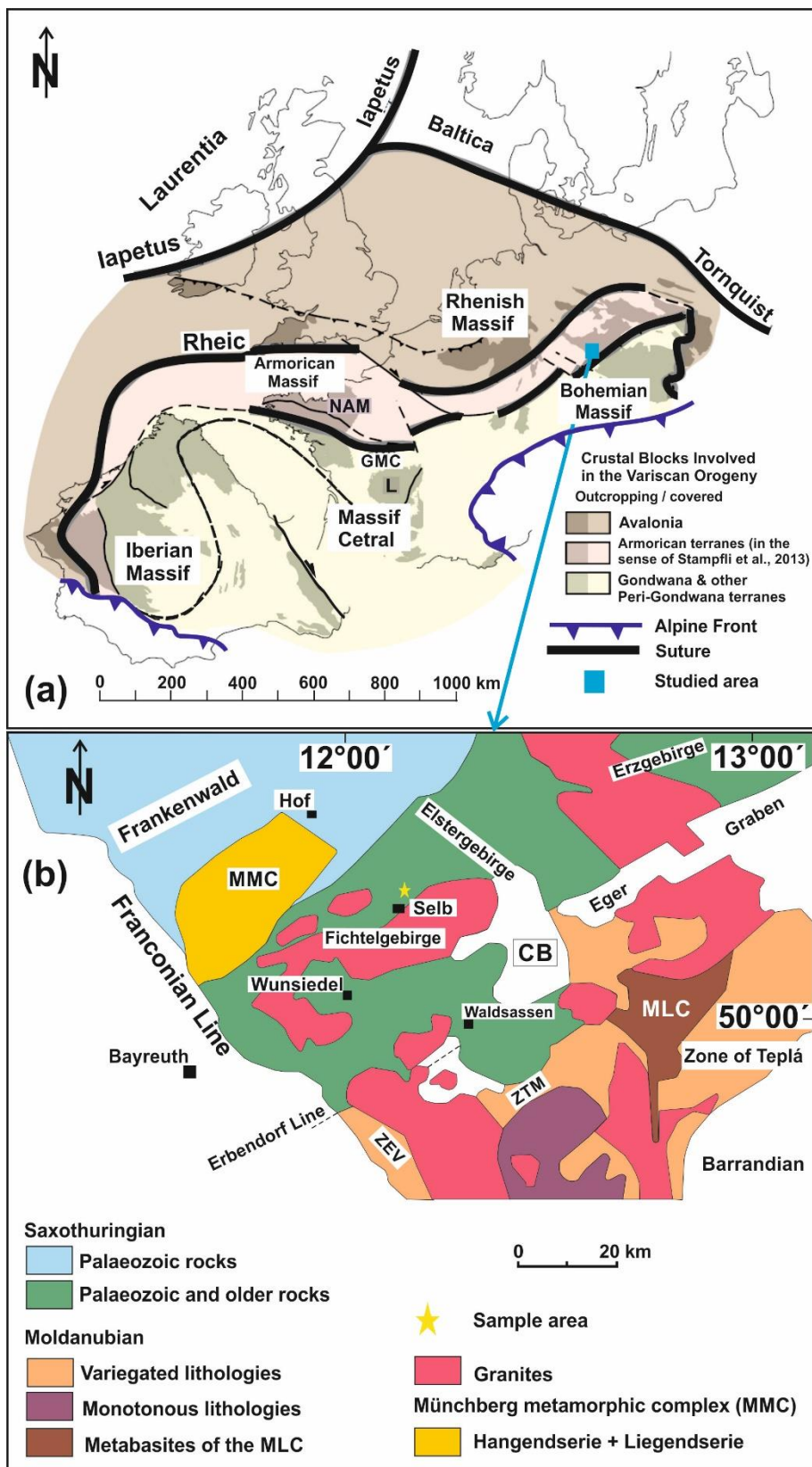


Fig. 4.1. (a) Sketch map of the crustal blocks involved in the Variscan orogeny, adapted from Ballèvre et al. (2014). Oceanic sutures: GMC, Galicia-Massif-Central Ocean. Regional subdivisions: NAM, North Armorican Massif; L, Limousin (Western Massif Central); and (b) Simplified geological map of the northwestern part of the Bohemian Massif based on the Geological Map of Bavaria 1: 500.000 (Stettner, 1981). CB, Cheb basin; MLC, Mariánské Lázně Complex; MMC, Münchber metamorphic complex; MO, Moldanubian Zone; ZEV, Zone of Erbendorf-Vohenstaub; and ZTM, Zone of Tirschenreuth-Mähring (see Kreuzer et al., 1989).

We can demonstrate in this work that these medium grade rocks experienced early high pressure (HP: ≥ 10 kbar) conditions of ~ 10 kbar, as in similar rocks from the nearby MMC and EC, and a heating event after exhumation to c. 4.5 kbar. Questions of particular importance are: (1) which P-T stages and tectonic mechanisms are actually depicted by the rock fabric and mineral assemblages preserved in the micaschists from the FC and (2) what are the timely relations of the corresponding metamorphic events? In addition, we wanted to clarify if our study area in the northern FC is an extension of the Variscan suture zone that was suggested by Faryad and Kachlík (2013) to occur in the Bohemian Massif, to the southwest. This zone is characterized by HP metamorphic rocks that had experienced peak temperatures between 350 and 550 °C in Early Variscan times (Faryad and Kachlík, 2013: cooling ages of c. 360 Ma).

4.2. Geological setting

The SZ in central Europe represents the northernmost Variscan unit in which higher grade metamorphic rocks occur. Such rocks of the SZ in the northern part of the Bohemian Massif are exposed in the MMC, FC, EC, and the Granulitgebirge metamorphic core complex (GC) which broadly form allochthonous domains (Kroner et al., 2008). Similar metamorphic rocks occur in the Sudetes (Fig. 4.1b). The metamorphism of these rocks is the result of collisional events in Middle Devonian to Lower Carboniferous times (e.g., Dallmeyer et al., 1995; Massonne, 2005; McCann et al., 2008; Schulmann et al., 2014).

In both MMC + FC and EC + GC the entire spectrum of regionally metamorphosed rocks is exposed, ranging from very-low to high grade. In addition, rocks that have experienced ultrahigh temperatures (GC: Rötzler et al., 2004) and ultrahigh pressures (MC: Klemd et al., 1991; EC: Massonne, 2003b) record processes related to subduction (Massonne and O'Brien, 2003), continental delamination (Massonne, 2005), and very fast exhumation (Müller et al., 2015).

The FC and EC (Fig. 4.1b) consist of several lithotectonic units recording distinct metamorphic conditions. From the bottom to the top, these units in the EC are as follows: the Cadomian Basement or Grey Gneiss Unit, the Gneiss-Eclogite Unit, the Micaschist-Eclogite Unit and the (Garnet)-Phyllite Unit (Willner et al., 2000): (i) The Cadomian Basement Unit is made up of medium pressure orthogneiss and migmatite with no evidence of HP conditions, but strongly affected by Variscan medium- to high temperature metamorphism (Willner et al., 2000).

(ii) The Gneiss-Eclogite Unit consists of gneiss, migmatite and various types of HP to ultrahigh pressure rocks such as coesite-bearing eclogite (Massonne, 2001), diamondiferous rock (Massonne, 2003b), and garnet peridotite (Massonne and Neuser, 2005). (iii) The Micaschist-Eclogite Unit is composed of chloritoid- and garnet-bearing micaschists (Konopásek et al., 2001; Rötzler et al., 1998) with intercalations of quartzite, marble (Gross et al., 2008) and eclogite (Massonne and Kopp, 2005).

The Arzberg Series of the FC could be correlated with this unit (Hecht et al., 1999; Kreuzer et al., 1989). (iv) The (Garnet)-Phyllite Unit forms a mantle around the gneiss dome of the EC. This unit, which is the uppermost one in the EC, is represented by phyllite and schist with intercalations of quartzite and metabasite. Blue amphibole has been reported from some metabasites in the basal part of the (Garnet)-Phyllite Unit (Holub and Souček, 1994; Frankenberg massif: Rötzler et al., 1999). Garnet is present in the eastern part, whereas the western part of this unit is free of garnet, but contains chloritoid (Rötzler et al., 1998). Faryad and Kachlík (2013) interpret the occurrences of various metamorphic rocks of the blue schist and low temperature eclogite facies from the Sudetes to the EC as evidence for a suture zone of the Early Variscan collision of plates. An uppermost allochthon is represented by several klippen (MMC and Wildenfels and Frankenberg Massifs, Fig. 4.1b), which could be interpreted as erosional remnants of a formerly coherent nappe unit derived from a position to the southeast of the present-day Fichtelgebirge, eventually marked by the Saxothuringian/Teplá-Barrandian plate boundary (Behr et al., 1982; Franke, 1984). The metasediments of the EC are suggested to represent lithological equivalents of the lower Palaeozoic succession of autochthonous domains (Mingram, 1998) such as those of low metamorphic grade exposed in the northern FC. The Arzberg Series in the central FC is also mainly composed of metasediments (e.g., phyllite, quartzite, graphite schist) characterized by the assemblage quartz-muscovite-chlorite-biotite-garnet-albite (Mielke et al., 1979) with some minor bodies and layers of marble, amphibolite and greenschist (Fig. 4.1b). Mielke and Schreyer (1972) concluded that the paragenesis magnetite-rutile found in metapelitic rocks of the FC indicates relatively low temperatures

between 450 and 500 °C. The occurrence of andalusite in FC metapelites was regarded as an indication of relatively low metamorphic pressures which were estimated to 3.5-5.5 kbar (Mielke et al., 1979). In the whole Bohemian Massif the Variscan evolution was terminated by intrusions of granitoid rocks (Dallmeyer et al., 1995). The plutons of the FC and western EC are such intrusions into the upper Saxothuringian crust (Behrmann and Tanner, 1997).

Based on field relations, petrography, geochemistry and radiometrical dating (Besang et al., 1976; Carl and Wendt, 1993; Richter and Stettner, 1979; Stettner, 1958), the granites of the FC can be subdivided into two main complexes: the older intrusive complex (~ 320 Ma) and the younger intrusive complex (290-280 Ma). However, the intrusion of the latter complex occurred between 300 and 290 Ma according to Carl and Wendt (1993) and Siebel et al. (2010). The age of the metamorphism in the EC was determined by various methods (Sm-Nd isochrons, Ar-Ar in phengite, U-Pb in zircon and monazite: see, Kröner and Willner, 1998; Massonne et al., 2007; Schmädicke et al., 1995; Tichomirowa et al., 2005; Werner and Lippolt, 2000). Ages around 340 Ma resulted from the application of these methods.

Tichomirowa (2002) and Tichomirowa et al. (2012) dated zircon of ortho- and paragneisses from the EC and determined age clusters at c. 575, 540-530 and 500-470 Ma which were related to Cadomian (and post-Cadomian?) magmatic events at the margin of Gondwana or peri-Gondwanan terranes (see Linnemann et al., 2000, 2010). A similar conclusion was drawn by Waizenhöfer and Massonne (2017) for a paragneiss of the MMC on the basis of monazite ages. Teufel (1988) suggested from ages of monazite occurring in paragneiss of the southern FC and adjacent Moldanubian units that the ages of the protolith of this rock type should be Ordovician or younger. Grauert et al. (1973) obtained U-Pb isotope data on zircon from a quartzite (Plattenquarzit) of the upper Arzberg Series suggesting that the sedimentation age of this rock was younger than 560 Ma. Metamorphism of MMC rocks occurred in Early Variscan times (410-370 Ma, see the summary in Massonne and O'Brien, 2003). However, the FC underwent low pressure metamorphism in the time interval 330-320 Ma (Okrusch et al., 1990).

An age of 316 ± 3 Ma was determined by Kreuzer et al. (1989) applying K-Ar dating to muscovite in a muscovite-biotite gneiss and schist, which both were sampled ~ 2.5 km northeast of the town of Selb. Hornblende from schistose amphibolites from localities at and near the town of Arzberg yielded ages of 332 and 299 Ma also using the K-Ar method (Kreuzer et al., 1989).

4.3. Analytical techniques

The chemical compositions of minerals in polished thin-sections were analysed with a CAMECA SX100 electron microprobe (EMP) with 5 wavelength-dispersive (WD) spectrometers. Concentrations of F, Na, Mg, Al, Si, K, Ca, Ti, Cr, Mn, Fe, and Ba were determined using counting times of 20 s at the peak and on the background except for F (30 s). Synthetic and natural minerals, glasses (e.g., Ba-rich glass for the BaL α 1 peak), and pure oxides were used as standards. The applied acceleration voltage and electric current were 15 kV and 30 nA, respectively, for analysing garnet. For other minerals an electric current of 10 nA was used. The beam diameter was usually 3-5 μ m. The PaP correction procedure provided by CAMECA was applied. The analytical errors of the applied method were reported by Massonne (2012), related to an electric current of 15 nA. Structural formulae were calculated with the CalcMin (Brandelik, 2009) program.

For the dating of monazite, full analyses of this mineral with the EMP, including the elements Si, P, S, Ca, Y, La, Ce, Pr, Nd, Sm, Eu, Gd, Pb, Th, and U, were performed. The analytical procedure was described by Massonne et al. (2012). However, the beam current of 180 nA, usually used, was reduced to 150 nA for the analysis of small monazite inclusions in garnet. The applied analytical conditions had been tested against different Palaeozoic monazite and/or zircon grains (see, Langone et al., 2011; Massonne, 2014; Li and Massonne, 2017; Waizenhöfer and Massonne, 2017; Massonne et al., 2007, 2018) which had been independently dated by other geochronological methods. For the calculation of ages and their errors the program MINCALC-V5 (Bernhardt, 2007) was used. Age histogram analysis was undertaken with the Isoplot program (Ludwig, 1999). Element concentration maps for major elements were prepared by step-wise movement of the thin section under the electron beam of the EMP and subsequent computer-aided evaluation (Bernhardt et al., 1995). Counting times per step were 80 ms.

An electric current of 40 and 20 nA was applied for areas with garnet and potassic white-mica, respectively. Major and trace element concentrations in the bulk rock (Table 4.1) were analysed using a rock slab, which was ground to powder. A glass disk was prepared by fusing this rock powder with Spectromelt® (ratio 1:6). This disk was analysed with a PHILIPS PW2400 X-ray fluorescence (XRF) spectrometer with a WD system calibrated with certified geostandards.

The contents of H₂O and CO₂ in the rock powder were determined with a LECO RC-412 C-O-H multiphase determinator after drying the powder at 110 °C for several hours. In order to correctly identify the aluminum silicate (Al₂SiO₅) polymorphs, Raman spectroscopy was additionally applied with a Raman microscope (HORIBA XploRa).

4.4. Petrography and chemical compositions of the minerals

The sample for this study (13F18) was taken from a larger gneissose micaschist block with mm-sized red brown garnet spots with unusual shape, about 100 m south of the hamlet of Lauterbach (4 km NNE of the centre of Selb), in the northeastern FC (Fig. 4.1b) (coordinates: N: 50.20349°, E: 12.14639°). Garnet in other micaschist samples taken from the same unit (mapped km-wide strip of medium grade metamorphic rocks, see above) were not as fresh as in 13F18. Phyllitic rocks, exposed, for instance, 2-3 km northwest of the locality of 13F18, are free of garnet.

Table 4.1. Bulk rock XRF analyses of metapelite (sample 13F18) and its normalized compositions used for pseudosection and melt calculations. M1, modified for 1st round calculations of O₂ free system; M2, modified for 2nd round calculations of O₂-bearing system; M3, modified for melt calculations of O₂-bearing system; M4, after subtraction of the 4 vol.% of garnet core and mantle of O₂ free system.

	XRF	M1	M2	M3	M4
SiO ₂ (wt.%)	77.976	78.458	77.858	79.063	80.185
TiO ₂	0.480	0.471	0.479	0.487	0.479
Al ₂ O ₃	9.759	9.376	9.744	9.895	8.982
Fe ₂ O ₃	6.894	-	-	-	-
FeO ^a	-	6.085	6.194	6.290	4.670
O ₂	-	0.000	0.069	0.070	0.000
MnO	0.026	0.026	0.026	0.026	0.010
MgO	0.546	0.536	0.545	0.554	0.521
CaO	0.510	0.185	0.184	0.187	0.300
Na ₂ O	0.306	0.300	0.306	0.310	0.309
K ₂ O	1.596	1.565	1.594	1.618	1.544
P ₂ O ₅ ^b	0.247	-	-	-	-
H ₂ O		3.000	3.000	1.500	3.000
Total	98.181	100.000	100.000	100.000	100.000

^a total Fe as FeO ^b corrected for apatite

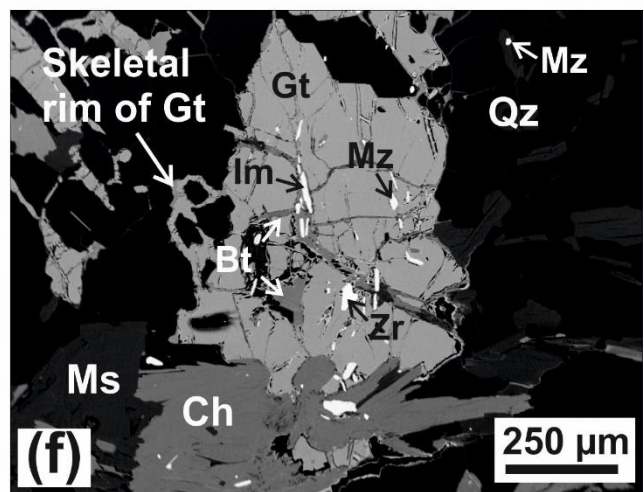
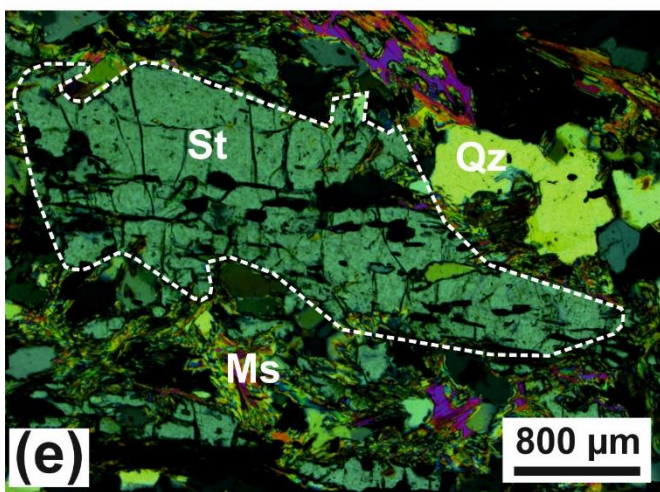
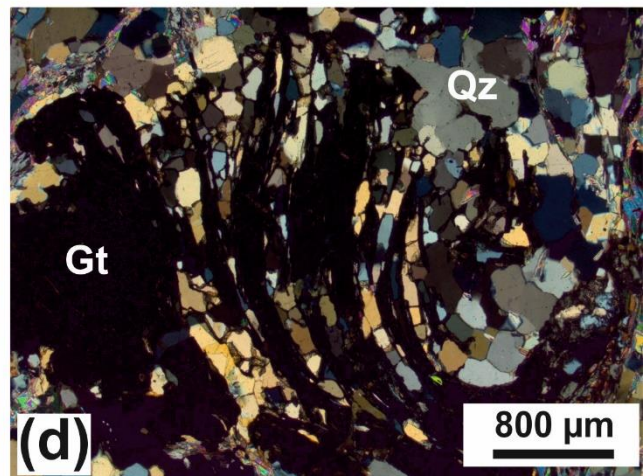
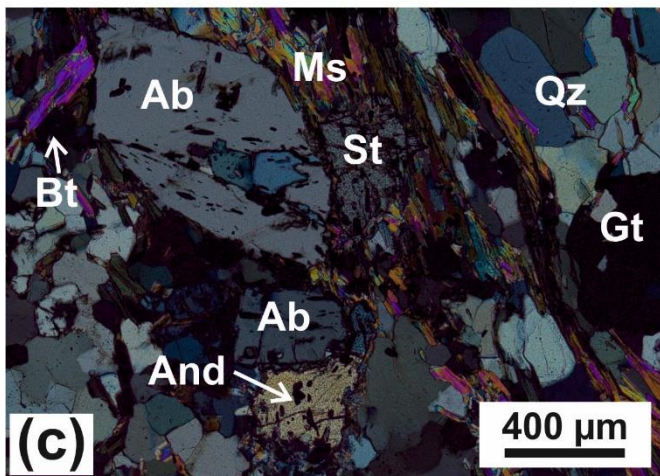
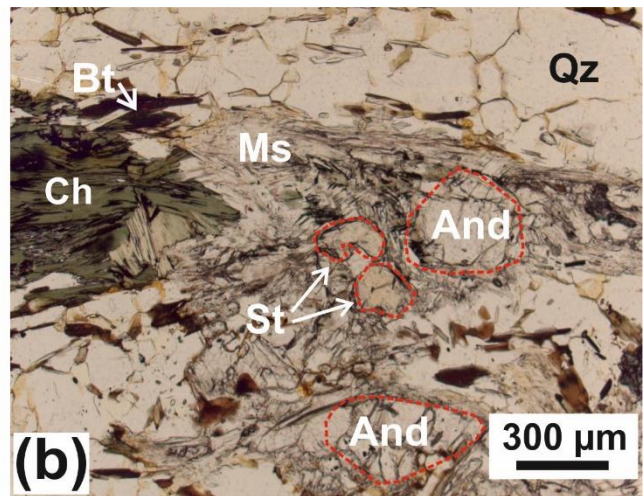
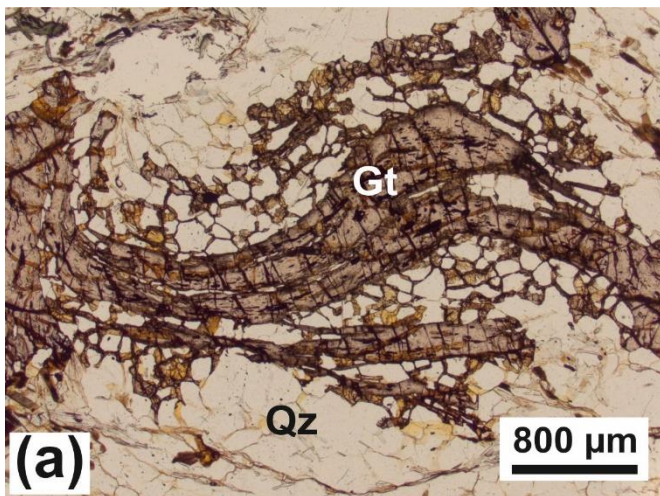


Fig. 4.2. Photomicrographs showing microstructural features of the garnet-bearing gneissose micaschist sample from the northwestern FC under plain-polarized light (a), (b) and crossed polarizers (c)-(e). (a) Garnet (Gt) porphyroblast characterized by a foam structure with quartz (Qz); (b) Relics of staurolite (St) and andalusite (And) surrounded by unoriented muscovite (Ms). In addition, larger chlorite (Ch) can be seen; (c) Rare albite (Ab) porphyroblast surrounded by biotite (Bt), potassic white-mica, staurolite and andalusite grains; (d) Garnet-quartz foam structure similar to (a) with curved garnet seams of different spacings; (e) Millimetre-sized staurolite grain surrounded by muscovite and quartz; and (f) Back-scattered electron image shows inclusions of ilmenite (Im), monazite (Mz), and zircon (Zr) in garnet. Biotite formed along cracks in garnet. Larger grains of muscovite and chlorite occur adjacent to garnet. The boundaries of a few grains in (b) and (e) were highlighted by broken lines.

4.4.1. Modal and textural aspects

Sample 13F18 consists mainly of quartz (60 vol.%). In addition, potassic white-mica (12-15 vol.%), biotite (8-10 vol.%), garnet (6 vol.%), chlorite (3-5 vol.%), andalusite (3 vol.%), staurolite (2 vol.%), and plagioclase (1-2 vol.%) occur (Fig. 4.2a, b). Accessory phases (2 vol.%) are zircon, monazite, apatite, and opaque phases (Fe oxides, sulphides and ilmenite). Millimetre-thick phyllosilicate-rich layers, characterized by intimate intergrowth of potassic white-mica and biotite, irregularly alternate with quartz-rich domains. These layers of oriented phyllosilicates are slightly folded. Most garnet grains are between 3 and 5 mm in size. The poikiloblastic structure of the garnet usually forms a three-dimensional cellular structure partially of thin seams, resembling a web or net in two-dimensional cross sections (Fig. 4.2a, d). Domains in this structure can be rich in quartz with irregular spacings frequently between 0.1 and 0.4 mm. At the skeletal rims of the garnet porphyroblasts, the planar structures are curved forming an S shape in favourable sections (Fig. 4.2d). This feature reflects deformation resulting in the rotation of garnet grains during a late stage of their growth (Stöckhert et al., 1997). Moreover, the net-like structure, commonly called foam structure (Underwood, 1970), shows that garnet has grown as thin seams along high-angle grain boundaries of matrix quartz with 120° angles at the edges between three quartz grains and 90° angles between these seams and the isometric quartz grains (Fig. 4.2d). Microlithons dominated by quartz can show rootless isoclinal folds with an axial plane sub-parallel to the main schistosity. Plastic deformation by dislocation creep is indicated by sutured high-angle grain boundaries (Fig. 4.2d). In addition, the shapes of the overgrown quartz in the outer zone of the garnet grains tend to be more irregular compared to quartz in the central part of the foam structure.

This is another indication, in addition to the rotation of garnet that the differential stress had increased during the final stage of garnet growth and eventually became sufficiently large to drive deformation of quartz by dislocation creep (see, Stöckhert et al., 1997). Millimetre-sized white-mica crystals are undeformed and form oriented layers (Fig. 4.2b). Finer-grained, unoriented white-mica occurs as replacement product of andalusite. Biotite with reddish brown and yellowish pleochroitic colours is 0.1 to 1 mm long with smaller crystals usually formed in the quartz-rich domains as opposed to those in the phyllosilicate-rich layers. This mineral and chlorite can also occur as small grains (~ 10-100 μm) in cracks in garnet (Fig. 4.2f).

Chlorite is pale green in colour. It can form grains up to 1 mm in size. Locally chlorite forms fan-like aggregates indicating that this mineral grew postkinematically. Plagioclase with grain sizes between 0.2 and 0.5 mm occurs in the matrix and dominantly in the layers rich in mica and chlorite. Plagioclase can show a sieve texture as well (Fig. 4.2c). Staurolite has replaced garnet at the outer zone of the foam structure. This can even concern the aforementioned thin garnet seams along high-angle quartz grain boundaries. The content of staurolite in the garnet foam structure (55% garnet, 30% quartz), which makes up 10-12% of the rock, is approximately 15%. Staurolite was also very rarely found even as 0.3-0.5 mm-sized grains enclosed in andalusite, which can form up to 6 mm long crystals. However, these crystals can be largely replaced by fine-grained muscovite (Fig. 4.2e).

On the basis of X-ray maps of Ca, Fe, Mg, and Mn, prepared for selected garnet porphyroblasts (Fig. 4.3a-e), and spot analyses with the EMP, the compositional change of garnet, being rich in almandine (Alm) component, during metamorphism could be elucidated. The correlation of the molar fractions X_{Mg} (X_{pyrope}) and X_{Mn} ($X_{\text{spessartine}}$) with X_{Ca} ($X_{\text{grossular}} + X_{\text{andradite}}$) in garnet are exhibited in Fig. 4.4. Garnet shows a prograde concentric zonation from core to the rim with the spessartine (Sps) and grossular (+ andradite: Grs + Andr) components decreasing from 1 to 0.1 mol% and 17 to 4 mol%, respectively, and the pyrope (Pyp) component increasing from 2 to 4 mol%. Correspondingly, the garnet composition of the innermost core is $(\text{Grs} + \text{Andr})_{16}\text{Alm}_{80}\text{Pyp}_1\text{Sps}_3$ (stage Ia). A typical intermediate composition is $(\text{Grs} + \text{Andr})_{10.5}\text{Alm}_{86}\text{Pyp}_3\text{Sps}_{0.5}$ (stage Ib, Fig. 4.4a, Table 4.2). At the outermost rim the garnet composition is $(\text{Grs} + \text{Andr})_5\text{Alm}_{89}\text{Pyp}_{5.5}\text{Sps}_{0.5}$ (stage II). The calculated andradite content is between 1.0 and 1.7 mol% (Table 4.2).

Potassic white-mica shows a compositional range (Fig. 4.4b, c, Table 4.3) with Si contents between 2.95 and 3.16 per formula unit (pfu) with the extreme values being due to under- or overestimation of

the true Si contents within the analytical errors (the value at 3.225 Si (pfu) is probably a mixed analysis of mica + some quartz owing to the too low Mg + Fe content). Several maps, as exemplarily shown in Fig. 4.3f, g, demonstrate that the rims are significantly poorer in Mg than the cores. The highest Mg contents resulted from analyses of some core regions of single grains of potassic white-mica. According to the spot analyses (Fig. 4.4b, c), the Mg-poorer domains are also poorer in Si.

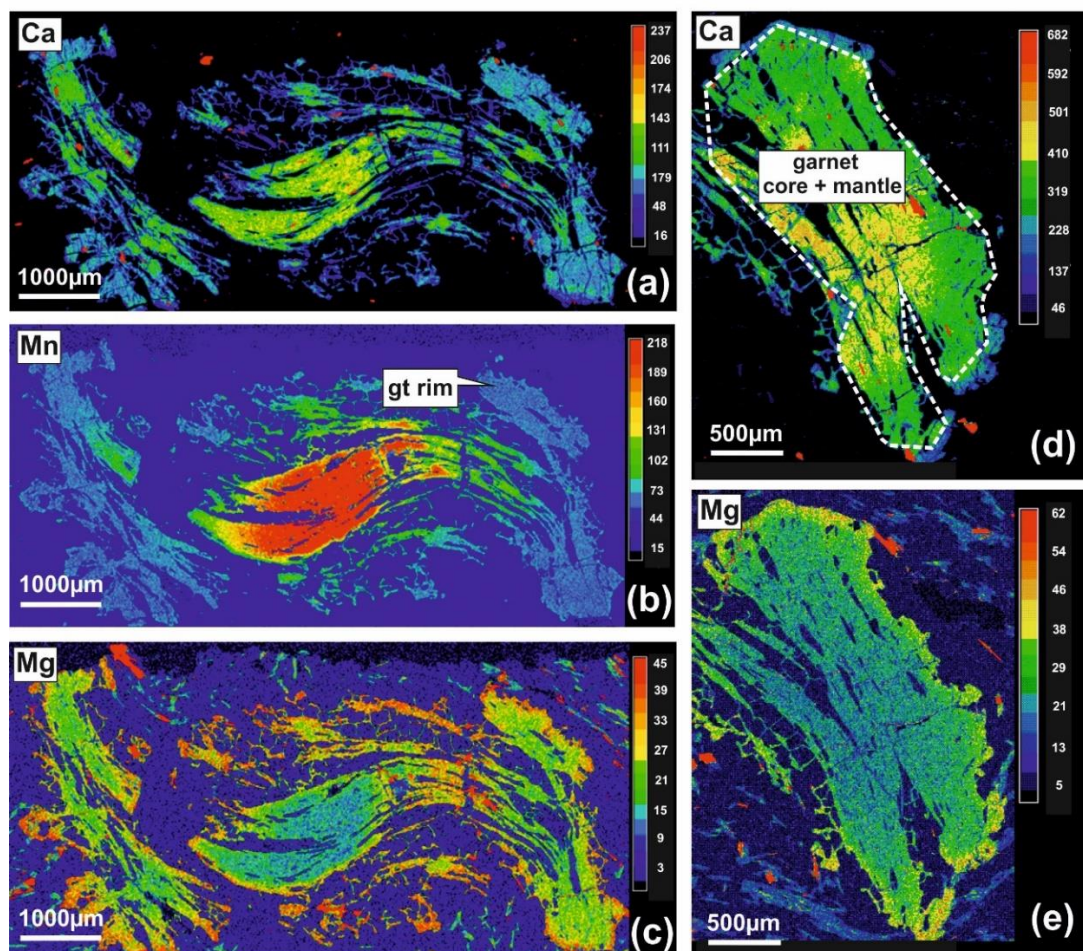
Iron contents first decrease similar to the Mg contents, according to the (inverse) Tschermak's substitution, but at the relatively low Si contents a clear increase of the Fe contents is discernable (Fig. 4.4c). With decreasing Si contents Na and Ba contents increase. Contents of Ti are fairly constant over the entire compositional range (Fig. 4.4b). According to the aforementioned elemental trends and the observations from the elemental maps, potassic white-mica can be subdivided into two generations (Fig. 4.3f, g). The older generation (related to metamorphic stage Ia, b) is characterized by Si contents up to 3.16 pfu, $X_{Mg} = Mg/(Mg+Fe) = 0.37-0.42$, $X_{Na} = Na/(Na+K+Ba) = 0.11-0.16$, and $X_{Ba} = Ba/(Ba+Na+K) \leq 0.01$ (Table 4.3), whereas the younger generation (stages Ic and II), overgrowing the older white-mica grains or andalusite during a post-deformational event, is specified by Si = 2.95-3.085 pfu, $X_{Mg} = 0.13-0.39$, $X_{Na} = 0.08-0.22$, and $X_{Ba} \leq 0.02$ (Fig. 4.4c).

Chlorite is Fe-Al-rich (chamosite: Fe^{2+} around 3.55 pfu, Mg around 1.2 pfu) with Mn contents lower than 0.015 pfu (Table 4.3). Chlorite has been analysed in the following textural positions: chlorite flakes in the phyllosilicate-quartz-rich matrix and in garnet fractures. Most chlorite from the matrix shows Al contents of 2.9 pfu and X_{Mg} values around 0.24, whereas this mineral in cracks of garnet has lower Al contents (~ 2.75 pfu) and lower X_{Mg} values around 0.14 (Fig. 4.4d).

Biotite has been analysed in the phyllosilicate-quartz-rich matrix and in garnet fractures. Both textural groups are characterized by Si contents around 2.63 pfu (Table 4.3), but higher FeO_t contents (~ 28 wt.%) were noted in biotite grown in garnet cracks compared to biotite from the matrix (~ 25 wt.%).

The analysed biotite shows TiO_2 contents close to 2 wt.%. X_{Mg} values range between 0.16 and 0.28 (Table 4.3). The chemical composition of plagioclase is close to pure albite. Orthoclase and anorthite contents are below 1 mol% (Table 4.3). Staurolite analyses yielded a fairly constant, Fe-rich composition ($X_{Mg} \sim 0.07$) with ~ 0.4 wt.% TiO_2 and up to 0.06 wt.% MnO.

13F18 garnet



13F18 potassic white mica

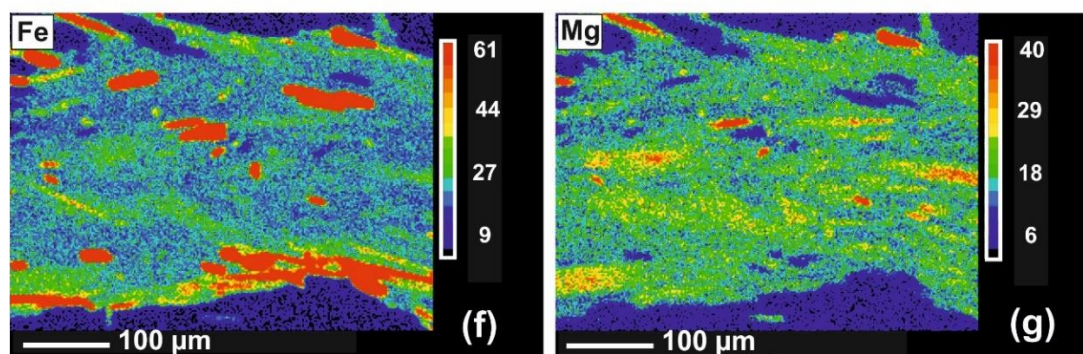


Fig. 4.3. (a-e) Ca, Mg and Mn concentration maps of two selected garnet crystals from sample 13F18; and (f, g) Fe and Mg concentration maps of a selected white-mica rich domains. Colour code on the right hand side of the images corresponds to counts per time unit.

4. Pressure-temperature-time evolution ...

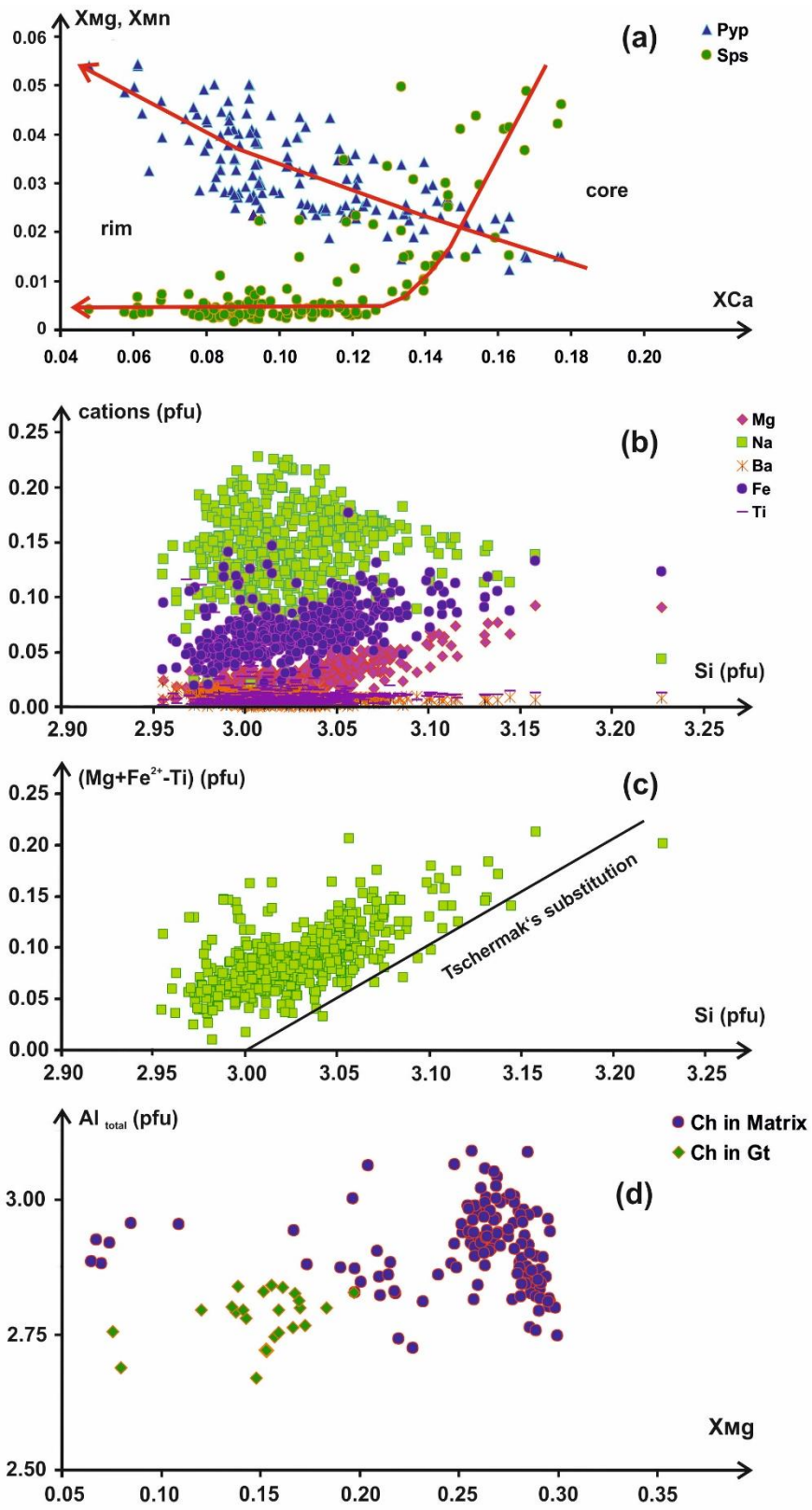


Fig. 4.4. Analytical data for minerals in sample 13F18: (a) Garnet in terms of molar fractions of pyrope (Pyp, X_{Mg}) and spessartine (Sps, X_{Mn}) vs. that of grossular + andradite (X_{Ca}). Chemical trends from core to rim are shown by arrows. Potassic white-mica in terms of (b) contents of various cations (pfu) versus the Si content (pfu); (c) in terms of $Mg + Fe^{2+}$ -Ti (pfu) versus Si (pfu); and (d) X_{Mg} vs. Al total (pfu) contents in chlorite (Ch) in matrix and garnet (Gt).

Table 4.2. Representative electron microprobe analyses (in wt.%) of garnet in the sample 13F18. The garnet structural formulae (per formula unit = pfu) was calculated on the basis of 12 O and 5 six- and eight-fold coordinated cations. Molar fractions of garnet components are given at the bottom. Note that the relatively low Si contents in garnet are probably real (see, Langone et al., 2011).

Sample	13F18					
Comment	Inner core	Outer-core	Mantle		Inner-rim	Outermost rim
SiO₂ (wt.%)	35.40	36.18	36.01	36.01	36.57	36.44
TiO₂	0.16	0.18	0.10	0.11	0.07	0.06
Al₂O₃	20.47	20.83	20.91	20.81	21.35	21.38
V₂O₃	0.00	0.00	0.00	0.00	0.00	0.00
Cr₂O₃	0.03	0.02	0.01	0.01	0.01	0.01
Fe₂O₃	0.99	0.68	0.15	0.88	0.02	0.24
FeO	34.87	38.32	37.85	38.38	39.18	40.08
MnO	1.62	0.14	0.22	0.28	0.13	0.20
MgO	0.38	0.61	0.79	1.00	1.13	1.38
CaO	5.84	4.22	3.80	3.70	2.96	2.18
Na₂O	0.00	0.01	0.03	0.01	0.02	0.00
Total	99.76	101.18	99.87	101.18	101.44	101.98
Si (pfu)	2.844	2.885	2.908	2.858	2.904	2.871
Ti	0.010	0.011	0.006	0.006	0.004	0.003
Al	1.938	1.958	1.990	1.947	1.998	1.985
V	0.000	0.000	0.000	0.000	0.000	0.000
Cr	0.002	0.001	0.001	0.001	0.001	0.001
Fe³⁺	0.060	0.041	0.009	0.053	0.002	0.014
Fe²⁺	2.343	2.556	2.557	2.548	2.602	2.641
Mg	0.045	0.072	0.095	0.118	0.134	0.162
Ca	0.502	0.361	0.329	0.315	0.252	0.184
Mn	0.110	0.009	0.015	0.019	0.009	0.014
Na	0.000	0.002	0.005	0.001	0.003	0.000
grossular	0.167	0.120	0.110	0.105	0.084	0.051
pyrope	0.015	0.024	0.032	0.039	0.043	0.056
spessartine	0.037	0.003	0.005	0.006	0.006	0.005
almandine	0.781	0.852	0.852	0.849	0.867	0.888

4. Pressure-temperature-time evolution ...

Table 4.3. Representative electron microprobe analyses (in wt.%) of various minerals from sample 13F18. Structural formulae (per formula unit = pfu) were calculated as follows: potassic white-mica (Ms) = 11 O, 21- (Ca + Ba) valencies neglecting interlayer cations; chlorite (Ch) = 14 oxygen and negligence of large cations (Na, Ca); biotite (Bt) = 11 O; plagioclase (Pl) = 8 O with Fe and Mn being trivalent; staurolite (St) = 30 cations; andalusite (And) = three cations; ilmenite (Im) = 3 O and 2 cations. Gt = garnet, tot = total, calc = calculated.

Mineral	Ms			Ch		Bt		Pl	St	And	Im	
	Occurrence	Early	Late	Late	In Gt	In matrix	In Gt				In matrix	In Gt
SiO ₂ (wt.%)	47.25	45.80	45.59	22.72	23.13	33.42	33.35	67.57	27.73	35.54		
TiO ₂	0.26	0.10	0.20	0.11	0.13	1.27	1.80	0.00	0.57	0.02	53.98	50.88
Al ₂ O ₃	33.28	36.48	35.16	21.46	22.48	20.09	19.81	19.68	55.69	60.84		
Cr ₂ O ₃										0.02	0.01	0.01
FeO	2.37	1.10	1.93	39.24	35.03	28.44	25.73		10.22		44.99	45.71
Fe ₂ O ₃								0.14		0.64		1.79
MnO				0.01	0.04	0.01			0.04	0.00	0.08	0.05
MgO	0.93	0.25	0.48	4.23	7.85	3.66	5.25	0.01	0.42	0.00	0.03	0.00
CaO								0.16		0.02		
Na ₂ O	1.07	1.51	1.33			0.04	0.20	11.66				
K ₂ O	9.79	9.58	9.85			9.05	9.31	0.06				
BaO	0.26	0.16	0.28			0.16	0.21	.				
ZnO									3.03			
H ₂ O _{calc}	4.49	4.50	4.45	10.51	10.88	3.80	3.82		1.05			
Total	99.69	99.47	99.28	98.29	99.57	99.95	99.47	99.28	98.75	97.08	99.08	98.44
Si (pfu)	3.163	3.0525	3.069	2.593	2.545	2.637	2.620	2.976	7.904	0.989		
Al _{tot}	2.622	2.866	2.79	2.887	2.916	1.868	1.835	1.022	18.712	1.996		
Ti	0.013	0.005	0.01	0.010	0.011	0.076	0.107		0.123	0.000	1.037	0.983
Fe ²⁺	0.1325	0.0615	0.109	3.745	3.224	1.877	1.691		2.437		0.961	0.982
Fe ³⁺								0.005		0.013	0.000	0.035
Mn				0.001	0.004	0.001			0.009		0.002	0.001
Mg	0.093	0.025	0.048	0.720	1.288	0.431	0.615		0.178		0.001	0.000
Ca	0.001	0.000	0.001					0.008		0.001		
Ba	0.007	0.004	0.008			0.005	0.006					
Na	0.139	0.195	0.174			0.006	0.031	0.996				
K	0.835	0.815	0.846			0.911	0.934	0.003				
F					0.014							
Cr										0.001	0.000	0.000
Zn									0.639			
H	2.000	2.000	2.000	8.000	8.000	2.000	2.000		2.000	2.000		

However, ZnO contents range between 1.0 and 4.0 wt.% (Table 4.3) with the highest contents in the core. All analysed andalusite is almost pure Al_2SiO_5 with contents of 0.6 wt.% Fe_2O_3 (Table 4.3).

4.5. Modelling of the P-T evolution

4.5.1. Calculation method

P-T pseudosections were constructed for the P-T range of 2-15 kbar and 400-700 °C, for a fixed bulk composition with the software PERPLE_X (Connolly, 2005, version from August 2011, downloaded from the web site <http://www.perplex.ethz.ch/>). For this purpose we used the internally consistent thermodynamic dataset and equation of state for H_2O of Holland and Powell (1998, updated 2002).

The following established solid-solution models, being compatible to this data set, were chosen from the downloaded version of the PERPLE_X solution model file (`newest_format_solut.dat`, see the appendix in Massonne et al., 2018): GlTrTsPg for amphibole (White et al., 2003), TiBio(HP) for biotite (see below), Chl(HP) for chlorite (Holland et al., 1998), Ctd(HP) for chloritoid (White et al., 2000), hCrd for cordierite (ideal solid-solution), Ep(HP) for clinozoisite-epidote (Holland and Powell, 1998), feldspar for plagioclase and K-feldspar (Fuhrman and Lindsley, 1988), Gt(HP) for garnet (Holland and Powell, 1998), IlGkPy for ilmenite, Omph(HP) for clinopyroxene (Holland and Powell, 1996), Mica(M), restricting the contents of the muscovite and margarite components, for paragonite (Massonne, 2010), Pheng(HP) for potassic white-mica (Coggon and Holland, 2002; using a maximum paragonite content of 50 mol%), MtUl(A) for magnetite (Andersen and Lindsley, 1988), St(HP) for staurolite (details in http://www.perplex.ethz.ch/perplex_solution_model_glossary.html), and Stlp(M) for stilpnomelane (Massonne, 2010). Although no evidence of the former presence of melt was detected in the studied rock, we calculated the solidus as an upper temperature limit. For this purpose, we used the whole-rock composition with 1.5 wt.% H_2O (Table 4.1), an older PERPLE_X version (downloaded in August 2006), and the melt(HP) model (White et al., 2001).

Fig. 4.5. P-T pseudosections calculated with the computer software package PERPLE_X (see text) for conditions (a) without and (b) with an O₂ content at water-saturated conditions without melt (left side of the dotted line = solidus) and a lower H₂O content with melt (right side of the solidus) according to the modified compositions of metapelite 13F18 given in Table 4.1. Abbreviations: And, andalusite; Bt, biotite; Ch, chlorite; Crd, cordierite; Ctd, chloritoid; Ep, epidote; Gt, garnet; Hm, hematite; Im, ilmenite; Ky, kyanite; Lw, lawsonite; M, silicate melt; Ms, potassic white-mica; Mt, magnetite; Nam, Na-rich amphibole; Om, omphacite; Pa, paragonite; Pl, plagioclase; Qz, quartz; Rt, rutile; Sil, sillimanite; St, staurolite; V, H₂O vapour; and Zo, zoisite. The grey tones of P-T fields are related to the variance (the darker the higher) of the corresponding mineral (+ H₂O) assemblage. Very small P-T fields are not labelled.

All calculations were performed in the Mn-Na-Ca-K-Fe-O₂-Mg-Al-Si-H-Ti system neglecting the O₂ buffers qfm and mthm and the abbreviated endmember phases ab (low-albite), mic (microcline), and ann1 (component in biotite) in the applied data file. The components tip and tbi (Ti end-members in micas) were ignored because of their untrustworthiness (see discussion in Massonne et al., 2018).

Thus, the applied biotite solid-solution model is identical to the former Bio(HP) model (Powell and Holland, 1999) used in earlier versions of PERPLE_X. The XRF composition was slightly simplified (Table 4.1) to fit the 11-component model chemical system: (1) CaO was somewhat reduced according to little phosphorus in the rock and the assumption that this element including Ca is bound exclusively to (ideally composed) apatite. (2) The H₂O content for the pelitic composition was increased to 3 wt.% to permit the saturation with a free hydrous fluid phase at relatively low temperatures. This free fluid phase exists in metapsammopelites at here relevant P-T conditions because of the formation of garnet resulting in a continuous, albeit not uniform, release of H₂O with increasing temperature (e.g., Massonne, 2016a). The option in PERPLE_X to undertake calculations with H₂O in excess was not used because otherwise the H₂O content in solids and, thus, the release of H₂O during prograde metamorphism could not have been easily presented by isopleths (see below). (3) An O₂ content to consider ferric iron was neglected because (i) magnetite is absent, (ii) the amount of ferric iron in minerals is low, and (iii) rutile + ilmenite (\pm pyrite) indicate low redox conditions (Diener and Powell, 2010; Groppo et al., 2010).

Another P-T pseudosection was calculated with 0.06 wt.% O₂ (Table 4.1) related to 10% of the iron being trivalent (Fig. 4.5b) to test the influence of enhanced Fe³⁺ contents in the bulk rock. Calculations with lower water contents (e.g., 1.5 wt.%) than 3 wt.% and some O₂ were also undertaken to eventually better understand the relations at a late metamorphic stage when H₂O, released by prograde metamorphic reactions, has left the system (see, e.g., Massonne et al., 2018).

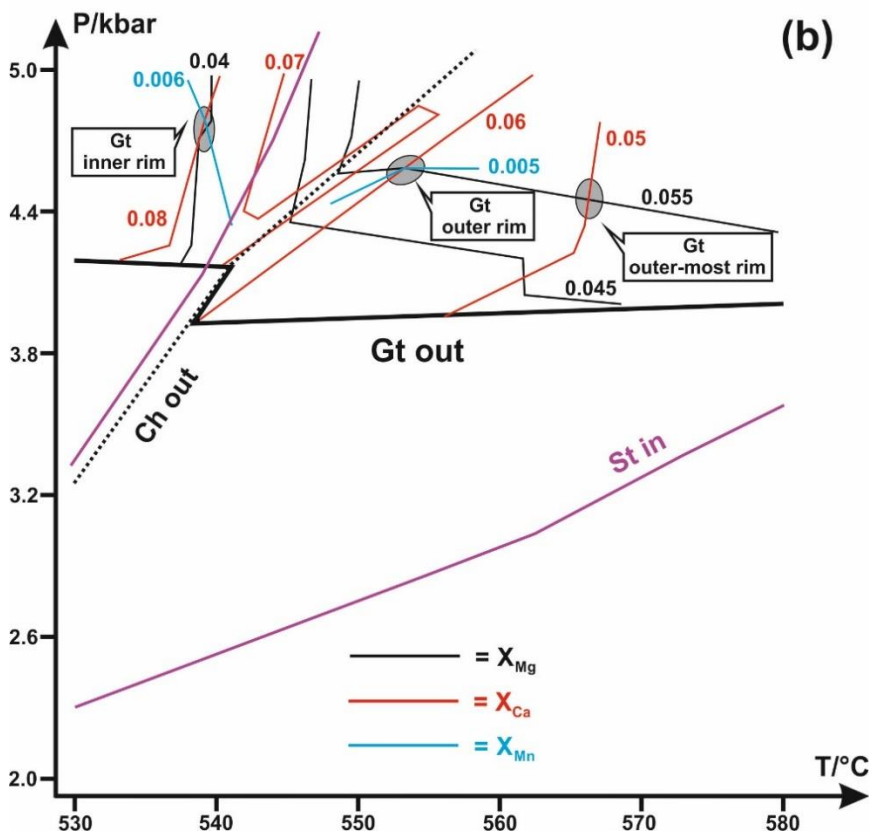
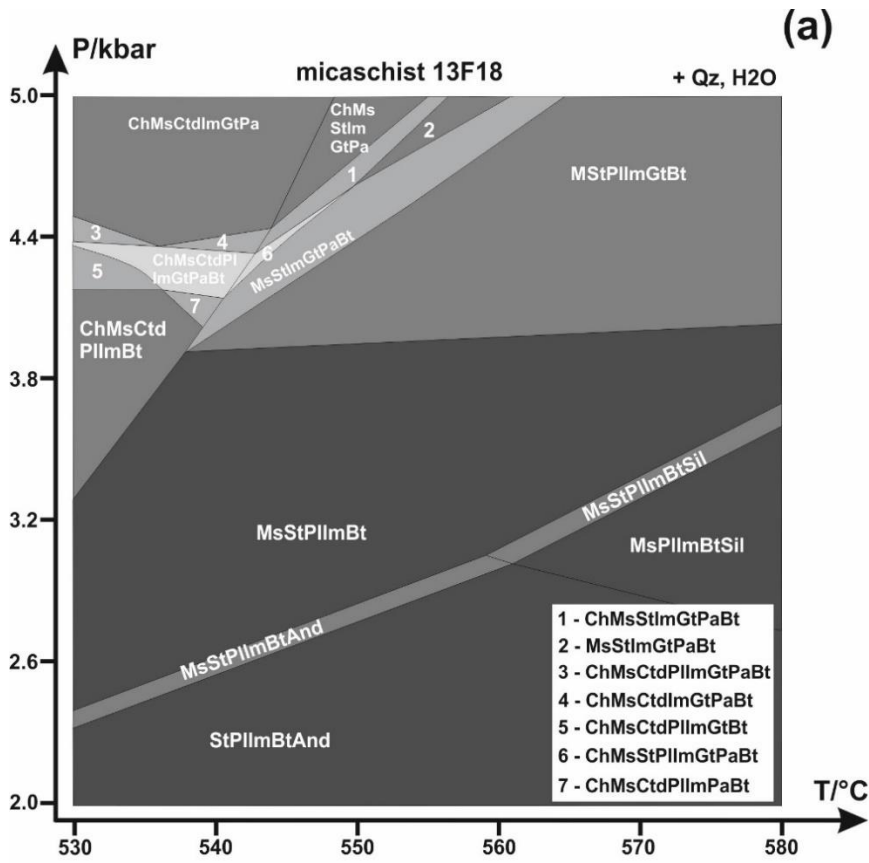


Fig. 4.6. (a) P-T pseudosection calculated for the effective bulk rock composition M4 (Table 4.1) to model the formation of the garnet rim; and (b) Mineral boundaries and P-T conditions (ellipses) for the growth of the garnet inner and outer rim for metapelite 13F18 derived mainly on the basis of various garnet isopleths. Abbreviations as in Fig. 4.5.

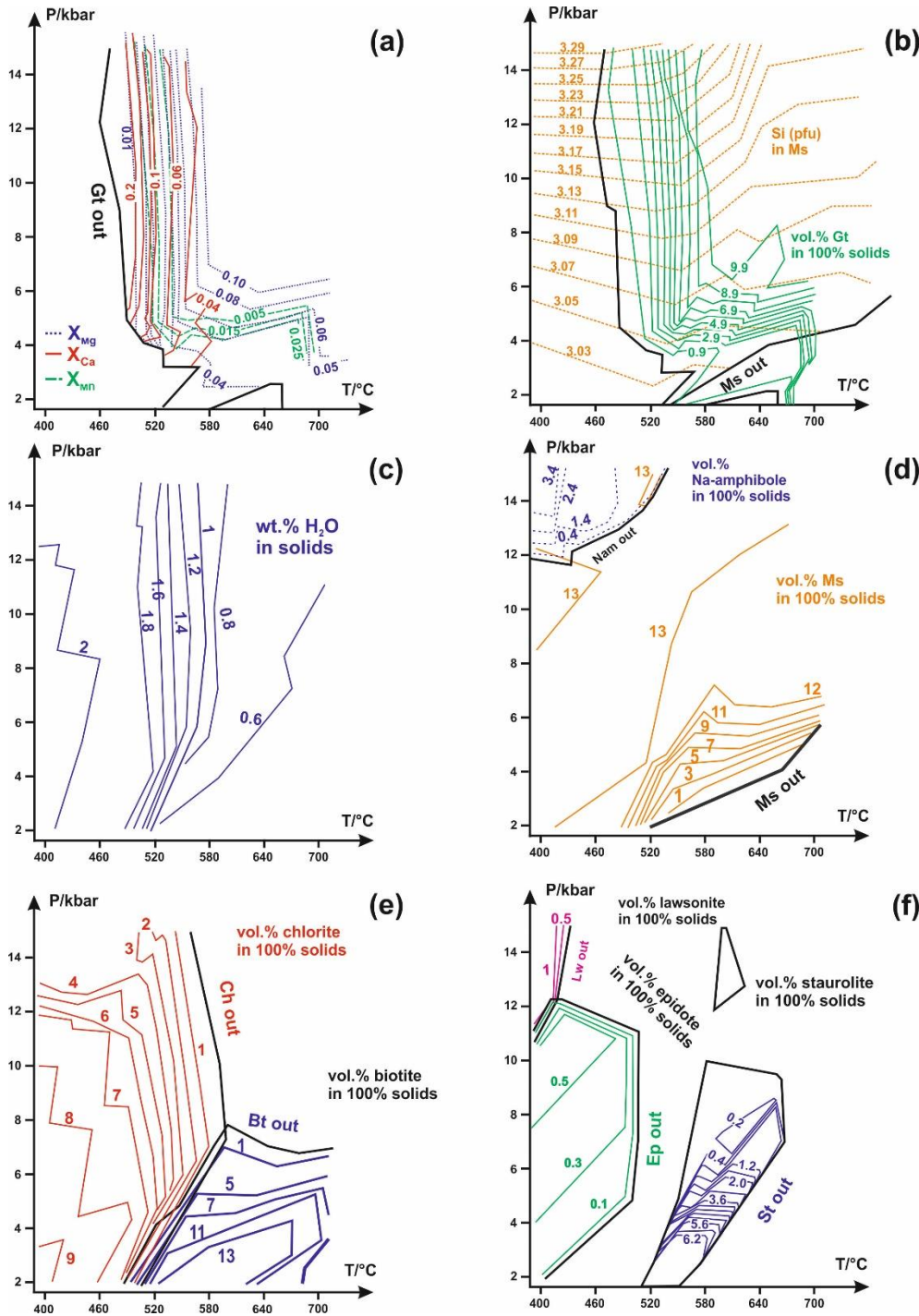


Fig. 4.7. Contouring of the P-T pseudosection of Fig. 4.5 was undertaken by isopleths for, (a) molar fractions of Ca, Mn and Mg in garnet (Gt); (b) the Si content (pfu) in potassic white-mica (Ms) and the modal content of garnet; (c) contents of H₂O bonded to solids; (d, e) Modal contents of potassic white-mica (Ms), Na-amphibole (Nam), chlorite (Ch) and biotite (Bt); and (f) those of epidote (Ep), and lawsonite (Lw). Mineral boundary lines were taken from Fig. 4.5.

In order to approach the effective bulk rock composition for a late metamorphic stage at which the garnet rim formed, we subtracted the chemical composition of the garnet core + mantle (intermediate garnet composition) from the bulk rock composition (see, e.g., Groppo and Rolfo, 2008; Marmo et al., 2002) according to the following strategy: The percentage of the volume (corresponding to the area) of the garnet core + mantle with respect to the whole garnet was roughly estimated from X-ray maps of garnet (see, Fig. 4.3a-e). Considering the garnet modal content in the rock, the garnet core + mantle volume amounts to 4 vol.%. Afterwards, the average chemical composition of the garnet core + mantle was calculated, based on the performed EMP analyses (see below), multiplied with 0.04, and subtracted from the bulk rock composition of sample 13F18.

The result of this procedure after addition of H₂O and normalization to 100% (O₂-free system) is given in Table 4.1. The calculated P-T pseudosections were contoured by isopleths of various garnet parameters (molar fractions of garnet components, modal content). We also calculated the P-T position of isopleths for the Si content in potassic white-mica. The final graphs were obtained by smoothing the calculated curves as demonstrated by Connolly (2005).

4.5.2. P-T pseudosection

The calculated P-T pseudosections for metapelite 13F18 (Figs. 4.5, 4.6; compositions M1, M2, and M4 of Table 4.1) show a relatively high number of P-T fields for different phase assemblages with quartz being ubiquitous. As no melt model was considered in the calculations of these pseudosections, the phase relations in the pseudosections are metastable with respect to melt at temperatures close to 700 °C (cf. the calculated solidus in Fig. 4.5b). Potassic white-mica is the only mineral phase (except quartz) that appears over almost the entire P-T range. This phase is only absent at pressures below 4 kbar and temperatures above 580 °C; instead, K-feldspar occurs. Comparing the pseudosections for the bulk rock with H₂O in excess and with and without Fe³⁺, the P-T pseudosection considering 0.06 wt.% O₂ (Table

4.1) resulted in significant modal contents of clinozoisite-epidote, the only silicate that can introduce Fe^{3+} in the PERPLE_X modelling according to the selected solid-solution models (Fig. 4.5b).

These pseudosections indicate: (1) A lower pressure limit of 12 kbar at temperatures below 530 °C exists for amphibole, which is rich in Na (Fig. 4.5b). (2) The upper temperature limit for chlorite is at about 600 °C. (3) This limit for clinozoisite is at c. 500 °C. (4) For the pseudosection calculated for 10% of iron being trivalent hematite appears only at higher pressures, whereas magnetite occurs at lower pressures (Fig. 4.5b). (5) Rutile occurs in a small P-T field close to 400 °C and 2 kbar, but mainly at high pressures (≥ 10 kbar in the system without Fe^{3+} ; Fig. 4.5a, ≥ 12 kbar with 10% of Fe being Fe^{3+} ; Fig. 4.5b).

Ilmenite is the low- and medium pressure Ti phase. (6) Biotite is absent at temperatures below 500 °C and at pressures above 8 kbar. (7) The P-T limit of lawsonite is at 430 °C and pressures ≥ 8.5 kbar (Fig. 4.5a) or ≥ 11.8 kbar (Fe^{3+} , Fig. 4.5b). (8) Omphacite occurs at 530 °C and pressures above 11 kbar (Fig. 4.5b) in the pseudosection for the O_2 -bearing bulk rock composition. (9) For this pseudosection a P-T field of epidote appears in the P-T range 400-520 °C and 2-12.2 kbar (Fig. 4.7f). (10) The temperature minimum for Mn-rich garnet is 490 °C (at HP conditions, see, Fig. 4.5b) in the pseudosection with O_2 and 460 °C in the Fe^{3+} -free pseudosection (Fig. 4.5a). (11) Chloritoid occurs over a significant temperature range from 400 to 510 °C at 2 kbar or to 610 °C at 15 kbar. (12) Kyanite appears only in a small P-T area ranging from 7.2 kbar and 660 °C to 15 kbar and 700 °C; sillimanite occurs at $T \geq 565$ °C below 8 kbar; a small P-T field of andalusite is present below 2.8 kbar (520-620 °C). (13) Staurolite occurs in the pressure range of 2-15 kbar at temperatures above 510 °C.

The calculations with significantly lower water contents than 3 wt.% and some O_2 resulted in minor changes of the pseudosection topology with no significant changes in relevant phase-in boundaries (e.g., cordierite-in; K-feldspar-in) unless relatively low water amounts of 1.5 wt.% H_2O are used, stabilizing K-feldspar (not observed in the rock) in subsolidus assemblages. The P-T field of garnet was contoured (Fig. 4.7a) by isopleths for the molar fractions X_{Ca} , X_{Mg} , and X_{Mn} of this mineral. Typically, X_{Mg} increases and X_{Mn} and X_{Ca} decrease with rising temperature at higher pressures. The modal amount of garnet (Fig. 4.7b) increases with rising temperature at high pressures but also with rising pressure at temperatures in excess of 640 °C. Maximum calculated garnet contents in the Fe^{3+} -free system are close to 9 vol.% neglecting the fluid phase. The calculated Si contents of potassic white-mica typically increase with rising pressure and vary between 3.03 and 3.29 pfu in the selected P-T range (Fig. 4.7b). A significant loss of water (~ 0.6 wt.%) bonded to solids occurs at temperatures between 530 and 580 °C

(Fig. 4.7c), especially in the pressure range 4-12 kbar, due to the formation of considerable quantities of garnet (Fig. 4.7b) from hydrous minerals such as chlorite and lawsonite.

The calculated content of potassic white-mica is around 14 vol.% except in P-T ranges for which considerable quantities of biotite were calculated (Fig. 4.7d, e). The P-T range with > 10 vol.% of biotite is at relatively low pressures and high temperatures. The maximum content of epidote in the Fe³⁺-bearing pseudosection is 0.5 vol.%. The highest content of staurolite in this pseudosection is 6 vol.%, which was calculated for 2.3 kbar at temperatures around 520 °C (Fig. 4.7f). This maximum content is 7 vol.% at P-T conditions of 530 °C and 2.3 kbar for the Fe³⁺-free pseudosection.

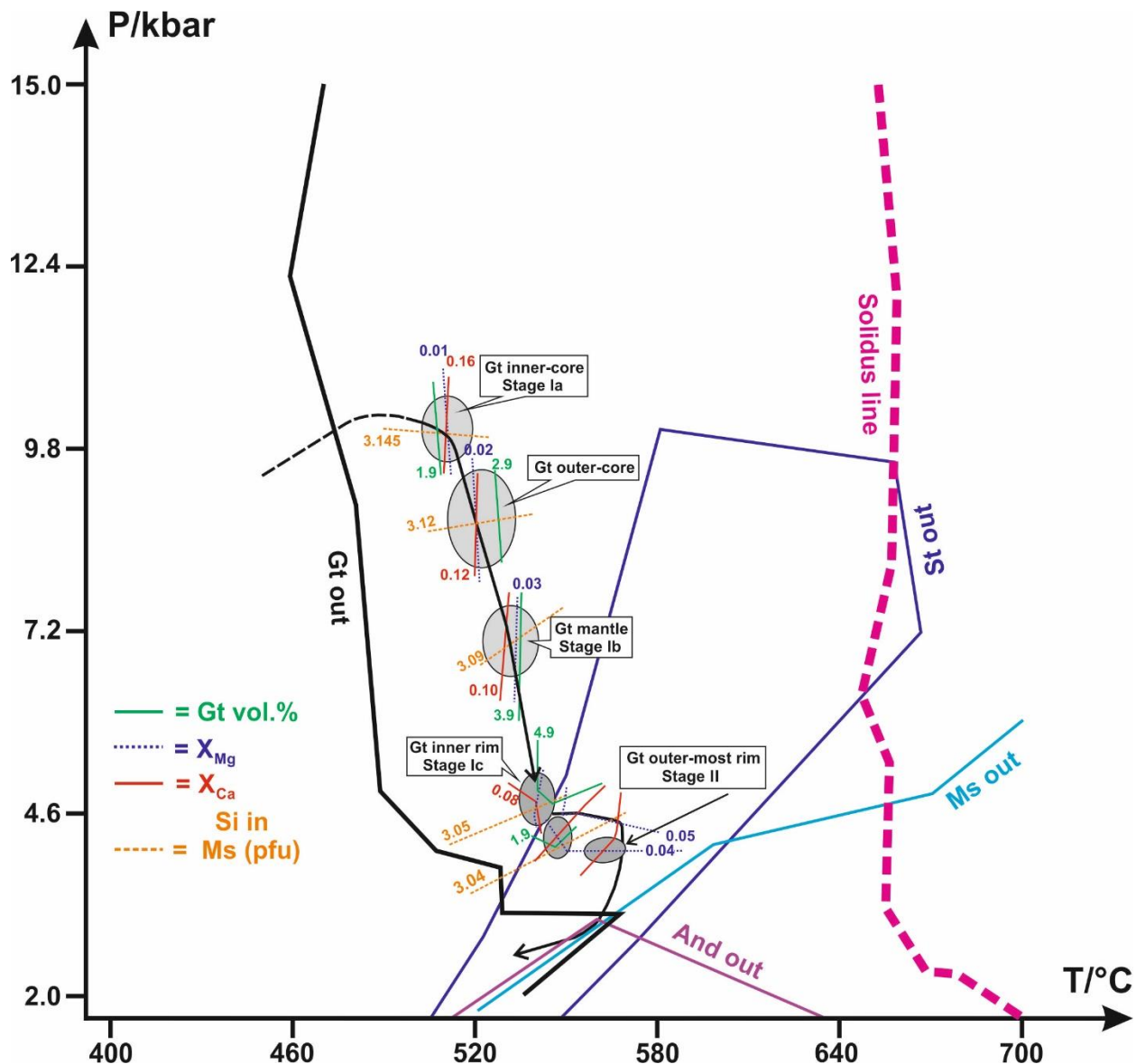


Fig. 4.8. P-T path for metapelite 13F18 derived on the basis of the various isopleths (exemplary shown by solid and dotted lines) for garnet and potassic white-mica (Ms) displayed in Fig. 4.7. Light grey ellipses mark the P-T conditions from the beginning of garnet growth (stage Ia) to the formation of the outer-most garnet rim (stage II) using bulk rock composition M4 (Table 4.1). The darker ellipses refer to the inner, outer and outer-most rim considering the effective bulk rock composition (Fig. 4.6). The P-T conditions of the subsequent retrograde path are compatible with the presence of staurolite and andalusite. The different size of the ellipses is related to the roughly estimated P and T errors as explained in the text. Abbreviations as in Fig. 4.5.

4.5.3. P-T path

For the construction of the P-T path of metapelite 13F18 we mainly used the changing muscovite and garnet compositions from core to rim and the P-T pseudosection for the Fe³⁺-free bulk rock composition. As Si-rich muscovite was observed to be enclosed in garnet (Fig. 4.4b, c), this mica was probably formed before or during early crystallization of garnet. If we assume that to the Si-richest muscovite (3.145 Si (pfu), average of 3 analyses) and the Mg-poorest garnet ($X_{Ca} = 0.16$, $X_{Mg} = 0.01$, Figs. 4.3a-e and 4.4a, Table 4.2) coexisted, stage Ia occurred at 10 kbar and 505 °C (see the isopleth diagrams of Fig. 4.5a, b). The errors of these quotations were roughly estimated to ± 0.4 kbar and ± 12 °C which might correspond to 1σ ranges in accordance to general error estimates, for instance, by Essene (1989) and Massonne (2013). Our roughly estimated errors are generally shown by ellipses drawn in Fig. 4.8 as proposed by Li and Massonne (2018).

At the derived HP conditions (10 kbar, 505 °C), accessory contents of ilmenite (~ 0.5 vol.%) and rutile were calculated to have coexisted with garnet, potassic white-mica, quartz, chlorite (7.2 vol.%), chloritoid (3.1 vol.%), and paragonite (3.5 vol.%). Epidote appears as accessory phase (~ 0.1 vol.%) in the calculation with the O₂-bearing bulk rock composition whereas zoisite appears only at P-T conditions lower than 10.5 kbar and 505 °C in the O₂-free system. If epidote was once present in the rock, it broke already down during an early stage of the subsequent pressure release to 7 kbar and 535 °C. At these conditions, reconstructed by intersecting garnet isopleths of $X_{Ca} = 0.10$ and $X_{Mg} = 0.03$ (additional intersections due to other garnet and muscovite compositions occur, e.g., at 9 kbar and 520 °C, see Fig. 4.7a), the intermediate zone of garnet (= mantle) had completely formed. Along the path from 10 to 7 kbar, the calculated modal content of garnet had increased to ~ 5 vol.%. The calculated mineral assemblage at 7 kbar and 535 °C contains still some chloritoid (1.9 vol.%) and chlorite (~ 4 vol.%).

In addition, minor biotite (< 1.5 vol.%) and paragonite (< 2.5 vol.%) was calculated to coexist with garnet, quartz, and Si poor (3.09 pfu) potassic white-mica. The P-T pseudosection for the effective bulk rock composition (after subtraction of the garnet core + mantle), constructed for the P-T range 530-580 °C and 2-5 kbar, was used to decipher the conditions for the late metamorphic stages (Ic and II) of the micaschist (Fig. 4.6). We received reasonable intersections of the isopleths for the molar fractions of grossular (+ andradite) and pyrope of the inner ($\text{Sps}_{0.6}\text{Pyp}_4\text{Grs}_{8.4}\text{Alm}_{87}$) and outer garnet rim domain ($\text{Sps}_{0.5}\text{Pyp}_{5.5}\text{Grs}_5\text{Alm}_{89}$) at 4.6-4.9 kbar, 535-540 °C and 4.4-4.6 kbar, 550-555 °C, respectively. The P-T conditions for the outermost rim ($\text{Sps}_{0.5}\text{Pyp}_{5.5}\text{Grs}_5\text{Alm}_{89}$) are 4.5 kbar and 565 °C (stage II, Fig. 4.8). These conditions are compatible with the presence of staurolite (calculated contents close to 5 vol.%), the absence of melt (Fig. 4.8) and the calculated Si content of potassic white-mica of 3.04 pfu.

During the metamorphic evolution from 7 to 4.5 kbar, paragonite, chloritoid, and chlorite disappeared according to the pseudosection modelling. The calculated content of biotite has increased to 11 vol.% (observed 8-10 vol.%, see above). In addition, some plagioclase has formed (calculated content: ~ 3 vol.%, observed: around 1.5 vol.%).

4.6. Monazite dating

Monazite, $(\text{Ce,Lu})\text{PO}_4$, is frequently used to date igneous and metamorphic rocks because it preferentially incorporates ThO_2 (e.g., Overstreet, 1967), sustains little radiation damage (e.g., Meldrum et al., 1998) and remains relatively impervious to Pb loss at high crustal temperatures (e.g., Smith and Giletti, 1997). In combination with geothermobarometry based on garnet and phengite, monazite in-situ dating with the EMP is a powerful tool to ascertain the evolution of metamorphic terranes (e.g., Massonne, 2014, 2016b). We found monazite in different microstructural positions in sample 13F18 (Fig. 4.9) using back-scattered electron (BSE) images. This mineral with anhedral to subhedral elongated to oval shape is common in both phyllosilicate- and quartz-rich domains of the matrix, but was rarely observed in garnet and plagioclase. The size of monazite grains, which are frequently significantly corroded, usually varies between 5 and 30 μm , but grains as large as ~ 50 μm (Fig. 4.9d) also occur.

The obtained monazite ages range between c. 200 and 480 Ma evaluating 168 monazite analyses after discarding those with totals below 97 wt.% or too high SiO_2 contents (> 0.9 wt.%) which frequently resulted from analyses of grains < 10 μm (Fig. 4.10d, e).

The probability density plot (Fig. 4.10d) shows an accumulation of ages between about 300 and 390 Ma. In the fitted curve obtained by histogram analysis with the Isoplot program (Ludwig, 1999), different age groups are proposed. However, the number of populations (10) discernable by age maxima and side maxima (at 203, 231, 275, 301, 324, 362, 385, 405, 437, and 472 Ma) might be exaggerated (Fig. 4.10e). In an attempt to use the chemical composition of monazite as a criterion to discriminate between several monazite populations, we arbitrarily subdivided the monazite analyses into three rough age populations: (i) younger than 300 Ma (31 ages yielding a mean age of 270 Ma), (ii) ranging from 300 to 360 Ma (100 ages yielding a mean age of 328 Ma) and (iii) older than 360 Ma (37 ages yielding a mean age of 390 Ma). BSE images of larger grains demonstrate moderate chemical zonation with high Y concentration in the apparent core and an inverse correlation with Th (Fig. 4.9d-f). Chemically different monazite is exemplarily shown in Table 4.4. The ThO₂ contents of monazite scatter around the average of ~ 4.5 wt.%. All monazite grains show La/Gd (pfu) ratios < 17 and Y₂O₃ contents > 0.3 wt.% (Fig. 4.10a). However, only the older populations (ages > 360 Ma) exhibit somewhat lower ThO₂/UO₂ (wt.%) ratios (mean: 6.07) than the younger populations (means: 6.34 for 300-360 Ma and 7.14 for < 300 Ma) in Fig. 4.10b.

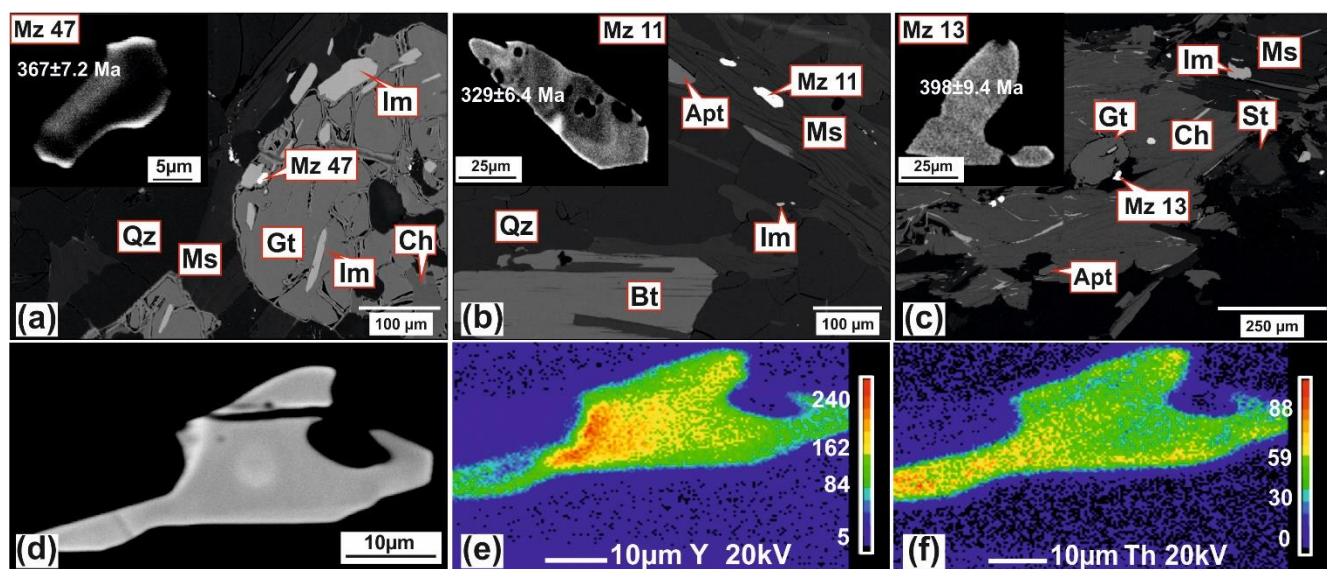


Fig. 4.9. Textural positions of selected monazite (Mz) shown by BSE images, (a) Mz 47 included in the garnet rim; (b) Mz 11 in white-mica; and (c) Mz 13 completely shielded by matrix chlorite. U-Th-Pb ages with 2σ errors (see Table 4.4) are reported. (d, e, f) BSE image and Th, Y chemical maps of a selected monazite. Note the discontinuous high-Y core. Apt, apatite; Mz, Monazite. Abbreviations as in Fig. 4.5.

4. Pressure-temperature-time evolution ...

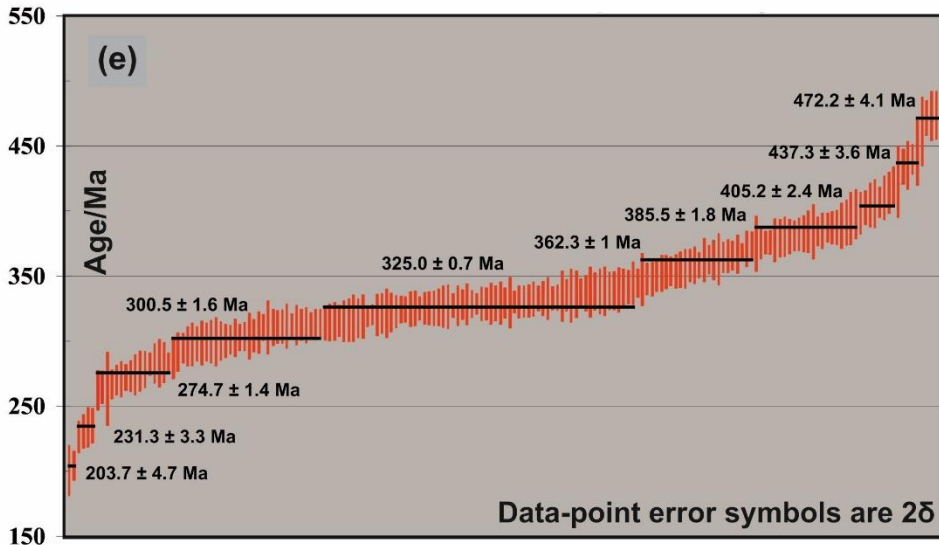
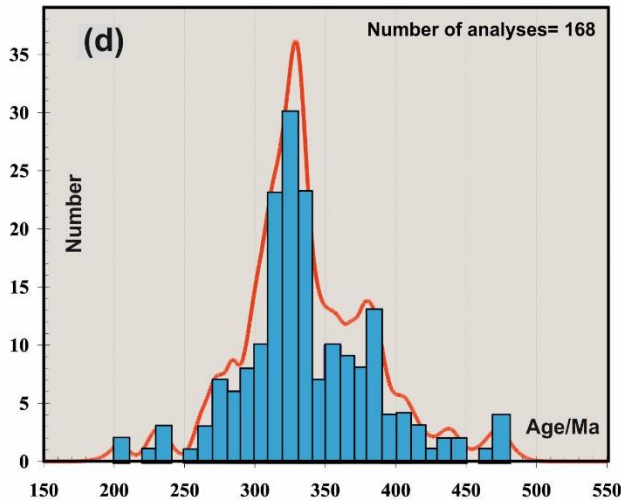
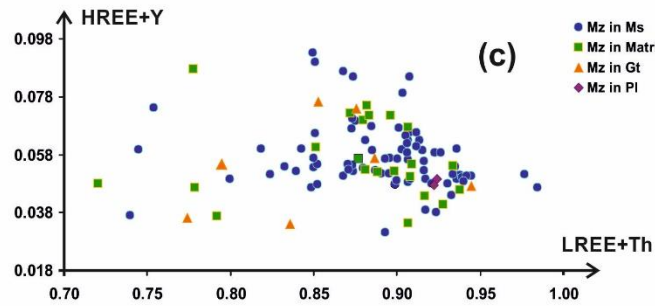
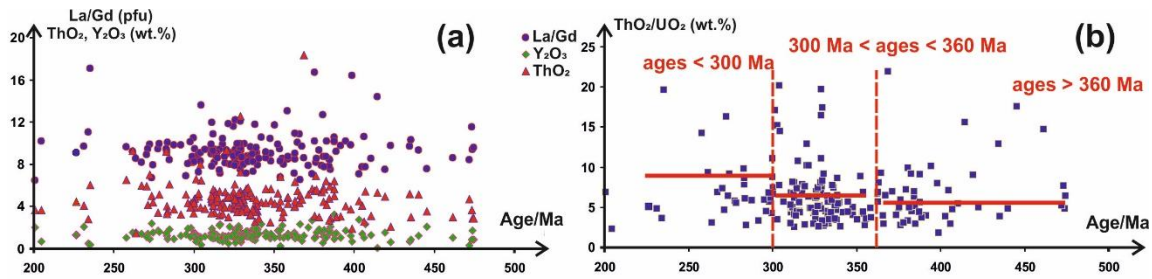


Fig. 4.10. Monazite chemical variation and ratios of rare earth elements REE versus age (Ma), (a) La/Gd (pfu) ratios, ThO₂ and Y₂O₃ contents in wt.% versus age (Ma); (b) ThO₂ to UO₂ (in wt.%) ratios versus age (Ma) with three mean values for the groups of ages; (c) Heavy rare earth elements (HREE) + Y versus light rare earth elements (LREE) + Th in monazite of different domains; (d) Probability density plot using Isoplot; and (e) Weighted average plot showing U-Th-Pb ages with 2 σ errors (red bars) and populations with average age (black bars) and 2 σ error.

Since the monazite HREE + Y budget in metapelites is largely controlled by garnet crystallization (e.g., Foster and Parrish, 2003; Spear and Pyle, 2010), the observed HREE + Y variations can be linked to garnet growth or resorption. Monazite grains enclosed in white-mica (Table 4.4, Fig. 4.10c) show an average value of heavy rare-earth elements (HREE) + Y (Y₂O₃: ~ 1.3 wt.%) with variable Th contents that are only somewhat lower than that of the matrix hosted grains (average 1.44 wt.% Y₂O₃) with generally lower contents for Th (average 4.8 wt.% ThO₂). Monazite included in garnet and plagioclase shows still lower HREE + Y contents (average 1.20 and 0.98 wt.% Y₂O₃, respectively, Fig. 4.10c).

4.7. Discussion

4.7.1. The metamorphic P-T evolution

The earliest metamorphic stage, recorded by the studied gneissose micaschist, is characterized only by the garnet inner core and relictic phengitic muscovite (average of 3.145 Si pfu), that was also found to be enclosed in garnet. P-T conditions of ~ 10 kbar and 505 °C (stage Ia) result when using these mineral compositions. The prograde metamorphic evolution before reaching stage Ia is probably characterized by a burial path outside the P-T field of garnet (Fig. 4.8).

The first garnet did not form immediately after crossing the “garnet-in” curve, but at stage Ia because of kinetic factors (energetic barriers) outlined by Spear (2017). At stage Ia, the predicted assemblages included ilmenite, rutile, quartz, chlorite, chloritoid, and paragonite (+ 0.1 vol.% of epidote in the O₂-bearing system). The latter two minerals do not occur in the rock because they were completely decomposed during subsequent prograde metamorphism as also predicted. Chlorite is present in the rock, but according to the observed textural relations, it should be exclusively a late stage mineral, so that its composition could not be used to refine the determined P-T conditions for stage Ia. The subsequent metamorphic evolution (stages Ib, c), accompanied by garnet growth and re-growth probably of stressed white-mica flakes, is characterized by a pressure release down to 5 kbar and slightly rising temperatures

to 535 °C. At these conditions still some paragonite and chloritoid had survived the prograde evolution according to the calculation result with an effective bulk rock composition (see Fig. 4.6).

However, the subsequent temperature increase to 565 °C at slightly decreasing pressure to 4.5 kbar (stage II) resulted in the complete decomposition of these minerals, including partial replacement of the garnet rim and of potassic white-mica by staurolite and biotite, respectively. We assume that this temperature increase was caused by the emplacement of large post-tectonic granite bodies in the FC. This interpretation is compatible with the crystallization level of the granites, which are presently exposed at the surface, at c. 15 km depth (4.3 kbar; Massonne, 1984). Andalusite could have been already metastably grown instead of sillimanite at the conditions of 4.5 kbar and 565 °C or even somewhat higher temperatures, which could not be verified because of the replacement of garnet (our P-T indicator). Alternatively, andalusite could have grown during early retrogression, for instance, at 3 kbar and 545 °C (Fig. 4.6a).

Although it might be possible that (only) mm-sized porphyroblast of andalusite can grow in a metamorphic rock by a fluid-mediated event triggered by the emplacement of nearby granitic magmas, we prefer the idea of metastable growth of andalusite with respect to fibrolitic sillimanite as advocated in the literature (e.g., Hodges and Spear, 1982; Holdaway, 1971; Pattison, 1992) already for a long time. The formation of relatively large fans of chlorite flakes, overgrowing the deformational fabric, and of small unoriented muscovite, with Si contents close to the ideal value of 3.00 pfu (Fig. 4.3f, g), around andalusite must be due to a late retrograde event probably at pressures ≤ 2 kbar (Fig. 4.5). The derived P-T path (Fig. 4.8) for the metamorphic evolution of garnet-bearing metapelite in the FC close to Selb is apparently incompatible with previously estimated metamorphic pressures (Mielke et al., 1979; Okrusch et al., 1990) of 3.5-5.5 kbar.

In addition, Mielke et al. (1979) and Mielke and Abraham (1980) suggested also somewhat higher temperatures of 580-640 °C for the staurolite-almandine-andalusite zone in the Fichtelgebirge, than found here. Mielke et al. (1979) reported, in fact, potassic white-mica analyses (Si = 2.95-3.47 pfu probably with the latter Si content being the result of additional quartz analysed) but considered only index minerals, such as chloritoid and garnet, and the minimum melting of granite for their P-T estimates.

The earlier researchers did not have the tools as applied in this work to decipher the HP event and were probably not aware of such an event as well. But the P-T conditions, for instance, derived by Mielke et al. (1979) for the final metamorphic event at low pressures, are compatible with our results.

Table 4.4. Representative EMP analyses of monazite in five different textural domains, recalculated on the basis of 4 O. (oxides in wt.%). Abbreviations as in Fig. 4.5.

Grain	Mz11	Mz13	Mz47	Mz25	Mz16
Textural position	In Ms	In Matrix	In Gt	In Bt	In Pl
SiO ₂ (wt.%)	0.24	0.85	0.23	0.80	0.43
P ₂ O ₅	28.65	29.29	28.30	28.46	28.15
SO ₃	0.01	0.00	0.00	0.00	0.01
CaO	0.94	0.73	1.07	1.31	1.35
Y ₂ O ₃	1.15	1.20	1.72	1.53	0.95
La ₂ O ₃	13.19	13.25	13.80	12.20	12.63
Ce ₂ O ₃	29.30	28.99	28.35	27.33	28.19
Pr ₂ O ₃	3.07	3.09	2.94	2.93	3.01
Nd ₂ O ₃	11.78	11.83	11.74	11.15	11.65
Sm ₂ O ₃	2.24	2.29	1.76	2.21	2.26
Gd ₂ O ₃	1.54	1.51	1.35	1.61	1.55
Dy ₂ O ₃	0.58	0.54	0.45	0.61	0.50
PbO	0.1047	0.0884	0.1079	0.1567	0.1188
ThO ₂	4.53	3.72	4.61	5.91	7.99
UO ₂	0.94	0.46	0.71	1.15	0.40
Total	98.26	97.85	97.13	97.34	99.19
Si (pfu)	0.0098	0.0416	0.0111	0.0321	0.0173
P	0.9785	0.9797	0.9568	0.9709	0.9626
S	0.0003	0.000	0.0001	0.0000	0.0002
Ca	0.0406	0.0311	0.0554	0.0567	0.0584
La	0.1963	0.193	0.2112	0.1813	0.1881
Ce	0.4328	0.4194	0.4325	0.4032	0.4168
Pr	0.0451	0.0445	0.052	0.043	0.0443
Nd	0.1697	0.167	0.1687	0.1605	0.1681
Sm	0.0311	0.0312	0.0294	0.0307	0.0315
Y	0.0246	0.0253	0.0185	0.0327	0.0204
Gd	0.0206	0.0197	0.0218	0.0215	0.0207
Dy	0.0075	0.0069	0.007	0.008	0.0065
Pb	0.0011	0.0009	0.0014	0.0017	0.0013
Th	0.0415	0.0334	0.0509	0.0542	0.0734
U	0.0084	0.0041	0.0076	0.0103	0.0036
Age (Ma)	329.0	398.0	367.2	384.7	304.1
2δ error (Ma)	6.4	9.4	7.2	5.6	5.4
La/Gd (pfu)	9.53	9.80	9.69	8.43	9.09

4.7.2. Geological interpretation of the new data

As no reasonable chemical discrimination in monazite was noted using La/Gd and ThO₂/UO₂ ratios and Y₂O₃ and ThO₂ contents (Fig. 4.10a, b), the interpretation of the obtained age clusters is difficult. Therefore, we strongly considered age information of the nearby granite intrusions and other medium-high grade metamorphic rocks from the MMC, FC, and EC (see, section Geological setting). Extended age variations are common in medium- to high grade metamorphic monazite (e.g., Foster et al., 2000, 2002; Li and Massonne, 2017; Martins et al., 2009; Palin et al., 2014; Rubatto et al., 2013). In fact, they can be due to mixed analyses of different monazite domains, but a successive growth during the entire metamorphism is more likely (Taylor et al., 2016). Therefore, we interpret the range between c. 200 and 480 Ma of all obtained monazite ages as follows: (1) Monazite ages below about 315 Ma are due to the influence of the emplacement of granites and later fluid interactions. (2) Monazite with ages older than about 395 Ma (age maxima: 405, 437, 472 Ma) can be assigned to the provenance area with late Cadomian and post-Cadomian magmatic arcs situated at the northern margin of Gondwana (or Peri-Gondwanan terranes) following Waizenhöfer and Massonne (2017) who had studied a nearby metasediment from the MC. When we relate the age maximum of 385 Ma (Fig. 4.10d, e) also to the provenance area, monazite could have been deposited in the sedimentary protolith of the studied micaschist in the Late Devonian. However, we favour the view that the maxima at 325, 362, and 385 Ma obtained by histogram analysis can be related to regional metamorphism. Unfortunately, the onset of garnet growth as a result of prograde metamorphism is not discernable by a drop of the HREE + Y contents in monazite as noted in similar studies on micaschists (Massonne, 2016b).

The reason, why Y₂O₃ contents in monazite are frequently above 1 wt.% over the entire age spectrum from 200 to 480 Ma, is probably due to a dissolution-precipitation process (Engi, 2017; Harlov et al., 2011; Williams et al., 2011), i.e., the chemical signature (except Pb) from an older monazite domain was, after partial dissolution, directly adopted from the newly grown monazite domain. The Upper Devonian ages (age peaks at 385 and 362 Ma) are compatible with zircon ages related to metamorphism in the nearby MC, zone of Erbendorf-Vohenstaub, and Mariánské Lázně complex (see, Fig. 4.1, section Geological setting, and Willner et al., 2000). In addition, HP metamorphism occurred in these crystalline complexes at that time. In analogy, we relate the peak pressure conditions of 10 kbar, identified in the studied rock, to an Upper Devonian event which would refer to the deep burial of Lower to Middle Devonian clastic sediments below an upper continental plate at the end of the complete closure

of the Rheic Ocean. According to recent plate reconstructions for the here relevant period of time, the upper continental plate in this scenario would be Avalonia, a peri-Gondwanan terrane being attached to Laurussia already in Silurian times (see, Li et al., 2017; Willner et al., 2013; Zeh and Will, 2010). The exhumation of the studied rock to depths of 15-20 km ($P \sim 4.5\text{-}5$ kbar) has ended at an age of 362 Ma which would be compatible with Ar-Ar cooling ages of c. 360 Ma and somewhat younger obtained for HP rocks of the SZ (Faryad and Kachlík, 2013).

Exhumation paths from HP conditions accompanied by slight heating, as reconstructed here, are typical for rocks which were deposited as sediments at the tip of a down going continental plate, deeply buried during the final subduction of an oceanic crust (see, Cruciani et al., 2013; Massonne and Calderón, 2008; Massonne and Toulkeridis, 2012), and then exhumed in an exhumation channel (Massonne, 2016a, 2016b). In addition, significant deformation in the exhumation channel, discernable by rotation of garnet during its growth in the studied rock, seems to be another characteristic for such HP rocks. In our case, the differential stress had increased during the final stage of garnet growth (see above) and, thus, of the exhumation to depths of 15-20 km. The dominant age peak at 325 Ma is assigned to the slight heating to 565 °C (or slightly more) at low pressures between 4.0 and 4.5 kbar (Fig. 4.8) being compatible with the inference that the FC underwent low pressure metamorphism in the time interval 330-320 Ma (Okrusch et al., 1990). According to our interpretation this metamorphic event can be related to the transport of a pile of crystalline nappes over the low grade metapsammopelites with intercalated acidic metavolcanics outcropping north of our sample locality as equivalents of Cambro-Ordovician sediments of the Thuringian lithofacies.

This event at the turn from the Early to the Late Carboniferous has probably already started with the collision of Gondwana and a northerly situated peri-Gondwanan terrane. Before this collision an ocean (e.g., Saxothuringian Ocean following Schulmann et al., 2009) south of the SZ was closed probably at c. 340 Ma, a common age of metamorphic rocks in the Bohemian Massif (Willner et al., 2000). The heating of our gneissose micaschist to c. 565 °C, also leading to the age peak at 325 Ma, should have been caused by post-collisional granitic melts of the older intrusive complex of the FC and, thus, after the crystalline nappe pile was already in place. Alternatively, the peak pressure conditions could have reached at the monazite age cluster around 362 Ma meaning that the derived P-T path was timely more condensed compared to the scenario outlined afore. If one of the scenarios, which relate the HP metamorphic event either to 362 or 385 Ma, is applicable to paragneisses and micaschists from the EC (Micaschist-Eclogite Unit) and MC, which had experienced similar but somewhat higher peak

pressure conditions of 12-13 kbar (Rötzler et al., 1998; Waizenhöfer and Massonne, 2017) or even 16 kbar (Faryad and Kachlík, 2013), must be left open because a decision cannot be made yet due to lacking age data for these EC and MC rocks.

In this respect, it is of interest that a polymetamorphic event (364 and 335 Ma) in a metasediment, was reported from the Orlica-Śnieżnik Dome in the Sudetes (Jastrzębski, 2010; Jastrzębski et al., 2016) to which Faryad and Kachlík (2013) has extended their Early Variscan suture zone. This metasediment, which had also experienced peak pressures close to 10 kbar, could possibly be related to the same unit as the rock studied here.

4.8. Conclusion

The studied gneissose micaschist from the northeastern FC had experienced a HP metamorphism at about 10 kbar and 505 °C. Exhumation to 15-20 km depths (~ 4.5 kbar) and heating to 565 °C followed. Only the latter event was recognized in previous studies (Mielke et al., 1979; Okrusch et al., 1990). Dating of monazite with the EMP resulted in ages between 200 and 480 Ma. Ages younger than 315 Ma are clearly related to the emplacement of the FC granites and subsequent hydrothermal processes, whereas Lower Devonian to Ordovician ages are assigned to detrital monazite in the former clastic sediment. The age cluster of 384.5 ± 1.8 (2 σ) Ma remains unclear, but we prefer to relate it to the HP metamorphism event instead of a Middle to Late Devonian provenance area. If our view is correct, the age cluster at 362.3 ± 1.0 Ma should correspond to the end of the exhumation to 15-20 km. The age peak at 325.0 ± 0.7 Ma might have caused by post-collisional granitic melts of the older intrusive complex of the FC. These melts had intruded a crystalline nappe pile that might have formed by a second collisional event of Gondwana and the peri-Gondwanan terrane which had been accreted to Laurussia after closure of the Rheic Ocean already in Late Devonian times. According to our interpretation, this event caused the overriding of crystalline nappes of the FC, of which the garnet-bearing micaschist unit of our sample was a lower part of, onto the Laurussian crust.

4.9. Acknowledgements

The authors thank Thomas Theye and Tillman Viefhaus (Stuttgart) for supporting our EMP and Raman microscopy works, respectively.

Note: This chapter was prepared as a manuscript to submit it to the geoscientific journal LITHOS. An improved version of it was published in Lithos 316-317, 366-384.

5. Metamorphic evolution of chloritoid-bearing micaschist from the Variscan Elstergebirge - evidence for stacking of high pressure rocks in the Saxothuringian Zone of central Europe

Abstract

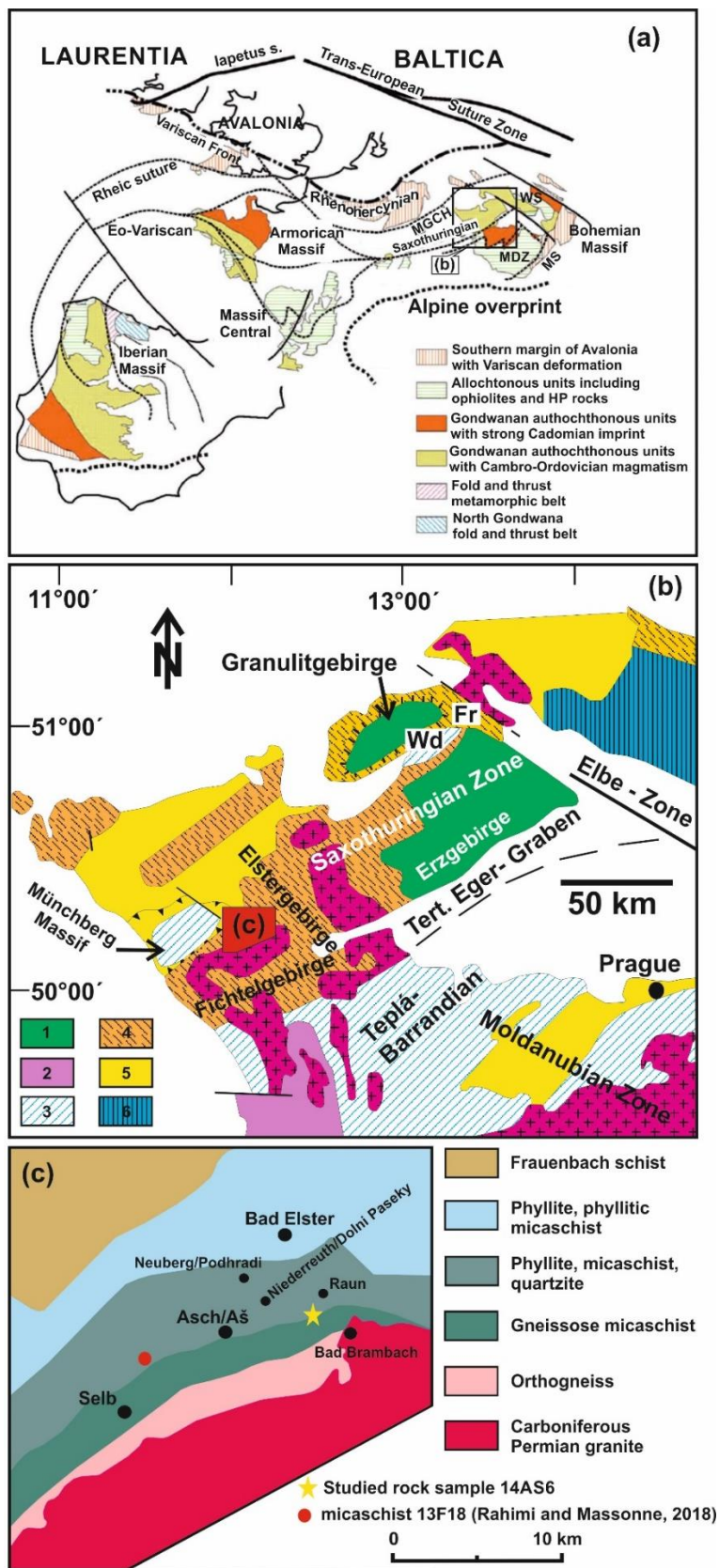
To better understand the evolution of the Variscan orogeny in the Saxothuringian Zone of the northwestern Bohemian Massif, a chloritoid-garnet-bearing micaschist from the southern part of the Elstergebirge was studied. After a careful investigation of the textural relations and compositions of minerals, especially of zoned garnet and potassic white-mica, a P-T path was reconstructed using contoured P-T pseudosections. U-Th-Pb dating of monazite in the micaschist was undertaken with the electron microprobe. This rock was formed along a clockwise P-T path starting at 16 kbar and 505 °C and ending at 5 kbar and 555 °C. Isobaric heating to about 600 °C followed. The monazite ages range between 315 and 480 Ma with the most prominent maxima and side maxima at 346.0 ± 1.1 (2σ), 357.3 ± 2.3 , and 368.3 ± 1.7 Ma. Ages older than 380 Ma were related to detrital monazite pointing to a Devonian sediment as protolith whereas those around 325 Ma were assigned to the isobaric heating by nearby post-tectonic granites. The high pressure event, being the result of the continent-continent collision of Laurussia and Gondwana after closure of the Rheic Ocean, occurred in the late Devonian. The exhumation to 15-20 km (5 kbar) ended probably in the early Carboniferous. We think that the high pressure micaschists from the Fichtelgebirge to the Erzgebirge crystalline complexes form a common nappe within a crystalline nappe pile. This nappe is composed of metasedimentary slices, which experienced different peak pressures, instead of representing a coherent crustal section.

Keywords: Saxothuringian Zone, chloritoid, garnet, monazite dating, Variscan orogeny, P-T path

5.1. Introduction

Significant progress was made in the last decade to better quantify the pressure (P) - temperature (T) - time (t) evolution of medium- to high grade metapelites especially when they have experienced polymetamorphic events (e.g., Gaidies et al., 2006; Massonne, 2014; Likhanova et al., 2015; Li and Massonne, 2018; Massonne et al., 2018a). These rocks frequently contain garnet, potassic white-mica, and accessory monazite. Mainly on the basis of the former rock-forming minerals, which are usually chemically zoned, a P-T path can be constructed using isochemical phase diagrams, called pseudosections (e.g., Johnson and Brown, 2004; Zuluaga et al., 2005; Massonne, 2013). Monazite, approximately $(\text{La,Ce})\text{PO}_4$, introduces relatively large quantities of Th and U (Parrish, 1990), so that much effort has been devoted over the last decades to develop methods for dating this mineral, including thermal ionization mass spectrometry, ion microprobe analysis, and electron microprobe (EMP) analysis (Cocherie and Albarède, 2001; Harrison et al., 2002). Especially the EMP dating was improved to obtain fairly accurate ages for small grains or chemical domains of monazite (e.g., Braun et al., 1998; Kelly et al., 2006; Schulz and Schüssler, 2013; Waizenhöfer and Massonne, 2017). Furthermore, monazite in metamorphic rocks has been shown to be not only a useful geochronometer, but also a sensitive and robust chemical recorder of prograde metamorphic processes and reactions (e.g., Foster et al., 2002; Pyle and Spear, 2003; Kohn and Malloy, 2004). In particular, the coexistence of garnet and monazite, both incorporating significant quantities of Y, allow petrogenetic interpretations upon which chronological relations are based on (e.g., Pyle et al., 2001; Catlos et al., 2002; Yang and Pattison, 2006; Tomkins and Pattison, 2007; Massonne, 2016a).

We have studied such monazite-bearing metamorphic rocks from the Elstergebirge, an area of the Saxothuringian Zone of the Variscan orogen (Fig. 5.1) for which no P-T path was derived so far. Only in adjacent areas, similar micaschists were investigated for their metamorphic evolution (southwesternmost Erzgebirge crystalline complex: Faryad and Kachlík, 2013; northeastern Fichtelgebirge crystalline complex: Rahimi and Massonne, 2018). In both cases, these rocks experienced, in fact, high pressure (HP: ≥ 10 kbar) conditions, but showed a peak pressure difference of 5-6 kbar.



5. Metamorphic evolution of chloritoid-bearing micaschist...

Fig. 5.1. (a) Schematic map of the Variscan Zones in Europe (modified after Franke, 1989; Keppie et al., 2009; Murphy et al., 2009); (b) Geological features of the northwestern Bohemian Massif, based on Willner et al. (2000) and Faryad, (2011) and the location of the studied area (red rectangular). 1) Medium to high grade units including rocks with HP-HT metamorphism around 340 Ma and mineral cooling ages > 320 Ma; 2) Units with LP-HT metamorphic imprint; 3) Medium to high grade units including rocks with HP-HT metamorphism around 400 Ma and mineral cooling ages > 370 Ma; 4) Low grade units (tectonically transposed) of the Saxothuringian and the Sudetes including LT-HP rocks; 5) Unmetamorphosed to very-low grade Upper Proterozoic to Lower Carboniferous sediments (supracrustal units); 6) Medium grade units of the Sudetes and Moravo-Silesian (undifferentiated). Abbreviations: Fr, Frankenberg; MGCH, Mid German Crystalline High; MO, Moldanubian Zone; MS, Moravo-Silesian; Wd, Wildenfelds; WS, West Sudetes; and (c) Simplified geological map of the Fichtelgebirge-Elstergebirge (based on Crender, 1902 and Bernstein et al., 1973) and approximate position of the studied rock.

The micaschists from the Elstergebirge can also contain chloritoid. This mineral in HP micaschists can provide information on P-T conditions in addition to potassic white-mica and garnet as was demonstrated, for instance, by Stöckhert et al. (1997), Rötzler et al. (1998), and Negulescu et al. (2009, 2018). Thus, in order to better understand the evolution of the medium grade HP unit(s) of the Saxothuringian Zone of the Bohemian Massif and its/their geodynamic position in the complex Variscan orogen, a P-T-t path for chloritoid-bearing micaschist of the Elstergebirge was derived.

5.2. Geological background

The northeastern portion of the Variscan orogen is exposed in the Bohemian Massif which is a collage of several basement complexes differing in age and metamorphic evolution (Fig. 5.1a). Traditionally, the Bohemian Massif and portions of the Variscan orogen exposed westerly of it are subdivided into Saxothuringian and Moldanubian Zones (e.g., Zulauf, 1993; Grandmontagne et al., 1994). These terms are still used in recent literature on the Bohemian Massif (e.g., Schulmann et al., 2009; Hajná et al., 2011; Faryad, 2011), which additionally consists of the Moravo-Silesian and Lugian-Sudetian Zones in the east and northeast, respectively.

The Moldanubian Zone is bounded to the north by the Saxothuringian Zone, which is one of the peri-Gondwanan fragments (microplates) of the lithosphere that became incorporated into the central European part of the Variscan orogenic belt (see, e.g., Linnemann et al., 2000). The autochthonous units

of the Saxothuringian Zone, including non-metamorphic nappes (Franke, 1995), represent Cadomian basement composed of Neoproterozoic to Early Cambrian arc-related volcano-sedimentary low grade rock complexes and plutonic bodies, transgressed by Cambro-Ordovician overstep sequences with passive margin signatures. The eastern margin of the Moldanubian Zone was thrust over the Moravo-Silesian Zone, which probably represents the margin of Baltica during the Lower Palaeozoic (Schulmann et al., 2005).

The Saxothuringian Zone of the Bohemian Massif including the Lugian-Sudetian Zone contain blueschist-facies and high grade rocks in several distinct lithotectonic units (Faryad, 2011). The Erzgebirge crystalline complex (Fig. 5.1b) as a well-studied major rock complex of the Saxothuringian Zone of the Bohemian Massif is composed of several lithotectonic units characterized by different metamorphic conditions. These units are from the bottom to the top: the Cadomian basement, the Gneiss-Eclogite Unit, the Micaschist-Eclogite Unit, the (Garnet)-Phyllite Unit and the uppermost allochthon represented by several klippen (Wildenfels, Frankenberg; Fig. 5.1b). (i) The Cadomian basement consists of medium pressure orthogneisses and migmatites with no evidence of HP metamorphism (Willner et al., 2000). (ii) The Gneiss-Eclogite Unit is composed of HP gneisses and migmatites (Willner et al., 1997) with lenses of various types of HP to ultrahigh pressure rocks such as coesite-bearing eclogite (Massonne, 2001), garnet peridotite (Schmädicke and Evans, 1997; Massonne and Neuser, 2005), and diamondiferous quartzofeldspathic rock (Massonne, 2003). (iii) The Micaschist-Eclogite Unit is composed of chloritoid- and garnet-bearing micaschists with intercalation of quartzites, marbles, and metabasites. Peak pressures close to ultrahigh pressure conditions (2.6 GPa at 650-700°C) were obtained for eclogites (Klápová et al., 1998; Massonne and Kopp, 2005), silicate marble (Gross et al., 2008), and eclogitic micaschist (Konopásek, 2001). The surrounding metasediments gave substantially lower pressures of 1.2-1.3 GPa (Rötzler et al., 1998). (iv) The (Garnet)-Phyllite Unit is represented by phyllites and schists with intercalations of quartzites and metabasites. Blue amphibole has been reported from some metabasites in the basal part of the unit (Holub and Souček, 1994; Rötzler et al., 1999). Our study area is located in the Elstergebirge (Czech: Halštrovské hory), a hilly area in the border region of the northwestern Czech Republic and southwestern Saxony. Schists and phyllites, assigned to the Cambrian and Ordovician in geological maps (e.g., scale 1:400.000, Bernstein et al., 1973), and micaschists are the dominant rocks of the Elstergebirge (Fig. 5.1c; Stumm, 2002). These rocks show similarities to those of the Micaschist-Eclogite and (Garnet)-Phyllite Units of the Erzgebirge crystalline complex, being

5. Metamorphic evolution of chloritoid-bearing micaschist...

adjacent to the northeast, although eclogite was never reported from the Elstergebirge. In addition, the Arzberg Series unit of the Fichtelgebirge crystalline complex also shows such similarities. This unit is situated southwest of the Elstergebirge and mainly composed of metasediments (phyllite, quartzite, graphite schist and marble) with some minor layers of amphibolite and greenschist. These metasediments underwent a low pressure greenschist- and amphibolite-facies metamorphism, characterized by the assemblage quartz-muscovite-chlorite-biotite-garnet-albite, during the Variscan orogeny (Mielke et al., 1979). As typical for the Erzgebirge and Fichtelgebirge crystalline complexes, several post-tectonic granitic plutons occur, which yielded ages either around 320 Ma or between 280 and 300 Ma (Richter and Stettner, 1979; Carl and Wendt, 1993; Siebel et al., 2010). Based on the composition of magmatic muscovite the intrusion level of these granites was in the depth range of 15-20 km (around 4.3 kbar: Massonne, 1984). Such a pluton (Fichtelgebirge granite, Fig. 5.1c) bounds the Elstergebirge to the south. Between this pluton and the micaschists and phyllites in the north para- and orthogneisses were mapped. These gneisses can contain andalusite (Stumm, 2002). Locally, shale layers with aegirine occur in these gneisses (Freyer and Tröger, 1965).

Various dating methods (Sm-Nd isochrons, Ar-Ar in phengite and amphibole, U-Pb in zircon and monazite) were achieved to determine the age of metamorphism in the Saxothuringian realm of the Bohemian Massif. U-Pb dating on zircon in medium- to high grade metamorphic rocks yielded ages of c. 340 Ma (Kröner and Willner, 1998; von Quadt and Gebauer, 1998; Romer and Rötzler, 2001) or somewhat younger (Massonne et al., 2007; Liati and Gebauer, 2009). Ar-Ar dating on phengite of two eclogites from the Erzgebirge crystalline complex revealed ages of 348 ± 2 and 355 ± 2 Ma (Schmädicke et al., 1995). The same dating method applied to white-mica and hornblende from 68 micaschists and gneisses of EC yielded 2 clusters at 340 ± 2 and 329.7 ± 1.5 Ma (Werner and Lippolt, 2000) confirming metamorphism in the Early Carboniferous. On the other hand, rocks from the Fichtelgebirge crystalline complex underwent low pressure regional metamorphism in the time interval 330-320 Ma (Okrusch et al., 1990). Kreuzer et al. (1989) reported K-Ar ages of 316 ± 3 Ma obtained on muscovite in a muscovite-biotite gneiss and schist, which both were sampled ~ 2.5 km northeast of the town of Selb (Fig. 5.1c).

In addition, these authors applied K-Ar dating of hornblende from schistose amphibolites of the Fichtelgebirge crystalline complex and revealed ages of 332 and 299 Ma. Dating of zircon and monazite also yielded information on protoliths of medium- to high grade metamorphic rocks from the Saxothuringian realm of the Bohemian Massif. Tichomirowa (2002) and Tichomirowa et al. (2012)

determined age clusters at c. 575, 540-530 and 500-470 Ma on zircon in ortho- and paragneisses from the Erzgebirge crystalline complex indicating Cadomian (and post-Cadomian?) magmatic events at the margin of Gondwana or peri-Gondwanan terranes (see, Linnemann et al., 2000, 2010). Teufel (1988) suggested Ordovician or younger protolith ages based on dating of monazite of paragneiss from the southern Fichtelgebirge crystalline complex and adjacent Moldanubian units. Waizenhöfer and Massonne (2017: mylonitic migmatite from the Münchberg metamorphic complex) and Rahimi and Massonne (2018: micaschist from the northern Fichtelgebirge crystalline complex) interpreted age clusters in the time interval between 575 and 455 Ma and 472 and 405 Ma, respectively, obtained by monazite dating with the EMP, as characteristic of provenance areas for detrital monazite that survived metamorphism of these former sediments.

5.3. Analytical methods

Major and trace element concentrations in the bulk rock were analysed using a rock slab, which was ground to rock powder. A glass disk was prepared by fusing this powder with Spectromelt® (ratio 1:6). This disk was analysed with a PHILIPS PW2400 X-ray fluorescence (XRF) spectrometer with a wavelength-dispersive (WD) system considering certified geostandards. The contents of H₂O and CO₂ in the rock powder were determined with a LECO RC-412 C-O-H multiphase determinator after drying the powder at 110 °C for several hours. The chemical compositions of minerals in polished thin sections were analysed with a CAMECA SX100 electron microprobe (EMP) with 5 WD spectrometers applying the PaP correction procedure provided by CAMECA. For silicates and oxides concentrations of F, Na, Mg, Al, Si, K, Ca, Ti, Cr, Mn, Fe, and Ba were determined using counting times of 20 s at the peak and on the background except for F (30 s). Synthetic and natural minerals, glasses (e.g., Ba glass for the BaL α_1 radiation), and pure oxides were used as standards. The applied acceleration voltage and electric current were 15 kV and 30 nA, respectively, for analysing garnet.

For other minerals an electric current of 10 nA was used. The beam diameter was usually 3-5 μ m. The analytical errors of the applied method were reported by Massonne (2012), related to an electric current of 15 nA. Full analyses of monazite with the EMP included the elements Si, P, S, Ca, Y, La, Ce, Pr, Nd, Sm, Eu, Gd, Pb, Th, and U. The procedure for a c. 17 minutes lasting analysis was described by

5. Metamorphic evolution of chloritoid-bearing micaschist...

Massonne et al. (2012). However, the usually used beam current of 180 nA was reduced to 150 nA for the analysis of small monazite inclusions in garnet. The applied analytical conditions had been tested against different Palaeozoic monazite (Waizenhöfer and Massonne, 2017) which had been dated also by other geochronological methods (see, Langone et al., 2011; Massonne et al., 2007). For the calculation of ages and their errors the program MINCALC-V5 (Bernhardt, 2007) was used. The age data were further processed with the Isoplot/Ex program by Ludwig (1999). Structural formulae were calculated with the CalcMin program (Brandelik, 2009). According to the five WD systems of the EMP up to five element concentration maps for specific elements (garnet: Ca, Mn, Fe, Mg; monazite: Y, Th, Ca, Ce, Nd; mica: Ba, Na, Mg, Fe, Ti) were simultaneously prepared by step-wise movement of the thin section under the electron beam of the EMP and subsequent computer aided evaluation (Bernhardt et al., 1995). Counting times per step were 80 ms. An electric current of 40 nA, 20 nA, and 150 nA was applied for areas with garnet, potassic white-mica and monazite, respectively. Back-scattered electron (BSE) images were taken with the EMP to document specific textural features.

5.4. Petrography and mineral compositions

5.4.1. Micaschist samples

In the area between the towns of Asch (Czech: Aš) and Bad Brambach and the village of Neuberg (Czech: Podhradí) several micaschists were sampled (for sample localities and characteristics see Table 5.1). From these rocks we selected micaschist sample 14AS6 because it contains garnet and chloritoid. In addition, this sample is relatively fresh with clearly defined mineral textures (Fig. 5.2a). Sample 14AS6 was taken from a 5-6 m high cliff in the forest c. 1 km southeast of the village of Raun (Fig. 5.1c). Macroscopically, the rock is light grey-green in colour with mm-sized dark-green chloritoid and red-brownish garnet porphyroblasts and a pervasive crenulated foliation which is mainly defined by aligned phyllosilicates.

Table 5.1. Localities, macroscopic and microscopic characterization of the samples micaschists. Abbreviation: Ab, albite; Bt, biotite; Ch, chlorite; Ctd, chloritoid; Kf, potassic-feldspar; Gt, garnet; Ms, potassic white-mica; Pl, plagioclase; and Qz, quartz.

Micaschist samples	Coordinates	Localities	Macroscopic features	Mineral assemblages and modal contents (vol.%)
14AS6	N: 50° 14.698 E: 12° 16.613	4.5 km NNE of Asch/Aš, 1 km SW of Raun	light grey-green, mm-sized dark-green chloritoid, red brownish garnet porphyroblasts, pervasive crenulated foliation	Qz 43 + Ms 30 + Gt 3 + Bt 5 + Ch 11 + Ctd 6 + accessory phases 2
14AS4	N: 50° 13.841 E: 12° 17.262	~1.5-2 km NW of Bad Brambach	light pink-grey, red brownish garnet porphyroblasts, strongly foliated	Qz 50 + Ms 25 + Gt 3 + Kf 2 + Ch 8 + Pl 10 + accessory phases 2
14AS5	N: 50° 14.418 E: 12° 16.731	~ 1.5 km SW of Raun	light red-pink, gneissose texture, 0.5 cm-sized red brownish euhedral garnet porphyroblasts, cm-sized foliated	Qz 50 + Ms 28 + Gt 4 + Pl (Ab) 2 + Ch 10 + St, And 3 + accessory phases 2
14AS11	N: 50° 13.730 E: 12° 12.080	~ 1 km NE of Asch/Aš	light grey, phyllitic to schistose structure, moderately foliated	Qz 56 + Ms 20 + Gt 2 + Pl (Ab) 2 + Kf 2 + Ch 10 + Bt 8 + accessory phases 2
14AS13	N: 50° 14.390 E: 12° 12.360	~ 1.5 km SSE of Neuberg/Podhradí	light-dark grey, porphyroblastic and strongly to moderately foliated as defined by the micas in the matrix	Qz 57 + Ms 27 + Gt 2 + Pl (Ab) 2 + Ch 10 + accessory phases 2
14AS18	N: 50° 14.777 E: 12° 13.543	~ 1.5 km NW Niederreuth/Dolní Paseky	dark grey, fine-grained and rich in quartz, foliated	Qz 66 + Ms 15 + Gt 1 + Pl (Ab) 2 + Ch 4 + Bt 10 + accessory phases 2

5.4.2. Minerals in sample 14AS6

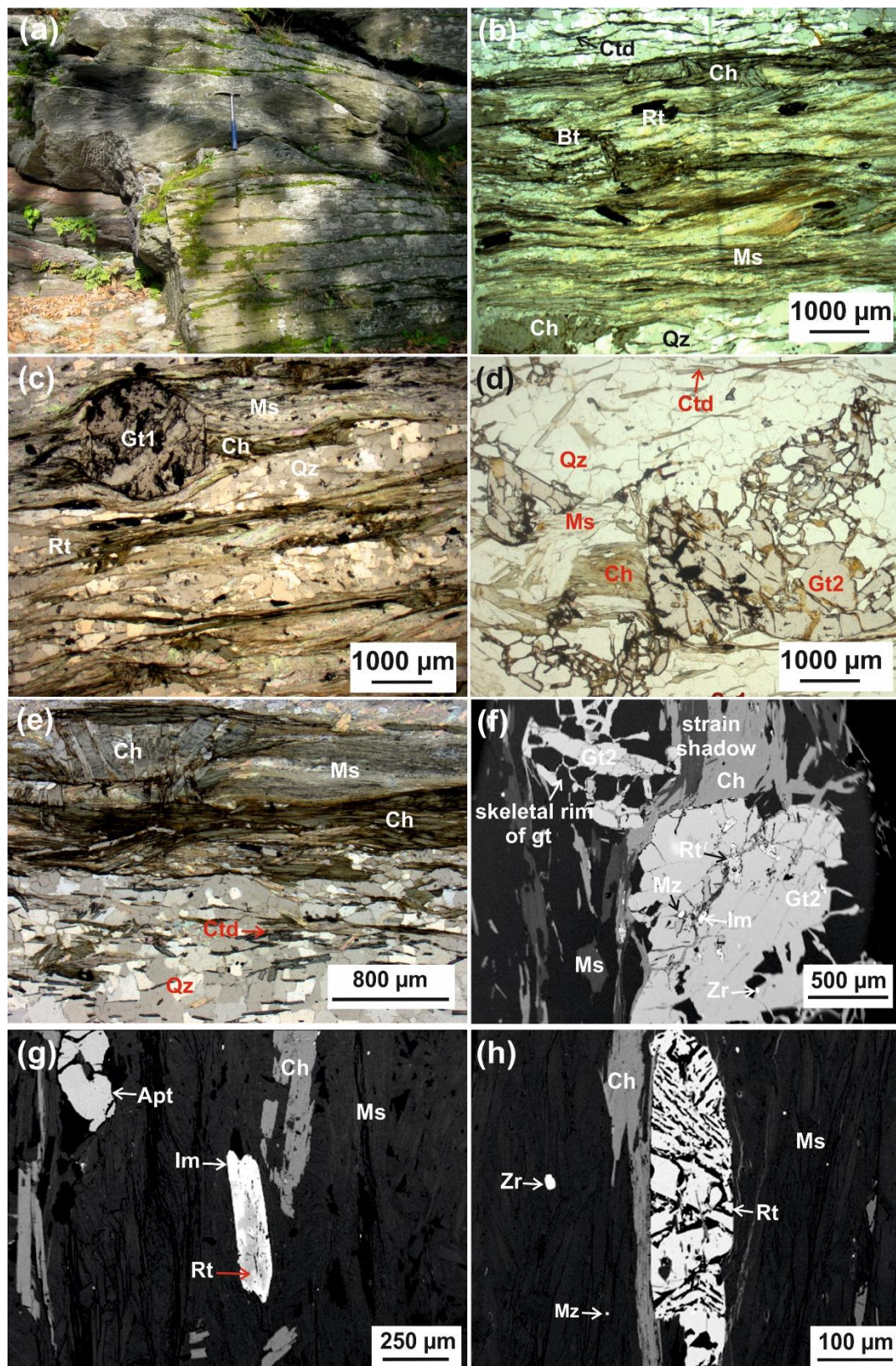
Quartz (43 vol.%), potassic white-mica (30-32 vol.%), biotite (5 vol.%), chlorite (10-11 vol.%) and chloritoid (5-6 vol.%) form the rock matrix of sample 14AS6 (Table 5.1). In addition, millimetre-sized porphyroblasts of garnet (3 vol.%) and accessory phases (~ 1-2 vol.%) of ilmenite, rutile, zircon, apatite and monazite are also present in the sample. Layers with thicknesses between 0.5 and 5 mm, consisting mainly of quartz (mean diameter 0.1-0.3 mm) slightly elongated along the main foliation, alternate with phyllosilicate layers (Fig. 2b-e) which are composed of oriented white-mica (mean size $2 \times 0.3 \text{ mm}^2$) and chlorite (mean size $1 \times 0.1 \text{ mm}^2$).

Two groups of garnet can be distinguished according to grain size and textural position. The middle-sized rare euhedral garnet (mean 1 mm, Gt1) occurs in phyllosilicate layers (Fig. 5.2c), whereas the large and subhedral garnet (3.5 mm, Gt2) appears in quartz domains and is elongated with the longer axis being at a low angle with the main foliation of the rock (Fig. 5.2d). The rim of Gt2 frequently shows a foam microstructure with quartz (Fig. 5.2f), i.e., the garnet has crystallized along the intergranular boundaries of a quartz aggregate (Stöckhert et al., 1997; Hawkins et al., 2007) as the size (0.1-0.7 mm) and fabric of the quartz grains are similar to those in the matrix. According to Engvik et al. (2000) and Hoschek (2001), we use the term skeletal for garnet in this intergrowth texture.

Inclusions in garnet (mostly Gt2) comprise single grains of zircon (up to 20 μm large), monazite, apatite, plagioclase, opaque phases, quartz, and rutile frequently surrounded or almost replaced by ilmenite (Fig. 5.2d, f). Mainly Gt1 is marginally replaced and locally entirely wrapped by potassic white-mica, chlorite and quartz. Chlorite and potassic white-mica fill garnet fractures.

Both Gt1 and Gt2 are rich in almandine component ($X_{\text{Fe}^{2+}} > 0.74$) and show the same prograde concentric zonation from core to rim exhibited in Fig. 5.3. The garnet core is characterized by pyrope, grossular (+ andradite), and spessartine components of $X_{\text{Mg}} = 0.035\text{-}0.04$, $X_{\text{Ca}} = 0.09$, and $X_{\text{Mn}} = 0.11$, respectively. Towards the rim, grossular (+ andradite) and spessartine components considerably decrease to $X_{\text{Ca}} = 0.02$ and $X_{\text{Mn}} = 0.05$, whereas pyrope contents increase to $X_{\text{Mg}} = 0.065$ (Fig. 5.3e, Table 5.2).

White-mica shows a compositional variability for Si from 3.00-3.31 per formula unit (pfu, Fig. 5.4b-d) with the highest values observed in inner parts of large grains.



5. Metamorphic evolution of chloritoid-bearing micaschist...

Fig. 5.2. (a) View of the outcrop of the chloritoid-garnet bearing micaschist between Bad Brambach and Bad Elster; and (b-e) Photomicrographs showing microstructural features of the chloritoid-garnet-bearing micaschist under plane-polarized light or partly crossed polarizers, (b) thick phyllosilicate layer containing potassic white-mica (Ms), biotite (Bt), chlorite (Ch), and accessory rutile (Rt) in the adjacent quartz (Qz) layers some chloritoid (Ctd) occurs; (c) garnet porphyroblast (Gt1) in a quartz-rich layer showing a strict, but crenulated foliation by oriented phyllosilicates; (d) garnet porphyroblast (Gt2) showing skeletal structure in a quartz-rich matrix; (e) A quartz-rich layer with chloritoid and a phyllosilicate-rich layer with oriented potassic white-mica and chlorite, which also forms a fan perpendicular to the main foliation. (f-h) Back-scattered electron images obtained with the CAMECA SX100 EMP show, (f) a garnet porphyroblast (Gt2) being skeletal at the rim and quartz, chlorite, and potassic white-mica in strain shadows; rutile, monazite (Mz), and zircon (Zr) occur as inclusion in Gt2; (g) Subhedral rutile (Rt) grain occurs in phyllosilicates and frequently replaced by ilmenite (Im); and (h) Large elongated rutile (Rt) grain surrounded by phyllosilicates. Abbreviations: Apt, apatite; Bt, biotite; Ch, chlorite; Ctd, chloritoid; Gt, garnet; Im, ilmenite; Ms, potassic white-mica; Mz, monazite; Qz, quartz; Rt, Rutile; and Zr, zircon.

In fact, potassic white-mica is not as concentrically zoned as garnet, but several maps, as shown in Figure 5.4a, demonstrate that the rims are significantly poorer in Mg than the cores. Thus, there is a clear trend, which developed during metamorphism, from the Si richest (Si ~ 3.31 pfu) to the Si-poorest (Si ~ 3.00 pfu) potassic white-mica. According to spot analyses (Fig. 5.4b-d), the Mg and Fe²⁺ poorer domains are richer in Na and Al and poorer in Si with values of Mg/(Mg+Fe) = Mg# and X_{Na} = Na/(Na+K) varying between 0.25 and 0.60 and 0.05 and 0.10, respectively. Fe contents first decrease as the Mg contents, according to the (inverse) Tschermak's substitution, but towards the low Si contents a clear increase of the Fe contents is discernable leading to the lowest Mg# values. Ti and Ba contents (0.01-0.02 pfu and around 0.005 pfu, respectively) remain fairly constant (Fig. 5.4, Table 5.3).

Analyses of pale to dark green chlorite in the matrix yielded contents of Si = 2.52-2.70 pfu, Al^{VI} = 1.38-1.49 pfu and Mg# values around 0.32 (Table 5.3). Locally, chlorite forms fan-like aggregates perpendicular to the main foliation indicating that this mineral also grew post-deformationally at a late metamorphic stage (Fig. 5.2b, e). Chloritoid exhibits a poor cleavage and a greenish gray to blue pleochroism, is locally elongated along the main foliation, and up to 1 mm in length (Fig. 5.2b). The composition of chloritoid (Table 5.3) is only slightly variable (Fig. 5.4e) with Mg# values between 0.08 and 0.10 and MnO contents between 0.20 and 0.40 wt.%. Contents of Ti are below the detection limit. Although no clear zonation of chloritoid was noted from elemental mapping, it seems to be that the Mg content decreases from core to rim (Fig 5.4e).

Table 5.2. Representative EMP analyses (oxides in wt.%) of garnet in sample 14AS6. The garnet structural formulae (double unit) was calculated on the basis of 24 O and 10 six- and eight-fold coordinated cations. Molar fractions of garnet components are given at the bottom.

Analyses No.	#131	#134	#64	#29	#52	#77
Comments	inner core	outer core	inner mantle	outer mantle	inner rim	outer rim
SiO₂ (wt.%)	35.74	35.42	37.11	37.38	37.20	37.06
TiO₂	0.10	0.13	0.07	0.08	0.06	0.05
Al₂O₃	21.16	20.99	20.65	20.76	20.82	20.51
Cr₂O₃	0.01	0.02	0.00	0.00	0.03	0.00
Fe₂O₃	0.72	0.72	0.71	0.51	0.35	0.88
FeO	34.34	34.92	36.11	35.89	37.21	38.20
MnO	5.29	4.80	2.43	3.23	2.56	1.92
MgO	0.97	1.08	1.47	1.41	1.61	1.65
CaO	3.33	2.86	2.61	2.25	1.45	1.07
Na₂O	0.01	0.00	0.04	0.01	0.00	0.03
Total	101.66	100.94	101.21	101.51	101.29	101.38
Si (dfu)	5.809	5.700	5.968	6.016	5.994	5.968
Ti	0.011	0.015	0.009	0.009	0.007	0.005
Al	3.914	3.912	3.914	3.938	3.954	3.893
Cr	0.001	0.002	0.000	0.001	0.003	0.000
Fe³⁺	0.085	0.086	0.086	0.061	0.043	0.107
Fe²⁺	4.507	4.618	4.856	4.831	5.014	5.145
Mg	0.227	0.255	0.352	0.338	0.387	0.397
Ca	0.560	0.484	0.449	0.388	0.250	0.185
Mn	0.703	0.643	0.331	0.440	0.349	0.262
Na	0.002	0.000	0.011	0.003	0.000	0.011
grossular	0.093	0.081	0.075	0.065	0.042	0.031
pyrope	0.038	0.042	0.059	0.056	0.064	0.066
almandine	0.751	0.770	0.809	0.805	0.836	0.857
spessartine	0.117	0.107	0.055	0.073	0.058	0.044

5. Metamorphic evolution of chloritoid-bearing micaschist...

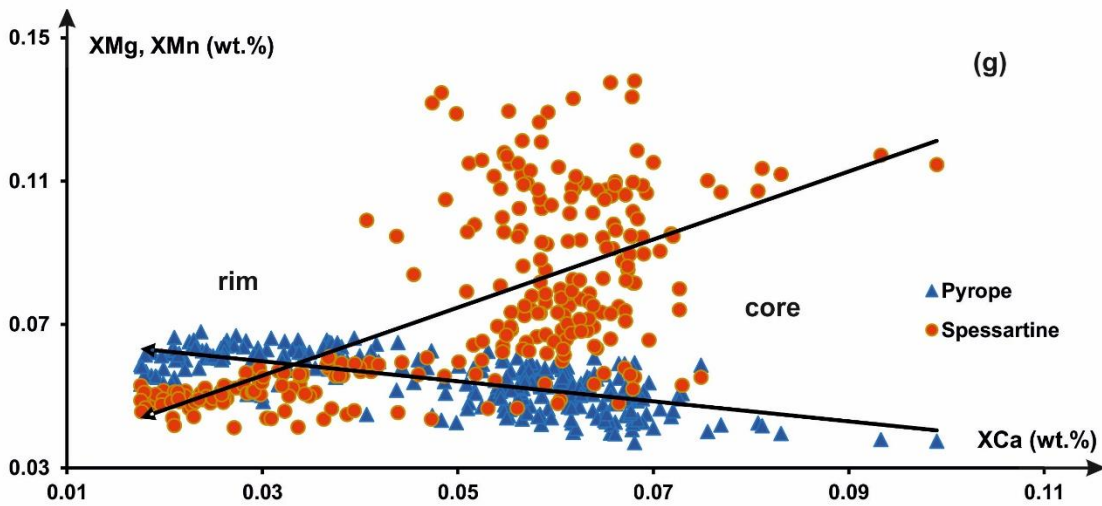
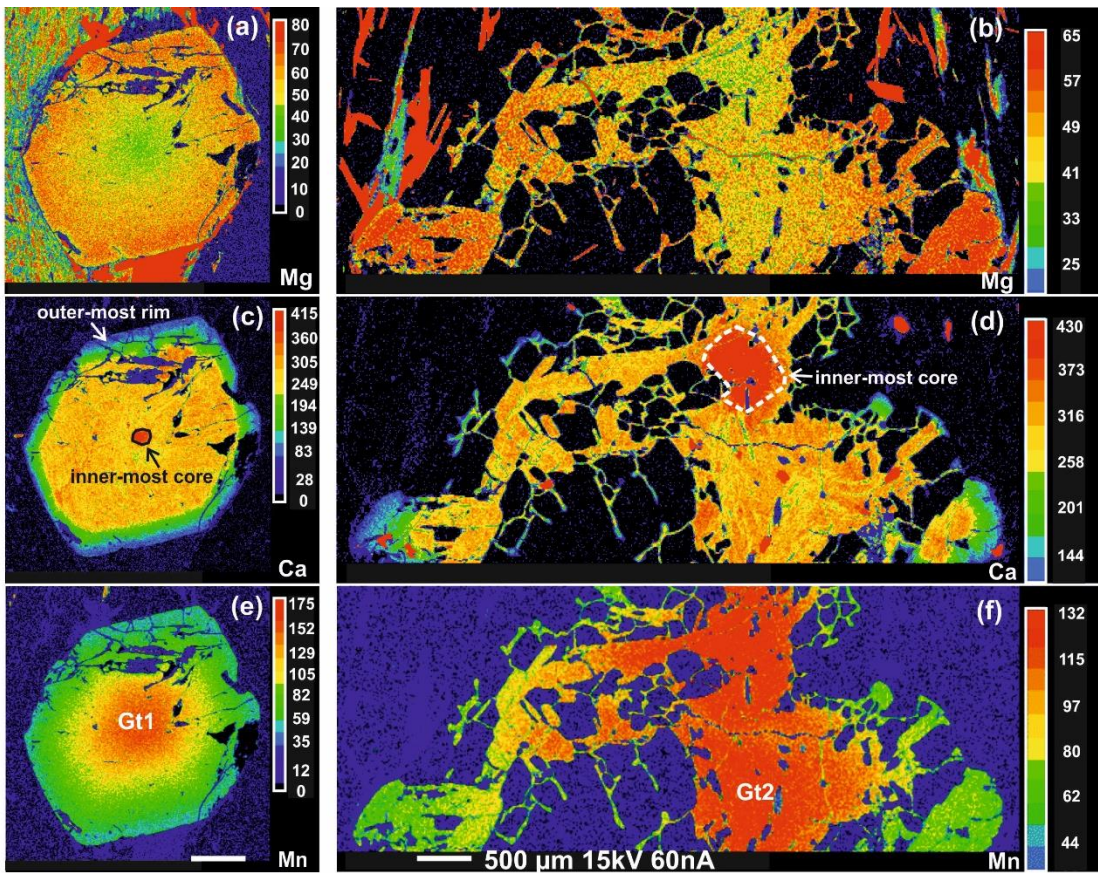


Fig. 5.3. X-ray compositional maps for two different textural garnets (a) and (b) for Mg; (c) and (d) for Ca; (e) and (f) for Mn. Black to red colours indicate increasing element concentrations; (g) garnet analyses obtained with an EMP in terms of molar fractions of pyrope (X_{Mg}) and spessartine (X_{Mn}) versus that of grossular (+ andradite) as X_{Ca} from core to the rim.

Biotite is reddish-brown and forms up to 1 mm-sized grains in the matrix. It also occurs enclosed in potassic white-mica. The contents of TiO₂ in biotite are around 1.7 wt.%. The Mg# values are also fairly constant (0.46-0.48, Table 5.3). Rare plagioclase with $X_{An} = Ca/(Ca+Na+K)$ of 0.01 and grain sizes between 0.1 and 0.4 mm occurs along boundaries of white-mica flakes. Rutile grains, which usually occur in the matrix, are subhedral with lengths up to 0.5-1 mm; those enclosed in garnet are smaller in size (up to 0.2-0.3 mm) (Fig. 5.2f). Sub-anhedral ilmenite occurs mostly in phyllosilicates and rarely included in garnet ranging in size from 0.1-0.3 mm (Fig. 5.2g-h). Compositionally, ilmenite is characterized by an average of 4.4 wt.% MnO (Table 5.3).

5.5. P-T pseudosection modelling

5.5.1. Calculation method

P-T pseudosections and their contouring with isopleths for modal contents and chemical compositions of minerals were computed with PERPLE_X (see Connolly, 2005; update in August 2011 downloaded from the internet site <http://www.perplex.ethz.ch/>) and the internally consistent thermodynamic data set (Holland and Powell, 1998; and updates) for minerals and H₂O (model CORK: Holland and Powell, 1991) for the P-T range of 2-22 kbar and 350-650 °C (Fig. 5a). The following solid-solution models (see, file solution_model taken from the PERPLE_X software and stored in Massonne et al. (2018b) were used: GlTrTsPg for amphibole (White et al., 2003), TiBio(HP) for biotite (see below), Carp(M) for carpholite (Massonne, 2010), Chl(HP) for chlorite (Holland et al., 1998), Ctd(HP) for chloritoid (see, White et al., 2000), feldspar for plagioclase and K-feldspar (Fuhrman and Lindsley, 1988), Gt(HP) for garnet (Holland and Powell, 1998), Opx(HP) for orthopyroxene (Powell and Holland, 1999), Omph(HP) for clinopyroxene (Holland and Powell, 1996), Mica(M), restricting the contents of the muscovite and margarite components to 30 mol%, for paragonite (Massonne, 2010), Pheng(HP) for potassic white-mica (see, Powell and Holland, 1999, with a maximum paragonite content of 50 mol%), St(HP) for staurolite (details in http://www.perplex.ethz.ch/perplex_solution_model_glossary.html), and Stlp(M) for stilpnomelane (Massonne, 2010).

5. Metamorphic evolution of chloritoid-bearing micaschist...

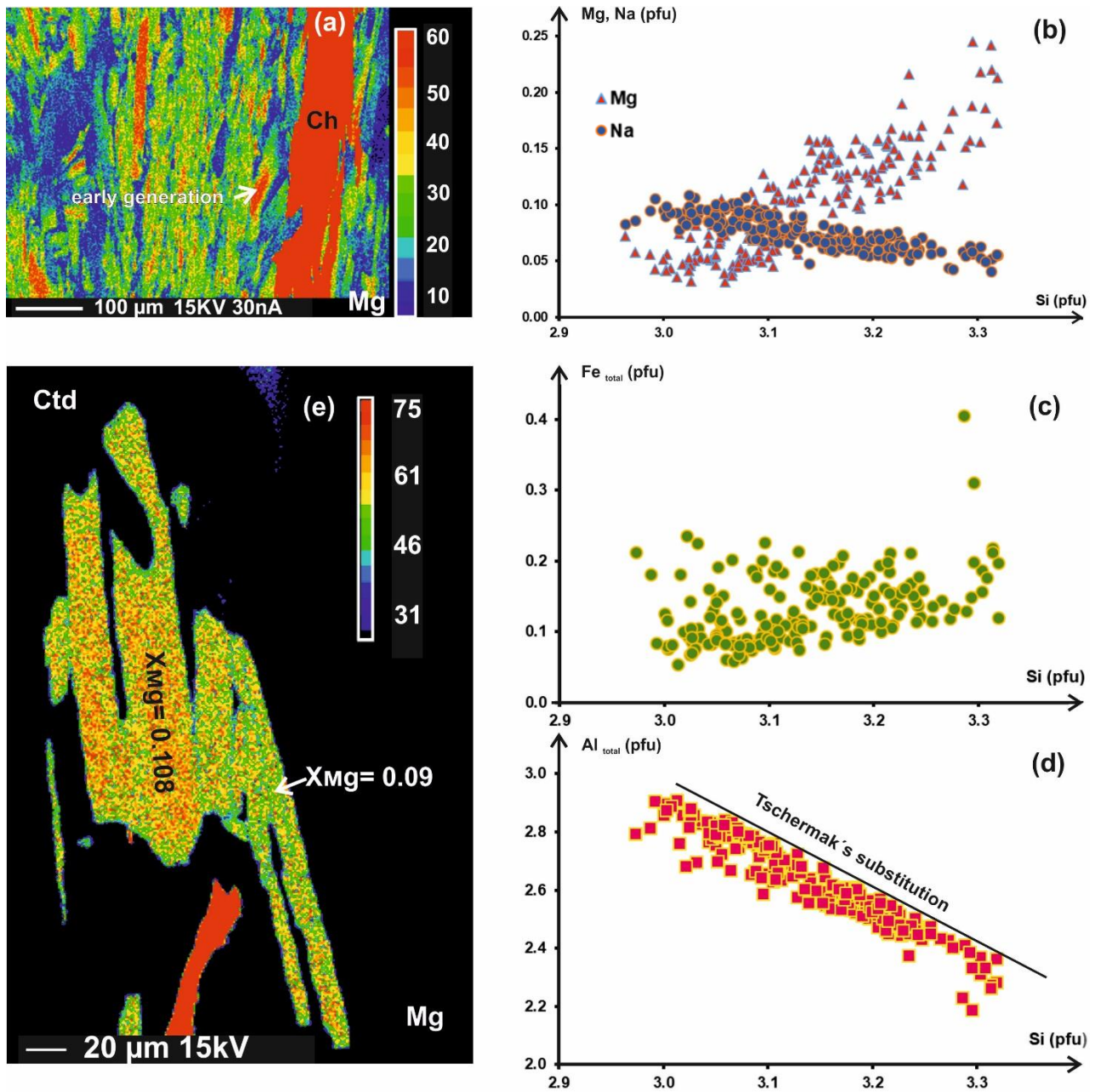


Fig. 5.4. (a) and (e) X-ray concentration maps for Mg obtained with a CAMECA SX100 EMP of white-mica and chloritoid respectively. Black to red colours indicate increasing element concentrations. Compositional diagrams for potassic white-mica in sample 14AS6; (b) Mg and Na vs. Si in potassic white-mica; (c) Fe_{total} vs. Si in potassic white-mica; and (d) Al_{total} vs. Si in potassic white-mica. All units are in pfu.

Table 5.3. EMP analyses (oxides in wt.%) of various minerals in sample 14AS6. Structural formulae were calculated as follows: biotite (Bt) = 11 O; chlorite (Ch) = 14 oxygen and the negligence of large cations (Na, Ca); chloritoid (Ctd) = 12 O, Ti + Al + Fe + Mn + Mg = 6, $Fe^{3+} = 4 - (Al + 2*Ti)$; ilmenite (Im) = 3 O; potassic white-mica (Ms) = 11 O, 21 - (Ca + Ba) valencies neglecting interlayer cations. tot= total, calc= calculated.

Mineral	Ph-Ms			Ms		Ch			Bt		Ctd			Im	
Analyses No.	#123	#69	#67	#23	#127	#3	#4	#8	#4	#11	#52	#53	#14	#8	#4
Comments	Early			Late					in Matrix			in Gt	in Ctd	in Ms	
SiO ₂ (wt.%)	49.25	49.9	49.83	45.7	46.73	25.03	24.27	23.48	35.73	35.26	24.44	24.35	26.25		
TiO ₂	0.23	0.27	0.24	0.26	0.27	0.07	0.07	0.08	1.73	1.71	0.03	0.02	0.01	53.05	52.56
Al ₂ O ₃	29.47	30.36	31.01	36.03	33.96	21.55	21.4	22.91	18.7	18.67	40.35	40.55	38.01		
FeO	3.14	2.84	2.34	1.09	1.87	33	33.21	34.29	19.14	19.19	26.02	25.74	23.77	40.87	40.76
Fe ₂ O ₃											0.84	0.78	2.19		
MnO	0.00	0.00	0.01			0.14	0.07	0.05	0.15	0.2	0.24	0.25	0.61	4.71	4.92
MgO	1.86	1.58	1.54	0.32	0.8	9.34	9.51	8.99	9.4	9.66	1.46	1.66	1.9		
CaO	0.01	0	0.00	0	0.02				0	0.04					
Na ₂ O	0.38	0.49	0.43	0.76	0.69				0.1	0.04					
K ₂ O	9.90	9.77	9.76	10.51	10.34				9.8	9.4					
BaO	0.30	0.19	0.22	0.24	0.21				0.04	0.05					
Nb ₂ O ₅															
ZrO ₂															
Cr ₂ O ₃														0.02	0.02
H ₂ O _{calc}	4.46	4.53	4.54	4.48	4.47	11.13	11.01	11.11	3.91	3.89	7.23	7.26	6.96		
Total	98.99	99.93	99.92	99.38	99.38	100.26	99.54	100.91	98.70	98.12	100.61	100.59	99.70	98.65	98.26
Si (pfu)	3.310	3.300	3.290	3.060	3.130	2.700	2.640	2.530	2.740	2.720	2.030	2.010	2.260		
Al _{tot}	2.330	2.370	2.410	2.840	2.680	2.740	2.750	2.910	1.690	1.690	3.940	3.950	3.860	0.000	0.000
Ti	0.010	0.010	0.010	0.010	0.010	0.010	0.010	0.010	0.100	0.100	0.000	0.000	0.000	1.020	1.020
Fe ²⁺	0.180	0.160	0.130	0.060	0.100	2.970	3.030	3.100	1.231	1.241	1.801	1.781	1.711	0.881	0.881
Fe ³⁺											0.05	0.05	0.14		
Mn	0.000	0.000	0.000			0.010	0.010	0.000	0.010	0.010	0.020	0.020	0.040	0.100	0.110
Mg	0.190	0.160	0.150	0.030	0.080	1.500	1.540	1.450	1.071	1.110	0.181	0.200	0.240		
Ca	0.000		0.000	0.000	0.000										
Ba	0.010	0.000	0.010	0.010	0.010										
Na	0.050	0.060	0.050	0.100	0.090				0.010	0.010					
K	0.850	0.820	0.820	0.900	0.880				0.960	0.920					
Nb															
Zr															
Cr															
H	2.000	2.000	2.000	2.000	2.000	8.000	8.000	8.000	2.000	2.000	4.000	4.000	4.000		

5. Metamorphic evolution of chloritoid-bearing micaschist...

For cordierite, ilmenite, and talc, the ideal solid-solution models hCrd, IlGkPy, and T, respectively, were used with thermodynamic data for corresponding end-members given by Holland and Powell (1998), Quartz, rutile, titanite, Al-silicates, zoisite and lawsonite were considered as pure phases. We excluded feldspar (ab, mic) and amphibole (cumm, grun) components. In addition, the mica components tip, tbi, and ann1 were neglected because of their untrustworthiness (Massonne et al., 2018b). Thus, the used solid-solution model of biotite is actually that applied in former versions of PERPLE_X (Powell and Holland, 1999: Bio(HP)).

However, the removal of inner garnet domains from the bulk rock (or previously defined effective bulk rock compositions) frequently has a minor effect on the P-T position of isopleths for the chemical parameters of garnet and potassic white-mica especially for the here relevant metapelitic compositions (see, Massonne, 2014; Massonne et al., 2018a, b; Rahimi and Massonne, 2018). Nevertheless, we calculated a P-T pseudosection for one effective bulk rock composition for the P-T range 2-9 kbar and 530-620 °C to better constrain the P-T conditions for the formation of the garnet rim following the procedure used by Marmo et al. (2002) and Waizenhöfer and Massonne (2017) (Fig. 5.5b). According to X-ray elemental mapping (see Fig. 5.3a-f) we defined the garnet portion (excluded garnet core + inner mantle volume amounts to 1.5 vol.%) to be included in the effective bulk rock composition and considered the average chemical compositions of the garnet domains, based on the achieved EMP analyses, and the higher density of garnet with respect to the main silicates in sample 14AS6. The result of this procedure after addition of H₂O and normalization to 100% is given in Table 5.4 (bulk2).

Since the PERPLE_X calculations were undertaken in the system Na₂O-K₂O-CaO-FeO-MnO-MgO-Al₂O₃-SiO₂-TiO₂-H₂O, the bulk rock composition (Table 5.4, bulk1) was slightly modified for these calculations. (1) The H₂O content was set to 5 wt.% to permit the formation of a free hydrous fluid phase already at relatively low temperatures to simulate the release of water during prograde metamorphism. (2) All iron was considered to be divalent (O₂ content = 0) because i) magnetite is absent, ii) the amount of ferric iron in minerals is very low, and iii) rutile + ilmenite (± pyrite) should indicate low oxidation conditions (Diener and Powell, 2010; Groppo et al., 2010). (3) For apatite-bearing rocks, Massonne (2012) and Massonne and Toulkeridis (2012) suggested to reduce the CaO content according to the analysed phosphorus content in the bulk rock. In contrast to these suggestions no Ca was subtracted here as monazite is present in the rock and apatite is rare.

The consequence of this decision and the low CaO content in sample 14AS6 (Table 5.4) results in a relatively high uncertainty of the P-T position of the X_{Ca} isopleths for garnet (cf. Massonne et al., 2018b). As the equilibration volume is the volume of rock at a set of P-T conditions in chemical equilibrium (Spear, 1995), early formed minerals, such as the core of garnet shielded by its own overgrowth domain, must be removed from the bulk rock for PERPLE_X calculations of later metamorphic stages. Such effective bulk rock compositions are difficult to assess as it is not always clear which are the minerals or mineral domains that have to be subtracted from the bulk rock. Commonly, garnet domains are stepwise removed to account for that (see, Evans, 2004; Konrad-Schmolke et al., 2008). Occasionally, potassic white-mica is considered as well (e.g., Waizenhöfer and Massonne, 2017).

Table 5.4. Bulk rock XRF analyses of sample 14AS6 and its normalized compositions used for pseudosection calculations. bulk1, modified for 1st round calculations and bulk2, modified for 2nd round calculations after subtraction of garnet core and inner mantle (1.5 vol.%).

	XRF analysis wt.%	Analyses modified for PERPLE_X (bulk1, see text) wt.%	Effective bulk-rock composition (bulk2, see text) wt.%
SiO ₂	60.292	60.594	61.040
TiO ₂	0.999	1.004	1.019
Al ₂ O ₃	20.897	21.002	21.002
Fe ₂ O ₃	6.277	-	-
FeO*	-	5.677	5.211
MnO	0.123	0.124	0.057
MgO	1.119	1.125	1.125
CaO	0.175	0.095	0.060
Na ₂ O	0.268	0.269	0.273
K ₂ O	5.085	5.110	5.194
P ₂ O ₅ **	0.203	-	-
H ₂ O	-	5.000	5.000
O ₂	-	0.000	0.000
Total	95.437	100.000	100.000

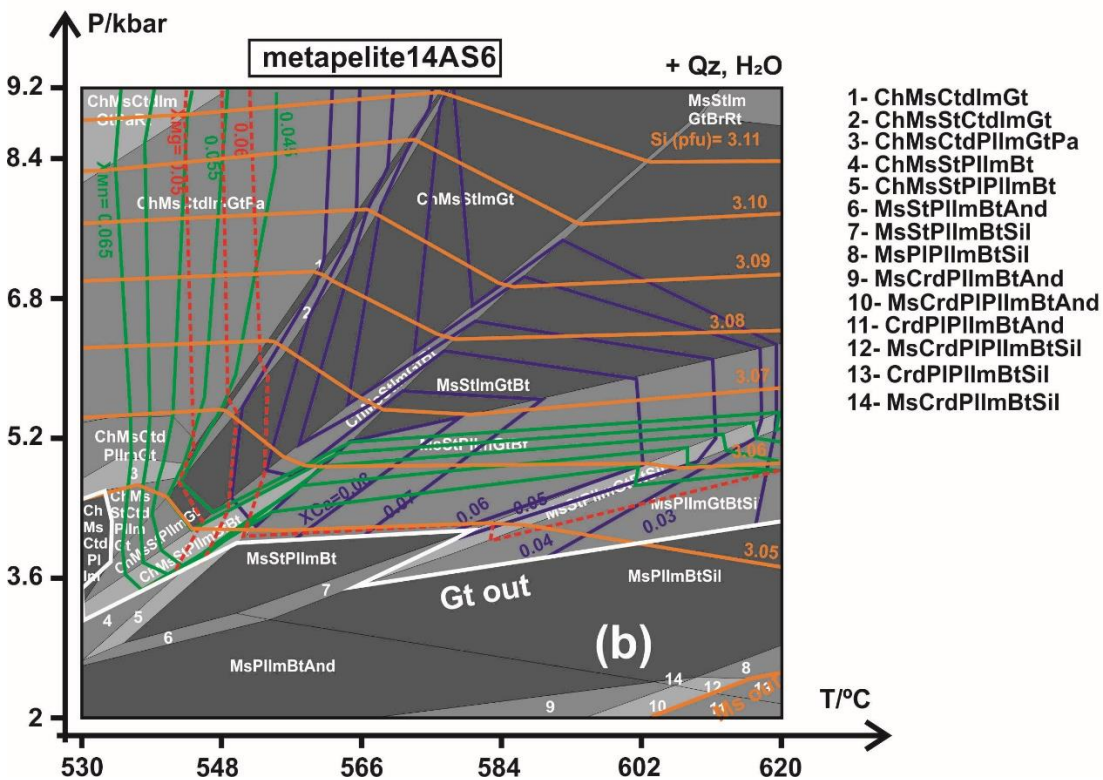
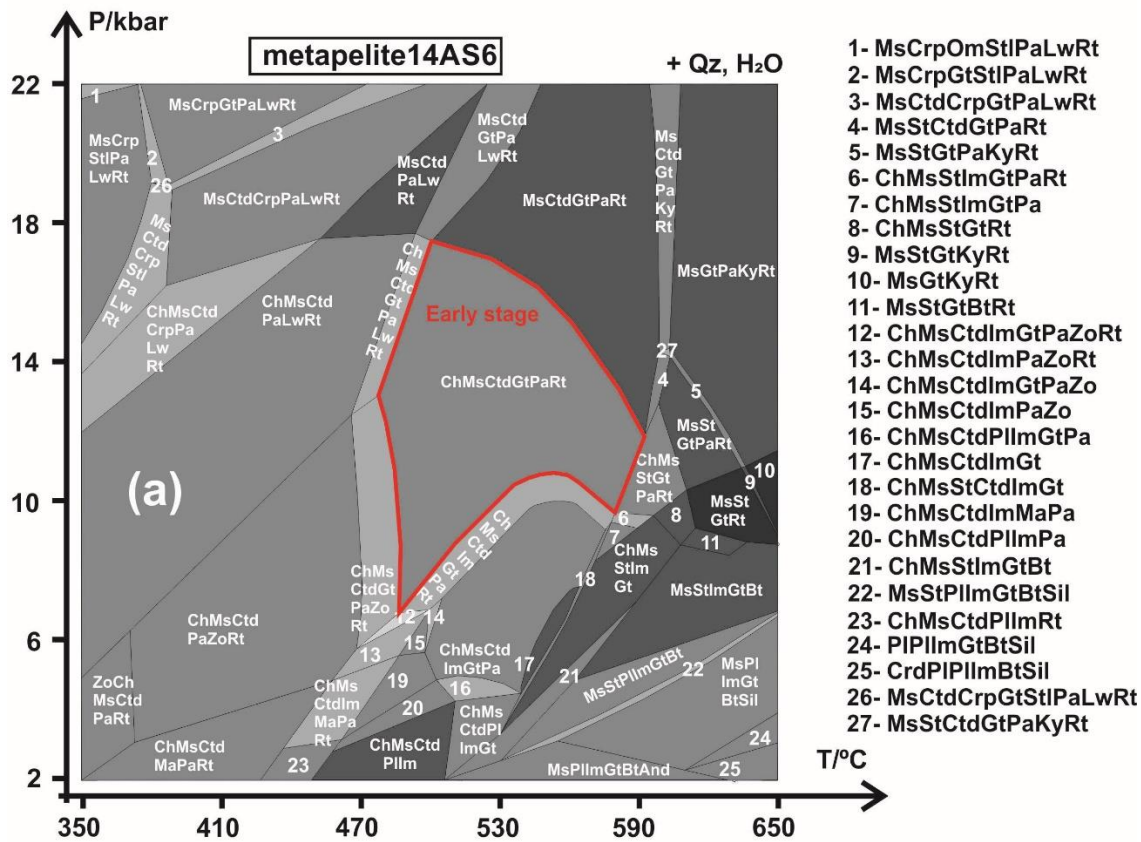
* total Fe as FeO ** corrected for apatite

5.5.2. Calculation results

The P-T pseudosections (Fig. 5.5a-b) are dominated by quadri- and tri-variant fields with pentavariant fields mostly confined at high pressure-high temperature conditions and some minor divariant fields. Only quartz and water are present over the entire P-T range. Potassic white-mica is present almost in the entire investigated P-T range whereas a lower pressure limit of 11.2 kbar at temperatures below 620 °C exists for paragonite (Fig. 5.6d). The Si content in potassic white-mica strongly depends on pressure: at 400 °C, this content is only 3.03 pfu at 2 kbar, but 3.43 pfu at 22 kbar (Fig. 5.6b).

Garnet appears at 420 and 520 °C and at ~ 20 and 10 kbar, respectively, in our P-T pseudosections. With rising pressure and temperature, increasing amounts of garnet occur in the various mineral assemblages. Maximum calculated garnet contents are close to 9.5 vol.% reached at 610 °C and 8.8 kbar (Fig. 5.6b). X_{Mg} increases with rising temperature and decreasing pressure. The highest X_{Mg} of 0.065 was found at $T \sim 600$ °C and $P \sim 2.6$ kbar. X_{Ca} decreases with rising temperature, but also with decreasing pressure. For instance, the lowest X_{Ca} value is 0.035 at P-T conditions of 4.8 kbar and 610 °C. The highest X_{Ca} of 0.09 is reached at 15.6 kbar and 525 °C for the P-T pseudosection calculated for bulk1 (Fig. 5.6a).

Multivariant fields at HP-LT conditions are characterized by the presence of Na-rich clinopyroxene and carpholite at temperatures below 520 °C and pressures higher than 12 kbar. Chlorite occurs at temperatures and pressures below 613 °C (9.3 kbar) and ~17.5 kbar (500 °C), respectively, whereas assemblages with staurolite appear at temperatures and pressures below $T \sim 537$ °C and $P \sim 14.5$ kbar. Maximum Mg contents of chlorite refer to $Mg\# = 0.32$ (see Fig. 5.6d). Plagioclase is present at pressures below ~ 6.4 kbar (650 °C, 2.2 kbar at 420 °C). At lower P-T conditions ($P \sim 2$ kbar and $T \sim 415$ °C) anorthite ($X_{An} \sim 0.97$) is the stable plagioclase. Kyanite appears at temperatures above 630 °C and at pressures above 10 kbar. Rutile occurs in a small P-T field close to 350 °C and 2 kbar, but mainly at high pressures above 10 kbar. Chloritoid is limited to temperatures between 350 and 610 °C in the pressure range 2-22 kbar (Fig. 5.6c). The highest Mg content of chloritoid ($Mg\# = 0.11$) is reached at this temperature limit (Fig. 5.6c). Biotite appears at $T > 510$ °C and $P < 9$ kbar. Contents of biotite above 10 vol.% occur only at pressures below 5.6 kbar and temperatures above 515 °C (Fig. 5.6c).



5. Metamorphic evolution of chloritoid-bearing micaschist...

Fig. 5. P-T pseudosections calculated for (a) the slightly modified composition of metapelite 14AS6 (Table 5.4, bulk1); and (b) an effective bulk rock composition (Table 5.4, bulk2) with the computer software package PERPLE_X (see text). The grey tones of P-T fields are related to the variance (the darker the higher) of the corresponding mineral (+ H₂O) assemblage. Very small P-T fields are not labeled. The pseudosection in (b) is contoured by isopleths of the molar percentage of Ca, Mn and Mg in garnet (Gt) and Si content (pfu) in k-white-mica (Ms). The P-T field with red boundaries in the pseudosection of (a) refers to the mineral assemblage of the early metamorphic stage. Abbreviations: And, andalusite; Bt, biotite; Ch, chlorite; Crd, cordierite; Crp, carpholite; Ctd, chloritoid; Gt, garnet; Im, ilmenite; Ky = kyanite; Lw, lawsonite; Ma, margarite; Ms, potassic white-mica; Om, omphacite; Pa, paragonite; Pl, plagioclase; Qz, quartz; Rt, rutile; Sil, sillimanite; St, staurolite; Stl, stilpnomelane; Wrk, wairakite; and Zo, zoisite.

The metamorphic assemblage of the studied micaschist (garnet + chloritoid + chlorite + white-mica + quartz) is compatible with multivariant P-T fields appearing in Figure 5.5a between 420 and 605 °C and 6.2 and 17.8 kbar. These fields are located at temperatures below those with staurolite and kyanite.

5.5.3. P-T path reconstruction

Isopleths of molar fractions of garnet, Mg# of chlorite and chloritoid, Si in phengite, and modal amounts of garnet and biotite were used to define the P-T conditions of various metamorphic stages. These stages are defined by a specific garnet domain each and related minerals and their compositional domains, which were selected based on mineral inclusions, contact relations or compatibility correlations. Error ellipses of the P-T determinations (Fig. 5.7) were estimated on the basis of compositional errors for the corresponding minerals and the kind of intersecting isopleths. For instance, small angles between intersecting isopleths result in ellipses strongly elongated along the bisecting line (see also, Li and Massonne, 2018).

The isopleths for the inner-most core of garnet ($X_{Ca} = 0.09$, $X_{Mg} = 0.037$, $X_{Mn} = 0.11$) and that for high Si contents in early potassic white-mica (Si = 3.30 pfu: average of 12 analyses) intersect close to 505 °C at 16 kbar (Fig. 5.7). At this HP stage, the calculated mineral assemblage is paragonite (2 vol.%), chlorite (1.5 vol.%, Mg# = 0.32), rutile, phengite, garnet (~ 1 vol.%), chloritoid (10.5 vol.%), and quartz (Fig. 5.5a).

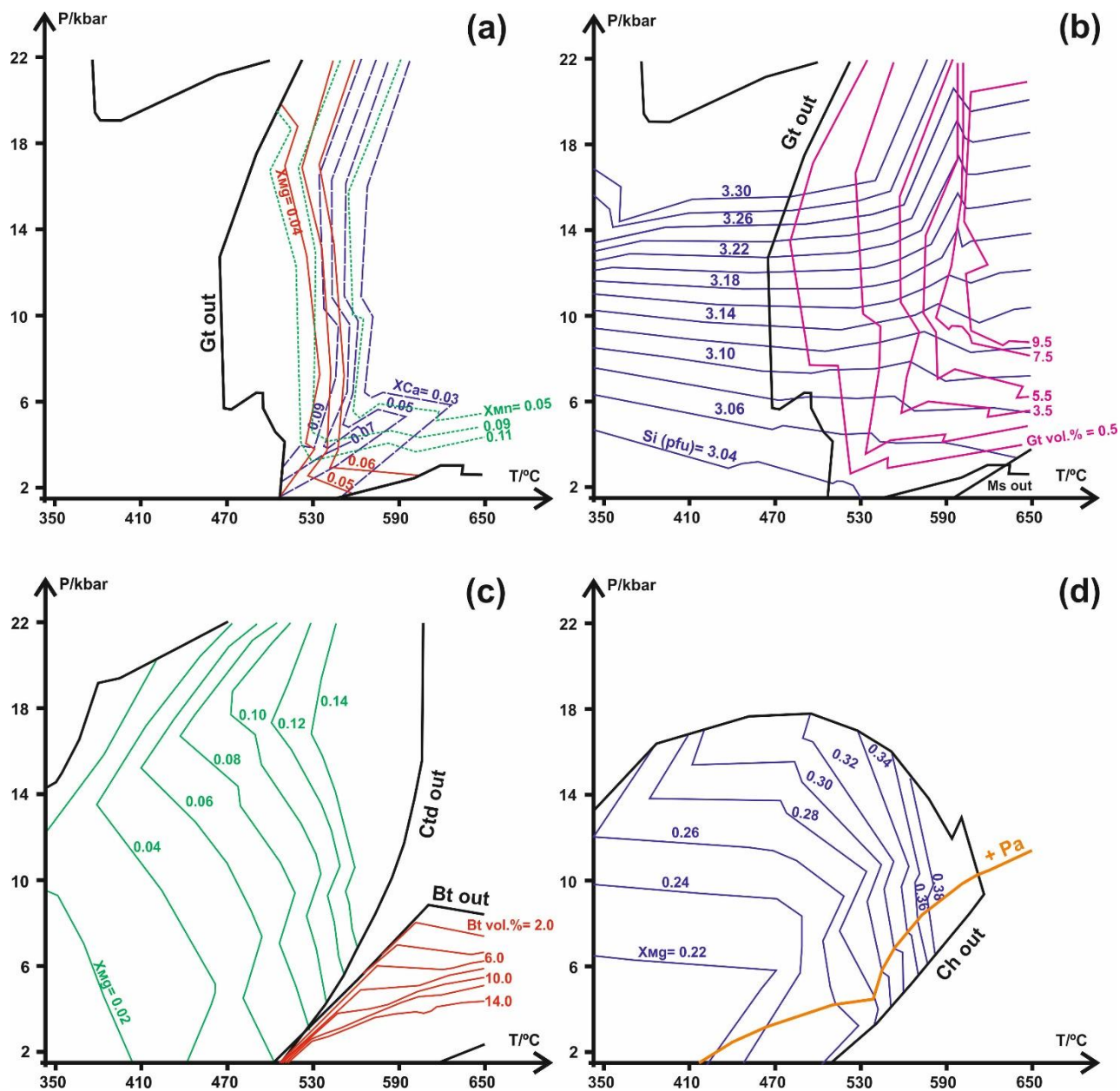


Fig. 5.6. Contouring of the P-T pseudosection of Figure 5.5a was undertaken by isopleths for (a) the molar percentage of Ca (blue), Mg (red) and Mn (green) in garnet (Gt); (b) the Si content (pfu) in potassic white-mica (Ms) (blue) and the modal content of garnet (purple); (c) X_{Mg} in chloritoid (Ctd) and the modal content of biotite (Bt) (red); and (d) X_{Mg} in chlorite (Ch). The orange line in (d) shows the limit of the paragonite (Pa) field. Mineral boundary lines were taken from Fig. 5.5.

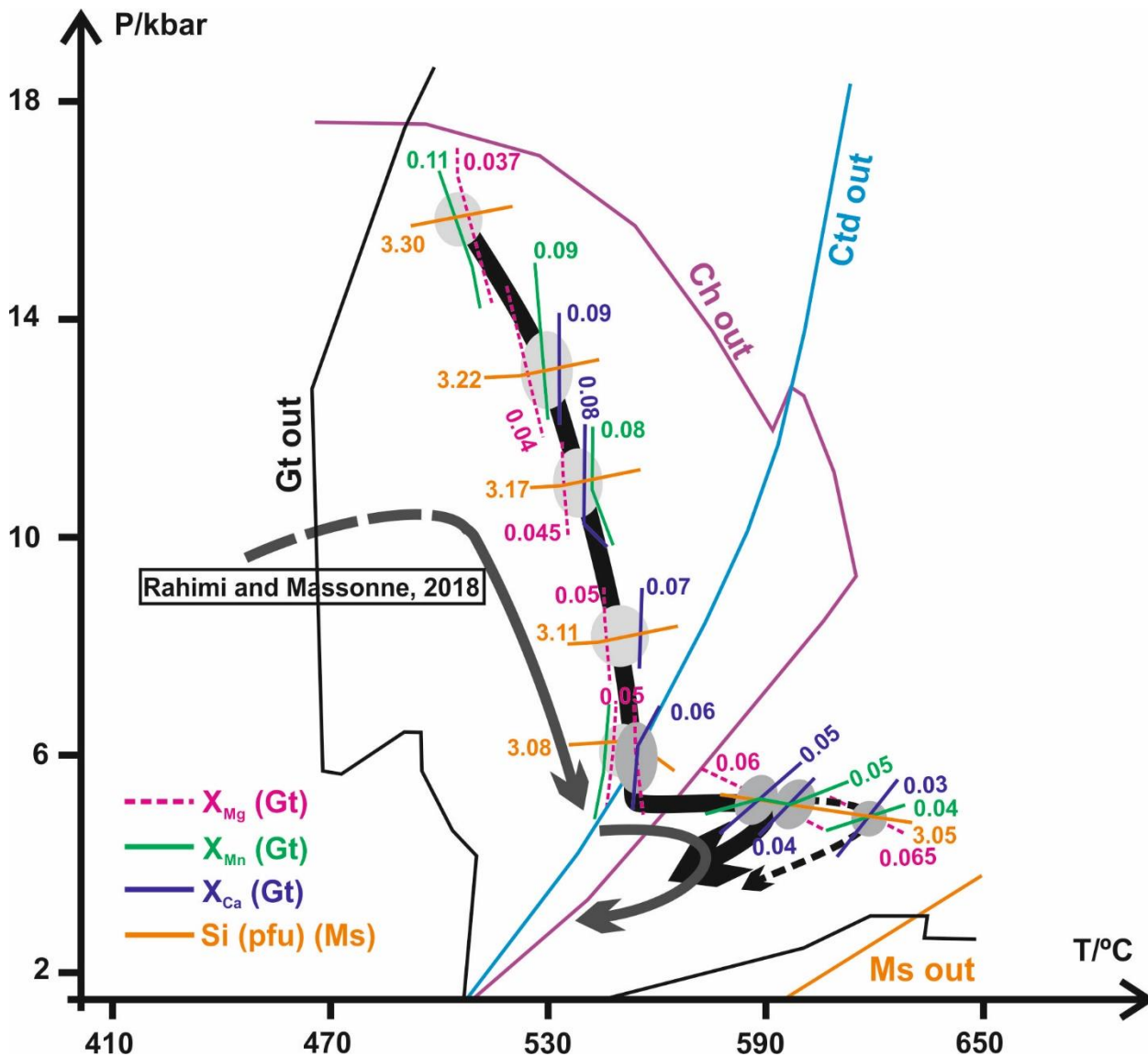


Fig. 5.7. P-T path (black with direction shown by the arrow) reconstructed for metapelite 14AS6 on the basis of intersections of various isopleths (coloured solid lines, see Fig. 5.6) for garnet (Gt) parameters and Si in potassic white-mica (Ms). Ellipses, the size of which might roughly reflect the P and T errors of these intersections, are shown in light grey when the bulk rock composition (Table 5.4, bulk 1) was considered. Grey ellipses refer to the effective bulk rock composition (Table 5.4, bulk 2). The end of the path for micaschist 14AS6 differs by a solid and a broken line. The reason why we prefer the solid line is given in the text. For comparison, the P-T path (solid-dotted dark grey arrow) for garnet-bearing micaschist 13F18 (see Fig. 5.1c) reported by Rahimi and Massonne (2018) is displayed. The limits for P-T fields are shown for four minerals (abbreviated as in Fig. 5.5) according to the results presented in Figure 5.5a.

A later metamorphic stage is defined by intersections of isopleths for the garnet outer-core ($X_{Ca} = 0.08$, $X_{Mg} = 0.045$, $X_{Mn} = 0.08$) with that of analysed potassic white-mica showing a lower Si content than the mica cores (Si = 3.17 pfu, average of 7 analyses) at 10-11 kbar and 535-540 °C (Fig. 5.7). We calculated garnet (1.5 vol.%), chlorite (4.5 vol.%), chloritoid (7 vol.%), paragonite (0.5 vol.%) coexisting with potassic white-mica, quartz, ilmenite, and rutile for this stage. Further P-T data of the metamorphic track were reconstructed, for instance, by intersecting isopleths for the garnet inner mantle ($X_{Ca} = 0.07$, $X_{Mg} = 0.05$, $X_{Mn} = 0.07$) and a Si poor (3.11 pfu) potassic white-mica at 8 kbar and 550 °C (see Fig. 5.7). Along the path from 11 to 8 kbar, the calculated modal content of garnet had increased to almost 2 vol.%. The calculated mineral assemblage at 8 kbar and 550 °C contains chlorite (~ 5.1 vol.%, Mg# = 0.34) and still some chloritoid (5.5 vol.%, Mg# = 0.14) and paragonite (0.5 vol.%).

To decipher the conditions for the late metamorphic stage of the micaschist, the P-T pseudosection for the effective bulk rock composition (bulk2 in Table 5.4) was used (Fig. 5.5b). We constructed intersections of the isopleths for the garnet outer mantle ($X_{Ca} = 0.06$, $X_{Mg} = 0.05$, $X_{Mn} = 0.05$), innermost rim ($X_{Ca} = 0.05$, $X_{Mg} = 0.06$, $X_{Mn} = 0.05$), inner rim ($X_{Ca} = 0.04$, $X_{Mg} = 0.06$, $X_{Mn} = 0.05$) and outer rim ($X_{Ca} = 0.03$, $X_{Mg} = 0.065$, $X_{Mn} = 0.04$) at about 6.2 kbar and 557 °C, 5.2 kbar and 590 °C, 5.0 kbar and 600 °C, and 4.8 kbar and 615 °C, respectively (Fig. 5.7). These isopleths for the innermost and inner rim intersect at about 10 °C lower temperatures when bulk1 was used instead of bulk2. The calculated mineral assemblage at 6.2 kbar and 557 °C involves chlorite (6 vol.%), staurolite (2.5 vol.%), and ilmenite (1 vol.%). At the peak T conditions of 615 °C, derived by the intersection of isopleths for the garnet outer rim, the calculated modal content of garnet has increased to 2.5 vol.%. The Si content of potassic white-mica has decreased to 3.05 pfu (Fig. 5.7). Further minerals in the calculated assemblage at 615 °C (Fig. 5.5b) are staurolite (4.5 vol.%), plagioclase (0.5 vol.%, $X_{An} = 0.26$), ilmenite (1 vol.%), biotite (8 vol.%, Mg# = 0.43), and sillimanite (1 vol.%).

5.6. Monazite age dating

Using BSE imagery (see, Scherrer et al., 2000), monazite was found in different microstructural positions. Petrographic and textural features of monazite are summarized in Figure 5.8.

5. Metamorphic evolution of chloritoid-bearing micaschist...

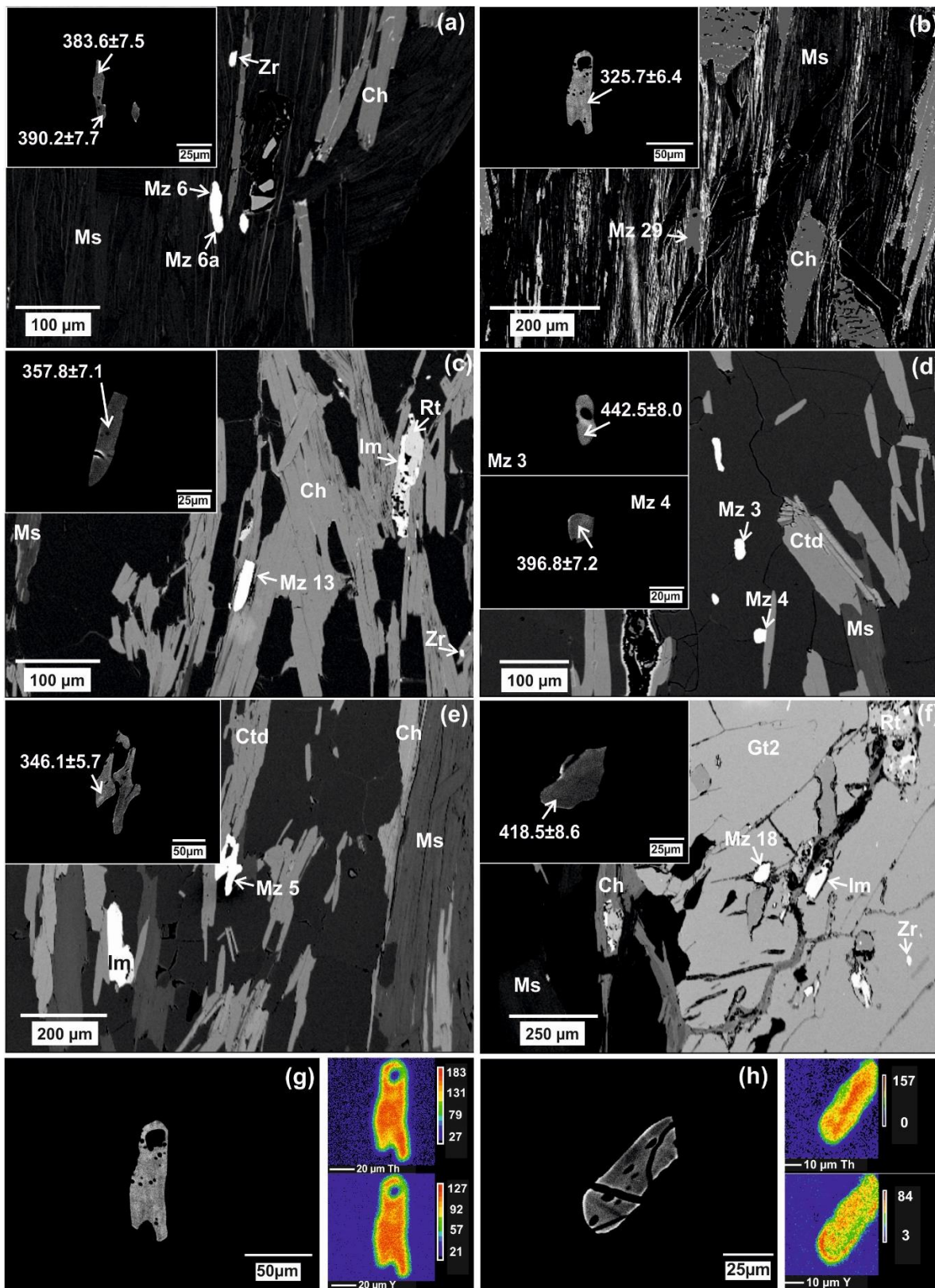


Fig. 5.8. BSE images showing monazite (Mz) in different textural positions. (a-b) Mz 6, Mz 6a, and Mz 29 occurring in a domain rich in potassic white-mica (Ms); (c) Mz 13 surrounded by chlorite (Ch); (d) Mz 3 and Mz 4 in a quartz-rich matrix; (e) Mz 5 in contact with chloritoid (Ctd) in a quartz-rich matrix; (f) Mz 18 enclosed in Gt2; and (g,h) X-ray concentration maps for Th and Y in monazite grains included in white-mica and chlorite. Cold to warm colours indicate increasing element concentrations (see the colour code on the right hand side of each map). The determined Th-Pb ages are reported with errors referring to a 2σ confidence level (see Table 5.5). (Abbreviated as in Fig. 5.5, Mz, monazite).

Monazite is commonly disseminated within the matrix of phyllosilicates (potassic white-mica, chlorite; Fig. 5.8a-c) and quartz (Fig. 5.8d), and rarely occurs in chloritoid (Fig. 5.8e) and garnet (Gt1, Gt2; Fig. 5.8f). For this study, monazite grains were dated that are an/subhedral, elongated, or oval shaped with grain sizes between 30 and 100 μm . In BSE images and elemental X-ray maps complex zonations and internal features are sometimes discernable. For instance, a grain within a white-mica aggregate was found to show a nearly homogeneous distribution of Y and Th (Fig. 5.8g), whereas another monazite grain, hosted by chlorite, shows an irregular zoning with enrichment of Th and Y in the core and partly in the rim, respectively (Fig. 5.8h).

Altogether 128 monazite analyses were conducted with the EMP on 87 grains leading also to U-Th-Pb ages (Table 5). The results are presented in Figure 9 in terms of Y_2O_3 content in wt.% and La/Gd and Th/U molar ratios plotted versus age. Some of the 128 monazite analyses were discarded because of low oxide sums (< 96.0 wt.%) and relatively high SiO_2 contents (> 0.9 wt.%). According to the remaining 113 EMP analyses (Table 5.5, Fig. 5.9a), monazite is characterized by Y_2O_3 contents less than 1.5 wt.%. Most monazite analyses yielded ThO_2 and UO_2 contents in the range of 3.6-6.3 and 0.6-0.8 wt.%, respectively (Table 5.5). These contents are more or less similar to those in igneous/high grade monazite that shows ThO_2 and UO_2 contents of 3-6 wt.% and 0.2-0.6 wt.% (Schandl and Gorton, 2004; Rasmussen and Muhling, 2007; Langone et al., 2011). However, monazite, formed at medium grade metamorphism, also shows such contents frequently with somewhat higher UO_2 contents (Gibson et al., 2004; Rasmussen and Muhling, 2007; Massonne, 2014). The obtained monazite ages are summarized in Figure 5.9b, c and range between 315 and 480 Ma without any significant age difference of monazite in distinct textural settings (see Fig. 5.8a-f). Due to the successive growth during a metamorphic cycle (Taylor et al., 2016) and probably some mixed analyses of different monazite domains, different age groups are not easily discernable.

5. Metamorphic evolution of chloritoid-bearing micaschist...

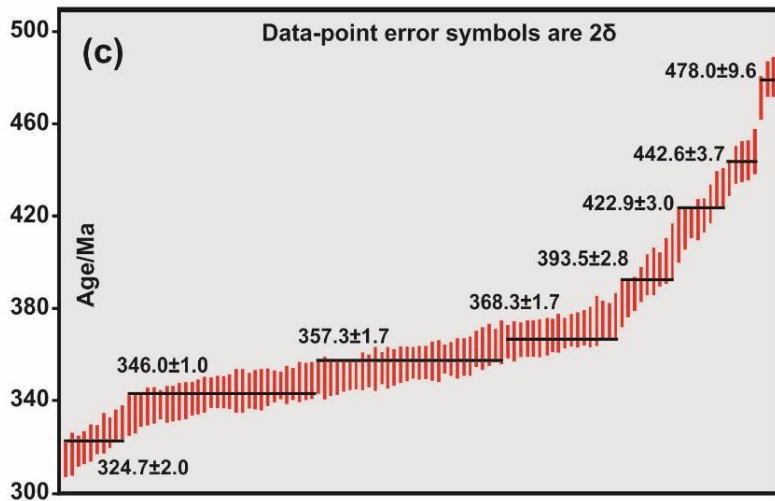
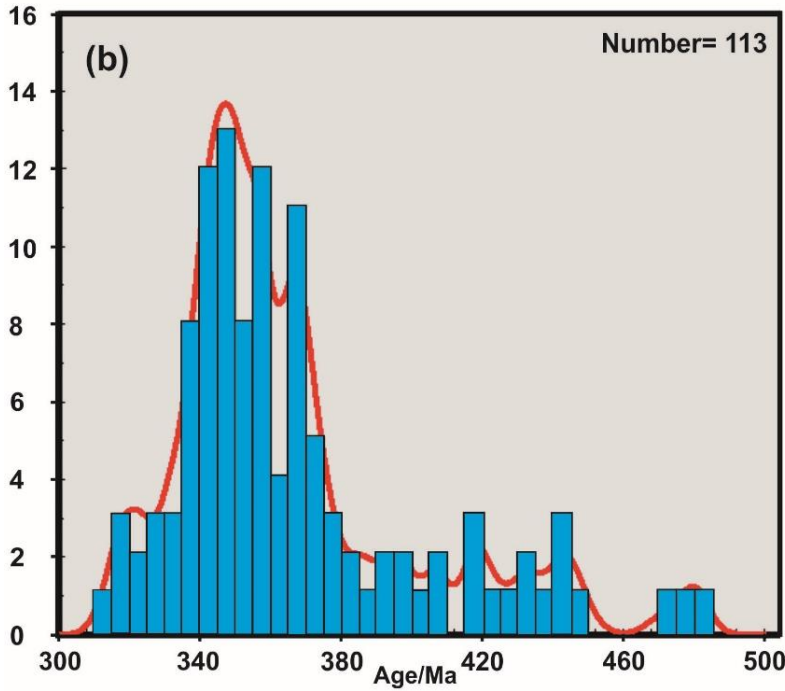
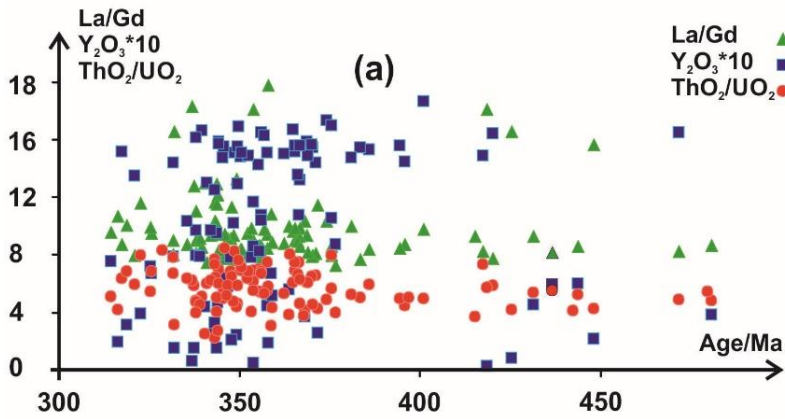


Fig. 5.9. EMP data of 113 analyses of monazite in sample 14AS6 (a) La/Gd (pfu), Y₂O₃ (wt.%)*10, and ThO₂/UO₂ (wt.%) plotted versus the determined age; (b) probability density; and (c) weighted average plots for the obtained U-Th-Pb monazite ages. Ages and their errors (2σ) of eight age populations are given in (c).

Table 5.5. Representative EMP analyses (oxides in wt.%) of monazite (Mz) in five different textural domains. The structural formulae of monazite was recalculated on the basis of 4 O.

Point analyses	Mz 29-Ms	Mz 5-Ctd	Mz 13-Ch	Mz 4-Matrix	Mz 18-Gt
SiO ₂ (wt.%)	0.42	0.43	0.28	0.41	0.25
P ₂ O ₅	28.25	27.69	28.57	29.70	26.38
SO ₃	0.01	0.01	0.02	0.01	0.00
CaO	0.70	0.75	0.62	0.58	0.56
Y ₂ O ₃	0.67	0.64	0.45	0.89	0.23
La ₂ O ₃	13.84	13.39	13.49	13.46	14.02
Ce ₂ O ₃	28.36	28.08	30.24	29.00	31.94
Pr ₂ O ₃	2.96	2.86	2.91	3.10	2.98
Nd ₂ O ₃	11.42	11.00	11.39	11.51	11.86
Sm ₂ O ₃	2.14	2.03	2.23	2.11	2.10
Gd ₂ O ₃	1.62	1.58	1.58	1.73	1.87
Dy ₂ O ₃	0.48	0.48	0.37	0.60	0.13
PbO	0.11	0.13	0.10	0.11	0.10
ThO ₂	5.17	6.28	4.27	4.13	3.59
UO ₂	0.75	0.74	0.77	0.83	0.63
Total	96.92	96.10	97.31	98.17	96.64
Si (pfu)	0.0172	0.0178	0.0113	0.0164	0.0109
P	0.9784	0.9729	0.9842	0.9978	0.9527
S	0.0004	0.0003	0.0007	0.0003	0.0000
Ca	0.0307	0.0332	0.0272	0.0248	0.0258
Y	0.0146	0.0142	0.0097	0.0188	0.0087
La	0.2088	0.2050	0.2025	0.1970	0.2206
Ce	0.4247	0.4266	0.4505	0.4214	0.4989
Pr	0.0442	0.0433	0.0432	0.0448	0.0463
Nd	0.1669	0.1630	0.1656	0.1631	0.1807
Sm	0.0302	0.0291	0.0313	0.0289	0.0309
Gd	0.0220	0.0218	0.0214	0.0228	0.0122
Dy	0.0064	0.0064	0.0048	0.0077	0.0017
Pb	0.0012	0.0014	0.0011	0.0012	0.0011
Th	0.0481	0.0594	0.0396	0.0373	0.0349
U	0.0069	0.0069	0.0070	0.0073	0.0059
Age	325.7	346.1	357.8	396.8	418.5
2 Sigma error	6.4	5.7	7.1	7.2	8.7

According to a histogram analysis with the Isoplot program (Ludwig, 1999), however, 8 populations with age maxima at 325, 346, 357, 368, 394, 423, 443, and 479 Ma could be defined. The most prominent maxima and side maxima are at 346.0 ± 1.1 (2σ), 357.3 ± 1.7 , and 368.3 ± 1.7 Ma (Fig. 5.9b, c). Among the monazite analyses (Fig. 5.9a), a group with ages ≤ 386 Ma can be only vaguely distinguished from a group with ages > 386 Ma by chemical parameters.

The younger age group is characterized by mean values for the La/Gd ratio, Y₂O₃ content, and Th/U ratio of 9.8, 1.02 wt.%, and 5.9, respectively, whereas these mean values for the older age group are somewhat higher (La/Gd = 10.05) or slightly lower (Y₂O₃ = 0.93 wt.%, Th/U = 5.4).

5.7. Discussion

The above derived P-T conditions and monazite age data shed light on the metamorphic evolution of the studied micaschist from the Elstergebirge. This evolution will be discussed in the following subsections. A geodynamic scenario is hypothesized to explain the new findings.

5.7.1. P-T evolution

The derived prograde P-T path (Fig. 5.7) for the studied chloritoid-bearing micaschist consists of 2 sections, the first one of which is an exhumation path to 15-20 km depths (~ 5 kbar). The second section indicates an isobaric heating event to about 600 °C. The path starts at 505 °C and 16 kbar. This temperature is defined by the inner core of garnet, whereas the pressure is determined by relatively Si-rich potassic white-mica (Si = 3.31 pfu) which was found as relic in the core of mica flakes. Even when our assumption of the coexistence of these garnet and mica domains would not hold true, the peak pressure would hardly be lower than 16 kbar as the corresponding Si isopleth for phengite is little temperature dependent above 400 °C (Fig. 5.6b). Thus, in any case the P-T path recorded by the studied rock is characterized by a significant pressure release to about 5 kbar at moderately rising temperature.

This temperature increase amounts to about 50 °C according to the growth of garnet from its core to the outer mantle and the consideration of an effective bulk rock composition for late garnet growth. However, the selection of diverse effective bulk rock compositions, based on the subtraction of specific early-formed garnet domains, is of nearly negligible influence as already shown in earlier works (Massonne, 2014; Massonne et al., 2018a, b). The isobaric heating path from 550 to 620 °C was exclusively reconstructed using the chemical composition of the garnet rim (see also below). Along the recorded exhumation path the calculated amount of garnet in the studied micaschist increases from 0.5 to 2.5 vol.%.

The heating path could have led to a further slight increase of this amount, which is then compatible with the observed quantity of garnet (3 vol.%) in the rock. Other minerals such as paragonite and

chloritoid, that were present at the peak pressure conditions, were already decomposed during the exhumation of the rock to 20 km depths according to the calculation results. Thus, no paragonite was found in sample 14AS6, but relicts of chloritoid exist. The remaining quantity of 5-6 vol.% (see above) corresponds to the calculated one at the derived P-T conditions of 8 kbar and 550 °C. It might be that the further metamorphic evolution was not accompanied by deformation, which usually enhances the attainment of mineral equilibrium. Lacking deformation at metamorphic pressures below 8 kbar is likely because of the observed skeletal texture of lately grown garnet around the grain boundaries of pre-existing equigranular quartz grains (Figs. 5.2 and 5.3). This texture is controlled by interfacial free energy rather than dislocation creep processes (Hawkins et al., 2007) and can, thus, only be achieved at very low differential stress, which led Stöckhert et al. (1997) to infer that deformation is, if at all, only localized to zones of weakness.

Along the exhumation path to 20 km depths the calculated amount of chlorite has increased from 1.5 to 6 vol.%. However, we observed slightly more than 10 vol.% in the rock. This means that during a late retrograde stage after the temperature climax additional chlorite has grown compatible with textural observations on micaschist 14AS6. The nearly isobaric heating path to more than 600 °C, at about 5 kbar should have led to significant amounts of staurolite (4.5 vol.%) and even some sillimanite (1 vol.%) but these minerals were not observed in sample 14AS6. We explain this discrepancy by an overestimation of the peak temperature because the composition of the outer garnet rim is probably only the result of local equilibria which can hardly be approached by the selection of an effective bulk rock composition. Thus, we think that the maximum temperatures were only around 580 °C although, at such temperatures staurolite should have already started to form at the expense of chloritoid and chlorite (Fig. 5.7).

However, significant amounts of biotite crystallized (5 vol.%) which prove the heating of the rock after exhumation to 20 km depths (see Fig. 5.6c). Compared to a garnet-bearing, but chloritoid-free and gneissose micaschist (sample 13F18) occurring 11 km WSW of the locality of sample 14AS6 (Fig. 5.1, Rahimi and Massonne, 2018), we noted a similar P-T evolution (Fig. 5.7). The P-T paths of both rocks show the same shape, but the peak pressure of 13F18 (10 kbar) is significantly lower than the here derived one (16 kbar). In addition, the temperatures of the exhumation path to 5 kbar are slightly lower for 13F18.

Both rocks (14AS6 and 13F18) experienced a heating event caused by the nearby intrusions of granitic magma at depths between 15 and 20 km (see above) corresponding to 4-5 kbar lithostatic

5. Metamorphic evolution of chloritoid-bearing micaschist...

pressure (Rahimi and Massonne, 2018). Although the peak temperature experienced by this event was somewhat lower for 13F18, the impact of the heating is more obvious in this rock due to the formation of staurolite, biotite, and andalusite, whereas in the micaschist 14AS6 only biotite newly formed. The occurrence of these minerals led to the view of earlier workers (e.g., Mielke and Schreyer, 1972) that the micaschists of the northeastern Fichtelgebirge crystalline complex experienced only low pressure metamorphism although Mielke et al. (1979) already reported the occurrence of phengite ($\text{Si} \sim 3.3$ pfu), but these authors were not aware of the geobarometric potential of potassic white-mica at that time. This mineral unequivocally evidences an early HP metamorphic stage of the studied micaschist before Barrovian-type metamorphism.

5.7.2. Interpretation of monazite ages

The obtained monazite ages, subdivided into 8 populations (see section 5.6.), range between 315 and 480 Ma. Such extended age variations are common in medium-high grade metamorphic monazite (e.g., Foster et al., 2000, 2002; Martins et al., 2009; Massonne, 2014; Palin et al., 2014; Rubatto et al., 2013). Different mechanism could be invoked to explain such age spreads (see, e.g., Foster et al., 2002). According to the discussion in Rahimi and Massonne (2018) we prefer the view that the presence of different chemical-age domains is the result of continuous and/or discontinuous monazite growth. In addition, we cannot exclude that a few age results are due to mixing of different monazite domains during EMP analysis. On the contrary, Pb loss in monazite due to diffusive processes is unlikely for a medium grade metamorphic rock as they are very slow and comparable with those in zircon (e.g., Cherniak et al., 2004; Gardés et al., 2007; Seydoux-Guillaume et al., 2002; Spear and Pyle, 2002). In addition, common observations of systematic correlation of intra-crystalline zoning (for example concerning Y and heavy rare-earth elements) with ages (e.g., Gibson et al., 2004; Williams and Jercinovic, 2002, 2012) make this diffusional process largely unlikely for being the reason of the age spread.

The determined monazite age populations (Fig. 5.9) show similarities to those reported from a metasediment (sample 13F18: Rahimi and Massonne, 2018) that occurs c. 11 km WSW of the cliff where sample 14AS6 was taken (Fig. 5.1c). There is a strict coincidence for the age cluster at 325 Ma. The cluster around 362 Ma given by Rahimi and Massonne (2018) might be represented in this work by two clusters at 357 and 368 Ma, whereas our cluster at 394 Ma is rather reproduced by two clusters at 386

and 405 Ma by these authors. In general, younger monazite ages were more intensively found in sample 13F18 than in the micaschist studied here. For instance, about one third of the EMP analyses of monazite in 13F18 yielded ages younger than 315 Ma which are completely lacking in monazite of micaschist 16AS6. In spite of some differences between the probability density plots for monazite ages in 13F18 and 16AS6, we can adopt the interpretation of age populations by Rahimi and Massonne (2018). According to these authors, we assign our age clusters at 394 Ma and older to detrital monazite providing that the studied rock is a metamorphosed pelitic sediment (see, its bulk rock composition in Table 5.4). The provenance areas of the detrital monazite were late Cadomian and post-Cadomian magmatic arcs located at the northern margin of Gondwana or Peri-Gondwanan terranes (see also, Waizenhöfer and Massonne, 2017). Our age clusters at 357 and 368 Ma are related to an Upper Devonian HP metamorphism and a subsequent exhumation in Upper Devonian to Lower Carboniferous times. This metamorphism was also reported from the nearby situated complexes of Münchberg, Erbendorf-Vohenstauß, and Mariánské Lázně (Willner et al., 2000; Fig. 5.1, section 5.2.) In fact, Rahimi and Massonne (2018) suggested that the exhumation from HP conditions to 20 km depths ended already in the Upper Devonian (362 Ma), but according to our new data the end of exhumation occurred somewhat later which would be still compatible with Ar-Ar cooling ages of c. 360 Ma and somewhat younger obtained for HP rocks situated WNW of the Elstergebirge by Faryad and Kachlík (2013). The age cluster at 325 Ma is assigned to the heating at pressures of ≤ 5 kbar (Fig. 5.7) being compatible with the low pressure metamorphism in the time interval 330-320 Ma (Okrusch et al., 1990) inferred for the adjacent Fichtelgebirge crystalline complex.

5.7.3. Geodynamic interpretation of the P-T-t evolution

If we relate our consideration to the entire belt of HP micaschists, which can be followed (with interruptions) over 100 km between the crystalline complexes of Fichtelgebirge and Erzgebirge, the original clastic sediments were deposited in the Devonian at the northern margin of Gondwana (Rahimi and Massonne, 2018). Such protoliths also refer to metasediments with HP signature in the Münchberg metamorphic complex as evidenced by a studied mylonitic migmatite (Waizenhöfer and Massonne, 2017). The burial of these metasediments started with the closure of the Rheic Ocean in Late Devonian times and proceeded with the subsequent continent-continent collision. In this scenario the upper

5. Metamorphic evolution of chloritoid-bearing micaschist...

continental plate should be Avalonia, a peri-Gondwanan terrane being accreted to Laurussia already in the Silurian (see, e.g., Li et al., 2017; Willner et al., 2013; Zeh and Gerdes, 2010; Zeh and Will, 2010). The HP stage was reached after the micaschists were fully overlaid by the Avalonian crust. This crust might have been thickened, eventually by a previously active magmatic arc as in the present-day Andes, in order to explain the depth of 55-60 km reached by the here studied micaschist at its pressure peak of 16 kbar. The exhumation occurred in an exhumation channel, which had developed between the collided plates (Massonne, 2016b). Typically, a P-T loop as shown in Figure 5.7 reflects this exhumation process as was observed for similar geotectonic settings elsewhere (e.g., Massonne and Calderón, 2008; Massonne and Toulkeridis, 2012; Massonne, 2016a).

Other metasediments of the belt of HP micaschist that have experienced peak pressures less than 16 kbar (Rahimi and Massonne, 2018: 10 kbar; Rötzler et al., 1998: 13 kbar) were involved in the upwards-directed mass flow of the exhumation channel either earlier, before they were overlaid by the thickened portion of the Avalonia crust, or later because of a larger distance to the tip of the downgoing plate. The latter reason could be more plausible when we also consider low grade metasediments, for instance, those outcropping at the margin of the Münchberg metamorphic complex. There, phyllites occur in the Prasinit-Phyllit-Serie, a nappe of this complex, showing K-Ar and Ar-Ar ages of metamorphism between 374 and 366 Ma (Koglin et al., 2018). Thus, the low grade metamorphism was contemporaneous to the HP metamorphism of the micaschists and suggests that the corresponding metasediments were not overridden by thick Avalonia crust as the here addressed HP rocks.

A further important geotectonic event is the stacking of a crystalline nappe pile. This event could have happened probably in the Viséan due to the collision of Gondwana and a northerly situated peri-Gondwanan terrane (northern Avalonia, the southern portion of it was the overriding plate in the Upper Devonian) after a short-lived ocean (e.g., Saxothuringian Ocean according to Schulmann et al., 2009) was closed probably around 340 Ma, a common age of metamorphism in the Bohemian Massif (Willner et al., 2000).

This Lower Carboniferous nappe pile was transported to the north or northwest over the autochthonous, low grade metapsammopelites with intercalated acidic metavolcanics occurring north and west of our sample locality (Fig. 5.1c) as equivalents of Cambro-Ordovician sediments of the Thuringian lithofacies. Within the pile, a nappe of HP metasediments occurred. However, this nappe does not present a coherent crustal section. On the contrary, it is composed of metasedimentary slices

that are characterized by similar P-T trajectories but clearly distinct peak pressure conditions (10-16 kbar). We assume that the mixing of these slices occurred already in the Upper Devonian exhumation channel as suggested above.

The heating of the studied micaschist to about 580 °C at 325 Ma (see above) was probably caused by post-tectonic melts of the older intrusive complex of the Fichtelgebirge granite (Rahimi and Massonne, 2018). At that time the aforementioned nappe pile was already in place. The period of time after 325 Ma is characterized by Late Variscan transpressional tectonics. Associated advective heat transfer to upper crustal levels from exhumed rocks and granitic melts is the likely reason for wide-spread regional high temperature, low pressure metamorphism in the late Lower Carboniferous (Kroner et al., 2007).

5.8. Conclusions

The detailed study of a chloritoid-bearing micaschist from the Saxothuringian Zone resulted in the following findings: (1) The studied rock underwent a HP metamorphism at about 16 kbar and 505 °C (Fig. 7). Exhumation to 15-20 km depths (~ 5 kbar) at slight heating to 555 °C followed. Subsequently, an isobaric heating to ~ 600 °C occurred. Such a P-T path, however with a significant lower peak pressure of 10 kbar, was already reported from a gneissose micaschist located 11 km WSW of the here studied rock (Rahimi and Massonne, 2018). Both HP micaschists disprove an earlier assignment to a low pressure metamorphism (Mielke et al., 1979; Okrusch et al., 1990). (2) EMP monazite dating suggests that the HP metamorphism occurred in the Upper Devonian (Fig. 5.9). The subsequent exhumation to 15-20 km depth ended in the early Carboniferous. The isobaric heating event is related to the intrusion of adjacent granites at 325 Ma.

We interpret our findings as follows: The burial of the protoliths of the micaschists started with the closure of the Rheic Ocean in Late Devonian times and proceeded with the subsequent continent-continent collision. At this stage, HP conditions were reached when the metasediments were overlaid by thick Avalonian crust. The following exhumation happened in a subduction channel. If the stacking of a crystalline nappe pile, of which the HP micaschists are part of as a nappe unit, occurred already in the subduction channel is not clear yet. A likely alternative for the stacking in the Viséan is a further

continent-continent collision after a short-lived ocean (Saxothuringian Ocean?) was closed. When early post-tectonic granites intruded the area at 325 Ma, the nappe pile was already in place.

We refer the HP micaschists from the Fichtelgebirge to the Erzgebirge crystalline complexes to a common nappe unit (see, e.g., Faryad and Kachlík, 2013), although they show different peak pressure conditions between 10 and 16 kbar. Thus, this nappe unit is composed of metasedimentary slices instead of representing a coherent crustal section.

5.9. Acknowledgements

The authors thank Thomas Theye (Stuttgart) for supporting our EMP work.

Note: This chapter was prepared as a manuscripts to submit to the geoscientific Journal of EARTH SCIENCE.

6. Protolith and Provenance

6.1. Protolith of metapelites

Chemical analyses of major, minor, and trace elements were performed for 11 metapelites of the Fichtelgebirge and Elstergebirge (see, Table 1). Sample preparation and analytical techniques were described in section 3.4; the analytical results are presented in Table 6.1.

The samples are chemically classified as subfeldspathic arenites in the $\text{Al}_2\text{O}_3 + \text{Fe}_2\text{O}_3 - \text{SiO}_2 - \text{MgO} + \text{CaO}$ diagram of Pettijohn et al. (1987) (Fig. 6.1a). The $\text{Zr} - 15*\text{Al}_2\text{O}_3 - 300*\text{TiO}_2$ ternary plot, which was proposed to monitor sediment sorting and recycling of Garcia et al. (1994), indicates greywackes and subgreywackes and a continuous trend extending from Al-rich shales towards mature sandstones (Fig. 6.1b). In this plot, the sandstone sample points show slight changes in $\text{Al}_2\text{O}_3/\text{Zr}$ ratios, suggesting poor to moderate sorting and comparatively rapid deposition. In order to constrain the protolith composition of the schists, the $\log(\text{Fe}_2\text{O}_{3\text{total}}/\text{K}_2\text{O})$ vs. $\log(\text{SiO}_2/\text{Al}_2\text{O}_3)$ discrimination diagram after Herron (1988) is also used (Fig. 6.1c). The investigated micaschist samples have shale and wacke compositions and plot close to the boundary of the Fe-sandstone field.

6.2. Provenance of metapelites

Although chemical components can be altered by diagenesis during plate tectonic movements, the major element compositions of shales can still be used to interpret the tectonic setting of the provenance area to supplement petrographic analysis (e.g., Bhatia, 1983; Roser and Korsch, 1986; Yan et al., 2007; Perri, 2014). In the TiO_2 versus $\text{Fe}_2\text{O}_3 + \text{MgO}$ and $\text{Al}_2\text{O}_3/\text{SiO}_2$ versus $\text{Fe}_2\text{O}_3 + \text{MgO}$ discrimination diagrams (Bhatia, 1983), most samples plot in or around the fields of active continental margin (ACM) and continental island arc (CIA). Some samples point to an oceanic island arc (OIA) (Fig. 6.2a-b).

According to the classification diagram by Roser and Korsch (1986), using $\text{SiO}_2/\text{Al}_2\text{O}_3$ vs. $\text{K}_2\text{O}/\text{Na}_2\text{O}$ ratios, samples of the Fichtelgebirge-Elstergebirge are PM (passive margin) or ACM (active continental margin) derived (Fig. 6.2d). The abundance rates of the highly incompatible trace elements Sc, Th, and $\text{Zr}/10$ (Fig. 6.2c) indicate that the precursor pelitic sediments were deposited at a continental island arc (Bhatia and Crook, 1986).

6. Protolith and Provenance

Most samples plot in the field of acidic arc source close to that of the upper continental crust (UCC) with a minor mixing of a felsic/basic source (Fig. 6.3e). However, certain samples with Hf enrichment suggest a considerable component of old sediments (Floyd and Leveridge, 1987). Upper continental crust normalized plots (Taylor and McLennan, 1981) were also used to discriminate the tectonic setting of the Fichtelgebirge-Elstergebirge (Fig. 6.3f). The following source-distinguishing anomalies were recognized: (1) Nb/Nb*: 0.06, (2) U, Sr, Nb, Zr and Ba anomalies which are typical for UCC. Trace element analyses show that the samples are depleted in Zr with abundances of Zr ranging from about 111 to 272 ppm. High Zr abundances are caused by concentration of zircon grains (Roser, 2000) and higher Zr contents in our samples correlate with high modal proportions of zircon (Shi et al., 2016). The average abundances of trace elements are generally similar to those in UCC, but there are some differences; relative enrichment in Hf and depletions in Ba and Sr. Alkali feldspar was probably the reservoir for Sr and Ba (e.g., Götze, 1998).

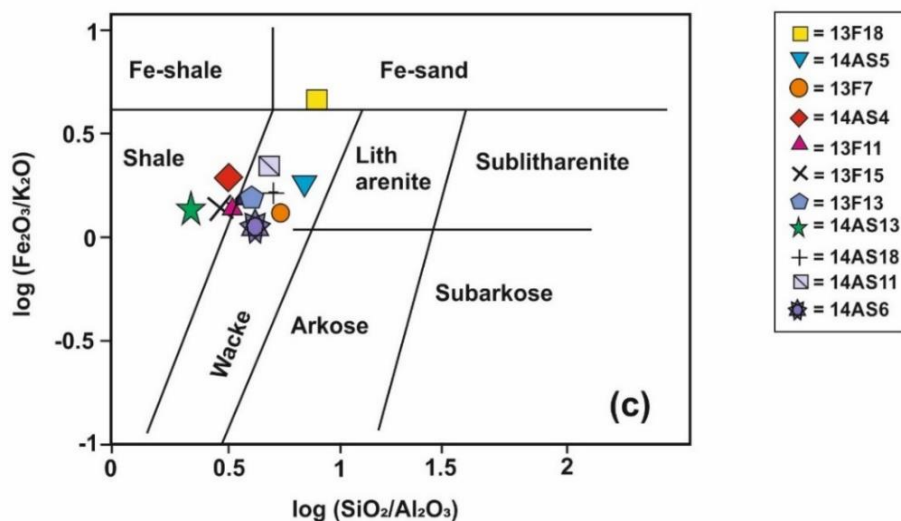
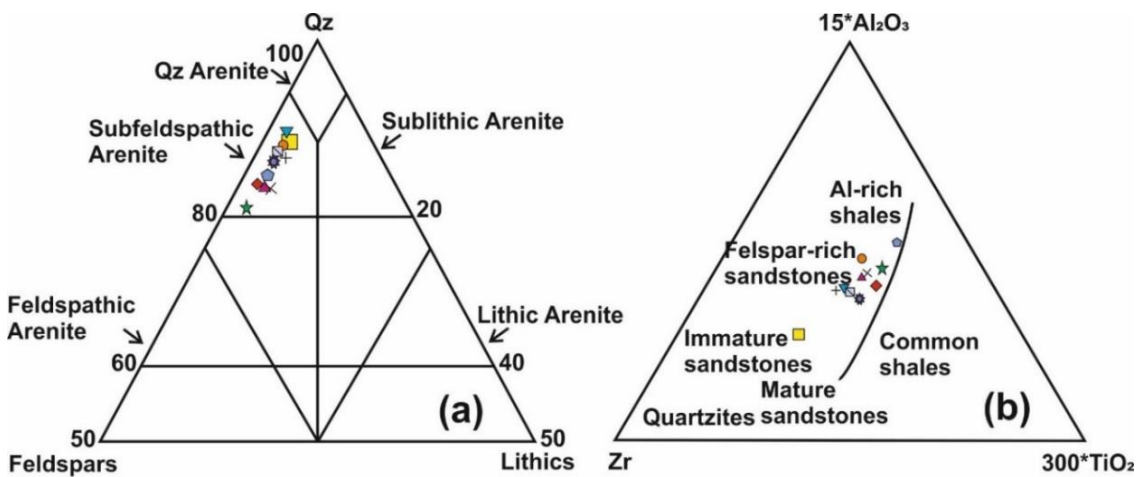


Fig. 6.1. (a) QFL triangular classification plot (Pettijohn et al., 1987) of metapelites from the Fichtelgebirge-Elstergebirge; (b) ternary $15 \cdot \text{Al}_2\text{O}_3 - \text{Zr} - 300 \cdot \text{TiO}_2$ plot (Garcia et al., 1994); and (c) the $\log(\text{SiO}_2/\text{Al}_2\text{O}_3)$ vs $\log(\text{Fe}_2\text{O}_3/\text{K}_2\text{O})$ diagram of Herron (1988).

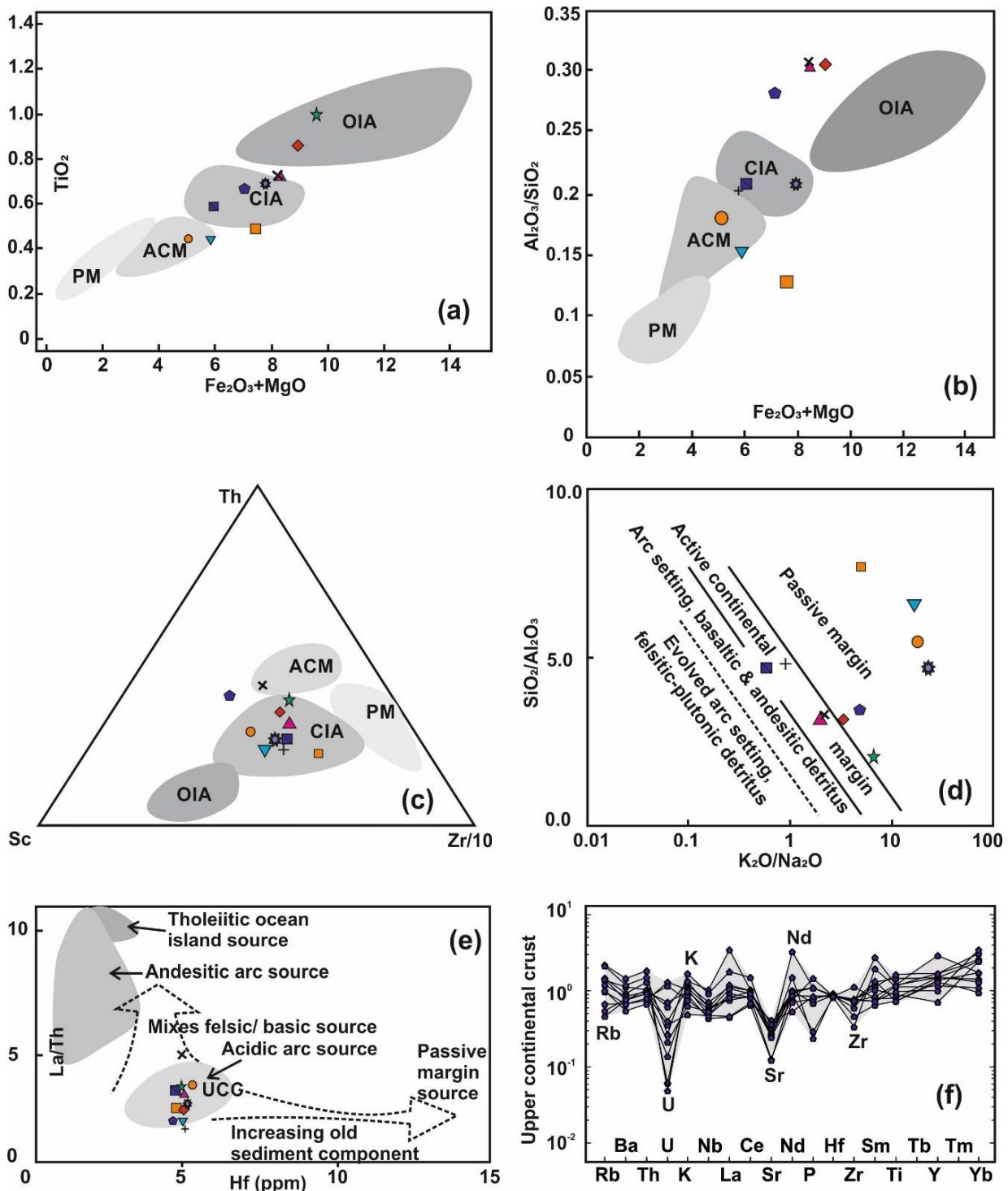


Fig. 6.2. Provenance discrimination diagrams, coloured symbols refer to the present study of metapelite from Fichtelgebirge-Elstergebirge. (a-b) Plots of $\text{Fe}_2\text{O}_3 + \text{MgO}$ vs. TiO_2 and $\text{Fe}_2\text{O}_3 + \text{MgO}$ vs. $\text{Al}_2\text{O}_3/\text{SiO}_2$

6. Protolith and Provenance

to discriminate tectonic settings (after, Bhatia, 1983); (c) Ternary tectonic diagram Th-Sc-Zr/10 of (Bhatia and Crook, 1986), (Discrimination fields of tectonic setting are after Bhatia and Crook (1986)); (d) $\text{SiO}_2/\text{Al}_2\text{O}_3$ vs. $\text{K}_2\text{O}/\text{Na}_2\text{O}$ diagram of Roser and Korsch (1986); e) Plot of La/Th vs. Hf (Floyd and Leveridge, 1987); Certain areas fields relate the compositions of sedimentary rocks to their deposition in different tectonic settings; and (f) Upper crust normalized, multi-element spider diagram for the studied metapelites. Upper crust values are from Taylor and McLennan (1981). ACM, Active Continental Margin; CIA, Continental Island Arc; OIA, Oceanic Island Arc; PM, Passive Margin; and UCC, Upper Continental Crust. Symbols as in Fig. 6.1.

Table 6.1. Bulk rock analyses for the studied rocks determined by X-ray fluorescence spectrometry = XRF (major and trace elements). The units for major and trace elements are wt.% and ppm, respectively.

Sample	13F7	13F11	13F13	13F15	13F18	14AS4	14AS5	14AS6	14AS11	14AS13	14AS18
SiO₂(wt.%)	63.19	62.18	66.30	62.01	77.98	75.66	77.58	70.87	70.94	54.54	71.89
Al₂O₃	19.17	18.79	18.55	18.80	9.76	13.37	11.33	14.64	14.57	25.41	14.32
Fe₂O₃	7.27	6.03	5.52	6.02	6.89	4.35	5.15	6.65	4.46	7.68	4.05
CaO	0.24	0.87	0.04	0.87	0.51	0.15	0.06	0.09	0.89	0.09	1.81
MgO	1.66	2.31	1.55	2.29	0.55	0.76	0.76	1.18	1.47	1.92	1.62
Na₂O	1.17	2.08	0.75	2.05	0.31	0.18	0.17	0.15	3.46	0.79	2.68
K₂O	3.90	4.43	3.63	4.41	1.60	3.39	2.87	3.25	2.08	5.55	2.48
TiO₂	0.86	0.72	0.67	0.72	0.48	0.44	0.44	0.68	0.59	0.99	0.53
MnO	0.06	0.05	0.12	0.05	0.03	0.04	0.07	0.08	0.06	0.06	0.06
P₂O₅	0.12	0.19	0.05	0.18	0.25	0.13	0.19	0.18	0.14	0.04	0.15
Total	97.66	97.65	97.17	97.42	98.18	98.47	98.61	97.77	98.67	97.01	99.58
Ag (ppm)	3.79	3.72	3.61	3.73	3.46	3.57	3.15	3.79	3.69	3.89	3.67
As	9.75	10.36	3.82	1.60	9.05	10.23	6.74	11.74	13.82	8.38	9.25
Ba	644.91	782.67	524.16	1026.34	519.29	469.91	384.98	589.33	537.58	821.77	462.90
Bi	12.44	12.16	11.57	11.56	9.38	12.85	15.19	13.52	20.00	14.67	14.08
Ce	63.90	63.43	54.36	65.05	51.62	53.03	41.46	62.47	59.22	97.03	44.19
Cd	2.55	7.15	3.75	5.71	4.09	6.63	4.63	6.12	7.55	3.45	6.67
Cr	73.77	89.57	69.28	105.28	39.13	41.92	42.05	66.05	63.02	84.53	52.61
Cs	7.78	16.17	11.52	18.35	1.18	8.19	9.32	16.19	6.58	17.02	7.42
Cu	1.70	1.67	1.61	1.71	1.66	1.68	2.15	1.64	1.70	1.57	1.62
Ga	19.57	19.19	19.47	28.40	10.12	12.64	9.56	13.49	10.09	25.31	11.21
Ge	0.83	0.82	0.79	0.83	0.80	0.93	0.82	0.81	0.83	0.86	0.80
Hf	5.00	4.95	4.71	5.08	4.87	5.32	5.00	5.02	4.82	4.98	5.09
I	4.40	4.35	4.20	4.42	4.19	4.47	4.69	4.62	4.79	4.26	4.58
La	33.57	35.50	22.20	102.32	24.42	27.57	13.40	24.84	31.50	54.00	13.93
Mo	0.37	0.36	0.35	0.37	0.37	0.38	0.38	0.36	0.32	0.34	0.36
Nb	17.91	14.70	15.45	25.52	11.88	12.22	10.82	14.07	13.22	22.62	11.85
Nd	26.37	24.61	22.85	84.44	19.32	18.29	26.30	25.53	22.62	39.33	13.87
Ni	13.35	13.06	22.31	35.94	0.81	6.38	20.26	12.94	18.36	23.33	32.86
Pb	29.94	27.92	34.45	37.21	24.97	28.96	36.04	26.95	31.97	36.87	28.36

Table 6.1. continued.

Pr	7.93	5.36	6.64	18.43	0.24	5.06	5.79	4.11	7.08	10.15	2.78
Rb	160.03	151.91	154.00	240.89	50.92	107.63	108.91	129.81	59.76	229.97	74.51
Sb	10.43	6.28	7.80	7.91	4.14	9.10	7.16	10.36	7.99	11.08	6.61
Sc	13.39	11.67	12.00	15.58	13.17	12.35	13.12	14.25	12.97	11.98	13.69
Se	2.73	2.66	1.64	3.05	0.50	1.26	1.63	2.02	1.60	2.93	0.20
Sm	5.85	3.80	8.78	12.39	3.54	2.95	6.03	3.25	3.26	5.08	4.63
Sn	2.31	2.28	2.20	2.28	2.14	2.31	2.03	1.12	0.08	0.63	0.89
Sr	106.35	97.12	91.92	94.35	86.84	43.63	42.81	129.37	126.77	84.31	142.72
Ta	0.10	0.63	1.89	2.74	5.66	2.25	1.23	3.79	1.85	3.40	3.28
Te	4.05	4.00	3.87	4.03	3.81	4.06	4.10	4.00	4.45	4.12	3.93
Th	13.75	10.90	10.86	19.34	9.62	7.94	6.95	10.09	9.59	15.91	8.44
Tl	5.45	4.13	2.98	3.55	2.81	2.57	3.68	1.72	2.84	2.41	2.78
U	0.15	1.54	1.00	0.12	0.88	3.26	0.35	1.79	0.53	0.66	2.89
V	102.10	116.75	93.37	134.70	58.94	55.20	53.16	85.11	62.61	119.01	53.68
Y	33.18	32.79	25.37	63.83	33.00	29.80	28.58	37.45	22.18	37.06	15.70
Yb	3.08	2.89	2.37	3.83	5.32	3.82	2.11	6.76	7.62	5.62	5.34
Zn	92.80	90.15	89.71	158.16	40.07	58.57	85.59	59.67	70.71	101.97	47.23
Zr	180.76	177.04	80.24	168.77	272.83	111.86	144.58	183.25	180.80	187.30	186.85
Nb/Nb*	0.06	0.06	0.06	0.06	0.06	0.06	0.06	0.06	0.06	0.06	0.06

7. Final conclusions

The Variscan orogeny of Europe and N-Africa is the result of the convergence of Gondwana and Laurussia plates, in the Palaeozoic. This orogen is characterized by the juxtaposition of blocks of continental crust. Petrological constraints in combination with chemical, geochemical and isotopic fingerprints of the protoliths, and tectonic regimes were used to obtain detail information on the Variscan evolution of the Fichtelgebirge crystalline complex (FC) and Elstergebirge in the Saxothuringian Zone (SZ). The thesis presents detailed P-T paths of metapelitic samples from these complexes. In addition, the sedimentary environment of pelitic rocks was elucidated by bulk rock analyses of 11 samples. Metamorphic ages were determined by U-Th-Pb monazite dating. The findings on dating, metamorphic evolution and protolith character were combined. The new results contribute significantly to a better understanding of the collisional situation in early- and mid- Variscan times (c. 400-340 Ma) for the northwestern portion of the Bohemian Massif. Since the existed various geological P-T models for this region are not fully compatible with the new findings, a revised one (see, discussion section in chapters 4 and 5) is presented, which also agrees with previously reported geochronological and geochemical data.

The detailed study of a garnet-bearing gneissose micaschist (sample 13F18) from an occurrence in the NNE of the town of Selb in the northern Fichtelgebirge (see, Fig. 4.1b) revealed that (1) this rock had experienced a high pressure (HP) metamorphism at about 10 kbar and 505 °C, followed by an exhumation to 15-20 km depths (~ 4.5 kbar) at 565 °C. (2) Monazite age dating with the electron microprobe (EMP) resulted in age populations between 200 and 480 Ma. The age cluster of 384.5 ± 1.8 (2σ) Ma can be related to the HP metamorphic event. The exhumation to 15-20 km ended at 362.3 ± 1.0 Ma. The post-collisional granitic melts of the older intrusive complex of the FC affected the metasediments at 325.0 ± 0.7 Ma. These melts had intruded a crystalline nappe pile that might have formed by a second collisional event of Gondwana and the peri-Gondwanan terrane which had been accreted to Laurussia after closure of the Rheic Ocean already in Late Devonian times. This event caused the overriding of crystalline nappes of the FC, of which the garnet-bearing micaschist unit of our sample was a lower part of, onto the Laurussian crust. Ages younger than 315 Ma are clearly related to the emplacement of the FC granites and subsequent hydrothermal processes.

The detailed study of another HP (> 10kbar) metapelite (sample 14AS6) located ~ 4.5 km NE of the town of Asch/Aš in the western Elstergebirge (see, Figs. 1.1, 3.2 and 5.1c), highlights that this chloritoid-bearing rock had experienced higher pressure conditions in the early stage (see, section 5.5). From these studies the following findings were concluded: (1) the studied rock underwent a HP metamorphism at about 16 kbar and 505 °C (Fig. 5.7). Exhumation to 15-20 km depths (~ 5 kbar) at slight heating to 555 °C followed. Subsequently, an isobaric heating to ~ 600 °C occurred. Such a P-T path, however with a significant lower peak pressure of 10 kbar, was already reported from sample 13F18 (chapter 4). Both HP micaschists disprove an earlier assignment to a low pressure metamorphism (Mielke et al., 1979; Okrusch et al., 1990). (2) EMP monazite dating suggests that the HP metamorphism occurred in the Upper Devonian. The subsequent exhumation to 15-20 km depth ended in the Early Carboniferous. The isobaric heating event is related to the intrusion of adjacent granites at 325 Ma.

We interpret our findings as follows: The burial of the protoliths of the micaschists started with the closure of the Rheic Ocean in Late Devonian times and proceeded with the subsequent continent-continent collision. At this stage, HP conditions were reached when the metasediments were overlaid by thick Avalonian crust. The following exhumation happened in an exhumation channel. If the stacking of a crystalline nappe pile, of which the HP micaschists are part of as a nappe unit, occurred already in the exhumation channel is not clear yet. A likely alternative for the stacking in the Viséan is a further continent-continent collision after a short-lived ocean (Saxothuringian Ocean?) was closed. When early post-tectonic granites intruded the area at 325 Ma, the nappe pile was already in place.

We refer the HP micaschists from the Fichtelgebirge to the Erzgebirge crystalline complexes to a common nappe unit (see, e.g., Faryad and Kachlík, 2013), although they show different peak pressure conditions between 10 and 16 kbar. Thus, this nappe unit is composed of metasedimentary slices instead of representing a coherent crustal section.

These findings are additionally supported by the different geotectonic nature (continental island arc, active continental and passive margin) of the protoliths according to the geochemical features of major and trace elements study. Lithologically, the precursor metasediments of the Fichtelgebirge and Elstergebirge may be clearly separated into three major rock groups irrespective of metamorphic grade: metagreywackes, feldspar-rich sandstones and shales which came from the upper continental crust of Avalonia.

8. Bibliography

- Abati, J., Gerdes, A., Fernández-Suárez, J., Arenas, R., Whitehouse, M.J., Díez Fernández, R., 2010. Magmatism and early-Variscan continental subduction in the Northern Gondwana margin recorded in zircons from the basal units of Galicia, NW Spain. *Geological Society of America Bulletin* 122, 219–235.
- Adam, J., Reuter, A., 1981. Das Paläozoikum von Erbdorf (NE-Bayern) – Ergebnisse Einer Neukartierung Unpubl. diploma thesis, Göttingen 63 p.
- Andersen, D.J., Lindsley, D.H., 1988. Internally consistent solution models for Fe-Mg-Mn-Ti oxides - Fe-Ti oxides. *American Mineralogist* 73, 714–726.
- Arenas, R., Díaz García, F., Martínez Catalán, J.R., Abati, J., González Cuadra, P., Andonaegui, P., González del Tanago, J., Rubio Pascual, F., Castiñeiras, P., and Gomez Barreiro, J., 2000, Structure and evolution of the Ordenes Complex: A Coruna, Spain, *Basement Tectonics* 15, Pre-Conference Field Trip.
- Asami, M., Suzuki, K., Grew, E.S., 2002. Chemical Th-U-total Pb dating by electron microprobe analysis of monazite, xenotime and zircon from the Archean Napier Complex, east Antarctica: evidence for ultra-high-temperature metamorphism at 2400 Ma. *Precambrian Research* 114, 249–275.
- Bahlburg, H., Vervoort, J. D., DuFrane, S. A., 2010. Plate tectonic significance of Middle Cambrian and Ordovician siliciclastic rocks of the Bavarian Facies, Armorican Terrane Assemblage, Germany–U–b and Hf isotope evidence from detrital zircons. *Gondwana Research* 17, 223–235.
- Ballèvre, M., Martinez Catalan, J.R., Lopez-Carmona, A., Pitra, P., Abati, J., Fernandez, R.D., Ducassou, C., Arenas, R., Bosse, V., Castineiras, P., Fernandez-Suarez, J., Gomez Barreiro, J., Paquette, J.L., Peucat, J.J., Poujol, M., Ruffet, G., Sanchez Martinez, S., 2014. Correlation of the nappe stack in the Ibero-Armorican arc across the Bay of Biscay: a joint French-Spanish project. In: Schulmann, K., Martínez Catalán, J.R., Lardeaux, J.M., Janoušek, V., Oggiano, G. (Eds.), *The Variscan Orogeny: Extent. Timescale and the Formation of the European Crust*. Geological Society of London Special Publications 405, 77–113.
- Behr, H.-J., Engel, W., Franke, W., 1982. Variscan wild flysch and nappe tectonics in the Saxothuringian Zone (northeast Bavaria, West Germany). *American Journal of Science* 282, 1438–1470.

- Behr, H.-J., Engel, W., Franke, W., Giese, P., Weber, K., 1984. The Variscan belt in Central Europe: main structures, geodynamic implications, open questions. *Tectonophysics* 109, 15–40.
- Behr, H.-J., Grosse, S., Heinrichs, T., Wolf, U., 1989. A reinterpretation of the gravity field in the surroundings of the KTB-implications for granite plutonism and terrane tectonics in the Variscan. In: Emmermann, R., and Wohlenberg, H. (Eds.), *The German Deep-Drilling Program: Pre-site Investigations in the Oberpfalz and Schwarzwald*. Springer, Berlin 501–526 pp.
- Behrmann, J.H. Tanner, D.C., 1997. Carboniferous tectonics of the Variscan basement collage in eastern Bavaria and western Bohemia. *Geologische Rundschau* 86, 15–27.
- Berman, R.G. 1988. Internally-consistent thermodynamic data for minerals in the system $\text{Na}_2\text{O}-\text{K}_2\text{O}-\text{CaO}-\text{MgO}-\text{FeO}-\text{Fe}_2\text{O}_3-\text{Al}_2\text{O}_3-\text{SiO}_2-\text{TiO}_2-\text{H}_2\text{O}-\text{CO}_2$. *Journal of Petrology* 29, 445–522.
- Berman, R.G., 1991. Thermobarometry using multi-equilibrium calculations: a new technique, with petrological applications. In: Gordon, T.M., and Martin, R.F. (Eds.), *Quantitative methods in petrology: an issue in honor of Hugh J. Greenwood*. *Canadian Mineralogist* 29, 833–855.
- Bernhardt, H.J., 2007. MINCALC-V5, a software tool for mineral analyses data processing. *Acta Microscopica* 16 (Suppl. 2), 43–44.
- Bernhardt, H.J., Massonne, H.-J., Reinecke, T., Reinhardt, J., Willner, A., 1995. Digital element distribution maps, an aid for petrological investigations. *Beihefte zum European Journal of Mineralogy* 7, 28.
- Bernstein, K.H., Gotte, W., Hirschmann, G., 1973. Erläuterung zur Geologischen Übersichtskarte der Bezirke Dresden, Karl-Marx Stadt und Leipzig 1:400 000. VEB Geologische Forschung und Erkundung Halle, Freiberg 78 p.
- Besang, C., Harre, W., Kreuzer, H., Lenz, H., Mülle, P., Wendt, I., 1976. Radiometrische Datierung, geochemische und petrographische Untersuchungen der Fichtelgebirgsgranite. *Geologisches Jahrbuch* E8, 3–71.
- Bhatia, M., 1983. Plate tectonics and geochemical composition of sandstones. *Journal of Geology* 9, 611–627.
- Bhatia, M.R., Crook, K.A., 1986. Trace elements characteristics of greywackes and tectonic setting discrimination of sedimentary basins. *Contribution to Mineralogy and Petrology* 92, 181–193.

- Brandelik, A., 2009. CALCMIN—an EXCEL™ Visual Basic application for calculating mineral structural formulae from electron microprobe analyses Source. *Computers and Geosciences* 35 1540–1551.
- Braun, I., Montel, J.M., Nicollet, C., 1998. Electron microprobe dating of monazites from high-grade gneisses and pegmatites of the Kerala Khondalite Belt, southern India. *Chemical Geology* 146, 65–85.
- Brouwer, P., 2006. Theory of XRF. Almelo, Netherlands: PANalytical BV, 11–14 pp.
- Brown, T.H., Berman, R.G., Perkins, E.H., 1988. Geo–Calc – Software package for calculation and display of pressure–temperature–composition phase-diagrams using an IBM or compatible personal-computer *Computers and Geosciences* 14, 279–289.
- Carl, C., Wendt, I., 1993. Radiometrische Datierung der Fichtelgebirgsgranite. *Zeitschrift für Geologische Wissenschaften* 21, 49–72.
- Catlos, E. J., Gilley, L.D., Harrison, T. M., 2002. Interpretation of monazite ages obtained via in situ analysis. *Chemical Geology* 188, 193–215.
- Cherniak, D.J., Watson, E.B., Grove, M., Harrison, T.M., 2004. Pb diffusion in monazite: a combined RBS/SIMS study. *Geochimica et Cosmochimica Acta* 68, 829–840.
- Cho, K.H., Takgaki, H., Suzuki, K., 1999. CHIME monazite age of granitic rocks in the Sungchang shear zone, Korea; timing of dextral ductile shear. *Geoscience Journal (Seoul)* 3, 1–15.
- Čizěk, P., Tomek, Č., 1991. Large-scale thin-skinned tectonics in the eastern boundary of the Bohemian Massif. *Tectonics* 10, 273–286.
- Cocherie, A., Albarède, F., 2001. An improved U-Th-Pb age calculation for electron microprobe dating of monazite. *Geochimica et Cosmochimica Acta* 65, 4509–4522.
- Cocks, L.R.N., Fortey, R.A., 1990. Biogeography of Ordovician and Silurian faunas. In: McKerrow, W.S., Scotese, C.F. (Eds.), *Palaeozoic Palaeogeography and Biogeography*, Geological Society of London Memoir 12, 97–104.
- Cocks, L.R.M., Torsvik, T.H., 2002. Earth geography from 500 to 400 million years ago: a faunal and palaeomagnetic review. *Journal of the Geological Society* 159, 631–644.
- Cocks, L.R.M., Torsvik, T.H., 2006. European geography in a global context from the Vendian to the end of the Palaeozoic. In: Gee, D.G., Stephenson, R.A. (Eds.), *European Lithosphere Dynamics*, Geological Society of London Memoir 32, 83–95.

- Cocks, L.R.M., Torsvik, T.H., 2011. The Palaeozoic geography of Laurentia and western Laurussia: a stable craton with mobile margins. *Earth Science Reviews* 106, 1–51.
- Coggon, R.M., Holland, T.J.B., 2002. Mixing properties of phengitic micas and revised garnet-phengite thermobarometers. *Journal of Metamorphic Geology* 20, 683–696.
- Connolly, J.A.D., 1990. Multivariable phase diagrams; an algorithm based on generalized thermodynamics. *American Journal of Sciences* 290, 666–718.
- Connolly, J.A.D., 2005. Computation of phase equilibria by linear programming: a tool for geodynamic modeling and its application to subduction zone decarbonation. *Earth and Planetary Science Letters* 236, 524–541.
- Connolly, J.A.D., 2009. The geodynamic equation of state: what and how. G3 10: Q10014, doi: 10.1029/2009GC002540.
- Connolly, J.A.D., Kerrick, D.M., 1987. An algorithm and computer program for calculating composition phase diagrams. *Calphad—computer Coupling of Phase Diagrams and Thermochemistry (CALPHAD)* 11, 1–55.
- Connolly, J.A.D., Petrini, K., 2002. An automated strategy for calculation of phase diagram sections and retrieval of rock properties as a function of physical conditions. *Journal of Metamorphic Geology*, 20, 697–708.
- Cooke, R.A., O'Brien, P.J., 2001. Resolving the relationship between high P–T rocks and gneisses in collisional terranes: an example from the Gföhl gneiss–granulite association in the Moldanubian Zone, Austria. *Lithos* 58, 33–54.
- Creder, H., 1902. *Erläuterungen zur geologischen Spezialkarte des Königreichs Sachsen. Section Bad Elster nebst Schönberg, 2. Auflage, Leipzig.*
- Crowley, Q.G., Floyd, P.A., Winchester, G.A., Franke, W., Holland, G., 2000. Early Palaeozoic rift-related magmatism in Variscan Europe: fragmentation of the Armorican Terrane Assemblage. *Terra Nova* 12, 171–180.
- Cruciani, G., Franceschelli, M., Massonne, H.-J., Carosi, R., Montomoli, C., 2013. Pressure–temperature and deformational evolution of high-pressure metapelites from Variscan NE Sardinia, Italy. *Lithos* 175–176, 272–284.
- Dallmeyer, R.D., Martínez García, E., 1990. *Pre-Mesozoic Geology of Iberia*. Springer, Berlin-Heidelberg-New York, 416 pp.

- Dallmeyer, R.D., Franke, W., Weber, K., 1995. Pre-Permian geology of central and eastern Europe: Berlin, Springer-Verlag, 604 p.
- DEKORP Research Group, 1994. The deep reflection seismic profiles DEKORP 3/MVE 90, *Zeitschrift für Geologische Wissenschaften* 22, 623–824.
- Diener, J.F.A., Powell, R., 2010. The influence of ferric iron on the stability of mineral assemblages. *Journal of Metamorphic Geology* 28, 599–613.
- Díez Fernández, R., Martínez Catalán, J.R., Arenas, R., Abati, J., Gerdes, A., Fernández-Suárez, J., 2012b. U–Pb detrital zircon analysis of the lower allochthon of NW Iberia: age constraints, provenance and links with the Variscan mobile belt and Gondwanan cratons. *Journal of the Geological Society* 169, 655–665.
- Drost, K., Gerdes, A., Jeffries, T., Linnemann, U., Storey, C., 2011. Provenance of Neoproterozoic and early Paleozoic siliciclastic rocks of the Teplá-Barrandian unit (Bohemian Massif): evidence from U–Pb detrital zircon ages. *Gondwana Research* 19, 213–231, doi:10.1016/j.gr.2010.05.003.
- Echtler, H., Malavieille, J., 1990. Extensional tectonics, basement uplift and Stephano-Permian collapse basin in a late Variscan metamorphic core complex (Montagne Noire, Southern Massif Central). *Tectonophysics* 177, 125–138.
- Emmert, U., von Horstig, G., Stettner, G., 1981. Geologische Übersichtskarte, Bayreuth. Scale, 1: 200000, Bl. Nr. CC6334, Hannover.
- Engel, W., Franke, W., Langenstrassen, F., 1983a. Palaeozoic sedimentation in the northern branch of the mid-European Variscides - essay of an interpretation. In: Martin, H., Eder, W. (Eds.), *Intracontinental Fold Belts - Case Studies in the Variscan Belt of Europe and the Damara Belt in Namibia*. Springer, Berlin 9–41 pp.
- Engel, W., Franke, W., Grote, C., Weber, K., Ahrendt, H., Eder, F.W., 1983b. Nappe tectonics in the southeastern part of the Rheinisches Schiefergebirge. In: Martin, H. Eder, F.W. (eds) *Intracontinental Fold Belts*. Springer, Berlin 267–287.
- Engi, M., 2017. Petrochronology based on REE-minerals: monazite, allanite, xenotime, apatite. *Reviews in Mineralogy and Geochemistry* 83, 365–418.
- Engvik, A.K., Austrheim, H., Andersen, T.B., 2000. Structural, mineralogical, and petrophysical effects on deep crustal rocks of fluid-limited polymetamorphism, Western Gneiss Region, Norway. *Journal of the Geological Society of London* 157, 121–134.

- Essene, E.J., 1989. The current status of thermobarometry in metamorphic rocks. In: Daly, J.S., Cliff, R.A., Yardley, B.W.D. (Eds.), *Evolution of Metamorphic Belts*. Geological Society of London Special Publications 43, pp. 1–44.
- Evans, P.-T., 2004. A method for calculating effective bulk composition modification due to crystal fractionation in garnet-bearing schist: implications for isopleth thermobarometry. *Journal of Metamorphic Geology* 22, 547–557.
- Falk, F., Franke, W., Kurze, M., 1995. VB1 - Saxothuringian Basin - autochthon and nonmetamorphic nappe units, stratigraphy. In: Dallmeyer, R.D., Franke, W., Weber, K. (Eds.), *Pre-Permian Geology of Central and Western Europe*. Springer, Berlin 221–234 pp.
- Faryad, S.W., 2011. Distribution and geological position of high-/ultrahigh pressure units within the European Variscan belt: a review. In: Dobrzhinetskaya, L., Faryad, S.W., Wallis, S., Cuthbert, S. (Eds.), *Ultrahigh Pressure Metamorphism: 25 years after the discovery of coesite and diamond*. Elsevier, 361–397.
- Faryad, S.W., Kachlík, V., 2013. New evidence of blueschist facies rocks and their geotectonic implication for Variscan suture(s) in the Bohemian Massif. *Journal of Metamorphic Geology* 28, 63–82.
- Fernández-Suárez, J., Dunning, G.R., Jenner, G.A., Gutiérrez-Alonso, G., 2000. Variscan collisional magmatism and deformation in NW Iberia: constraints from U–Pb geochronology of granitoids. *Journal of the Geological Society of London* 157, 565–576.
- Fielitz, W., Mansy, J.-L., 1999. Pre- and synorogenic burial metamorphism in the Ardenne and neighbouring areas (Renohercynian zone, central European Variscides). *Tectonophysics* 309, 227–256.
- Floyd, P.A., Leveridge, B.E., 1987. Tectonic environment of the Devonian Gramscatho Basin, South Cornwall: Framework mode and geochemical evidence from turbiditic sandstones. *Journal of the Geological Society* 144, 531–542.
- Foster, G.L., Parrish, R.R., 2003. Metamorphic monazite and generation of P–T–t paths, in: Vance, D., Müller, W., Villa, I.M. (Eds.), *Geochronology: Linking the Isotopic Record with Petrology and Textures*. Geological Society of London Special Publications 220, 25–47.
- Foster, G., Kinny, P., Vance, D., Prince, C., Harris, N., 2000. The significance of monazite U–Th–Pb age data in metamorphic assemblages; a combined study of monazite and garnet chronometry.

- Earth and Planetary Science Letters 181, 327–340.
- Foster, G.L., Gibson, H.G., Parrish, R.R., Horstwood, M.S.A., Fraser, J., Tindle, A., 2002. Textural, chemical and isotopic insights into the nature and behavior of metamorphic monazite. *Chemical Geology* 191, 183–207.
- Franke, W., 1984. Variszischer Deckenbau im Raum Münchberger Gneismasse – abgeleitet aus der Fazies, Deformation und Metamorphose im umgebenden Paläozoikum. *Geotekt. Forsch.* 68, 1–253.
- Franke, W., 1989a. The Geological Framework of the KTB Drill Site, Oberpfalz. In: Emmermann, R., and Wohlenberg, J. (Eds.), *The German Continental Deep Drilling Program (KTB)*. Springer, Berlin, 37–54 p.
- Franke, W., 1989b. Tectonostratigraphic units in the Variscan belt of Central Europe. In: Dallmeyer, R.D. (Eds.), *Terranes in the Circum-Atlantic Paleozoic Orogens*. Geological Society of America, Special Paper 230, 67–90.
- Franke, W., 1995. III Rhenohercynian Foldbelt, III.B Autochthon and Nonmetamorphic Nappe Units, III.B.1 Stratigraphy. In: Dallmeyer, R.D., Franke, W., Weber, K. (Eds.), *Pre-Permian Geology of Central and Eastern Europe*. Springer, Berlin, 33–49.
- Franke, W., 2000. The mid-European segment of the Variscides: Tectonometamorphic units, terrane boundaries and plate tectonic evolution, In Franke, W., Haak, V., Oncken, O., and Tanner, D., (Eds.), *Orogenic processes—Quantification and modelling in the Variscan belt of central Europe*: London, Geological Society of London Special Publication 179, 35–61.
- Franke, W., Prössl, K., Schwarz, J., 1992. Devonische Grauwacken im Erbendorfer Paläozoikum - Alter, tektonische Stellung und geotektonische Bedeutung. *KTB Report* 92–4, 213–224.
- Franke, W., Dallmeyer, R.D., Weber, K., 1995. XI - geodynamic evolution. In: Dallmeyer, D., Franke, W., Weber, K. (Eds.), *Pre-Permian Geology of Central and Western Europe*. Springer, Berlin, 579–594 pp.
- Franke, W., Haak, V., Oncken, O., Tanner, D., 2000. Orogenic processes: Quantification and modelling in the Variscan belt. *Geological Society Special Publication* 179, 459 p.
- Franke, W., Cocks, R.L.M., Torsvik, T.H., 2017. The Palaeozoic Variscan oceans revisited. *Gondwana Research* 48, 257–284.
- Franz, G., Glodny, J., Gerdes, A., 2014. New age constraints for the development of the Münchberg Massif. Abstract. *Deutsche Mineralogische Gesellschaft, Jena*, 176p.

- Freyer, G., Tröger, K.-A., 1965. Geologischer Führer durch das Vogtland. VEB Deutscher Verlag für Grundstoffindustrie, Leipzig, 279 p.
- Fuhrman, M.L., Lindsley, D.H., 1988. Ternary-feldspar modeling and thermometry. *American Mineralogist* 73, 201–215.
- Gaidies, F., Abart, R., De Capitani, C., Schuster, R., Connolly, J.A.D., Reusser, E., 2006. Characterization of polymetamorphism in the Austroalpine basement east of the Tauern Window using garnet isopleth thermobarometry. *Journal of Geology* 24, 451–475, doi:10.1111/j.1525-1314.2006.00648.x
- Garcia, D., Fonteilles, M., Moutte, J., 1994. Sedimentary fractionations between Al, Ti and Zr and the genesis of strongly peraluminous granites. *Journal of Geology* 102, 411–422.
- Gardés, E., Montel, J.M., Seydoux-Guillaume, A.M., Wirth, R., 2007. Pb diffusion in monazite: new constraints from the experimental study of $\text{Pb}^{2+}=\text{Ca}^{2+}$ interdiffusion. *Geochimica et Cosmochimica Acta* 71, 4036–4043.
- Gerdes, A., Zeh, A., 2006. Combined U–Pb and Hf isotope LA-(MC) ICP-MS analyses of detrital zircons: comparison with SHRIMP and new constraints for the provenance and age of an Armorican metasediment in Central Germany. *Earth and Planetary Science Letters* 249, 47–61.
- Geyer, G., Wiefel, H., 1997. Fränkisch-Thüringisches Schiefergebirge. In: Stratigraphische Kommission Deutschlands, ed., *Stratigraphie von Deutschland II, Teil I: Thüringen, Sachsen, Ostbayern*. Cour Forsch Inst Senckenberg 200, 57–102.
- Geyer G, Buschmann B, Elicki, O., 2014. A new lowermost middle Cambrian (Series 3, Stage 5) fauna from Saxony (Germany) and its bearing on the tectonostratigraphic history of the Saxothuringian domain. *Paläontologische Zeitschrift* 88, 239–262.
- Gibson, H.D., Carr, S.C., Brown, R.L., Hamilton, M.A., 2004. Correlations between chemical and age domains in monazite, and metamorphic reactions involving major pelitic phases: an integration of ID-TIMS and SHRIMP geochronology with Y–Th–U X-ray mapping. *Chemical Geology* 211, 237–260.
- Gómez Barreiro, J., Martínez Catalán, J.R., Arenas, R., Castiñeiras, P., Abati, J., Díaz García, F., and Wijbrans, J.R. 2007. Tectonic evolution of the upper allochthon of the Ordenes Complex (northwestern Iberian Massif): structural constraints to a polyorogenic peri-Gondwanan terrane. In *The evolution of the Rheic Ocean: from Avalonian–Cadomian active margin to Alleghenian–*

- Variscan collision. Edited by U. Linnemann, R.D. Nance, P. Kraft, and G. Zulauf. Geological Society of America, Special Paper 423, 315–332.
- Götze, J., 1998. Geochemistry and provenance of the Altendorf feldspathic sandstone in the Middle Bunter of the Thuringian basin, Germany. *Chemical Geology* 150, 43–61.
- Grandmontagne, N., Heinisch, H., Franke, W., 1994. The South Krkonoše Mountains: Saxothuringian/Moldanubian boundary in the Czech Sudetes. *Journal of the Czech Geological Society* 39, 38–39.
- Grauert, B., Hännly, R., Soptrajanová, G., 1973. Age and origin of detrital zircons from the pre-Permian basement of the Bohemian Massif and the Alps. *Contributions to Mineralogy and Petrology* 40, 105–130.
- Green, T. H., Hellman, P. L., 1982. Fe–Mg partitioning between coexisting garnet and phengite at high pressure, and comments on a garnet–phengite geothermometer. *Lithos* 15, 253–266.
- Grew, E.S., Suzuki, K., Asami, M., 2001. CHIME ages of xenotime, monazite, and zircon from beryllium pegmatites in the Napier complex, Khmara Bay, Enderby Land, East Antarctica. *Polar Geoscience* 14, 99–118.
- Groppo, C., Rolfo, F., 2008. Counterclockwise P-T evolution of the Aghil Range: metamorphic record of an accretionary melange between Kunlun and Karakorum (SW Sinkiang, China). *Lithos* 105, 365–378.
- Groppo, C., Rubatto, D., Rolfo, F., Lombardo, B., 2010. Early Oligocene partial melting in the Main Central Thrust Zone (Arun valley, eastern Nepal Himalaya). *Lithos* 118, 287–301.
- Gross, J., Burchard, M., Schertl, H.P., Maresch, W.V., 2008. Common high-pressure metamorphic history of eclogite lenses and surrounding metasediments: a case study of calc-silicate reaction zones (Erzgebirge, Germany). *European Journal of Mineralogy* 20, 757–775.
- Grünthal, G., Schneck, V., Zeman, A., and Schenková, Z., 1990. Seismotectonic model for the earthquake swarm of 1985-1986 in the Vogtland / West Bohemia focal area. *Tectonophysics* 174, 369–383.
- Grygar, R., 2016. Geology and Tectonic Development of the Czech Republic. In: Pánek, T., and Hradecký J., (Eds.), *Landscapes and Landforms of the Czech Republic*. World Geomorphological Landscapes, 422 p, doi: 10.1007/978-3-319-27537-6.
- Gümbel, C.W. von. 1879. *Geognostische Beschreibung des Fichtelgebirges mit dem Frankenwalde und dem westlichen Vorlande*. Perthes, Gotha 698 p.

- Hajná, J., Žák, J., Kachlík, V., 2011. Structure and stratigraphy of the Teplá–Barrandian Neoproterozoic, Bohemian Massif: a new plate-tectonic reinterpretation. *Gondwana Research* 19, 495–508, doi:10.1016/j.gr.2010.08.003.
- Harley, S.L., Kelly, N.M., 2007. Zircon: tiny but timely. *Elements* 3, 13–18.
- Harley, S.L., Kelly, N.M., Möller, A., 2007. Zircon behaviour and the thermal histories of mountain chains. *Elements* 3, 25–30.
- Harlov, D.E., Wirth, R., Hetherington, C.J., 2011. Fluid-mediated partial alteration in monazite: the role of coupled dissolution–reprecipitation in element redistribution and mass transfer. *Contributions to Mineralogy and Petrology* 162, 329–348.
- Harrison, T.M., Catlos, E.J., Montel, J.M., 2002. U–Th–Pb dating of phosphate minerals. In: *Phosphates: Geochemical, geobiological, and materials importance. Reviews in Mineralogy and Geochemistry* 48, 523–558.
- Hawkins, A.T., Selverstone, J., Brealey, A.J., Beane, R.J., Ketcham, R.A., Carlson, W.D., 2007. Origin and mechanical significance of honeycomb garnet in high-pressure metasedimentary rocks from the Tauern Window, Eastern Alps. *Journal of metamorphic Geology* 25, 565–583.
- Haydoutov, I., 1989. Precambrian ophiolites, Cambrian island arc, and Variscan suture in the South Carpathian–Balkan region. *Geology* 17, 905–908.
- Hecht, L., Thuro, K., Plinninger, R., Cuney, M., 1999. Mineralogical and geochemical characteristics of hydrothermal alteration and episyenitization in the Königshain granites, northern Bohemian Massif, Germany. *International Journal of Earth Sciences* 88, 236–252.
- Herron, M.M., 1988. Geochemical classification of terrigenous sands and shales from core or log data. *Journal of Sedimentary Petrology* 58, 820–829.
- Heuse, T., Blumenstengel, H., Elicki, O., Geyer, G., 2010. Biostratigraphy – The faunal province of the southern margin of the Rheic Ocean. In: Linnemann, U., Romer, R.L. (Eds.), *Pre-Mesozoic Geology of Saxo-Thuringia*. Schweizerbart, Stuttgart 99–170 p.
- Hirschmann, G., 1996. KTB - The structure of a Variscan terrane boundary: seismic investigation – drilling – models. *Tectonophysics* 264, 327–339.
- Hodges, K.V., Spear, F.S., 1982. Geothermometry, geobarometry and the Al₂SiO₅ triple point at Mt. Moosilauke, New Hampshire. *American Mineralogist* 67, 1118–1134.
- Höhn, S., Koglin, N., Klopff, L., Tragelehn, H., Schüssler, U., Frimmel, H.E., Zeh, A., Brätz, H., 2018.

- Geochronology, stratigraphy and geochemistry of Cambro-Ordovician, Silurian and Devonian volcanic rocks of the Saxothuringian Zone in NE Bavaria (Germany) – new constraints for Gondwana break up and Rheic Ocean island magmatism. *International Journal of Earth Sciences (Geologische Rundschau)* 107, 359–377, doi: 10.1007/s00531-017-1497-2.
- Holdaway, M.J., 1971. Stability of andalusite and the aluminosilicate phase diagram. *American Journal of Science* 271, 97–131.
- Holdaway, M. J., 2000. Application of new experimental and garnet Margules data to the garnet–biotite geothermometer. *American Mineralogist* 85, 881–892.
- Holdaway, M. J., 2001. Recalibration of the GASP geobarometer in light of recent garnet and plagioclase activity models and versions of the garnet–biotite geothermometer. *American Mineralogist* 86, 1117–1129.
- Holder, M.T., Levridge, B.E., 1986. Correlation of the Rhenohercynian Variscides. *Journal of the Geological Society London* 143, 141–147.
- Holland, T.J.B., Powell, R., 1991. A compensated-Redlich-Kwong (CORK) equation for volumes and fugacities of CO₂ and H₂O in the range 1 bar to 50 kbar and 100–1600 °C. *Contributions to Mineralogy and Petrology* 109, 265–273.
- Holland, T.J.B., Powell, R., 1996. Thermodynamics of order-disorder in minerals. 2. Symmetric formalism applied to solid solutions. *American Mineralogist* 81, 1425–1437.
- Holland, T.J.B., Powell, R., 1998. An internally consistent thermodynamic data set for phases of petrological interest. *Journal of Metamorphic Geology* 16, 309–343.
- Holland, T.J.B., Powell, R., 2011. An improved and extended internally consistent thermodynamic dataset for phases of petrological interest, involving a new equation of state for solids. *Journal of Metamorphic Geology* 29, 333–383.
- Holland, T.J.B., Baker, J., Powell, R., 1998. Mixing properties and activity-composition relationships of chlorites in the system MgO-FeO-Al₂O₃-SiO₂-H₂O. *European Journal of Mineralogy* 10, 395–406.
- Holub, F., Souček, J., 1994. Blueschist-greenschist metamorphism of metabasites in the Krušné Hory (Erzgebirge) Mts. *Zentralblatt für Geologie und Paläontologie Teil 1*, 1992, 815–826.
- Holzförster, F., Peterek, A., Rabold, J. M., 2011. KTB Deep Drilling Site and Czech-Bavarian Geopark- Two best practice examples of geoscience outreach. In book: *Geological Field Trips in Central Western Europe: Fragile Earth International Conference, Munich*, 7–27 pp.

- Hoschek, G., 2001. Thermobarometry of metasediments and metabasites from the eclogite zone of the Hohe Tauern, Eastern Alps, Austria. *Lithos* 59, 127–150.
- Huckriede, H., Ahrendt, H., Wemmer, K., 2002. Das K/Ar Abkühlungsalter der detritischen Muskovite des Nereiten-Sandsteins (Unterdevon, Thüringisches Schiefergebirge) und seine paläogeographische Bedeutung. *Geowissenschaftliche Mitteilungen Thüringen*. 10, 15–19.
- Hynes, A., Forest, R. C., 1988. Empirical garnet–muscovite geothermometry in low-grade metapelites, Selwyn Range (Canadian Rockies). *Journal of Metamorphic Geology* 6, 297–309.
- Jastrzębski, M., 2010. A Variscan continental collision of the West Sudetes and the Brunovistulian terrane: a contribution from structural and metamorphic record of the Stronie Formation, the Orlica-Śnieżnik Dome, SW Poland. *International Journal of Earth Science* 98, 1901–1923.
- Jastrzębski, M., Budzyń, B., Stawikowski, W., 2016. Structural, metamorphic and geochronological record in the Goszów quartzites of the Orlica-Śnieżnik Dome (SW Poland): implications for the polyphase Variscan tectonometamorphism of the Saxothuringian terrane. *Geological Journal* 51, 455–479.
- Johnson, T., Brown, M., 2004. Quantitative constraints on metamorphism in the Variscides of southern Brittany - a complementary pseudosection approach. *Journal of Petrology* 45, 1237–1259.
- Kalt, A., Corfu, F., Wijbrans, J.R., 2000. Time calibration of a P–T path from a Variscan high-temperature low-pressure metamorphic complex (Bayerische Wald, Germany), and the detection of inherited monazite. *Contributions to Mineralogy and Petrology* 138, 143–163.
- Karioris, F.G., Gowda, K., Cartz, L. 1991. Heavy ion bombardment on monoclinic ThSiO₄, ThO₂, and monazite. *Radiation Effects Letters* 58, 1–3.
- Kelly, N.M., Clarke, G.L., Harley, S.L., 2006. Monazite behaviour and age significance in poly-metamorphic high-grade terrains: a case study from the western Musgrave Block, central Australia. *Lithos* 88, 100–134.
- Keppie, J.D., 1994. *Pre-Mesozoic geology in France: Berlin-Heidelberg-New York*, Springer Verlag, 514 p.
- Keppie, D.J., Nance, D.R., Murphy, B.J., Dostal, J., Brad, J.A., 2009. The high-pressure Iberian-Czech belt in the Variscan orogen: extrusion into the upper (Gondwanan) plate? *Gondwana Research* 17, 306–316.

- Kim, B. C., Choi, S.J., Suzuki, K., Adachi, M., Obayashi, T., Yu, K.M. 1997. Provenance of Cretaceous sandstones in the southeastern Youngdong Basin, Korea; CHIME geochronology of detrital monazites. *Geoscience Journal* 1, 37–49.
- Klápová, H., Konopásek, J., Schulmann, K., 1998. Eclogites from the Czech part of the Erzgebirge: multi-stage metamorphic and structural evolution. *Journal of the Geological Society London*, 155, 567–583.
- Klein, C., Philpotts, A., 2013. *Earth Materials: Introduction to Mineralogy and Petrology*. Cambridge University Press, New York, 552 p.
- Klemd, R., 2010. Early Variscan allochthonous domains: the Münchberg Complex, Frankenberg, Wildenfels, and Góry Sowie. In: Linnemann, U., Romer, R.L. (Eds.), *Pre-Mesozoic Geology of Saxo-Thuringia — From the Cadomian Active Margin to the Variscan Orogen*. Schweizerbart, Stuttgart 221–232 pp.
- Klemd, R., Matthes, S., Okrusch, M., 1991. High pressure relics in meta-sediments intercalated with the Weissenstein eclogite, Münchberg gneiss complex, Bavaria. *Contributions to Mineralogy and Petrology* 107, 328–342.
- Koglin, N., Franz, G., Glodny, J., Schüssler, U., Zeh, A., Gerdes, A., Brätz, H., 2015. Münchberg nappe complex: nature and ages of the nappe protoliths. *Abstracts GeoBerlin*, 215 p.
- Koglin, N., Zeh, A., Franz, G., Schüssler, U., Glodny, J., Gerdes, A., Brätz, H., 2018. From Cadomian magmatic arc to Rheic ocean closure: The geochronological-geochemical record of nappe protoliths of the Münchberg Massif, NE Bavaria (Germany). *Gondwana Research* 55, 135–152.
- Kohn, M. J. & Malloy, M. A., 2004. Formation of monazite via prograde metamorphic reactions among common silicates: implications for age determinations. *Geochimica et Cosmochimica Acta*, 68, 101–113.
- Konopásek, J., 2001. Eclogitic micaschist in the central part of the Krušné Hory Mts (Bohemian Massif). *European Journal of Mineralogy*, 13, 87–100.
- Konopásek, J., 2011. Tectonic position of eclogites and blueschists in the Bohemian Massif. *Geolines* 23, 11–17.
- Konopásek, J., Schulmann, K., Lexa, O., 2001. Structural evolution of the central part of the Krušné Hory (Erzgebirge) Mountains in the Czech Republic—evidence for changing stress regime during Variscan compression. *Journal of Structural Geology* 23, 1373–1392.

- Konrad-Schmolke, M., O'Brien, P.J., De Capitani, C., Carswell, D.A., 2008. Garnet growth at high- and ultra-high pressure conditions and the effect of element fractionation on mineral modes and composition. *Lithos* 103, 309–332.
- Korzhinskii, D.S., 1959. Physico-chemical basis of the analysis of the paragenesis of materials. Consultants Bureau, New York, 142 p.
- Kossmat, F., 1927. Gliederung des varistischen Gebirgsbaues. *Abhandlungen des Sächsischen Geologischen Landesamts*. 1, 1–39 pp.
- Kreuzer, H., Seidel, E., Schüssler, U., Okrusch, M., Lenz, K.L., Raschka, H., 1989. K-Ar geochronology of different tectonic units at the northwestern margin of the Bohemian Massif. *Tectonophysics* 157, 149–178.
- Kreuzer, H., Seidel, E., Schussler, U., Okrush, M., Lentz, K.L., Rashka, H., 1989. K-Ar geochronology of different tectonic units at the northwestern margin of the Bohemian Massif. *Tectonophysics* 157, 149–178.
- Krogh, J. E., Råheim, A., 1978. Temperature and pressure dependence of Fe–Mg partitioning between garnet and phengite, with particular reference to eclogites. *Contributions to Mineralogy and Petrology* 66, 75–80.
- Krohe, A., 1998. Extending a thickened crustal bulge: toward a new geodynamic evolution model of the Palaeozoic NW Bohemian Massif, German Continental Deep Drilling site (SE Germany). *Earth Science Reviews* 44, 95–145.
- Krohe, A., Wawrzenitz, N., 2000. Domainal variations of U-Pb monazite ages and Rb-Sr whole-rock dates in polymetamorphic paragneisses (KTB drill core, Germany): influence of strain and deformation mechanisms on isotope systems. *Journal of Metamorphic Geology* 18, 271–291.
- Kröner, A., Willner, A.P., 1998. Time of formation and peak of Variscan HP-HT metamorphism of quartz-feldspar rocks in the central Erzgebirge, Saxony, Germany. *Contributions to Mineralogy and Petrology* 132, 1–20.
- Kröner, A., Jäckel, P., Reischmann, T., and Kroner, U., 1998. Further evidence for an early Carboniferous (~340 Ma) age of high-grade metamorphism in the Saxothuringian Granulite complex: *Geologische Rundschau* 86, 751–766.
- Kroner, U., Romer, R.L., 2013. Two plates – Many subduction zones: The Variscan orogeny reconsidered. *Gondwana Research* 24, 298–329.

- Kroner, U., Hahn, T., Romer, R.L., Linnemann, U., 2007. The Variscan orogeny in the Saxo-Thuringian zone—Heterogenous overprint of Cadomian/Paleozoic Peri-Gondwana crust. *Geological Society of America Special Paper* 423, 153–172, doi: 10.1130/2007.2423(06).
- Kroner, U., Mansy, J.-L., Mazur, S., Aleksandrowski, P., Hann, H.P., Huckriede, H., Lacquement, F., Lamarche, J., Ledru, P., Pharaoh, T.C., Zedler, H., Zeh, A., Zulauf, G., 2008. Variscan tectonics. In: McCann, T. (Eds.), *The Geology of Central Europe. Precambrian and Palaeozoic* vol. 1. Geological Society, London, 383–410 pp.
- Kukal, Z., 1971. Sedimentology of Cambrian deposits of the Barrandian area, Central Bohemia. *Sborník Geologických Věd, Geologie* 20, 53–100.
- Langone, A., Braga, R., Massonne, H.-J., Tiepolo, M., 2011. Preservation of old (prograde metamorphic) U-Th-Pb ages in unshielded monazite from the high-pressure paragneisses of the Variscan Ulten Zone (Italy). *Lithos* 127, 68–85.
- Lenz, H., 1986. Rb / Sr-Gesamtgesteins-Altersbestimmungen am Weissenstadt-Marktleuthener Porphyrganit des Fichtelgebirges. *Geologisches Jahrbuch, Reihe E* 34, 67–76.
- Li, B., Massonne, H.-J., 2017. Contrasting metamorphic evolution of metapelites from the Malpica-Tuy unit and the underlying so-called parautochthon at the coast of NW Spain. *Lithos* 286–287, 92–108.
- Li, B., Massonne, H.-J., 2018. Two Tertiary metamorphic events recognized in high-pressure metapelites of the Nevado-Filábride Complex (Betic Cordillera, S Spain). *Journal of Metamorphic Geology* 36, 603–630, doi:10.1111/jmg.12312.
- Li, B., Massonne, H.-J., Opitz, J., 2017. Clockwise and anticlockwise P-T paths of high-pressure rocks from the 'La Pioza' eclogite body of the Malpica-Tuy zone, NW Spain. *Journal of Petrology* 58, 1363–1392.
- Liati, A., Gebauer, D., 2009. Crustal origin of zircon in a garnet peridotite: A study of U-Pb SHRIMP dating, mineral inclusions and REE geochemistry (Erzgebirge, Bohemian Massif). *European Journal of Mineralogy* 21, 737–750.
- Likhanova, I.I., Reverdatto, V.V., Kozlov, P.S., Khiller, V.V., Sukhorukov, V.P., 2015. P–T–t constraints on polymetamorphic complexes of the Yenisey Ridge, East Siberia: Implications for Neoproterozoic paleocontinental reconstructions. *Journal of Asian Earth Sciences* 113, 391–410.

- Linnemann, U., 2007. Ediacaran rocks from the Cadomian basement of the Saxo-Thuringian Zone (NE Bohemian Massif, Germany): age constraints, geotectonic setting and basin development. Geological Society London, Special Publications 286, 35–51.
- Linnemann, U., Gemmlich, M., Tichomirowa, M., Buschmann, B., Nasdala, L., Jonas, P., Lützner, H., and Bombach, K., 2000. From Cadomian subduction to Early Palaeozoic rifting: the evolution of Saxo-Thuringia at the margin of Gondwana in the light of single zircon geochronology and basin development (Central European, Germany). In: Franke, W., Haak, W., Oncken, O., Tanner, D., (Eds.), *Orogenic processes: quantification and modelling Variscides in the Variscan Belt*. Geological Society London Special Publications 179, 131–153.
- Linnemann, U., McNaughton, N.J., Romer, R.L., Gehmlich, M., Drost, K., Tonk, C., 2004. West African provenance for Saxo-Thuringia (Bohemian Massif): Did Armorica ever leave pre-Pangean Gondwana? U/Pb-SHRIMP zircon evidence and the Nd-isotopic record. *International Journal of Earth Sciences* 93, 683–705.
- Linnemann, U., Gerdes, A., Drost, K., Buschmann, B., 2007. The continuum between Cadomian orogenesis and opening of the Rheic Ocean: constraints from LA-ICP-MS U-Pb zircon dating and analysis of plate-tectonic setting (Saxo-Thuringian zone, northeastern Bohemian Massif, Germany). In: Linnemann, U., Nance, R.D., Kraft, P., Zulauf, G. (Eds.), *The Evolution of the Rheic Ocean: From Avalonian-Cadomian Active Margin to Alleghenian-Variscan Collision*. Geological Society of America Special Papers 423, 61–96.
- Linnemann, U., Pereira, F., Jeffries, T.E., Drost, K., Gerdes, A., 2008. The Cadomian Orogeny and the opening of the Rheic Ocean: the diachrony of geotectonic processes constrained by LA-ICPMS U–Pb zircon dating (Ossa-Morena and Saxo-Thuringian Zones, Iberian and Bohemian Massifs). *Tectonophysics* 461, 21–43. doi:10.1016/j.tecto.2008.05.002.
- Linnemann, U., Romer, R.L., Gerdes, A., Jeffries, T.E., Drost, K., Ulrich, J., 2010a. The Cadomian Orogeny in the Saxo-Thuringian Zone. In: Linnemann, U., Romer, R.L. (Eds.), *Pre-Mesozoic Geology of Saxo-Thuringia*. Schweizerbart, Stuttgart 37–58 pp.
- Linnemann, U., Hofmann, M., Romer, R.L., Gerdes, A., 2010b. Transitional stages between the Cadomian and Variscan Orogenies: Basin development and tectonomagmatic evolution of the southern margin of the Rheic Ocean in the Saxo-Thuringian Zone (North Gondwana shelf). In:

- Linnemann, U., Romer, R.L. (Eds.), Pre-Mesozoic Geology of Saxo-Thuringia – From the Cadomian Active Margin to the Variscan Orogen. Schweizerbart, Stuttgart, 59–98 pp.
- Linnemann, U., Gerdes, A., Hofmann, M., Marko, L., 2014. The Cadomian Orogen: Neoproterozoic to Early Cambrian crustal growth and orogenic zoning along the periphery of the West African Craton—Constraints from U–Pb zircon ages and Hf isotopes (Schwarzburg Antiform, Germany). *Precambrian Research* 244, 236–278, doi:10.1016/j.precamres.2013.08.007.
- Lorenz, W., Hoth, K., 1990. Lithostratigraphie im Erzgebirge—Konzeption, Entwicklung, Probleme und Perspektiven: Abhandlungen des Staatlichen Museums für Mineralogie und Geologie zu Dresden 37, 7–35.
- Lotze, F., 1945. Zur Gliederung der Varisziden der Iberischen Mesetas. *Geotektonische Forschungen* 6, 78–92.
- Ludwig, K. R., 1999. Isoplot/Ex, Version 2.06: A Geochronological Tool-kit for Microsoft Excel. 1a. Berkeley Geochronology Center, Special Publications, 1–49 pp.
- Mac Niocaill, C., van der Pluijm, B.A., Van der Voo, R., 1997. Ordovician paleogeography and the evolution of the Iapetus Ocean. *Geology* 95, 159–162.
- Marmo, B.A., Clarke, G.L., Powell, R., 2002. Fractionation of bulk rock composition due to porphyroblast growth: effects on eclogite facies mineral equilibria, Pam Peninsula, New Caledonia. *Journal of Metamorphic Geology* 20, 151–165.
- Martínez Catalán, J.R., Arenas, R., Abati, J., SánchezMartínez, S., Díaz García, F., Fernández-Suárez, J., González Cuadra, P., Castiñeiras, P., Gómez Barreiro, J., Díez Montes, A., González Clavijo, E., Rubio Pascual, F.J., Andonaegui, P., Jeffries, T.E., Alcock, J.E., Díez Fernández, R., López Carmona, A., 2009. A rootless suture and the loss of the roots of a mountain chain: the Variscan belt of NW Iberia. *Comptes Rendus Géoscience* 341, 114–126.
- Martins, L., Vlach, S.R.F., Janasi, V.A., 2009. Reaction microtextures of monazite: correlation between chemical and age domains in the Nazaré Paulista migmatite, SE Brazil. *Chemical Geology* 261, 271–285.
- Massonne, H.-J., 1984. Bestimmung von Intrusionstiefen variszischer Granite Mitteleuropas und Neuschottlands anhand der Chemie ihrer Hellglimmer. *Fortschr. Mineral.* 62, 147–149 Beiheft 1.
- Massonne, H.-J., 1999. A new occurrence of microdiamonds in quartzofeldspathic rocks of the Saxonian Erzgebirge, Germany, and their metamorphic evolution. In: Gurney, J.J., Ž. Gurney, J.L., Pascoe,

- M.D., Richardson, S.H. (Eds.), Proceedings of the 7th International Kimberlite Conference, vol. 2. Red Roof Design, Cape Town, 533–539.
- Massonne, H.-J., 2001. First find of coesite in the ultrahigh-pressure metamorphic region of the Central Erzgebirge, Germany. *European Journal of Mineralogy* 13, 565–570.
- Massonne, H.-J., 2003a. Paläozoische Hochdruck- und Ultrahochdruck-Metamorphite in Mitteleuropa und ihre Beziehungen zur variszischen Orogenese. *Zeitschrift für geologische Wissenschaften* 31, 239–249.
- Massonne, H.-J., 2003b. A comparison of the evolution of diamondiferous quartz-rich rocks from the Saxonian Erzgebirge and the Kokchetav Massif: are so-called diamondiferous gneisses magmatic rocks? *Earth and Planetary Science Letters* 216, 345–362.
- Massonne, H.-J., 2005. Involvement of crustal material in delamination of the lithosphere after continent-continent collision. *International Geology Review* 47, 792–804.
- Massonne, H.-J., 2010. Phase relations and dehydration behaviour of calcareous sediments at very-low to low grade metamorphic conditions. *Periodico di Mineralogia* 79 (2), 21–43.
- Massonne, H.-J., 2012. Formation of amphibole and clinozoisite–epidote in eclogite owing to fluid infiltration during exhumation in a subduction channel. *Journal of Petrology* 53, 2115–2138.
- Massonne, H.-J., 2013. Constructing the pressure-temperature path of ultrahigh-pressure rocks. *Elements* 9, 267–272.
- Massonne, H.-J., 2014. Wealth of P–T–t information in medium-high grade metapelites: example from the Jubrique Unit of the Betic Cordillera, S Spain. *Lithos* 208–209, 137–157.
- Massonne, H.-J., 2016a. Tertiary high-pressure metamorphism recorded in andalusite-bearing micaschist, southern Pirin Mts., SW Bulgaria. *European Journal of Mineralogy* 28, 1187–1202.
- Massonne, H.-J., 2016b. Hydration of the lithospheric mantle by the descending plate in a continent-continent collisional setting and its geodynamic consequences. *Journal of Geodynamics* 96, 50–61.
- Massonne, H.-J., O'Brien, P.J., 2003. The Bohemian Massif and the NW Himalaya. In: Carswell, D.A., Compagnoni, R. (Eds.), *Ultrahigh Pressure Metamorphism*. EMU Notes in Mineralogy. Budapest 5, 145–187 pp.
- Massonne, H.-J., Neuser, R.D., 2005. Ilmenite exsolution in olivine from the serpentinite body at Zöblitz, Saxonian Erzgebirge - microstructural evidence using EBSD. *Mineralogical Magazine* 69, 119–124.

- Massonne, H.-J., Calderón, M., 2008. P-T evolution of metapelites from the Guarguaráz Complex, Argentina: evidence for Devonian crustal thickening close to the western Gondwana margin. *Revista Geológica de Chile* 35, 215–231.
- Massonne, H.-J., Toulkeridis, T., 2012. Widespread relics of high-pressure metamorphism confirm major terrane accretion in Ecuador: a new example from the Northern Andes. *International Geology Review* 54, 67–80.
- Massonne, H.-J., Kennedy, A., Nasdala, L., Theye, T., 2007. Dating of zircon and monazite from diamondiferous quartzofeldspathic rocks of the Saxonian Erzgebirge. *Mineralogical Magazine* 71, 407–425.
- Massonne, H.-J., Dristas, J.A., Martínez, J.C., 2011. Metamorphic evolution of the Río de la Plata craton in the Cinco Cerros area, Buenos Aires Province, Argentina. *Journal of South American Earth Sciences* 38, 57–70.
- Massonne, H.-J., Dristas, J.A., Martínez, J.C., 2012. Metamorphic evolution of the Río de la Plata craton in the Cinco Cerros area, Buenos Aires Province, Argentina. *Journal of South American Earth Sciences* 38, 57–70.
- Massonne, H.-J., Opitz, J., Theye, T., Nasir, S., 2013. Evolution of a very deeply subducted metasediment from As Sifah, northeastern coast of Oman. *Lithos* 156–159, 171–185.
- Massonne, H.-J., Barr, S.M., White, C.E., Miller, B.V., 2018a. The Pocologan metamorphic suite of southern New Brunswick, Canada: New constraints on age and conditions of medium- to high-pressure metamorphism. *Tectonophysics* 747–748, 177–190.
- Massonne, H.-J., Cruciani, G., Franceschelli, M., Musumeci, G., 2018b. Anti-clockwise pressure-temperature paths record Variscan upper-plate exhumation: example from micaschists of the Porto Vecchio region, Corsica. *Journal of Metamorphic Geology* 36, 55–77.
- Matte, P., 1986. Tectonics and plate tectonic model for the Variscan belt of Europe. *Tectonophysics* 126, 329–374.
- Matte, P., 1991. Accretionary history and crustal evolution of the Variscan Belt in Western Europe. *Tectonophysics* 196, 309–339.
- Matte, P., 1998. Continental subduction and exhumation of HP rocks in Paleozoic orogenic belts: Uralides and Variscides: *Geologiska Forhandlingar a Föreningar* 120, 209–222.

- Matte, P. 2001. The Variscan collage and orogeny (480–290 Ma) and the tectonic definition of the Armorica microplate: a review. *Terra Nova*, 13, 122–128.
- Matte, P., Maluski, H., Rajlich, P. and Franke, W., 1990. Terrane boundaries in the Bohemian Massif: Results of largescale Variscan shearing. *Tectonophysics* 177, 151–170.
- McCann, T., Skompski, S., Poty, E., Dusar, M., Vozárová, A., Schneider, J., Wetzels, A., Krainer, K., Kornpohl, K., Schäfer, A., Krings, M., Oplustil, S., Tait, J., 2008. Carboniferous. In: McCann, T. (Eds.), *The Geology of Central Europe. Precambrian and Palaeozoic 1*. Geological Society London, 411–529 pp.
- Meldrum, A., Boatner, L.A., and Ewing, R.C. 1997. Displacive radiation effects in the monazite- and zircon-structure orthophosphates. *Physics Reviews B* 56, 13805–13814.
- Meldrum, A., Boatner, L.A., Weber, W.J., Ewing, R.C., 1998. Radiation damage in zircon and monazite. *Geochimica et Cosmochimica Acta* 62, 2509–2520.
- Mielke, H., Schreyer, W., 1969. Mineralparagenesen in Metasedimenten des Fichtelgebirges. *Geologica Bavarica* 60, 29–44.
- Mielke, H., Schreyer, W., 1972. Magnetite-rutile-assemblages in metapelites of the Fichtelgebirge, Germany. *Earth and Planetary Science Letters* 16, 423–428.
- Mielke, H., Abraham, K., 1980. Retrograde Mineralumwandlungen in Metasedimenten des Fichtelgebirges. *Neues Jahrbuch Mineralogie Abhandlungen* 138, 178–197.
- Mielke, H., Blümel, P., Langer, K., 1979. Regional low- pressure metamorphism of low and medium grade in metapelites and -psammites of the Fichtelgebirge area, NE-Bavaria. *Neues Jahrbuch für Mineralogie Abhandlungen* 137, 83–112.
- Mingram, B., 1998. The Erzgebirge Germany—A subducted part of northern Gondwana: Geochemical evidence for repetition of early Palaeozoic metasedimentary sequences in metamorphic thrust units. *Geological Magazine* 135, 785–801.
- Mingram, B., Rötzler, K., 1999. Geochemische, petrologische und geochronologische Untersuchungen im Erzgebirgskristallin - Rekonstruktion eines Krustenstapels. *Schriftenreihe für Geowissenschaften* 9, 1–80.
- Mingram, B., Kröner, A., Hegner, E., Krentz, O., 2004. Zircon ages, geochemistry, and Nd isotopic systematics of pre-Variscan orthogneisses from the Erzgebirge, Saxony (Germany), and geodynamic interpretation. *International Journal of Earth Sciences* 93, 706–727.

- Montel, J.-M., Foret, S., Veschambre, M., Nicollet, N., Provost, A. 1996. Electron microprobe dating of monazite. *Chemical Geology* 131, 37–53.
- Müller, T., Massonne, H.-J., Willner, A.P., 2015. Timescales of exhumation and cooling inferred by kinetic modeling: An example using lamellar garnet pyroxenite from the Variscan Granulitgebirge, E Germany. *American Mineralogist* 100, 747–759.
- Murphy, D. B., 2001. *Fundamentals of light microscopy and electronic imaging*. A John Wiley and Sons INC., Publication, USA, 357 p.
- Murphy, J.B., Nance, R.D., 2008. The Pangea conundrum. *Geology* 36, 703-706.
- Murphy, J.B., Gutiérrez-Alonso, G., Nance, R.D., Fernandez-Suarez, J., Keppie, J.D., Quesada, C., Dostal, J., Braid, J.A., 2009. Rheic Ocean mafic complexes: overview and synthesis. In: Murphy, J.B., Keppie, J.D., Hynes, A. (Eds.), *Ancient Orogens and Modern Analogues*. Geological Society of London, Special Publication 327, 343–369.
- Murphy, J.B., Cousens, B.L., Braid, J.A., Strachan, R.A., Dostal, J., Keppie, J.D., Nance, R.D., 2011. Highly depleted oceanic lithosphere in the Rheic Ocean: implications for Palaeozoic plate reconstructions. *Lithos* 123, 165–175.
- Nance, R.D., Murphy, J.B., 1994. Contrasting basement isotopic signatures and the palinspastic restoration of peripheral orogens: example from the Neoproterozoic Avalonian–Cadomian belt. *Geology* 22, 617–620.
- Nance, R.D., Linnemann, U., 2008. The Rheic Ocean: Origin, Evolution, and Significance. *GSA Today* 18, 4-12, doi: 10.1130/GSATG24A.1.
- Nance, R.D., Gutiérrez-Alonso, G., Keppie, J.D., Linnemann, U., Murphy, J.B., Quesada, C., Strachan, R.A., Woodcock, N.H., 2010. Evolution of the Rheic Ocean. *Gondwana Research* 17, 194–222.
- Nance, R. D., Gutiérrez-Alonso, G., Keppie, D., Linnemann, U., Murphy, B., Quesada, C., Strachan, R. A., Woodcock, N. H., 2012. A brief history of the Rheic Ocean. *Geoscience Frontiers* 3, 125–135, doi:10.1016/j.gsf.2011.11.008.
- Negulescu, E., Săbău, G., Massonne, H.-J., 2009. Chloritoid-bearing mineral assemblages in high-pressure metapelites from the Bughea Complex, Leaota Massif (South Carpathians). *Journal of Petrology* 50, 103–125.
- Negulescu, E., Săbău, G., Massonne, H.-J., 2018. Growth of chloritoid and garnet along a nearly isothermal burial path to 70 km depth: an example from the Bughea Metamorphic Complex, Leaota

- Massif, South Carpathians. *Mineralogy and Petrology* 112, 535–553.
- Nesse, W. D., 2013. *Introduction to Mineralogy*. Fourth Edition Publication. Oxford University Press. 512 p.
- Neubauer, F., and Handler, R., 2000. Variscan orogeny in the Eastern Alps and Bohemian Massif: How do these units correlate? In: Neubauer, F., Höck, V. (Eds.), *Aspects of Geology in Austria*. *Mitteilungen Österreichische Geologische Gesellschaft* 92, 35–59.
- O'Brien, P.J., 2000. The fundamental Variscan problem: high temperature metamorphism at different depths and high pressure metamorphism at different temperatures. In: Franke, W., Haak, V., Oncken, O., Tanner, D. (Eds.), *Orogenic Processes: Quantification and Modelling in the Variscan Belt*. *Geological Society of London Special Publication* 179, 369–386 pp.
- O'Brien, P.J., Carswell, D.A., 1993. Tectonometamorphic evolution of the Bohemian Massif: evidence from high pressure metamorphic rocks. *Geologische Rundschau* 82, 531–555.
- Ogenhall, E., 2010. *Geological Evolution of the Supracrustal Palaeoproterozoic Hamrånge Group: A Svecofennian Case Study*. Uppsala: *Acta Universitatis Upsaliensis*, 53 p.
- Okrusch, M., Schüssler, U., Seidel, E., Kreuzer, H., Raschka, H., 1990. Pre- to early Variscan magmatism in the Bohemian Massif. In: Franke, W. (Ed.), *Mid-German Crystalline Rise & Rheinisches Schiefergebirge: field-guide to pre-conference excursion*. *Terranes in the Circum-Atlantic Paleozoic Orogen*. Conference on Paleozoic Orogens in Central Europe. *Geology and Geophysics* 233. IGCP, Göttingen-Giessen, pp. 81–91.
- Oncken, O., Winterfeld, C.V., Dittmar, U., 1999. Accretion of a rifted passive margin: the Late Palaeozoic Rhenohercynian fold and thrust belt (Middle European Variscides). *Tectonics* 18, 75–91.
- Overstreet, W.C., 1967. The geologic occurrence of monazite. *U.S. Geological Survey Professional Paper* 530, 1–327.
- Palin, R.M., Searle, M.P., St-Onge, M.R., Waters, D.J., Roberts, N.M.W., Horstwood, M.S.A., Parrish, R.R., Weller, O.M., Chen, S., Yang, J., 2014. Monazite geochronology and petrology of kyanite- and sillimanite-grade migmatites from the northwestern flank of the eastern Himalayan syntaxis. *Gondwana Research* 26, 323–347.
- Pan, Y. Stauffer, M.R., 2000. Cerium anomaly and Th/U fractionation in the 1.85 Ga Flin Flon palaeosol: clues from REE- and U-rich accessory minerals and implications for palaeoatmospheric

- reconstruction. *American Mineralogist* 85, 898–911.
- Parrish, R.R., 1990. U–Pb dating of monazite and its application to geological problems. *Canadian Journal of Earth Sciences* 27, 1431–1450.
- Pattison, D.R.M., 1992. Stability of andalusite and sillimanite and the Al_2SiO_5 triple point: Constraints from the Ballachulish Aureole, Scotland. *Journal of Geology* 100, 423–446.
- Perri, F., 2014. Composition, provenance and source weathering of Mesozoic sandstones from Western-Central Mediterranean Alpine Chains. *Journal of African Earth Science* 91, 32–43.
- Pettijohn, F., Potter, P., Siever, R. 1987. *Sand and Sandstones*. Springer-Verlag, Berlin, 617 p.
- Pin, C., Paquette, J.L., Santos Zalduegui, J.F., Gil Ibarguchi, J.I., 2002. Early Devonian suprasubduction-zone ophiolite related to incipient collisional processes in the Western Variscan Belt: the Sierra de Careón unit, Ordenes Complex, Galicia. *Geological Society of America Special Paper* 364, 57–71.
- Powell, R., Holland, T., 1999. Relating formulations of the thermodynamics of mineral solid solutions; activity modeling of pyroxenes, amphiboles, and micas. *American Mineralogist* 84, 1–14.
- Pyle, J.M., Spear, F.S., 2003. Four generations of accessory-phase growth in low-pressure migmatites from SW New Hampshire. *American Mineralogist* 88, 338–351.
- Pyle, J. M., Spear, F. S., Rudnick, R. L., McDonough, W. F., 2001. Monazite–Xenotime–Garnet Equilibrium in Metapelites and a New Monazite–Garnet Thermometer. *Journal of Petrology* 42, 2083–2107.
- Quinn, D., Meere, P. A., Wartho, J.-A., 2005. A chronology of foreland deformation: ultra-violet laser $^{40}\text{Ar}/^{39}\text{Ar}$ dating of syn/lateorogenic intrusions from the Variscides of southwest Ireland. *Journal of Structural Geology*, 27, 1413–1425.
- Rahimi, G., Massonne, H.-J., 2018. Pressure-temperature-time evolution of a Variscan garnet-bearing micaschist from the northern Fichtelgebirge, NW Bohemian Massif in central Europe. *Lithos* 316–317, 366–384, doi:10.1016/j.lithos.2018.07.023.
- Rasmussen, B., Muhling, J. R., 2007. Monazite begets monazite: Evidence for dissolution of detrital monazite and reprecipitation of syntectonic monazite during low-grade regional metamorphism. *Contributions to Mineralogy and Petrology* 154, 675–689.
- Reed, S.J.B., 2005. *Electron microprobe analysis and scanning electron microscopy in geology*. Cambridge University Press, 7–11 pp.

- Reinhard, J., Kleemann, U., 1994. Extensional unroofing of granulitic lower crust and related low-pressure, high temperature metamorphism in the Saxonian Granulite Massif, Germany. *Tectonophysics* 238, 71–94.
- Richter, P., Stettner, G., 1979. Geochemische und petrographische Untersuchungen der Fichtelgebirgsgranite. *Geologica Bavarica* 78, 1–127.
- Rodríguez, J., Cosca, M.A., Gil-Ibarguchi, J.I., Dallmeyer, R.D., 2003. Strain partitioning and preservation of $^{40}\text{Ar}/^{39}\text{Ar}$ ages during Variscan exhumation of a subducted crust (Malpica-Tui complex, NW Spain). *Lithos* 70, 111–139, doi: 10.1016/S0024-4937(03)00095-1.
- Romer, R., Rötzler, J., 2001. P-T-t evolution of ultrahigh temperature granulites from the Saxon Granulite Massif, Germany. Part II: U-Pb dating of trace and major phases. *Journal of Petrology* 42, 2015–2032.
- Roser, B.P., 2000. Whole-rock geochemical studies of clastic sedimentary suites. *Memoir Geological Society of Japan* 57, 73–89.
- Roser B. P., Korsch R. J., 1986. Determination of tectonic setting of sandstone-mudstone suites using SiO_2 content and $\text{K}_2\text{O}/\text{Na}_2\text{O}$ ratio. *Journal of Geology* 5, 635–650.
- Rötzler, J., Carswell, D.A., Gerstenberger, H., Haase, G., 1999. Transitional blueschist-epidote amphibolite facies metamorphism in the Frankenberg massif, Germany, and geotectonic implications. *Journal of Metamorphic Geology* 17, 109–125.
- Rötzler, K., Schumacher, R., Maresch, W.V., Willner, A.P., 1998. Characterization and geodynamic implications of contrasting metamorphic evolution in juxtaposed high-pressure units of the western Erzgebirge (Saxony, Germany). *European Journal of Mineralogy* 10, 261–280.
- Rötzler, J., Romer, R.L., Budzinski, H., Oberhänsli, R., 2004. Ultrahigh-temperature high-pressure granulites from Tirschheim, Saxon Granulite Massif, Germany. *European Journal of Mineralogy* 16, 917–937.
- Rubatto, D., Hermann, J., 2007. Zircon behaviour in deeply subducted rocks. *Elements* 3, 31–35.
- Rubatto, D., Chakraborty, S., Dasgupta, S., 2013. Time scale of crustal melting in the Higher Himalayan Crystallines (Sikkim, Eastern Himalaya) inferred from trace element-constrained monazite and zircon chronology. *Contributions to Mineralogy and Petrology* 165, 349–372.
- Santos Zalduegui, J.F., Schärer, U., Gil-Ibarguchi, J.I., 1995. Isotope constraints on the age and origin of magmatism and metamorphism in the Malpica-Tuy allochthon, Galicia, NW-Spain. *Chemical*

- Geology 121, 91–103, doi: 10.1016/0009-2541(94)00123-P.
- Schäfer, J., Neuroth, H., Ahrendt, H., Dörr, W., Franke, W., 1997. Accretion and exhumation at a Variscan active margin, recorded in the Saxothuringian flysch. *Geologische Rundschau* 86, 599–611.
- Schandl, E.S., Gorton, M.W., 2004. A textural and geochemical guide to the identification of hydrothermal monazite: Criteria for selection of samples for dating epigenetic hydrothermal ore deposits. *Economic Geology* 99, 1027–1035.
- Schätz, M., Reischmann, T., Tait, J., Bachtadse, V., Bahlburg, H., Martin, U., 2002. The Early Palaeozoic break-up of northern Gondwana, new palaeomagnetic and geochronological data from the Saxothuringian Basin, Germany. *International Journal of Earth Sciences* 91, 838–849.
- Scherrer, N.C., Engi, M., Gnose, E., Jakob, V., Liechti, A., 2000. Monazite analysis; from sample preparation to microprobe age dating and REE quantification. *Schweizerische Mineralogische und Petrographische Mitteilungen* 80, 93–105.
- Schmädicke, E., Evans, B.W., 1997. Garnet-bearing ultramafic rocks from the Erzgebirge, and their relation to other settings in the Bohemian Massif. *Contributions to Mineralogy and Petrology* 127, 57–74.
- Schmädicke, E., Mezger, K., Cosca, M.A., Okrusch, M., 1995. Variscan Sm–Nd and Ar–Ar ages of eclogite facies rocks from the Erzgebirge, Bohemian massif. *Journal of Metamorphic Geology* 13, 537–552.
- Scholtz, H., 1930. Das varistische Bewegungsbild. *Fortschritte der Geologie und Palaeontologie* 25, 235–316.
- Schulmann, K., Kröner, A., Hegner, E., Wendt, I., Konopásek, J., Lexa, O., Štípská, P., 2005. Chronological constraints on the pre-orogenic history, burial and exhumation of deep-seated rocks along the eastern margin of the Variscan orogen, Bohemian Massif, Czech Republic. *American Journal of Science* 305, 407–448.
- Schulmann, K., Konopásek, J., Janoušek, V., Lexa, O., Lardeaux, J.M., Edel, J.B., Štípská, P., Ulrich, S., 2009. An Andean type Palaeozoic convergence in the Bohemian Massif. *Comptes Rendus Géoscience* 341, 266–286.
- Schulmann, K., Martínez Catalán, J. R., Lardeaux, J. M., Janoušek, V., Oggiano, G., 2014. The Variscan Orogeny: Extent, Timescale and the Formation of the European Crust. Geological Society, London, Special Publications, 405, doi.org/10.1144/SP405.15.

- Schulz, B., Schüssler, U., 2013. Electron-microprobe Th–U–Pb monazite dating in Early-Palaeozoic high-grade gneisses as a completion of U–Pb isotopic ages (Wilson Terrane, Antarctica). *Lithos* 175–176, 178–192.
- Scotese, C.R., 1997. *Continental Drift*, 7th ed. PALEOMAP Project, Arlington, Texas. 79 p.
- Sdzuy, K., 1971. The Ordovician in Bavaria. *Colloque Ordovicien—Silurien. Mém Bur Rech Géol Minières* 73, 379–390.
- Sebastian, U., 2013. *Die Geologie des Erzgebirges*. Berlin, (Springer Spektrum), 267 p.
- Seydoux-Guillaume, A.M., Paquette, J.L., Wiedenbeck, M., Montel, J.M., Heinrich, W., 2002. Experimental resetting of the U–Th–Pb system in monazite. *Chemical Geology* 191, 165–181.
- Shi, G., Song, G., Wang, H., Huang, C., Zhang, L., Tang, J., 2016. Late Paleozoic tectonics of the Solonker Zone in the Wuliji area, Inner Mongolia, China: Insights from stratigraphic sequence, chronology, and sandstone geochemistry. *Journal of Asian Earth Sciences* 127, 100–118.
- Siebel, W., Raschka, H., Irber, W., Kreuzer, H., Lenz, K.-L., Höhndorf, A., Wendt, I., 1997. Early Palaeozoic Acid Magmatism in the Saxothuringian Belt: New Insights from a Geochemical and Isotopic Study of Orthogneisses and Metavolcanic Rocks from the Fichtelgebirge, SE Germany. *Journal of Petrology* 38, 203–230.
- Siebel, W., Shang, C.K., Presser, V., 2010. Permo-Carboniferous magmatism in the Fichtelgebirge: dating the youngest intrusive pulse by U–Pb, $^{207}\text{Pb}/^{206}\text{Pb}$ and $^{40}\text{Ar}/^{39}\text{Ar}$ geochronology. *Zeitschrift für geologische Wissenschaften* 38, 85–98.
- Spear, F.S., 1995. *Metamorphic phase equilibria and pressure-temperature-time paths*. Mineralogical Society of America, Washington, 799 p.
- Spear, F.S., 2017. Garnet growth after overstepping. *Chemical Geology* 466, 491–499.
- Spear, F.S., Pyle, J.M., 2002. Apatite, monazite, and xenotime in metamorphic rocks. *Reviews in Mineralogy and Geochemistry* 48, 293–331.
- Spear, F.S., Pyle, J.M., 2010. Theoretical modeling of monazite growth in a low-Ca metapelite. *Chemical Geology* 273, 111–119.
- Stampfli, G.M., 1996. The intra-alpine terrain: a paleotethyan remnant in the Alpine Variscides. *Eclogae Geologicae Helveticae* 89, 13–42.

- Stampfli, G.M., Borel, G.D., 2002. A plate tectonic model for the Paleozoic and Mesozoic constrained by dynamic plate boundaries and restored synthetic oceanic isochrones. *Earth and Planetary Science Letters* 196, 17–33.
- Stein, E., 1988. Die strukturgeologische Entwicklung im Übergansbereich Saxothuringikum/Moldanubikum in NE Bayem. *Geologica Bavarica* 92, 5–131.
- Steiner, J., Falk, F., 1981. The Ordovician Lederschiefer of Thuringia. In: Hambrey, M.J., Harland, W.D. (Eds.), *Earth's pre-Pleistocene Glacial Record*. University Press Cambridge 579–581 pp.
- Stettner, G., 1958. Erläuterungen zur Geologischen Karte von Bayern 1:25000, Bl. Nr. 5937. Bayerisches Geologisches Landesamt München, Fichtelberg, 1–166 pp.
- Stettner, G., 1975. Zur geologisch-tektonischen Entwicklung des Oberpfälzer Grundgebirges. *Aufschluss*, Sonderband 26, 11–38.
- Stettner, G., 1980. Zum geologischen Aufbau des Fichtelgebirges. *Aufschluss* 31, 391–403.
- Stettner, G., 1981. 1. Grundgebirge. In: Haunschild, H., Jerz, H. (Eds.), *Erläuterungen zur Geologischen Karte von Bayern 1:500 000*, 3 Auflage Bayerisches Geologisches Landesamt, München, 7–29 pp.
- Stille, H., 1951. Das mitteleuropaishe varistische Grundgebirge im Bilde des gesamteuropäischen. *Geologisches Jahrbuch Beihefte* 2, 1–138.
- Stöckhert, B., Massonne, H.-J., Nowlan, E.U., 1997. Low differential stress during high pressure metamorphism: the microstructural record of a metapelite from the Eclogite Zone, Tauern Window, Eastern Alps. *Lithos* 41, 103–118.
- Stöckhert, B., Duyster, J., Trepmann, C., Massonne, H.-J., 2001. Microdiamond daughter crystals precipitated from supercritical COH silicate fluids included in garnet, Erzgebirge, Germany. *Geology* 29, 391–394.
- Stumm, A., 2002. *Genese und Entwicklung der Mineralwässer in Bad Brambach.*, Dr. rer. nat. thesis, Technische Universität Bergakademie Freiberg, 119 p.
- Sturm, R., 2017. Cordierite from a high-temperature low-pressure shear zone of the south-western Bohemian Massif (Moldanubian terrain, Austria). *Chemie der Erde* 77, 195–206.
- Suess, E., 1888. *Das Antlitz der Erde*. Tempsky, Wien.
- Suess, F.E., 1903. Bau und Bild der Böhmischen Masse. In: Diener, C., Hoernes, R., Suess, F.E., and Uhlig, V. (Eds.), *Bau und Bild Österreichs: Temsky-Freytag*, 1110 p.

- Suess, F.E., 1926. Intrusions- und Wandertektonik im varistischen Grundgebirge. Verlag Bornträger, Berlin.
- Suzuki, K., Adachi, M., 1991. Precambrian provenance and Silurian metamorphism of the Tsubonosawa paragneiss in the South Kitakami terrane, Northeast Japan, revealed by the chemical Th-U-total Pb isochron ages of monazite, zircon and xenotime. *Geochemical Journal* 25, 357–376.
- Suzuki, K., Adachi, M., Kajizuka, I. 1994. Electron microprobe observations of diffusion in metamorphosed detrital monazites. *Earth and Planetary Science Letters* 128, 391–405.
- Taylor, S.R., McLennan, S.M., 1981. The composition and evolution of the continental crust: rare earth element evidence from sedimentary rocks. *Philosophical Transactions of the Royal Society London* 301, 381–398.
- Taylor, R.J.M., Kirkland, C.L., Clark, C., 2016. Accessories after the facts: constraining the timing, duration and conditions of high-temperature metamorphic processes. *Lithos* 264, 239–257.
- Teufel, S., 1988. Vergleichende U–Pb- und Rb–Sr-Altersbestimmungen an Gesteinen des Übergangsbereiches Saxothuringikum/Moldanubikum. NE-Bayern. *Göttinger Arbeiten für Geologie und Paläontologie* 35, 1–87.
- Thompson, J.B., 1959. Local equilibrium in metasomatic processes. In: Abelson, P.H. (Ed.), *Researches in Geochemistry*, Wiley, New York, 42–457.
- Tichomirowa, M., 2002. Die Gneise des Erzgebirges – hochmetamorphe Äquivalente von neoproterozoisch – frühpaläozoischen Grauwacken und Granitoiden der Cadomiden. *Freiburger Forschungshefte, Reihe C* 495, 1–222.
- Tichomirowa, M., Whitehouse, M.J., Nasdala, L., 2005. Resorption, growth, solid state recrystallisation, and annealing of granulite facies zircon—a case study from the Central Erzgebirge, Bohemian Massif. *Lithos* 82, 25–50.
- Tichomirowa, M., Sergeev, S., Berger, H.J., Leonhardt, D., 2012. Inferring protoliths of high-grade metamorphic gneisses of the Erzgebirge using zirconology, geochemistry and comparison with lower-grade rocks from Lusatia (Saxothuringia, Germany). *Contributions to Mineralogy and Petrology* 164, 375–396.
- Timmermann, H., Štědrá, V., Gerdes, A., Noble, S.R., Parrish, R.R., Dörr, W., 2004. The problem of dating high-pressure metamorphism: a U–Pb isotope and geochemical study on eclogites and related rocks of the Mariánské Lázně complex, Czech Republic. *Journal of Petrology* 45, 1311–1338.

- Tischendorf, G., Förster, H.-J., 1994. Mineral deposits of the Erzgebirge/Krušné Hory (Germany/Czech Republic). In: Gehlen von, K., and Klemm, D.D. (Eds.), *Monogr. Series on Mineral Deposits* 31; Gebrüder Borntraeger: Berlin, 5–23 pp.
- Tomkins, H.S., Pattison, D.R.M., 2007. Accessory phase petrogenesis in relation to major phase assemblages in pelites from the Nelson contact aureole, southern British Columbia. *Journal of Metamorphic Geology* 25, 401–421.
- Torsvik, T.H., Smethurst, M.A., Meert, J.G., Van der Voo, R., McKerrow, W.S., Brasier, M.D., Sturt, B.A., Walderhaug, H.J., 1996. Continental break-up and collision in the Neoproterozoic and Palaeozoic: a tale of Baltica and Laurentia. *Earth-Science Reviews* 40, 229–258.
- Underwood, E.E., 1970. *Quantitative Stereology*. Reading in Massachusetts Addison-Wesley 274 pp.
- van Staal, C.R., Dewey, J.F., Mac Niocaill, C., McKerrow, W.S., 1998. The Cambrian-Silurian tectonic evolution of the Northern Appalachians and British Caledonides; history of a complex, west and southwest Pacific-type segment of Iapetus. In: Blundell, D., Scott, A.C. (Eds.), *Lyell: The Past is the Key to the Present*. Geological Society of London Special Publication 143, 199–242.
- Vejnar, Z., 1965. Bemerkungen zur lithostratigraphischen Beziehung zwischen dem mittelböhmischen Algonkium und dem Moldanubikum. *Neues Jahrbuch für Geologie und Paläontologie* 2, 102–111.
- Vollbrecht, A., Weber, K., Schmoll, J., 1989. Structural model for the Saxothuringian-Moldanubian suture in the Variscan basement of the Oberpfalz (northeastern Bavaria, F.R.G.) interpreted from geophysical data. *Tectonophysics* 157, 123–133.
- von Quadt, A., 1993. The Saxonian Granulite Massif: New aspects from geochronological studies: *Geologische Rundschau* 82, 516–530, doi: 10.1007/BF00212414.
- von Quadt, A., Gebauer, D., 1998. Evolution of eclogitic rocks in the Erzgebirge; a conventional and SHRIMP U–Pb zircon and Sm–Nd study. *Acta Universitatis Carolinae Geologica* 42, 324–325.
- von Raumer, J.F., Neubauer, F., 1993, *The Pre-Mesozoic geology in the Alps*: Springer, Heidelberg, 671p.
- von Raumer, J.F., Neubauer, F., 1994, *The Paleozoic evolution of the Alps*. *Schweizerische Mineralogisch Petrographische Mitteilungen* 74, 459–467.
- Waizenhöfer, F., Massonne, H.-J., 2017. Monazite in a Variscan mylonitic paragneiss from the Münchberg Metamorphic Complex (NE Bavaria) records Cadomian protolith ages. *Journal of Metamorphic Geology* 35, 453–469.

- Waldron, J.W.F., Murphy, J.B., Schofield, D.I., 2011. A Caribbean-style plate in the Iapetus Ocean. Geological Society of America, Abstracts with Programs 5, 43–45.
- Weber, K., Vollbrecht, A., 1989. The Crustal Structure at the KTB Drill Site, Oberpfalz. In: Emmermann, R., and Wohlenberg, J., (Eds), The German Continental Deep Drilling Program (KTB). Springer, Berlin, 5–36 p.
- Weil, A.B., Van der Voo, R., van der Pluijm, B.A., 2001. Oroclinal bending and evidence against the Pangea megashear: the Cantabria–Asturias arc (northern Spain). *Geology* 29, 991–994.
- Wendt, I. Carl, C. 1991. The statistical distribution of the mean squared weighted deviation. *Chemical Geology (Isotope Geoscience Section)* 86, 275–285.
- Werner, O., Lippolt, H. J., 2000. White mica $^{40}\text{Ar}/^{39}\text{Ar}$ ages of Erzgebirge metamorphic rocks: simulating the chronological results by a model of Variscan crustal imbrication. In: Franke, W., Haak, V., Oncken, O., Tanner, D., (Eds.), *Orogenic Processes: Quantification and Modelling in the Variscan Belt*. Geological Society of London, Special Publications 179, 323–336
- White, R.W., Powell, R., Holland, T.J.B., Worley, B.A., 2000. The effect of TiO_2 and Fe_2O_3 on metapelitic assemblages at greenschist and amphibolite facies conditions: mineral equilibria calculations in the system $\text{K}_2\text{O}-\text{FeO}-\text{MgO}-\text{Al}_2\text{O}_3-\text{SiO}_2-\text{H}_2\text{O}-\text{TiO}_2-\text{Fe}_2\text{O}_3$. *Journal of Metamorphic Geology* 18, 497–511.
- White, R.W., Powell, R., Holland, T.J.B., 2001. Calculation of partial melting equilibria in the system $\text{Na}_2\text{O}-\text{CaO}-\text{K}_2\text{O}-\text{FeO}-\text{MgO}-\text{Al}_2\text{O}_3-\text{SiO}_2-\text{H}_2\text{O}$ (NCKFMASH). *Journal of Metamorphic Geology* 19, 139–153.
- White, R.W., Powell, R., Phillips, G.N., 2003. A mineral equilibria study of the hydrothermal alteration in mafic greenschist facies rocks at Kalgoorlie, Western Australia. *Journal of Metamorphic Geology* 21, 455–468.
- Wiegand, B., 1996. Isotopengeologische und geochemische Untersuchungen zur prävariskischen magmatischen und sedimentären Entwicklung im saxothuringisch-moldanubischen Übergangsbereich (Grenzgebiet BRD/CR). Dissertation Theses, Universität Göttingen, 1–146 pp.
- Will, T.M., Schmädicke, E., 2001. A first find of retrogressed eclogites in the Odenwald Crystalline Complex, Mid-German Crystalline Rise, Germany: evidence for a so far unrecognised high-pressure metamorphism in the Central Variscides. *Lithos* 59, 109–125.
- Williams, I.S., 2013. 30 Years of Progress in Applying Micro dating Techniques to Understanding

- Precambrian Crustal Evolution Precambrian Evolution and Deep Exploration of the Continental Lithosphere, 7–9 October 2013, Beijing, China, Abstract Volume, IAGR Conference Series 15, 110–112.
- Williams, M.L., Jercinovic, M.J., 2002. Microprobe monazite geochronology: putting absolute time into micro structural analysis. *Journal of Structural Geology* 24, 1013–1028.
- Williams, M.L., Jercinovic, M.J., 2012. Tectonic interpretation of metamorphic tectonites: integrating compositional mapping, microstructural analysis and in situ monazite dating. *Journal of Metamorphic Geology* 30, 739–752.
- Williams, M.L., Jercinovic, M.J., Terry, M.P. 1999. Age mapping and dating of monazite on the electron microprobe: deconvoluting multistage tectonic histories. *Geology* 27, 1023–1026.
- Williams, M.L., Jercinovic, M.J., Harlov, D.E., Budzyń, B., Hetherington, C.J., 2011. Resetting monazite ages during fluid-related alteration. *Chemical Geology* 283, 218–225.
- Willner, A.P., Rötzler, K., Maresch, W.V., 1997. Pressure temperature and fluid evolution of quartzo–feldspathic metamorphic rocks with a relic high-pressure, granulite–facies history from the Central Erzgebirge (Saxony, Germany). *Journal of Petrology* 38, 307–336.
- Willner, A.P., Krohe, A., Maresch, M.V., 2000. Interrelated P–T–t–d paths in the Variscan Erzgebirge dome (Saxony, Germany): constraints on the rapid exhumation of high-pressure rocks from the root zone of a collisional orogen. *International Geology Review* 42, 64–85.
- Willner, A.P., Sebazungu, E., Gerya, T.V., Maresch, W.V. & Krohe, A., 2002. Numerical modelling of PT-paths related to rapid exhumation of high-pressure rocks from the crustal root in the Variscan Erzgebirge Dome (Saxony/Germany). *Journal of Geodynamics* 33, 281–314.
- Willner, A.P., Barr, S.M., Gerdes, A., Massonne, H.-J., White, C.E., 2013. Origin and evolution of Avalonia: evidence from U–Pb and Lu–Hf isotopes in zircon from the Mira terrane, Canada, and the Stavelot–Venn Massif, Belgium. *Journal of the Geological Society* 170, 769–784.
- Wilson, J.T., 1966. Did the Atlantic close and then re-open? *Nature* 211, 676–681.
- Winchester, J.A., Pharaoh, T.C., Verniers, J., 2002. Palaeozoic amalgamation of central Europe: An introduction and synthesis of new results from recent geological and geophysical investigations, in Winchester, J.A., Pharaoh, T.C., Verniers, J. (Eds.), *Palaeozoic amalgamation of central Europe*: London, Geological Society of London Special Publication 201, 1–18.

- Winter, J. D. 2010. Principles of igneous and metamorphic petrology (2nd Ed.), Upper Saddle River, NJ: Prentice Hall, 745 p.
- Wu, C.M., Cheng, B.H., 2006. Valid garnet-biotite (GB) geothermometry and garnet-aluminum silicate-plagioclase-quartz (GASP) geobarometry in metapelitic rocks. *Lithos*, 89, 1–23.
- Wu, C.M., Wang, X.S., Yang, C.H., Geng, Y.S., Liu, F.L., 2002. Empirical garnet–muscovite geothermometry in metapelites. *Lithos* 62, 1–13.
- Wurm, A., 1925. Geologie von Bayern: Nordbayern, Fichtelgebirge u. Frankenwald. Gebr. Borntraeger, Berlin, 373 pp.
- Wurm, A., 1961. Geologie von Bayern – Frankenwald, Münchberger Gneismasse, Fichtelgebirge, Nördlicher Oberpfälzer Wald. Borntraeger, Berlin, 555 pp.
- Yan, Y., Xia, B., Lin, G., Cui, X., Hu, X., Yan, P., Zhang, F., 2007. Geochemistry of the sedimentary rocks from the Nanxiong Basin, South China and implications for provenance, palaeoenvironment and paleoclimate at the K/T boundary. *Sedimentary Geology* 197, 127–140.
- Yang, P., Pattison, D., 2006. Genesis of monazite and Y zoning in garnet from the Black Hills, South Dakota. *Lithos* 88, 233–253.
- Zeh, A., Gerdes, A., 2010. Baltica- and Gondwana-derived sediments in the Mid-German Crystalline Rise (Central Europe): Implications for the closure of the Rheic Ocean. *Gondwana Research* 17, 254–263.
- Zeh, A., Will, T.M., 2010. The Mid-German Crystalline Zone. In: Linnemann, U., Romer, R.L. (Eds.), *Pre-Mesozoic Geology of Saxo-Thuringia - From the Cadomian Active Margin to the Variscan Orogen*. Schweizerbart, Stuttgart, 195–220 pp.
- Zeh, A., Brätz, H., Millar, I.L., Williams, I.S., 2001. A combined zircon SHRIMP and Sm–Nd isotope study on high-grade paragneisses from the Mid-German Crystalline Rise: evidence for northern Gondwanan and Grenvillian provenance. *Journal of the Geological Society of London* 158, 983–994.
- Zitzmann, A., 1968. Das Paläozoikum im Grenzbereich zwischen Bayerischer und Thüringischer Faziesreihe des Frankenwaldes. *Geologisches Jahrbuch* 86, 579–654.
- Zulauf, G., 1993. The Moldanubian/Saxothuringian boundary at the western border of the Bohemian Massif - a polyphase strike-slip zone. *Zeitschrift der Deutschen Geologischen Gesellschaft* 144, 68–87.

Zuluaga, C.A., Stowell, H.H., Tinkham, D.K., 2005. The effect of zoned garnet on metapelite pseudosection topology and calculated metamorphic P-T paths. *American Mineralogist* 90, 1619–1628.

Zwart, H.J., 1967. The duality of orogenic belts. *Geologie en Mijnbouw* 46, 283–309.

Acknowledgements

First of all, I would like to express my deepest gratitude to Prof. Hans-Joachim Massonne for his extensive work as my supervisor, and he gave me the best supervision. During my doctorate work, he was always patient and silent to help me and encourage me in every way. He review through my manuscripts for publications many times for each, and did careful corrections again and again to improve them. He has also been a very dedicate guide for me. He supported me to go to geological field and international conferences, which allowed me to greatly broaden my scientific horizons. He is always at service and patient to answer every of my questions making sure that my work was always on the right track. His broad knowledge and calm personality have been very inspiring on my future work and life.

Secondly, I would like to thank Prof. Michael Hunger for participate to my dissertation as my second supervisor. He is a responsible professor, and he was caring on the progress of my doctorate work, giving me good tips how to manage my work and prepare final exam. Thirdly, I would like to mention the institute team. Dr. Thomas Theye, who taught me how to use the instruments of EMP and XRF, and I troubled him tens of thousands of times during my analytical work. He introduced books and papers to me from time to time. He is a good advisor, and he solved a lot of my scientific questions. I also would like to give my deepest thank to Dr. Joachim Opitz, as others said “he taught us to enjoy sunshine everyday”. He always can find fun from stressful life, which makes the work place so happy. He is a kind of culture dictionary, and I know a lot of interesting stories about different countries from him. Another one of my most respective persons is Prof. Arne Willner. Every time when I met him, he asked me about my work progress and gave me constructive suggestions. Dr. Tillmann Viefhaus is also a helpful person, he was always welcoming to give me valuable information and I troubled him a lot about chemistry and German language questions. I appreciate my best friend, Volker Spieth, for his existence, whenever I needed him. He encouraged me to improve my German and plan my future career and private life. He was always next to me immediately if I required help or consultant. I thank Alexander Schopf for kindly providing me many useful information about my thesis preparation and university administrations. Botao Li and Florian Waizenhöfer are thanked for unforgettable experiences of common study, field trip and daily discussions. I also would like to give my deep gratitude to Bettina Wieland, Moritz Schmelz, Gisela Kwiatkowski, Matthias Leiss and Zeljka Zigovecki Gobac for their help and support. In such international atmosphere, I had also the opportunity to know interesting people from all

over the world, giving me the curiosity and priceless information about different cultures and point of views. It was Wentao Cao from USA, Federico Rossetti, Deborah Lo Pò, Salvatore Iaccarino, Dario Fancello, Gabriele Cruciani and Federico Lucci from Italy, Christian Soder from Heidelberg, Sérgio Benjamin Baggio and Rossana Vicente Goulart from Brazil, Mauricio Calderón from Chile, Juan Cruz Martínez and Jorge Dristas from Argentina, became very close friends to me. We were chatting, traveling, and eating during our leisure time, which are very unforgettable memories. My family is thanked for giving me total freedom for following my dreams.

Finally, I would like to thank my partner, Axel Watzlawek. He donated much endless help and support, he was so patient and caring and motivated me anytime time. Without him I would not be able to finish my doctorate work.

Erklärung über die Eigenständigkeit der Dissertation

Ich versichere, dass ich die vorliegende Arbeit mit dem Titel

„Evolution of Variscan metamorphic rocks from the Fichtelgebirge and Elstergebirge“

selbständig verfasst und keine anderen als die angegebenen Quellen und Hilfsmittel benutzt habe; aus fremden Quellen entnommene Passagen und Gedanken sind als solche kenntlich gemacht.

Declaration of Authorship

I hereby certify that the dissertation entitled

„Evolution of Variscan metamorphic rocks from the Fichtelgebirge and Elstergebirge“

is entirely my own work except where otherwise indicated. Passages and ideas from other sources have been clearly indicated.

Name/Name: Gelareh Rahimi

Unterschrift/Signed:

Datum/Date: 21.01.2019

Lebenslauf des Autor

Personal Data

Birth date and place: 31 October 1978, Teheran

Nationality: Iranian

Email: ra_gelareh@yahoo.com

Education

10/2013 **Promotion** an der Fakultät Chemie der Universität Stuttgart bei Prof. Dr. Hans-Joachim Massonne

Research project or dissertation: „Evolution of Variscan metamorphic rocks from the Fichtelgebirge and Elstergebirge“

09/2006 – 09/2009 **M.Sc. Petrology (Hons.)** University of Tehran, School of Science, Faculty of Geology

Research project or dissertation: „Petrology and geochemistry of the volcanic rocks of North and North-East of Qazvin (Abazar District) “

09/2001 – 09/2005 **B.Sc. Geology (Hons.)** Azad University – North of Tehran Branch, School of

Work Experience

10/2013 – 31.03.2019 – University of Stuttgart, Institut für Mineralogie und Kristallchemie

09/2012 – 08/2013 – Self-employed in Tehran, Iran – Consulting and advising for various clients

04/2011 – 09/ 2012 – TÜV Nord Iran-Germany

09/2009 – 03/201 – Exploration Directorate, National Iranian Oil Company

09/ 2007 – 08/2009 – Off-shore oil company, National Iranian Oil Company - Teaching experience in University for bachelor students, participating in national and international seminars and conferences, having publications in different international scientific journals.